Development and Characterization of *nano*-Hydroxyapatite based Bioabsorbable Polymeric Internal Fixation Devices

Thesis submitted in the partial fulfillment of the requirement for the degree of

Doctor of Philosophy

By

Arbind Prasad

Department of Mechanical Engineering

Indian Institute of Technology, Guwahati

Guwahati-781039, Assam, India

August, 2019

Statement

This is to certify that the research work in the thesis entitled "**Development and characterization of *nano*-Hydroxyapatite based Bioabsorbable Polymeric Internal Fixation Devices**" is carried out by me at the Mechanical Engineering Department and Centre of Excellence for Sustainable Polymers (CoE-SusPol) Lab, Department of Chemical Engineering, Indian Institute of Technology Guwahati, under the supervision of Professor Vimal Katiyar and Dr. Mamilla Ravi Sankar. The results documented in this thesis are achieved by me and it has not been submitted to any other university or Institute for the award of any degree or diploma.

(Arbind Prasad)
Roll no. 136103034
Department of Mechanical Engineering
Indian institute of Technology Guwahati
Guwahati -781039, India

Certificate

This is to certify that the thesis entitled "**Development and characterization of nano Hydroxyapatite based Bioabsorbable Polymeric Internal Fixation Devices**" being submitted by Arbind Prasad for the award of PhD. Degree has been carried out by him at the Mechanical Engineering Department and Centre of Excellence for Sustainable Polymers (CoE-SusPol), Department of Chemical Engineering, Indian Institute of Technology Guwahati, under our guidance and supervision. The work documented in this thesis has not been submitted to any other university or Institute for the award of any degree or diploma.

Prof. Vimal Katiyar
Professor
Department of Chemical Engineering
Principal Investigator
Centre of Excellence for Sustainable Polymers
Indian Institute of Technology Guwahati
Guwahati -781039, India

Dr. Mamilla Ravi Sankar
Associate Professor
Department of Mechanical Engineering
Indian Institute of Technology Guwahati
Guwahati -781039, India

Dedicated

To

My Beloved Parents

for their Endless love, Support and Encouragement

Acknowledgement

I would like to express my sincere and profound sense of gratitude, to both my learned guide Prof. Vimal Katiyar and Dr. Mamilla Ravi Sankar for their valuable guidance and steady encouragement throughout my Ph.D. work. Their constant encouragement, enormous goodwill and unruffled patience made me work at ease and kept me highly motivated throughout my stay. The innovative ideas and consistent support by extending all the necessary facilities are helpful in the successful completion of my research work. I would like to acknowledge Prof. P. S. Robi, Prof. S. Senthilvelan and Prof. Mohd. Qureshi, members of my Doctoral Committee who have directed me in the right path by providing comments, suggestions and sharing their expertise at various stages of my experimental work. I thank the Head, Department of Mechanical Engineering, IIT Guwahati for their support during the course of my research work. I extend my sincere thanks to Tool Room Training Centre, Amingaon staff and deputy managers and especially Mr. Sanjiv Kumar for his valuable suggestions during fabrication of critical parts machining during fabrications of moulds and fixtures.

I would like to thank Mr. N. K. Das and his associates for helping me during the fabrication processes in the central workshop, IITG. Especially I would like to thank Mr. Mrinal Sarma, Fitting Shop who patiently helped me throughout my experimental work. I am very grateful to the technical staff of Mechanical Engineering Department, Mr. Sanjib Sarma, Mr. Jiten Basumatary, Mr. Nip Borah, Mr. Saiffuddin Ahmed, Mr. Pranjol Paul, Mr. Dhruba Jyoti Bordoloi and Mr. Rituraj Saikia for their contribution and help throughout my research work. I am also thankful to the Mechanical Engineering Department office staffs Mr. Nabajyoti Dutta and Mr. Raju Talukdar who have supported me in the academic and administration works.

I am thankful to my seniors and lab colleagues Dr. Sachin Singh, Mr. Rasmi Ranjan, Dr. Kishor Kumar Gajrani, Dr. A. Muthuraja, Vignesh Babu, Srikant Prasad, Dipendra Roy, Dr. Ashish Rajak, Dr. Ramesh Kumar, Nabajyoti, Abhishek of Mechanical Engineering department and Dr. Arvind

Gupta, Dr. Akhilesh Pal, Dr. Prodyut Dhar, Dr. Rahul Patwa, Dr. Melakuu Tesfaye, Dr. Purabi, Dr. Prasanta, Siddharth Mohan Bhasney, Narendren, Surendra Gaur, Kiran Gali, Naba kalita, Shasanka, Gourhari, Monika, Modu, Neha, Tabli, Devleena, Bhanupriya, Deepshikha, Munmi, Doli, Chethana, Khalid, Durlov, Sayan, Sunny, Sourav, Partha, Lakhya of Chemical Engineering Department and summer interns, Aditya, Manmohan, Abhishek, Kakoli for their valuable help in my thesis work. I also thank my Mechanical Engineering Department colleagues who rendered direct and indirect support in my work.

I thank Chemical Engineering Department staff and Physics Department staff and Central Instruments Facility, IIT Guwahati for permitting to utilize their resources throughout my thesis work. I thank all of them for helping me directly and indirectly to complete my work. I wish to extend my deepest gratitude to my parents and my wife Ragni and son Shubham for their love, affection and cooperation throughout my research work. Finally, I extend my gratitude to the Almighty god for giving me this opportunity and good health for the successful completion of this breakthrough in my career.

Arbind Prasad

Abstract

Increasing population density and expanding health care market leads to the imports of orthopaedic and prosthetic devices. Due to an abnormal lifestyle of living, quality of food, nutrition intake and deficiency in calcium intake lead towards the bone weakness day by day. Additionally, the growing incidence of diabetes, obesity, osteoarthritis and osteoporosis are further expanding the clinical needs. Traditional metallic internal fixation devices provide reliable fixation, but after fracture healing, retraction without pain and discomfort is almost not possible. The main limitations associated with metal implants are a frequent need for non-intended secondary surgical removal of hardware (e.g. due to implant migration, discomfort, pain, or stress shielding phenomena). To overcome these problems, bioabsorbable internal fixation devices (IFDs) have been developed and fabricated. The advantages associated with these devices are that the concerned patient need not go for resurgery for removal of implants, as they were in the case of metallic implant devices. The mechanical properties of the bone and developed IFDs are almost in the same range thus avoiding stress shielding phenomenon. Thus the mechanical properties should match with the properties of bone, and elastic modulus value must lie in the limit of bone properties so that stress shielding phenomenon could be avoided.

Bioabsorbable IFDs are the implants used inside in our body to fix the fractured bones. The widely used IFDs are cortical screws, cancellous screws, bone plate, Steinmann pins and U-type bone staples. In this research, bioabsorbable IFDs are based on biocompatible, bioabsorbable polymers as matrix and functional nano powders as a reinforcing phase. Since the natural bone is also consisting of both inorganic and organic components, it combines the strength and stiffness of the inorganic compound (nano Hydroxyapatite (nHAp)) and flexibility. The toughness and resorbability of an organic phase such as pure bioabsorbable polymers (poly lactic acid (PLA)), this will combine the osteoconductivity and biodegradability of polymers/ceramic composite which is further expected to mimic the natural bone to some extent.

To achieve the above stated objectives, Natural biowastes such as fish scales were collected from the local market and deproteinized with standard protocols to clean and ultimately produce pure nHAp as a filler material. Commercial PLA was purified for medical grade

purposes and crushed into powders to mix with filler materials as a matrix phase. Various moulds were designed and fabricated for IFDs such as cortical screws, cancellous screws, bone plates, Steinmann pins and U-type bone staples. Optimization of injection moulding process parameters such as screw speed, temperature and residence time were set to produce the optimum IFDs. Preliminary experiments were conducted for finding the significant concentration in weight percentage of filler materials and base materials after that parameter (extrusion temperature, injection moulding temperature, cylinder temperature, mould temperature, residence time, holding time, screws speed and air pressure). Once the concentration of filler and base material were optimized, all IFDs were produced through twin screws extruder cum injection moulding process.

In vitro bioactivity studies were conducted as per the standard protocol in simulated body fluid at 37°C of pH 7.4. *In vitro* hydrolytic degradation studies were conducted on PLA and PLA/nHAp biocomposites. Once the process parameters and involved machinery were optimized the bioabsorbable IFDs were studied one by one using ASTM standards. Various fixtures of metals and wooden materials were fabricated to know the near exact properties and its durability.

For every IFDs, separate test arrangement has been done with the help of fabricated fixtures such as for cortical screws, axial pull out strength, flexural strength, torsional test and double shear strength etc. These all have been determined with varying concentrations of filler to base materials. Similarly, a separate arrangement for hydrolytic degradation has been studied to know the degradation time of every type of IFDs. Development, fabrication of moulds, related fixtures, bioactivity studies, cytotoxicity studies, *In vitro* hydrolytic degradation studies of each IFDs and ultimately conclusion about its application and targeting for various age group people makes this finding impactful, affordable and replacement of existing metallic internal fixation devices. Therefore this doctoral thesis focuses on the development and characterization of nano Hydroxyapatite based bioabsorbable polymeric IFDs.

Key findings

The major contributions and findings of the current work are summarized as below:

1. Bioactive bio fillers (nHAp) from natural biowastes such as fish scale biowastes through mechanical route.

2. PLA was purified in order to get medical grade fibrous PLA, which ease to crush in powder form results uniform mixing with the nHAp effectively.
3. Fabrication of standards molds for cortical screws, cancellous screws, bone plates, steinmann pins and u- type bone staples.
4. Parametric optimization of process parameters of extrusion cum injection molding process of all IFDs. Generally, the processing parameter was set as mold temperature at 100-110°C, screw speed was maintained 100-120 rpm, cylinder temperature kept at 190-210°C,and residence time was maintained 1-1.25 min.
5. In case of cortical screws, axial pull out strength increases to 38% in 10% nHAp, 30% in torsional strength, 12% in double shear strength was observed. The flexural strength was reduced between 4% -16% with compared to neat PLA.
6. In cancellous screws, axial pull out strength of 10% nHAp gives 39%, 48% torsional strength (10% nHAp), 8% double shear strength (10% nHAp) enhancement was observed. The flexural strength was reduced between 5% -18% with compared to neat PLA.
7. In bone plates, 19% torsional strength (5% nHAp), 3% Single plate pull out test (3% nHAp) and double plate pull out test (7% nHAp) enhancement was observed. The flexural strength was reduced between 4% -8% with compared to neat PLA.
8. In case of steinmann pins, 11% double shear strength (10% nHAp) enhancement was observed. The flexural strength was increased between 9% -11% with compared to neat PLA. While in case of bone staples, torsional strength of 3% nHAp gives 5% increment and reduction of 3% (3% nHAp) to 30 % (10% nHAp) was observed in ultimate tensile strength.
9. *In vitro* hydrolytic degradation studies were carried out for 90 days. Mechanical strength after *In vitro* hydrolytic degradation observed ~30% - 44% reduction after 90 days.
10. Invitro bioactivity studies were carried as per standard protocol in simulated body fluid environment and was observed the formation of apatite layer on it.
11. Dimensional deviation from the standard geometry to the obtained geometry were measured through optical and stereomicroscopes. The deviation in their dimensions were observed insignificant.

TABLE OF CONTENTS

Statement i
Certificate ii
Acknowledgement iv
Abstract vi
Table of Contents ix
List of Figures xv
List of Tables xxvii
Nomenclature xxix

Chapter 1

1 Introduction and Literature Review…….....1

1.1 Global and Indian scenario of orthopedic devices market…….....1

1.2 Internal fixation devices (IFDs) and its requirement …….3

1.3 Fixations of fractured bones……4

1.3.1 Cortical screws……5

1.3.2 Cancellous screws……...5

1.3.3 Bone plates…….....6

1.3.4 Steinmann pins……6

1.3.5 U type bone staples……6

1.4 Problems with metallic internal fixation devices……7

1.5 An alternative solution for the metallic internal fixation devices……...8

1.6 Bioabsorbable polymeric internal fixation devices…….....10

1.7 Challenges of bioabsorbable polymers and IFDs……..10

1.8 Bone and its remodeling……13

1.9 Bone fixation device materials…….....15

1.9.1 Mechanical properties of some implant materials and tissues..……16

1.10 Statistics of bone related diseases……..18

1.11 Bone fracture healing……...18

1.12 Statistics of fish scales bio wastes……19

1.13 Bone and Hydroxyapatite……..19
1.14 Bioabsorbable polymers……21
1.15 Poly lactic acid……....23
1.16 Literature review……...25
1.16.1 Literature review of internal fixation devices……...25
1.16.2 Gaps observed in the prior art……...36
1.16.3 Motivation and objectives of the present work…….37
1.16.4 Hypothesis……38
1.16.5 The objective of the research ……...38
1.16.6 Organization of thesis……39

Chapter 2

2 Polylactic acid and *nano*-Hydroxyapatite based Biocomposites……..……..……42
2.1 Introduction……...42
2.2 Materials and methodology…….....44
2.2.1 Poly lactic acid…….....44
2.2.2 Hydroxyapatite…….....44
2.3 Processing of PLA/nHAp biocomposites…….……47
2.4 Characterization of PLA/nHAp biocomposites……50
2.5 Results and discussion…….....50
2.5.1 Field emission scanning electron microscopy……...……50
2.5.2 Transmission electron microscope……51
2.5.3 X-ray diffraction studies……53
2.5.4 Thermogravimetric analysis……..54
2.5.5 Gel permeation chromatography……...57
2.5.6 Differential scanning calorimetry……..58
2.5.7 Fourier transform infrared spectroscopy……...60
2.5.8 Mechanical properties……...61
2.5.9 Hardness test…….……65
2.5.10 Density measurement……66
2.5.11 Surface wettability……68

2.5.12 Polarizing optical microscopic studies…..70
2.5.13 Bioactivity studies……73
2.5.14 Hydrolytic degradation studies……..75
2.5.15 Water absorption test……78
2.6 Summary……80

Chapter 3

3 Fabrication and characterization of cortical screws……82
3.1 Introduction……...82
3.2 Development of cortical screws……90
3.3 Development of molds and fixtures for cortical screws…..90
3.4 Mechanical Testing of Cortical screws……92
3.4.1 Axial pull out strength……92
3.4.2 Torsional strength……..95
3.4.3 Flexural testing……..98
3.4.4 Double shear strength……102
3.5 Degradation studies……105
3.6 Dimensional deviation studies……108
3.7 Summary……..111

Chapter 4

4 Fabrication and characterization of cancellous screws……114
4.1 Introduction……114
4.2 Development of cancellous screws……123
4.3 Development of molds and fixtures for cancellous screws……123
4.4 Mechanical testing of cancellous screws…..125
4.4.1 Axial pull out strength……125
4.4.2 Torsional strength……129
4.4.3 Flexural testing……132
4.4.4 Double shear strength……136
4.5 Degradation studies……138
4.6 Dimensional deviation studies……142
4.7 Summary……..144

Chapter 5

5 Fabrication and characterization of bone plates……147

5.1 Introduction……147

5.2 Development of bone plate……..161

5.3 Mechanical Testing of bone plate……162

5.3.1 Flexural testing……163

5.3.2 Torsional strength……165

5.3.3 Uniaxial single plate tensile test……..168

5.3.4 Uniaxial double plate tensile strength……171

5.4 Degradation studies……175

5.5 Dimensional deviation studies……178

5.6 Summary……..179

Chapter 6

6 Fabrication and characterization of Steinmann Pins and Staples……182

6.1 Introduction and fabrication process……...182

6.2 Introduction to U-type bone staples and fabrication process…….....187

6.3 Development of Steinmann pins and U-type bone staples……..……191

6.4 Development of molds and fixtures for Steinmann pins and U–type bone staples……191

6.5 Mechanical testing of steinmann pins……194

6.5.1 Flexural strength……..194

6.5.2 Double shear test…..197

6.6 Mechanical Testing of U-type bone staples…….....200

6.6.1 Ultimate tensile test……201

6.6.2 Torsional test……...204

6.7 Degradation studies……207

6.8 Dimensional deviation studies……209

6.9 Summary……..211

Chapter 7

7 Conclusion and future scope…….....213

7.1. Conclusion…….....213

7.2. Implication of the findings……..214
7.3. Future scope…….....215
References…….....216
Research outcomes……..242
Product developed in the lab and ready to commercialize…….....247

LIST OF FIGURES

Figure 1.1: The global scenario of marketing in the case of orthopedic devices……1

Figure 1.2: The graphical profiles of the market size of various orthopedic problems……..2

Figure 1.3: Competitions involved in Indian orthopedic devices markets……2

Figure 1.4: Bone screws and its arrangement attached with bone……...3

Figure 1.5: Bone plates and their arrangement for bone…….....3

Figure 1.6: Bone staples, wires and pins arrangement for bone support……4

Figure 1.7: Intramedullary rods and nails for bone support…….....4

Figure 1.8: The widely used internal fixation devices…….....5

Figure 1.9: The major problems associated with metallic internal fixation devices…….....7

Figure 1.10: The desired properties should be with the materials targeted for IFDs……..8

Figure 1.11: The advantages associated with bioabsorbable polymeric IFDs……9

Figure 1.12: The challenges faced by bioabsorbable polymers and IFDs…….....10

Figure 1.13: Major complication observed in orthopedic implants……...……12

Figure 1.14: Pictorial presentation of the architectural structure of natural bone…….……14

Figure 1.15: Materials properties and its responses towards nearby tissues formation…….15

Figure 1.16: The cycle of PLA in nature…….……..24

Figure 1.17: Characteristic properties of PLA……..……24

Figure 1.18: Application of PLA in various areas…….....25

Figure 1.19: Summary of the proposed objectives for the research work……39

Figure 2.1: The cycle of PLA in nature…….....43

Figure 2.2: Stepwise process for the synthesis of nHAp powders…….....45

Figure 2.3: EDX analysis of nHAp particles…….….....46

Figure 2.4: EDX analysis of commercial PLA……..……46

Figure 2.5: EDX analysis of purified fibrous PLA……..…….47

Figure 2.6: Schematic of PLA/nHAp biocomposite production……..…….48

Figure 2.7: Schematic of extrusion cum injection molding process ……..……49

Figure 2.8: Properties of PLA and nHAp for suitable application….....49

Figure 2.9: (a) and (b) The Surface micrograph of nHAp powders, (c) The crossectional surface micrograph of neat PLA and (d) Crossectional surface micrograph of PLA/nHAp composite……...……..……51

Figure 2.10: Field emission transmission electron microscope image of nHAp (b) SAED pattern of nHAp…….....52

Figure 2.11: XRD diffractographs of the fabricated nHAp and PLA/nHAp composites……..54

Figure 2.12: TGA thermos gram of the fabricated PLA and PLA/nHAp composites……..56

Figure 2.13: DTG profile of PLA and PLA/nHAp composites…….56

Figure 2.14: DSC profile of PLA and PLA/nHAp composites….....59

Figure 2.15: FTIR spectroscopy profile of the nHAp and PLA/nHAp composites…….……60

Figure 2.16: Value of Elastic modulus of the PLA with varying concentration of nHAp…….62

Figure 2.17: Values of percentage elongation of the PLA with varying concentration of nHAp……..…….....63

Figure 2.18: Values of ultimate tensile strength of the PLA with varying concentration of nHAp……..……..……..…..63

Figure 2.19: Values of flexural strength of the PLA with varying concentration of nHAp…….....64

Figure 2.20: Values of the hardness of the PLA with varying concentration of nHAp…..…..66

Figure 2.21: Values of the density of the PLA with varying concentration of nHAp….……67

Figure 2.22: Contact angle measurement of (a) nHAp, (b) Neat PLA, (c) 3% nHAp, (d) 5% nHAp, (e) 7% nHAp, (f) 10% nHAp biocomposite strips…….....69

Figure 2.23: Contact angle value of nHAp, PLA and PLA/nHAp composites…….……70

Figure 2.24: Radial growth of spherulite of the PLA and PLA/nHAp biocomposite…….....71

Figure 2.25: Polarized optical micrograph of neat PLA, and PLA/nHAp composites at a particular time interval……..……...…....72

Figure 2.26: Profile of pH value concerning a number of immersion day in SBF……..……73

Figure 2.27: Formation of apatite layer on the surface of PLA/nHAp composites after five weeks……..……..74

Figure 2.28: The EDX profile of apatite layer formed on PLA/nHAp composite……..…….76

Figure 2.29: Profile of pH value concerning a number of immersion day in PBS solution….76

Figure 2.30: Mass loss profile of PLA and PLA/nHAp composite……..…….77

Figure 2.31: FESEM images of the surface of (a) before degradation (b), (c), (d) after the degradation of the PLA/nHAp composites……...……..…….78

Figure 2.32: Profile of water uptake of the PLA and PLA/nHAp composite concerning a number of days……...…..79

Figure 3.1: (a) Lab synthesized fibrous PLA and (b) Grinded PLA into powder form….……89

Figure 3.2: Schematic diagram of cortical screws (a) 3D line diagram of cortical screw (b) Photographic images of neat PLA (top) and PLA/nHAp (bottom) cortical Screws….89

Figure 3.3: Schematic diagrams for fabrication of cortical screw molds. (a) H13 material for mold (b) machining in lathe machine (c) surface grinding (d) Heat treated mold (e) mold in final shape (f) side view of screw mould……91

Figure 3.4: 3D model of cortical screw mold……..……..92

Figure 3.5: (a) Fixture for cortical screws (b) fixture setup (c) magnified the view of axial pull out test arrangement…..……...93

Figure 3.6: Surface micrograph from FESEM after axial pull-out test of cortical screws (a) neat PLA and (b) PLA/nHAp…..…….94

Figure 3.7: Axial pull out strength value of cortical screws with varying concentration of nHAp fillers .... ……...95

Figure 3.8: Axial pull out strength of neat PLA and 10% nHAp before and after *In vitro* hydrolytic degradation..……...…….95

Figure 3.9: (a) Torsion test set up (b) fixation of cortical screws (c) magnified the view of cortical screw arrangement for torsion test……..…….....96
Figure 3.10: Ultimate torque and angle at maximum torque of cortical screws with respect to nHAp filler. ……..……97
Figure 3.11: Ultimate torque value of neat PLA and 10% nHAp cortical screws before and after *In vitro* hydrolytic degradation……..……..97
Figure 3.12: Angle at maximum torque of neat PLA and 10% nHAp cortical screws before and after *In vitro* hydrolytic degradation…….…..……..98
Figure 3.13: (a) Flexural test set up (b) arrangement of cortical screw for 3 point bend test (c) fracture of cortical screw during test…….……..99
Figure 3.14: Flexural Strength value obtained through three point bend test of cortical screws concerning nHAp fillers……..…….……..99
Figure 3.15: Fractured surface micrographs of a) neat PLA b) 7% nHAp from FESEM after flexural strength. ……..……..……100
Figure 3.16: Flexural strength value of neat PLA and 7% nHAp cortical screw before and after hydrolytic degradation……..……..……..100
Figure 3.17: (a) Double shear strength set up (b) Arrangement of cortical screw into the fixture (c) Magnified view of cortical screws……..……..102
Figure 3.18: Double shear strength of cortical screws concerning variation……..……104
Figure 3.19: Values of double shear strength for neat PLA and 10% nHAp cortical screws before and after hydrolytic degradation……..……..……104
Figure 3.20: (a) cortical screws in the glass jar (b) storing of glass jar in air oven (c) after drying cortical screws……..…….....105
Figure 3.21: Profile of mass (wt. %) of neat PLA and 10% nHAp before and after hydrolytic degradation……...……..…….....106
Figure 3.22: (a) The surface profile of the degraded cortical screws. (b) The surface profile of the degraded screws after 90 days……...……..……107

Figure 3.23: Photographic images of fractured cortical screws after double shear strength and torsional strength test……..…….....108
Figure 3.24: Photographic images of fractured cortical screws after flexural test and axial pull-out test……..……..…….....108
Figure 3.25: Deviation in pitch of the fabricated cortical screws….....109
Figure 3.26: Photographic image of surface profile optical micrograph of cortical screws……..…….....110
Figure 3.27: (a) Profile of cortical screw head (b) Profile of thread of cortical screw (c) Measurement of pitch in the cortical screw (d) threaded portion of the cortical screws……..……..……110
Figure 4.1: Schematic diagram of cancellous screws (a) 3D and line diagram of cancellous screws (b) Photographic images of neat PLA (top) PLA/nHAp (bottom) cancellous screws……..…….123
Figure 4.2: Schematic diagrams for fabrication of cancellous screw molds (a) Machining of mold (b) Mold in prefinal shape (c) fabrication of copper electrode (d) Mold in final shape after machining……..……..……124
Figure 4.3: 3D solid model diagram (inset) and 3D line model diagram of fabricated cancellous screws mold…….……..……125
Figure 4.4: Fixtures for axial pull out the test (b) Arrangement of cancellous screw fixture in universal tensile test machine (c) Magnified pictorial images of fixture set up……..…..……126
Figure 4.5: Axial pull out strength value of cancellous screws with varying concentrations…….……...…….127
Figure 4.6: Axial pull out strength of Neat PLA and 10PLA after *In vitro* hydrolytic degradation……..…….....128
Figure 4.7: Surface micrograph from FESEM after axial pull-out test of cancellous screws (a) neat PLA and (b) PLA/nHAp…….……..…….....129

Figure 4.8: (a) Torsion machine set up (b) cancellous screw holding in the torsion set up the machine (c) After torsion testing……..……..130

Figure 4.9: Torsional strength value and corresponding twisting angle of cancellous screws with varying concentrations……..……...……131

Figure 4.10: Torsional strength of neat PLA and 10%nHAp after *In vitro* hydrolytic degradation…….…….....131

Figure 4.11: Twisting angle corresponding to the ultimate torque of Neat PLA and 10 % nHAp after *In vitro* hydrolytic degradation……...……132

Figure 4.12: Flexural test set up for the cancellous screw (b) Magnified view of the set up (c) side view of the arrangement of the cancellous screw for flexural strength measurement……...……...133

Figure 4.13: Flexural strength value of cancellous screws with varying concentrations…..133

Figure 4.14: Flexural strength of Neat PLA and 7% nHAp after *In vitro* hydrolytic degradation……...……..…….....135

Figure 4.15: Fractured surface micrograph of neat PLA and PLA/nHAp from FESEM…..135

Figure 4.16: (a) Double shear strength test set up for cancellous screw (b) fixture attachment in Universal tensile test machine (c) magnified pictorial view of the cancellous screw in the fixture……..…….....136

Figure 4.17: Double shear strength value of cancellous screws with varying concentrations……...……...…….137

Figure 4.18: Double shear strength of Neat PLA and 10% nHAp after *In vitro* hydrolytic degradation……...……..…….....138

Figure 4.19: (a) *In vitro* hydrolytic degradation of cancellous screw arrangement in a glass jar (b) Hot air oven maintained at 37° C (c) pH measurement of PBS solution for maintaining the pH routinely……..…….……139

Figure 4.20: (a) Surface micrograph from FESEM after three weeks *In vitro* hydrolytic degradation of PLA (b) Surface profile of the hydrolytically degraded PLA

surface through surface profilometer…..……..…….139
Figure 4.21: Mass loss profile of neat PLA and 10% nHAp before and after *In vitro* hydrolytic degradation……...……...……140
Figure 4.22: FESEM images of cancellous screw surface after 90 days *In vitro* hydrolytic degradation……..…….....140
Figure 4.23: Photographic images of fractured cancellous screws after torsion test and double shear strength test……...……...……141
Figure 4.24: Photographic images of fractured cancellous screws after the pull-out test and flexural test……..…….....142
Figure 4.25: Deviation in pitch of the fabricated cancellous screw……..…….143
Figure 4.26: Photographic image of surface profile optical micrograph of cortical screws……...……..…….....144
Figure 4.27: Stereomicroscopic images of cancellous screw thread (a) neat PLA cancellous screws (b) PLA/nHAp composites……...……..……..144
Figure 5.1: Bone plate assembly during implantation of a bone plate for fracture fixations……..…….....151
Figure 5.2: Tibia bone fracture fixations by bone plates….....152
Figure 5.3: Schematic of a compression plate for bone fracture fixations……..……154
Figure 5.4: (a) H13 metals in form of raw materials (b) machining to the lathe machines for giving shapes as per the injection molding machine mold cavity (c) Heat treatment of the H13 metal (d) Cylinderical turning of the heat treated mould (e) Bone plate electrode made of copper (f) Bone plate mold in final shape……...…….....160
Figure 5.5: Fabrication of wooden fixtures for bone plate mechanical testing…….……161
Figure 5.6: (a) 3D and line diagram of a bone plate (b) Photographic images of neat PLA (top) and PLA/nHAp (bottom) bone plate……..……161
Figure 5.7: 3D solid model diagram (inset) and 3D line model diagram of fabricated bone

plate mold……..……..…….162
Figure 5.8: Arrangement of 3 point bend test performed on bone plates……..……163
Figure 5.9: Flexural Strength value obtained through 3 point bend test of a bone plate concerning nHAp…….……...……164
Figure 5.10: Flexural strength of neat PLA and 3% nHAp after *In vitro* hydrolytic degradation……...……..…….....164
Figure 5.11: Arrangement of bone plates to the torsion machine for torsion testing (a) before fracture (b) in the machine (c) After fracture…….……..165
Figure 5.12: Surface micrograph of the fractured bone plates (a) neat PLA (b) PLA/nHAp after torsion testing……..…….....166
Figure 5.13: Values of ultimate torque concerning nHAp filler concentration……..……166
Figure 5.14: Values of the angle at which maximum torque was observed concerning nHAp filler concentration……..…….....167
Figure 5.15: Torsional strength of neat PLA and 5% nHAp after *In vitro* hydrolytic degradation…….....167
Figure 5.16: Values of corresponding twisting angle before and after *In vitro* hydrolytic degradation test……...……...…...168
Figure 5.17: (a) Arrangement of the bone plate to the wooden fixtures (b) Bone fixtures along with bone plate arrangement in the universal tensile testing machine (c) Fractured bone plate after the axial pull out testing……..……168
Figure 5.18: Values of uniaxial tensile strength concerning varying nHAp filler concentration……...……..……169
Figure 5.19: Surface micrograph of the fractured crossectional surface after uniaxial tension test (a) neat PLA (b) Magnified view of PLA (c) PLA/nHAp (d) Magnified surface micrograph of PLA/nHAp…….…….....……170
Figure 5.20: Values of uniaxial tensile strength of neat PLA and 3% nHAp before and after *In vitro* hydrolytic degradation…..171

Figure 5.21: (a) Arrangement of the bone plate to the wooden fixture for the pull out test. (b) Machine set up for fixture arrangement (c) magnified view of the attached bone plate in the universal tensile testing machine for the pull out test….....172

Figure 5.22: Fractured bone plates after uniaxial double plate pull out the test. (b) Attachment of fixture in the machine (c) Fractured bone plate during tension test……...…..…..172

Figure 5.23: Uniaxial tensile strength values of the double plate concerning varying nHAp filler concentration……..……..……..…….....173

Figure 5.24: Uniaxial tension values of Neat PLA and 7PLA after *In vitro* hydrolytic degradation……...……...……..173

Figure 5.25: Fractured bone plate profile after the mechanical test……174

Figure 5.26: Photographic images captured by stereomicroscope (a) neat PLA bone plate at fracture site. (b) neat PLA bone plate fractured near combination holes.....175

Figure 5.27: Glass jars used for *In vitro* hydrolytic degradation studies. (b) Magnified view of the bone plate kept in PBS medium (c) arrangement of PBS filled glass jar in hot air oven maintaining the temperature at 37.5°C…….175

Figure 5.28: Mass loss profile of neat PLA and 7% nHAp before and after *In vitro* hydrolytic degradation……..…….....176

Figure 5.29: Mechanism of *In vitro* hydrolytic degradation……...……177

Figure 5.30: (a) surface micrograph from FESEM of *In vitro* hydrolytic degraded bone plate sample (b) Magnified at 10 thousand zooms (c) magnified image at the 20kX (d) *In vitro* hydrolytic degradation of the bone plate surface exposed towards PBS for 28 days……..…..…....177

Figure 5.31: Photographic image of surface profile optical micrograph of bone plates..……178

Figure 6.1: (a) 3D and line diagram of pins (b) Photographic images of neat PLA (top) and PLA/nHAp (bottom) steinmann pins……..……...……186

Figure 6.2: (a) 3D line diagram of U-type bone staples (b) Photographic images of neat

PLA (bottom) and PLA/nHAp (top) U-type bone staples……189

Figure 6.3: (a) Application of bone staples at foot ankle joint as compression devices. (b) Applications of bone staples in foot heel joints. (c) Hammer toe joints. (d) Combinations of internal fixation devices applications in foot bone fracture joints. (e) Bone staple before insertion and (f) Bone staples after insertion.....190

Figure 6.4: (a) Fabrication of H13 metals in form of mold cavity (b) Machining after heat treatment of the molds (c) Bone staples electrode for electric discharge machining (d) Electric discharge machining process during mold fabrication (e) Fabricated mold of pins (f) Fabricated molds of bone staples……..…....192

Figure 6.5: 3D solid model diagram (inset) and 3D line model diagram of fabricated Steinmann pin mold…….....193

Figure 6.6: 3D solid model diagram (inset) and 3D line model diagram of fabricated U-type staples mold……..……..193

Figure 6.7: Arrangement of 3 point bend test performed on Steinmann pins (a) Universal tensile testing machine (b) Fabricated steinmann holding on the fabricated flexural molds (c) Magnified view of the three point bend test of the PLA pins……..…....194

Figure 6.8: Flexural Strength value obtained through three point bend test of Steinmann pins concerning nHAp filler……...195

Figure 6.9: Flexural strength value of Neat PLA and 7% nHAp after *In vitro* hydrolytic degradation…….…….....196

Figure 6.10: (a) universal tensile testing machine for double shear test measurement. (b) The arrangement of the steinmann pin in to the fabricated molds (c) Fabricated steinmann pins during the double shear test.……..197

Figure 6.11: Double shear strength of Steinmann pins concerning variation in the nHAp filler……..…….198

Figure 6.12: Double shear strength values of neat PLA and 10% nHAp after *In vitro*

hydrolytic degradation……...……..…….198
Figure 6.13: Photographic images of the fractured fabricated steinmann pins after flexural test and double shear strength…….....199
Figure 6.14: Stereomicroscopic surface images of the fabricated steinmann pins (a) neat PLA (b) Magnified view at fracture site of fabricated neat PLA (c) PLA/nHAp steinmann pins (d) magnified images at the fractured site of the PLA/nHAp steinmann pin……...…….....200
Figure 6.15: Arrangement of testing of bone staples for the tensile test……201
Figure 6.16: UTS value of PLA/nHAp U-type staples concerning nHAp fillers….……202
Figure 6.17: Peak load value of PLA/nHAp U-type staples concerning nHAp fillers ….. …202
Figure 6.18: Ultimate tensile strength value of PLA/nHAp U-type staples concerning nHAp fillers…….....203
Figure 6.19: Peak load value of PLA/nHAp U-type staples concerning nHAp (wt. %)……203
Figure 6.20: (a) Torsional test fixture for bone staples. (b) Torsion testing machine (c) Magnified photographic images of attached bone staples in the fabricated fixtures for torsion testing…….....204
Figure 6.21: Value of ultimate torque concerning nHAp filler concentration…….205
Figure 6.22: Value of breaking angle at which the maximum torque was observed concerning varying filler concentration……...……..……206
Figure 6.23: Torque value of neat PLA and 3 % nHAp after hydrolytic degradation studies……...…….....206
Figure 6.24: Angle at maximum torque of neat PLA and 3 % nHAp after degradation studies……...…….207
Figure 6.25: Photographic images of Fractured bone staples after torsion and ultimate tensile strength test……...…….....207
Figure 6.26: Loss of mass profile after *In vitro* hydrolytic degradation studies in case of neat PLA and 7 % nHAp in case of steinmann pins……..……..208

Figure 6.27: Loss of mass profile after *In vitro* hydrolytic degradation studies in case of neat PLA and 3% nHAp for U-type bone staples…….…….209

Figure 6.28: Optical profilometer of steinmann pins (a) whole steinmann pin on the bed (b) magnified view of one of the ends of Steinmann pins (c) Enlarged view of one of the ends of Steinmann pins (d) end view of the Steinmann pins…...…….210

Figure 6.29: Optical surface profile of fabricated bone staples (a) Staples kept on the profilometer base (b)Magnified view of the bridge length of the staples (c) leg of the staples (d) both leg of the staples(e) Bridge length of the staples……..……210

Figure 6.30: The stereomicroscopic images of U-type bone staples (a) neat PLA (b) Magnified view of neat PLA fabricated U-type bone staple (c) PLA/nHAp based U-type bone staples (d) Distance between two teeth of the fabricated U-type bone staple…..211

LIST OF TABLES

Table 1.1: Mechanical Properties of various materials for internal fixation devices……...13

Table 1.2: Materials used as bio implants and its principal applications. ……16

Table 1.3: Mechanical properties of some implant materials and tissues……..17

Table 1.4: The presence of elements in bone and HAp. ……..20

Table 1.5: Properties of Polymers and ceramics for orthopedic implants…….....22

Table 1.6: Properties of various polymers, bone and steel. ……22

Table 2.1: Parameters for extrusion of dumbbells and strips.……48

Table 2.2: Thermal behavior of PLA and PLA/nHAp biocomposites. ……55

Table 2.3: Molecular weight of PLA and PLA/nHAp biocomposites. ……..57

Table 2.4: Value of density and Spherulite growth rate for composites. ……..72

Table 3.1: Parameters for cortical screws production. ……..……88

Table 4.1: Parameters for cancellous screws production. ……122

Table 5.1: Extruder cum injection molding parameters for bone plate fabrication……..159

Table 6.1: Parameters for Steinmann pins production. ……186

Table 6.2: Parameters for U-type bone staples production……189

NOMENCLATURE

PLA	Poly(lactic acid)
nHAp	Hydroxyapatite
PP	Polypropylene
PE	Polyethylene
PBS	Polybutylene succinate
PLLA	Poly(L-lactic acid)
PDLA	Poly(D-lactic acid)
PGA	Poly glycolic acid
HAp	Hydroxyapatite
DSC	Differential scanning calorimetry
XRD	X-ray diffraction
FESEM	Field emission scanning electron microscopy
FETEM	Field emission transmission electron microscope
TEM	Transmission electron microscope
SAED	Selected area diffraction pattern
PGF	Phosphate glass fibre
POM	Polarizing optical microscopy
TGA	Thermogravimetric analysis
DTG	Derivative thermogravimetry
IFDs	Internal Fixation devices
ACL	Anterior Cruciate Ligament
UTM	Universal testing machine
CA	Contact angle
GPC	Gel permeation chromatography
Mw	Molecular weight
RH	Relative humidity
EDX	Energy dispersive X-ray spectroscopy

rpm	Revolutions per minute
NaOH	Sodium hydroxide
PMMA	Poly(methyl methacrylate)
Tg	Glass transition temperature
HCl	Hydrochloric acid
Tm	Melting temperature
Tc	Crystallization temperature
Wt.	weight
FTIR	Fortier transform infrared Spectroscopy
3D	Three dimensional
μ	micro
$\boldsymbol{\sigma}$	Flexural strength
MPa	Mega Pascal
GPa	Giga Pascal
$\boldsymbol{\tau}$	Shear strength
ρ	Specific gravity

Chapter 1

1 Introduction and Literature Review

1.1 Global and Indian scenario of orthopedic devices market

The global orthopedic device market is expected to reach $41.2 billion by 2019. The market is expected to grow at a compounded annual growth rate of 4.9% during the period. North America dominates the market for orthopaedic devices because of the prevalence of obesity and osteoarthritis and higher value per device. The Asia Pacific market will see significant growth due to increasing population density and expanding health care markets [1-3]. Imports account for over 85% of the orthopedic and prosthetic market. In 2014, USA accounted for over 50% of India's imports, followed by the European Union accounting for 26.6%, led by Ireland (16.3%), mainly due to the manufacturing activities of United States multinationals in the Europe. Switzerland supplied 9.1% of imports, including 20% of all imported artificial joints. The key foreign players in this segment are Stryker, Zimmer, Medtronic, ArthroCare, ConMed and Exatec. Major Indian players in this segment are Atlas Surgical, Narang Medical, Apothecaries Sundries Manufacturing Co. (ASCO) and Invicta Meditek Ltd. Artificial joints and fixation devices are the two major segments in the orthopaedic segment. Concerning these two, the Indian players are almost equal to foreign companies; however, foreign players provide a larger product portfolio [4-8]. Figure 1.1 shows the trends of the market of orthopedic fixations devices.

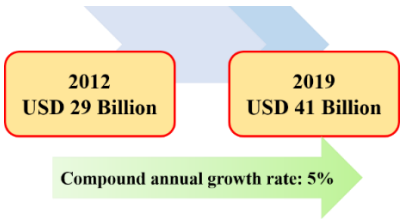

Figure 1.1: The global scenario of marketing in the case of orthopedic devices.

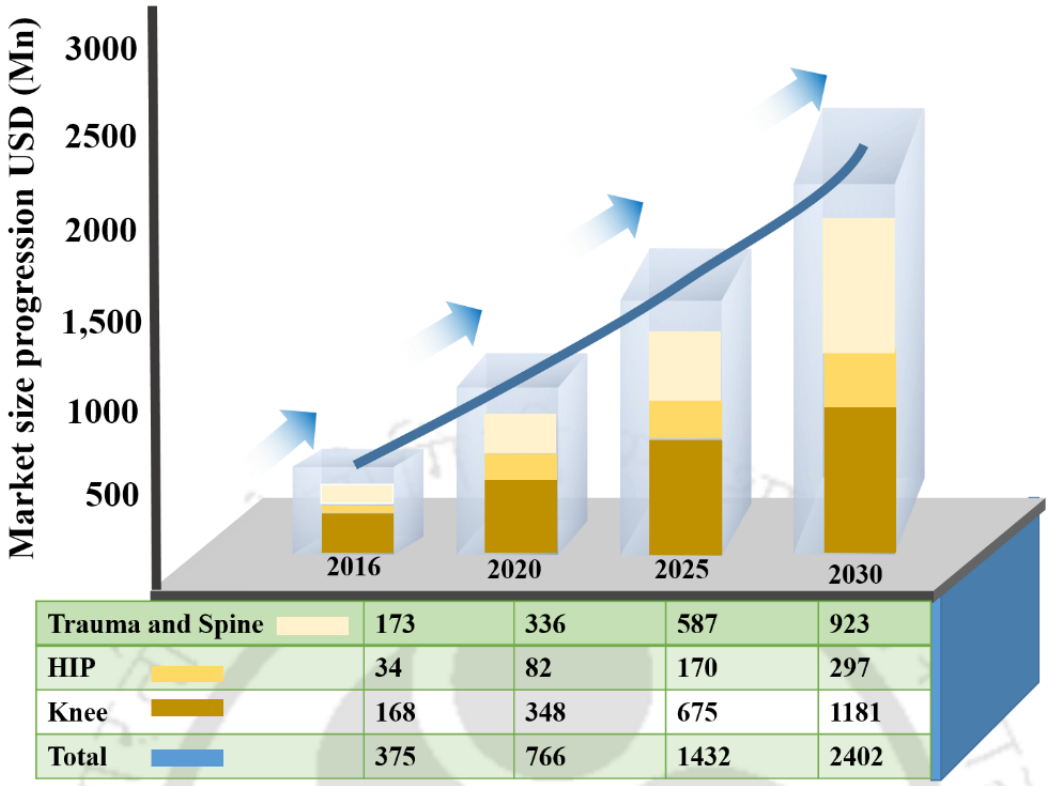

Trauma and Spine	173	336	587	923
HIP	34	82	170	297
Knee	168	348	675	1181
Total	375	766	1432	2402

Figure 1.2: The graphical profiles of the market size of various orthopedic problems.

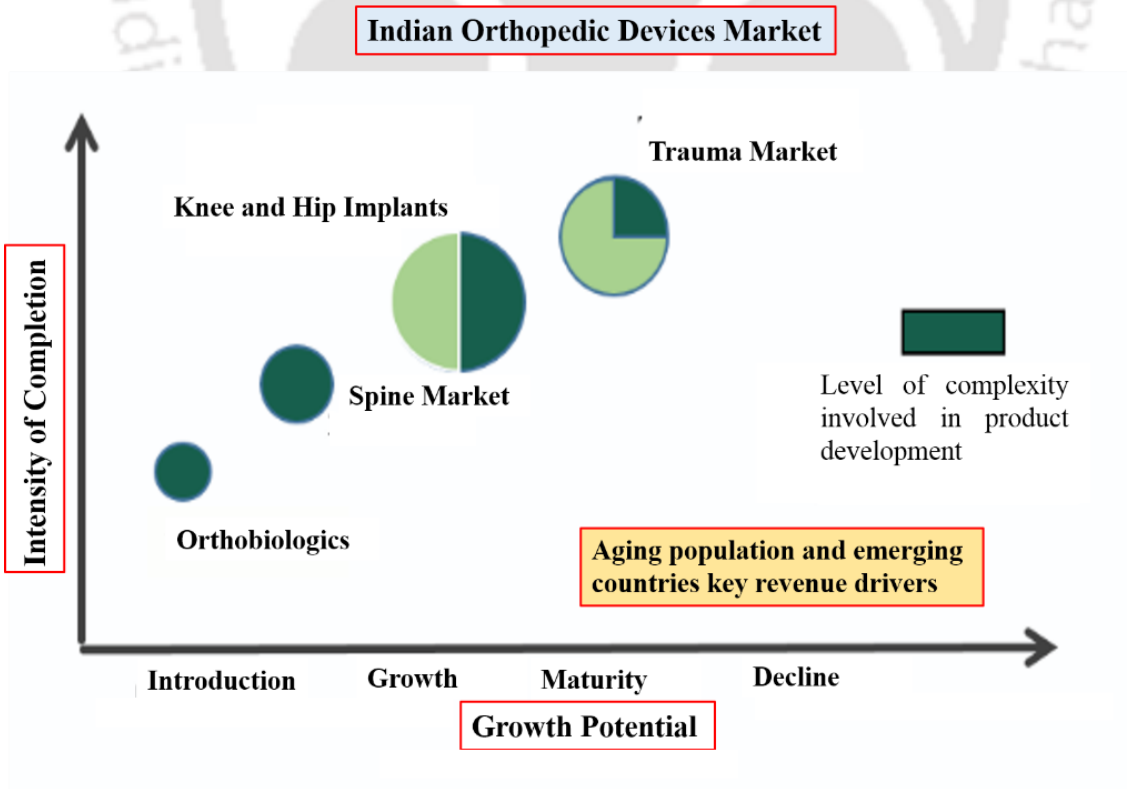

Figure 1.3: Competitions involved in Indian orthopedic devices markets.

The market for Indian orthopaedics is around Rs.2, 400 crores and it will grow at around 20% every year for the next decade to reach Rs.16, 000 crores by 2030 [9]. Additionally, the growing incidence of diabetes, obesity, osteoarthritis and osteoporosis are further expanding the clinical needs [10]. Figure 1.2 shows the size of the market of orthopedic fixations related to their problems. Figure 1.3 shows the intensity of completion concerning growth potential in the Indian orthopedic market.

1.2 Internal fixation devices and its requirement

Internal fixation devices (IFDs) are used to support the alignment of bone fragments during the healing process. These fixation devices are shown in Figure 1.4, Figure 1.5, Figure 1.6, and Figure 1.7 [11-13] are available in various ranges like for internal, external or intermediate bone fracture. The fixation device should have enough mechanical strength and also secure enough to allow early mobilization of the injured part.

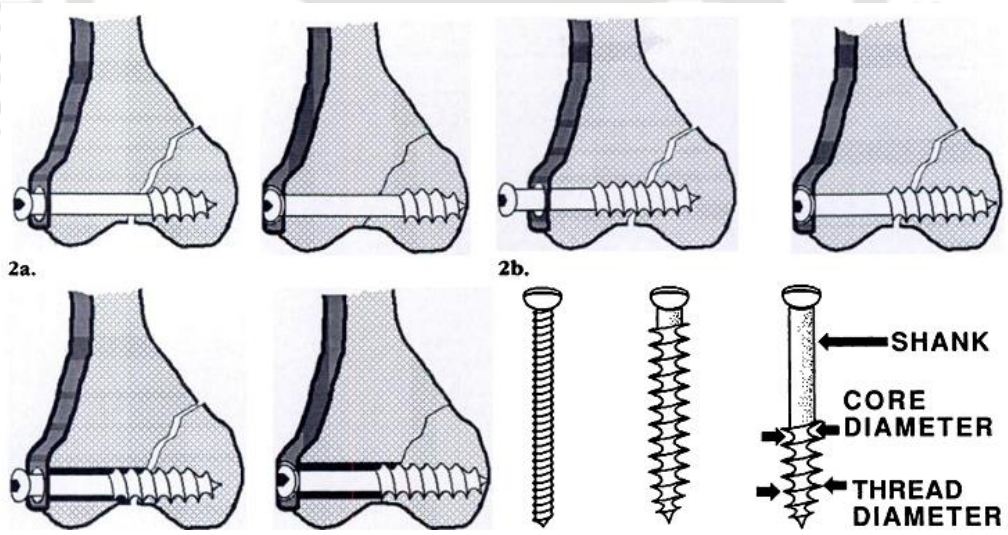

Figure 1.4: Bone screws and its arrangement attached with bone [11-13].

Figure 1.5: Bone plates and their arrangement for bone [11-13].

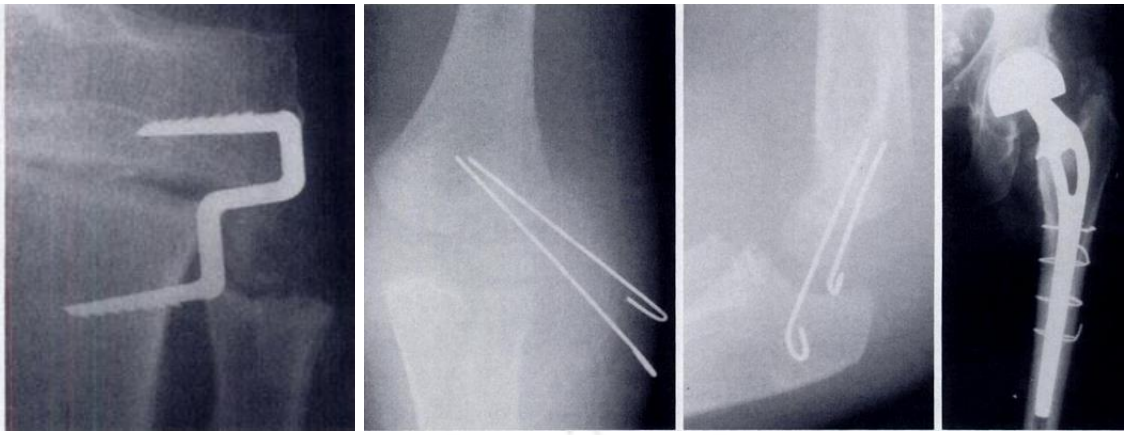

Figure 1.6: Bone staples, wires and pins arrangement for bone support (as adopted from various sources) [11-13].

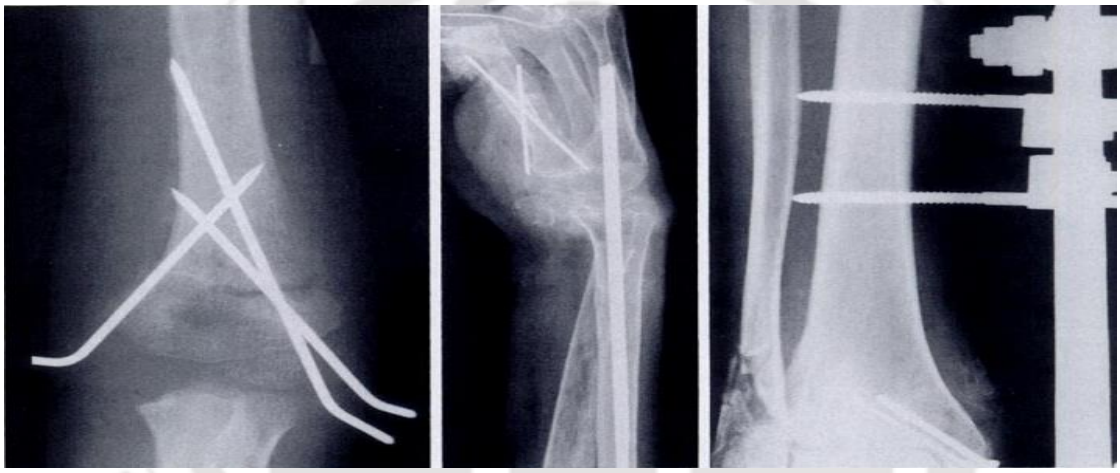

Figure 1.7: Intramedullary rods and nails for bone support (as adopted from various sources) [11-13].

1.3 Fixations of fractured bones

Generally, the fractured bone are fixed by using internal fixation devices. The bioabsorbable IFDs have several advantages over conventional, i.e. metallic fixation devices. It has discussed in the previous sections. Sometimes scaffolds are used for minor fracture occurred the soft bone, but when the fracture is severe and it need support to carry the loads transferred to the bone, thus internal fixation devices is the only option left for this fixations applications. The major five IFDs have been extensively used for the fixations. These are as shown in Figure 1.8.

1.3.1 Cortical screws

The cortical crew is a cylinder with spiral threads running on its outer surface. It converts torsional forces into compression. The primary functional objective in the design of a screw is to dissipate and distribute the mechanical load [14].

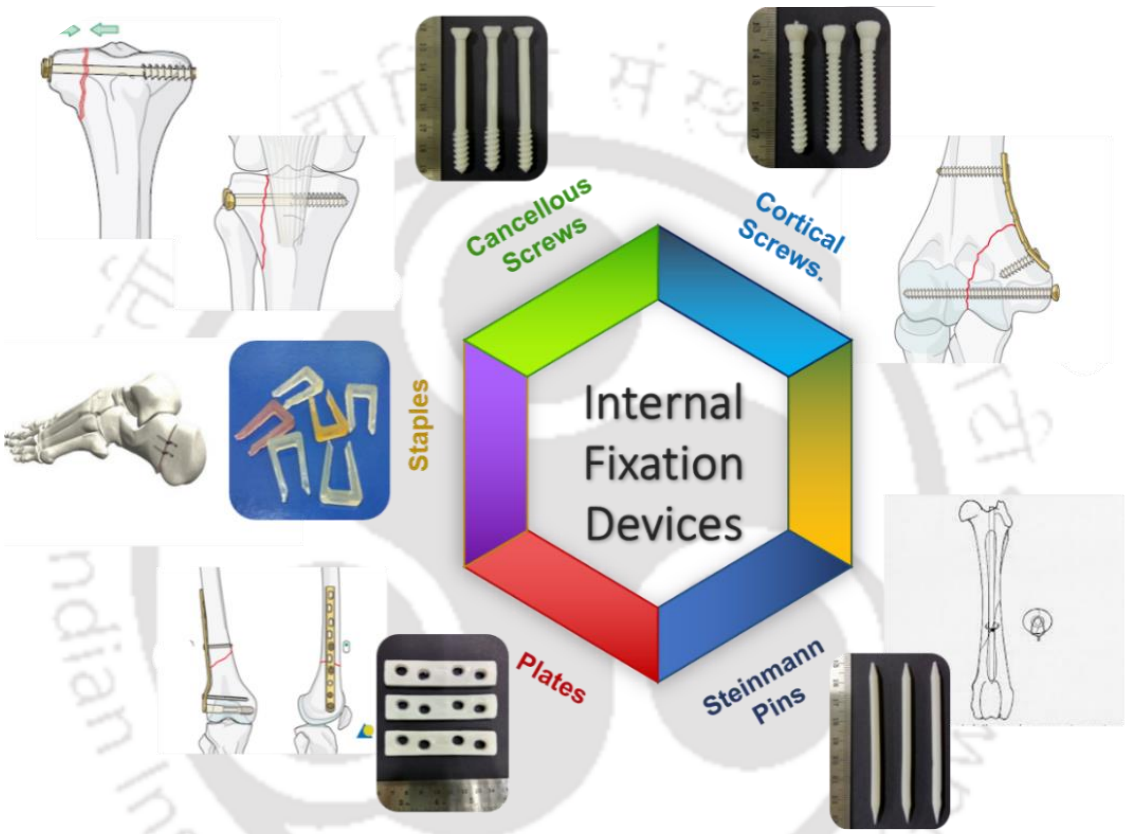

Figure 1.8: The widely used internal fixation devices.

1.3.2 Cancellous screws

The cancellous screws are used to join the fracture of long bones. These screws are designed for fixation of cancellous bone. They are most commonly used in the metaphysis of long bones where cancellous bone is abundant. They have more deeply cut and more widely spaced threads compared to cortical screw [15]. Since cancellous bone is much less dense than cortical bone, the screw threads cut their path in the bone when the screw

is inserted, i.e. cancellous screws are self-tapping. Partially threaded cancellous screws are often used as lag screws for metaphyseal fractures.

1.3.3 Bone plates

A bone plate is a thin implant used to immobilize bone segments. The plate is affixed with screws to properly align the bone and aid in the healing process. It is also called as orthopedic bone plates and is used to hold the broken bones together with screws. It comes in different types like dynamic compression plate (DCP) or least contact dynamic compression plate (LCDCP). Bone plates may be left in place after healing is complete, or they may be removed (in select cases) [16].

1.3.4 Steinmann Pins

Steinmann pins are often used to pin the bones back together. These are often used to hold together pieces of bone that are too small to be fixed with screws. In many cases, they are used in conjunction with other forms of internal fixation, but they can be used alone to treat fractures of small bones, such as those found in hand or foot [17]. Steinmann pins are generally made from implant-grade stainless steels. Steinmann pins are similar to K-wires (Kirschner wires) but typically have larger diameters. These pins typically have trocar, chisel, or spherical ends with partially threaded or smooth outside diameters [18].

1.3.5 U type bone staples

Bone staples have a shape of a hook with sharp conical or trapezoidal points. Their size and shape are given by the extent of the osteotomy. Some staples have thin ribs inside. Bone staples fixate adjusted bandy or valgus deformations in upper osteotomy of the tibia. Staples are constructed in a way so that they could compress the osteotomy slit during infixing. Staples keep the cutting surfaces together with required extend of bone tissue growing until complete healing. These staples can be recommended even for the treatment of bandy or valgus inflammation of knee joint [19].

The bone staples in the market are available in design various cross sectional shapes, leg lengths, bridge shapes, tip contours and the presence and absence of leg barbs [20].

1.4 Problems with metallic internal fixation devices

Traditional metallic fixation implants provide reliable and stable initial postoperative fixation allowing early mobilization, but they and their permanent support become redundant and are often even harmful after consolidation. The main disadvantage associated with metal implants (Figure 1.9) is the frequent need for non-intended secondary surgical removal of hardware (e.g. due to implant migration, discomfort, pain, or stress shielding phenomena). Furthermore, when rupture of the knee joints is treated with a metallic screw, the removal of hardware is usually done routinely in all cases 6-10 weeks postoperatively to enable normal movement of the ankle after healing of fractured bone sites [21].

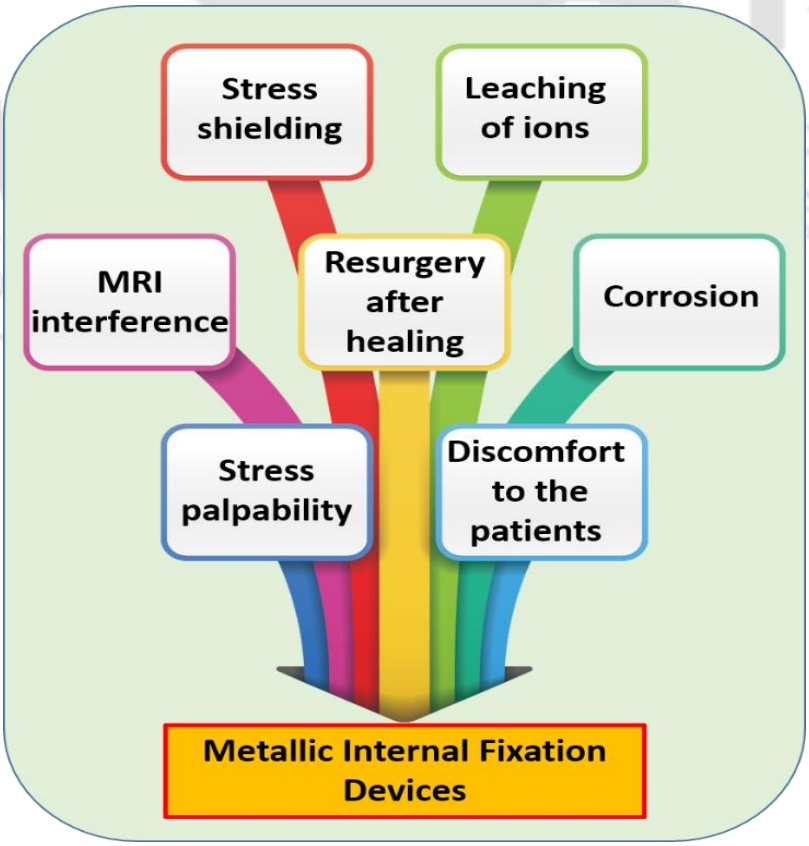

Figure 1.9: The major problems associated with metallic internal fixation devices.

The disadvantages associated with secondary surgery is required to remove these materials after the reunion of fractures bones. The temporary weakening of bone as a result of the removal of implants may lead to bone refracture. Very stiff metallic materials may cause osteoporosis beneath the implants because of stress shielding and may lead to bone fracture at the implant site. While relatively rare, corrosion of metallic implants is not a negligible concern. Metallic implant interferes with or distort post-operative radiography, CT and MRI images. During post-operative radiotherapy in patients who have had the tumor removed, the presence of metallic implants may alter the local dose distribution (i.e., over dosage proximal to the implant and under dosage distal to the implant) [22].

1.5 An alternative solution for the metallic internal fixation devices

The alternative solution could be the application of bioabsorbable polymeric IFDs, which properties lies almost in the range of our natural bone properties. The materials or structure of the proposed materials must fulfil certain medical and physical demands to be safe for clinical applications [23].

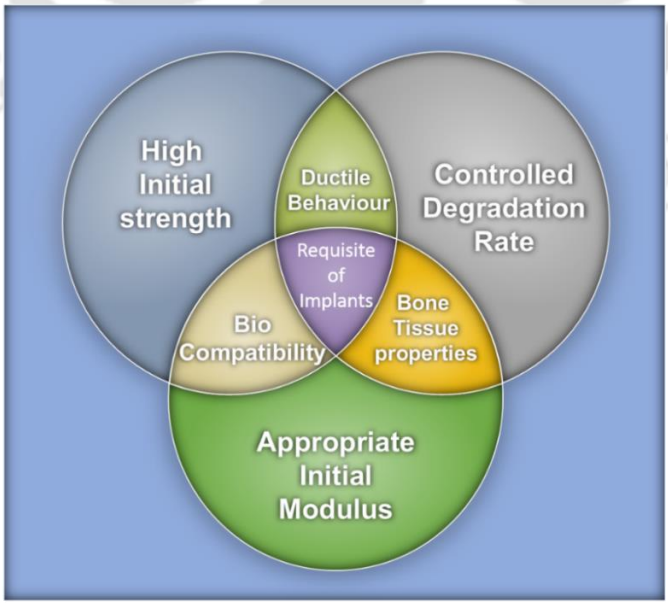

Figure 1.10: The desired properties should be with the materials targeted for IFDs.

The medical demands are mainly bound with the biocompatibility of the material and its degradation products. The physical properties, which is much essential for the safe absorbable implants is shown in Figure 1.10. The high strength is essential because the implant must resist mechanical stresses during a surgical procedure and it must carry external and physiological loads during the early stage of healing when the healing tissue is still weak. The appropriate modulus means that the material must not be too stiff or too flexible for the special purpose where it is used. The material should possess ductile behavior so that it does not fracture with a brittle mechanism [24]. The loss of strength and modulus *In vivo* must be in coordination with the increase of strength and modulus of healing tissues.

1.6 Bioabsorbable Polymeric Internal Fixation Devices

The bioabsorbable internal fixation devices are generally made of absorbable materials which can be considered as substitutes of metallic fixations. Since the metallic fixation has many limitations already mentioned in section 1.4.

Figure 1.11: The advantages associated with bioabsorbable polymeric IFDs.

The difficulties associated with the metals and advantages of polymeric materials make bioabsorbable polymeric IFDs ideal for bone fracture fixation. Bioabsorbable IFDs have been used successfully in certain orthopedic applications for more than two decades. The main advantage of bioabsorbable polymeric IFDs is to avoid of secondary removal of hardware, often required after treatment with conventional metallic devices [25]. The advantages associated with bioabsorbable polymeric IFDs is shown in Figure 1.11.

1.7 Challenges of bioabsorbable polymers and IFDs

Orthopedic fixation devices of synthetic biodegradable polymers have advantages over metal implants in that they transfer stress over time to the damaged area, allowing healing of the tissues, and eliminate the need for a subsequent operation for implant removal. The general criteria for selecting the polymer for use as bioabsorbable IFDs are its ability to combine mechanical properties with degradation time to the needs of the applications. The chosen materials should have sufficient strength remains until the fractured bone is healed. Although, the widely used synthetic polymers may have excellent properties, but the challenges associated are still there as mentioned in Figure 1.12.

Figure 1.12: The challenges faced by bioabsorbable polymers and IFDs.

Sometimes it happens that the materials have sufficient mechanical strength but the resorption time is very less which leads to early degradation of its structure. The approximate time for complete resorption of PGA is between 6-12 months, for PCL and PLLA is beyond 36 months, while for PDLLA is between 12-15 months so based upon the patient age, the healing periods also differs in this the selection of appropriate materials plays a vital role [26]. The mechanical strength for a particular location of fractured sites is different; thus customization is also one of the challenges. The compatibility issues and to avoid complications and failure of surgery, it is necessary for the complete degradation of polymers to match the bone healing time. This thus requires a creation of new materials that can degrade at a specific rate which satisfy the condition of healing and load carrying ability. However, bioabsorbable implants are usually not suitable for high-load bearing applications unless used in conjunction with traditional rigid fixation or appropriate additional external immobilization [26].

The Figure 1.13 shows the various complications related to orthopedic implants [27-30]. Generally, complication rises due to many reasons like patient conditions and material chosen for implants. In order to achieve sufficient fixation stability, biodegradable fixation implants are typically made thicker and wider than the corresponding metal implants. The various inorganic fillers are available such as Hydroxyapatite and additive active fillers like silver, zinc, copper etc. for antimicrobial properties [31-32], which could be used in various combination of loading in order to optimize the stability of the fixation devices in all aspects. Moreover the degradation behaviour is also not similar as of metallic implants as the properties of polymer based materials vary with temperature, conditions and surrounding environments but the combination of different polymers leads to giving useful results for fabrication of perfect internal fixation devices. Mostly used internal fixation devices are screws, plates, rods,

pins and staples. The current scenario of the market of these bioabsorbable implants are very much demanding, but the cost of these implants are not easily affordable. The companies which manufacture these biodegradable internal fixation devices are also limited and has their own market monopoly.

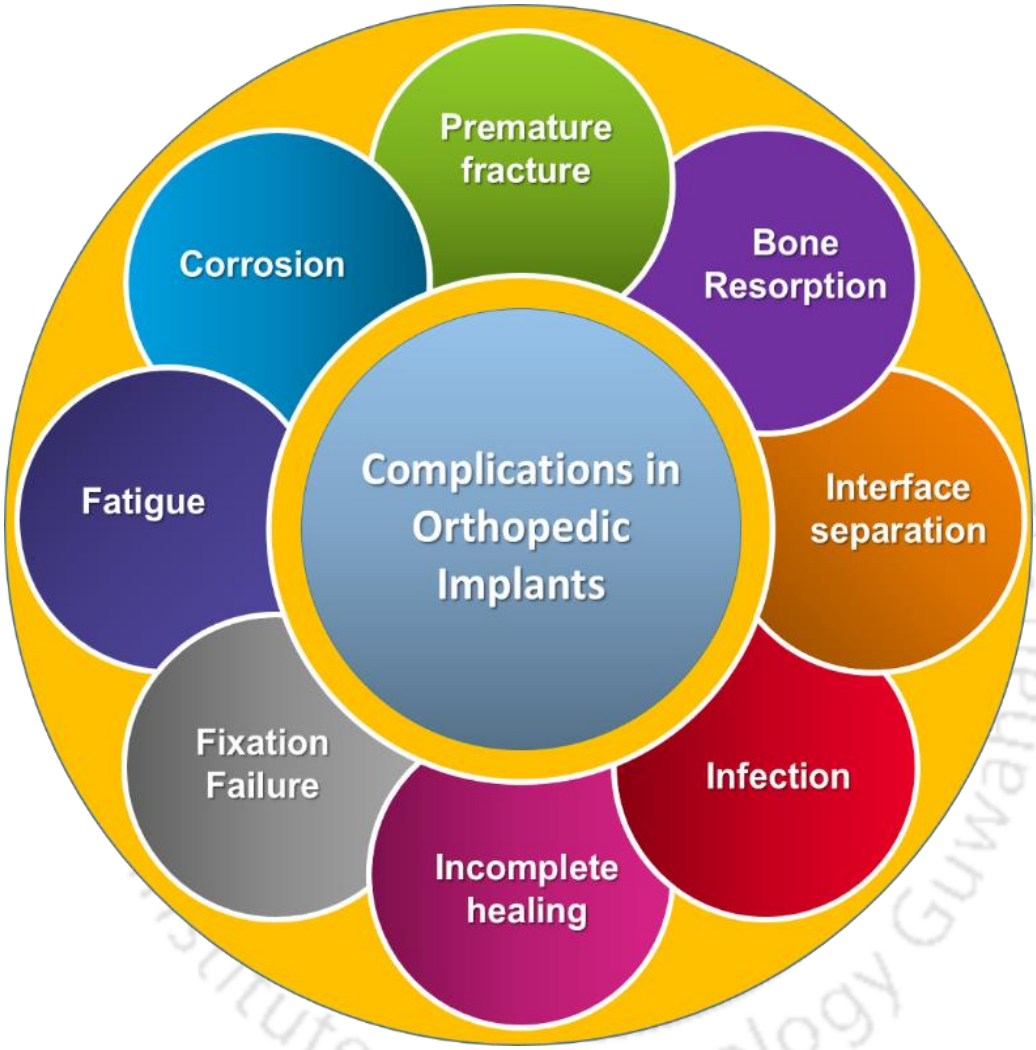

Figure 1.13: Major complication observed in orthopedic implants

Mechanical properties of implant devices made of biomaterials have a significant role in supporting the healing bone, such as gross motion at the repair site promoted by insufficient stiffness result in adequate healing or that complete elimination of micro motion results in stress shielding [33]. Table 1.1 summarizes about various mechanical properties of the biomaterials used as internal fixation devices [34-35].

Table 1.1: Mechanical Properties of various materials for internal fixation devices

S.no.	Materials	Elastic Modulus (GPa)	Tensile strength (MPa)	Elongation (%)
1.	Al_2O_3	350	1000 to 10,000	0
2.	SS316	210	600-1000	55
3.	Ti6Al4V	120	900	18
4.	Bone (cortical)	12 to 30	70-150	0-8
5.	Spongy Bone	1.3 to 8	50-100	--
6.	PGA	4 to 7	75-142	15-20
7.	PLLA	2.7 to 5.1	40-140	5-10
8.	PLDLA	1.9	42-51	3-10
9.	Ti	100	620	18

The current studies are expected to build up such internal fixation devices that not only quickens bone joining without harming the bone physiology but also completely resorbable in our body after doing its intended functions. The development of bio absorbable internal fixation devices is based on biocompatible, bioabsorbable polymers as matrix and functional nano powders as a reinforcing phase. Since natural human bone is a complex organic-inorganic composite, which consists of hybrid materials that combine the strength and stiffness of the inorganic compound such as *nano*-Hydroxyapatite (nHAp) and flexibility, toughness and resorbability of an organic phase such as pure bioabsorbable polymers like poly (lactic acid) (PLA). This will combine the osteoconductivity and biodegradability of polymers/ceramic composite which further expected to mimic the natural bone to some extent.

1.8 Bone and its remodeling

Bone is natural composite materials and the main supporting systems in the human body. It is a unique combination of mineral and tissue that provides excellent tensile and loading

strength. The inorganic mineral phase that is responsible for its stiffness [36]. Cells and tissue constitute the organic phase, responsible for maintenance, tensile strength and elasticity. Its properties depend on the composition of the matrix which has two components: a mineral part, made of Hydroxyapatite and an organic part, composed of glycol proteins, proteoglycans, sialo proteins and gla proteins. Mineral part contributes 65-70% of the matrix whereas the organic part consists of remaining 30-35% of the matrix [37]. In an adult skeleton, bone tissue is organized in two structural forms: spongy or cancellous bone, which consist of 20% of the total skeleton and cortical bone consist of 80% of total skeleton [38]. Cancellous part of bone shows a porosity of 50-90% whereas cortical bone has the porosity of only 10%. The modulus and strength of cancellous bone are 20 times lower than cortical bone. Cancellous bone is arranged with a honeycomb structure of branching bars, plates and rods of various sizes. Cortical bone has three types: long bone, short bones and flat bones.

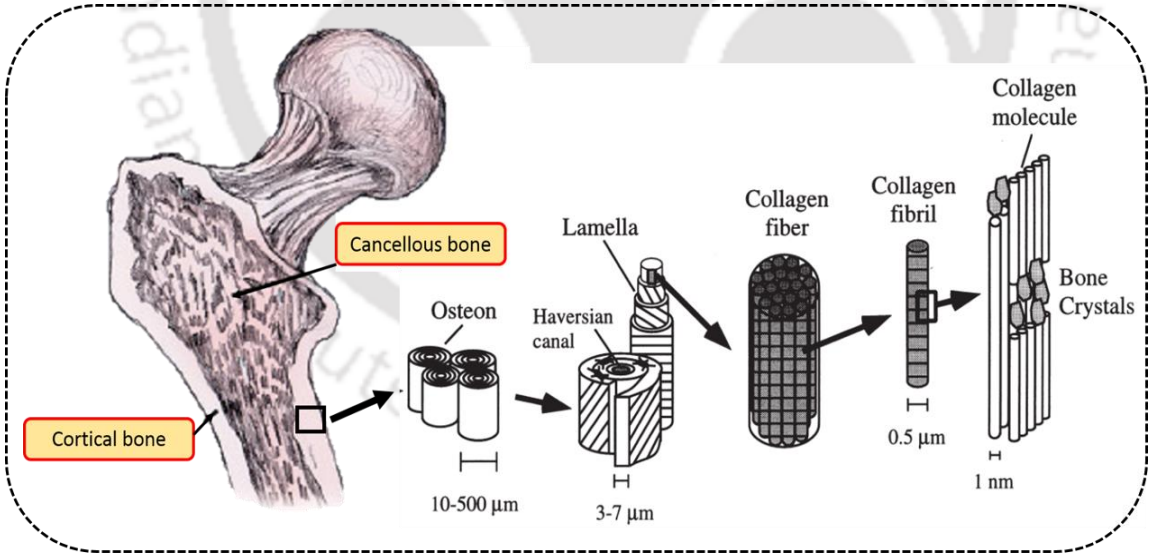

Figure 1.14: Pictorial presentation of the architectural structure of natural bone.

There are three types of cells, which are generally active during the bone remodeling process, they are osteoblast, osteocytes and osteoclasts responsible for elaboration,

maintenance and resorption of bone tissue from their interactions respectively [39-40]. Figure 1.14 shows the pictorial images of the architectural structure of natural bone.

The normal bone regenerates continuously at a relatively slow rate. In the injured bone, the remodeling and regenerative process are highly activated. One important precondition for bone healing is immobilization. Depending on the local conditions, different bone repair mechanism can occur. Generally, these are secondary and primary bone healing, secondary bone healing takes place if relatively wide fracture gaps exist and a certain amount of mobility ions present [41]. The bone heals through callus formation; that is fibrous tissue and cartilage form first, followed by bone [42].

1.9 Bone fixation device materials

The use of biomaterials for internal fixation devices is one of the important factors to be considered for its performance. A variety of metals, polymers, and ceramics are used for such applications. One of the most prominent application areas for biomaterials is for orthopedic implant devices, and it is depend on the material properties and the nearby tissues responses as shown in Figure 1.15.

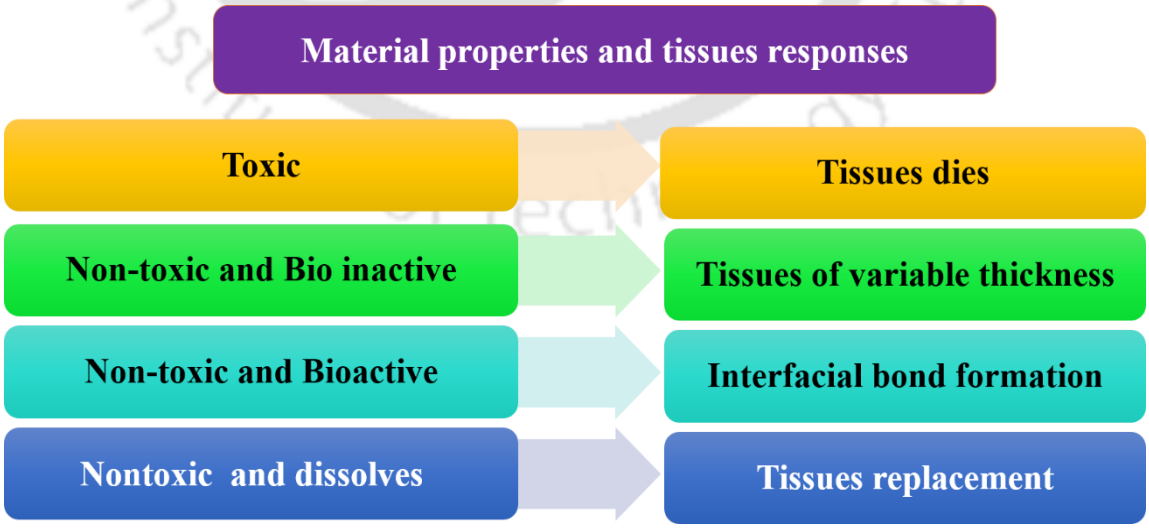

Figure 1.15: Materials properties and its responses towards nearby tissues formation.

Initially, stainless steel (SS316 L) was used to produce the fixation devices. It was widely used because of cheaper and easily converted into various shapes, but the durability was the main issues [43]. After that cobalt chromium alloy was in fashion due to its less susceptible to corrosion, fatigue and wear but it was also observed heavy. After that titanium alloys came, and it was observed lighter than another. It was also observed very good compatibility concerning others available metallic internal fixations thus is the most widely used in the last two decades [44]. Generally, the use of metallic materials used for fixation provides the stable fixation to the fractured bones but the unable to transmit the load during the process of fracture bone healing process. It was also observed that some inflammation reactions near the surrounding tissues caused by corrosion and leaching of ions take place, which leads to the removal of the implants through surgery. The list of materials used for internal fixation or bio implants for orthopedics is listed in Table 1.2 [45].

Table 1.2: Materials used as bio implants and its principal applications.

Materials	***Principal applications***
316L stainless steel	Fracture fixation, stents, surgical instruments
CP-Ti, Ti-Al-V, Ti-13Nb-13Zr, Ti-Mo-Zr-Fe	Bone and joint replacement, fracture fixation, dental implants, pacemaker encapsulation
Co-Cr-Mo, Cr-Ni-Cr-Mo	Bone and joint replacement, dental implants, dental restorations, heart valves
Ni-Ti	Bone plates, stents, orthodontic wires, dental
Alumina	Joint replacement, dental implants
Calcium phosphates	Joint replacement
Zirconia	Bone repair and augmentation, surface coatings on metals
PLA	Bone screw, pins, staples, plates, scaffolds
PGA	Bone screw, pins, staples, scaffolds, sutures.
PLA/PGA	Bone screw, pins, staples, scaffolds
PCL	Bone screw, pins, staples, scaffolds

1.9.1 Mechanical properties of some implant materials and tissues

Mechanical properties of internal fixation devices provides a role in support of healing bone, such as gross motion at the repair site promoted by insufficient stiffness result in adequate healing or that complete elimination of micro motion results in stress shielding. The elastic modulus measured the strain in response to a given tensile or compressive stress along the force, flexural modulus measured the relationship between the bending stress and resulting strain in response to a given tensile or compressive stress perpendicular under load, Tensile strength deals with the maximum stress that the material can withstand before it breaks and maximum strain checks the ductility of a material or total strain exhibited prior to fracture [46]. Table 1.3 explains about the mechanical properties of some implant material and tissues [47-48].

Table 1.3: Mechanical properties of some implant materials and tissues

S.no.	Materials	Elastic Modulus (GPa)	Tensile strength (MPa)	Percentage Elongation
1.	SS316	210	600-1000	55
2.	Ti6Al4V	120	900	18
3.	Co-Cr alloy	210	1085	
4.	Cortical bone	12 to 30	70-150 (Compressive strength=131-224)	0-8
5.	Cancellous bone	1.3 to 8	Compressive strength=5-10	
6.	PGA	4 to 7	75-142	15-20
7.	PLLA	2.7 to 5.1	40-140	5-10
8.	PLDLA	1.9	42-51	3-10
9.	Ti	100	620	18
10.	Bioglass	35	42	
11.	Zirconia	220	820	
12.	HAp	95	50	

In the case of ceramics application for the orthopedic fracture fixations, it consists of low toughness and limitation for application high load bearing applications. Although this

material has good compatibility, corrosion resistance and is good for filling of bony defects, but the brittleness, low fracture strength, difficult to fabricate, low mechanical reliability and high density is the main problems.

1.10 Statistics of bone related diseases

According to International osteoporosis foundation (IOF), statistics for Asia is about more than 50% hip fractures will occur in Asia by 2050 [49]. It is also said that this date will also increase if the living life style is not improved as per standards. All Asian countries fall very low in calcium intake daily basis per individuals. The recommended diet for calcium by world health organization is about in the range of 1000-1300mg/day, but the real fact is only 450 mg/day, which may also be the main reason behind this. Worldwide, osteoporosis causes more than 8.9 million fractures annually, resulting in an osteoporotic fracture every 3 seconds. Osteoporosis is estimated to affect 200 million women worldwide - approximately one-tenth of women aged 60, one-fifth of women aged 70, two-fifths of women aged 80 and two-thirds of women aged 90. In India, the number of osteoporosis patients was at approximately 26 million (in the year 2003) with the numbers projected to increase to 36 million by 2013. The major cause of bone related problems was due to inadequate nutrition intake and poor life style [50].

1.11 Bone fracture healing

The major problems associated with the fractures healing is the selection of proper implants at the right time through the right procedure. Orthopedic surgeon also plays a vital role while fixing the fractured bone. If the bone fracture is more severe than various scaffold is introduced in between the fractures sites to support the bone shape, there after metallic internal fixation devices were implanted in order to the proper adjustment of the fractured bone to get in to shapes [51]. The healing time for fractured bones also dependent on the fracture part and nearby site conditions. Generally, bone fracture healing

takes places in major four steps. Initially where bone was fractured the inflammation occurs, which led to swelling of the fractured sites and if it is for a long time then there may be chances of more severe inflammation which led to the development of yellow push coming through the outer skin [52-53]. After inflammation curing, the soft callus formation starts which completes like completely woven bones. This process continues till 6-12 weeks. Hard Callus formation is a complex process that is guided by the release of mineral compounds such as Calcium and Phosphate into the Cartilage tissue, which subsequently transforms into a bridge of Hard Callus over the fracture site. Once the Hard Callus has formed at the former fracture site, then fracture Union is said to have occurred. Fracture Union can be seen on X-ray at around six weeks in upper limb fractures and twelve weeks in lower limb fractures. One of the factors that encourage hard Callus formation in lower limb fractures is gentle weight bearing exercise which stimulate hard callus formation because bone responds to repeated gentle loading by laying down more bone tissue [54].

1.12 Statistics of fish scales bio wastes

Each year, 18-30 million tons of fish waste is being discarded throughout the world. By weight, about 50% of the total waste generated by the fish processing industry is waste, and about 4% of the waste is fish scale [55]. Generally, the fish scale is considered worthless, impracticable, and dismissed as a waste. However, it is known that fish scale contains numerous valuable organic and inorganic components, mainly collagen and hydroxyapatite, which have commercial value for use in manufacturing functional foods, cosmetics, and biomedical products [56].

1.13 Bone and Hydroxyapatite

Bone is a structure composed of Hydroxyapatite ($Ca_{10}(PO_4)_6(OH)_2$) (HAp) crystals deposited within organic matrix collagen. The nano sized biomaterial and compatibility

with the inorganic bone crystal of the human body is extensively considered for orthopedic fracture fixation devices. The nano size Hydroxyapatite powder (nHAp) is an excellent bioactive site because of high surface to volume ratio, and reactivity than the same micron size HAp material. Thus, nHAp particles have aroused intensive interest, and the same time high effort concentrate since the last decade to synthesis and understand their structure and properties. However, it is always difficult to synthesize nHAp with well-defined size, morphology and crystallinity concerning desire biological applications. The nHAp promotes bone in growth, biocompatible and regenerate neo bone tissues. It has a Ca/P ratio (1.50-1.67) within the range known to promote bone regeneration [57-58].

Table 1.4: The presence of elements in bone and HAp.

Elements	Bone	HAp
Ca (wt. %)	36.6	39.6
P (wt.%)	17.1	18.5
CO_2 (wt.%)	4.8	--
Na (wt.%)	1.0	--
K (wt.%)	0.07	--
Mg (wt.%)	0.6	--
Sr (wt.%)	0.05	--
F (wt.%)	0.1	--
Zn (ppm)	39	--
Ca/P ratio	1.65	1.67

It has been widely employed for hard tissue repair in orthopedic surgery and dentistry. Hydroxyapatite was first identified as being the mineral component of bone in 1926 **[59]**. It consists of calcium (wt. %) and phosphate (wt. %) as similar as in natural bone (shown in Table 1.4). It is one of a limited number of materials that form strong chemical bonds

with bone *In vivo* while remaining stable under the harsh conditions encountered by the human body.

1.14 Bioabsorbable Polymers

Bioabsorbable polymers are those polymers, which dissolve (or disperse) in bio fluids and are eliminated from the body without chain scission [60]. The degradation product resorbs in the body, i.e. can be metabolized and enter the general metabolic pathways. These include poly (alpha hydroxyl acid) such as poly glycolide (PGA), poly (lactic acid) (PLA) and their copolymers. The PGA is partially crystalline, with high melting points (220-230°C) and a glass transition temperature of 34-40. It has a tensile strength in the order of 57 MPa and tensile modulus ranging from 6-7 GPa [60]. The strength of the PGA is increased when spinning into a fiber form, because of the preferred high molecular orientation of the polymer [61]. Poly (lactic acid), on the other hand, is a polymer with initial molecular weights of 180, 000 to 530,000 and a melting point of about 174°C [62]. In orthopedic implants, poly-L-lactic acid (PLLA) has been used more extensively because it retains its initial strength longer than poly-D-lactic acid (PDLA). PGA belongs to the category of fast degrading polymers, and intra-osseous implanted PGA screws have been shown to completely disappear within six months [63]. PLLA, on the other hand, has a very long degradation time and has been shown to persist in tissues for as long as five years post implantation [64]. Poly caprolactane (PCL) was first synthesized in the 1930s by ring opening polymerization of ε-caprolactane. PCL is partially crystalline, with a melting point of 59-64° C and a glass transition temperature of -60°C. It has a tensile strength of 16 MPa and tensile modulus of 0.4 GPa. PCL is highly hydrophobic and thus has longer degradation time than PLA (2-5 years) [65], which makes it suitable for applications where long degradation times are required.

Due to low melting temperature, PCL is easily processed by conventional melting techniques and can be filled with stiffer materials (particles of fibers) for better mechanical properties. Table 1.5 and Table 1.6 shows the properties of various bioabsorbable polymers and other suitable materials for applications as orthopedic fixations along with their properties [66-70].

Table 1.5: Properties of polymers and ceramics mostly used for orthopedic implants.

Materials		Molecular weight (Da)	Density (gcm^{-3})	Melting point (K)	Tensile strength (MPa)	Young modulus (GPa)	Degradation time (months)
Polymers	LPLA	108,600	1.25-1.3	456.4-466.7	50-60	3-5	>24
	DPLA	107,300	1.24	443.3-452.5	50-60	3-5	>24
	PDL	88,400	1.25	Amorphous	28-41	1.38-2.75	12-16
	75/25 PDL/PG	104,500	1.30	Amorphous	41-55	1.38-2.75	4-5
	50/50 PDL/PG	49,900	1.34	Amorphous	41-55	1.38-2.75	1-2
	PCL	80,000	1.145	333	15-30	0.15-0.3	6-12
Ceramics	HAp	--	3.2		100-900	35-120	--

Table 1.6: Properties of various polymers, bone and steel.

Polymers	Melting temperature (ºC)	Glass transition temperature (ºC)	Modulus (GPa)	Elongation (%)	Degradation time (months)
DLPLA	Amorphous	55-60	1.9	3-10	12 to 16
PGA	220-230	35-45	6-7		6-12
PLA	150-162	45-60	0.35-3.5		6-24
PLLA	170-200	55-65	2.7-4.14	5-10	>24
P-DL-LA	Amorphous	50-60	1-3.45		12-16
PCL	59-64	-60-(-65)	0.2-0.4	300-500	>24

PDO	N/A	-10-0	1.5	N/A	6 to 12
PGA-TMC	N/A	N/A	2.4	N/A	6 to 12
85/15 DLPLG	Amorphous	50-55	2.0	3-10	5 to 6
75/25 DLPLG	Amorphous	50-55	2.0	3-10	4 to 5
65/35 DLPLG	Amorphous	45-50	2.0	3-10	3 to 4
50/50 DLPLG	Amorphous	45-50	2.0	3-10	1 to 2
PLGA (50/50)	Amorphous	50-55	1.4-2.8	--	3-6
PHB	168-182	5-15	3.5-4	5-8	
PPF	30-50	-60	--	--	>24
Bone	----	--	10-20	--	--
Steel	----	--	210	--	--

1.15 Poly lactic acid

PLA, an aliphatic polyester, has outstanding advantages over other polymers. As early as the 1970's, PLA products were approved by the US Food and Drug Administration (FDA) for direct contact with biological fluids [71]. PLA is derived from renewable and degradable resources such as plant sources (corn and potato), which is shown in Figure 1.16. PLA degrades inside into our body in form of H_2O and CO_2, which is not toxic to the human body, hence making it an excellent material for biomedical applications [72]. Figure 1.17 shows the characteristic properties of PLA which have wide application in many areas as mentioned in Figure 1.18.

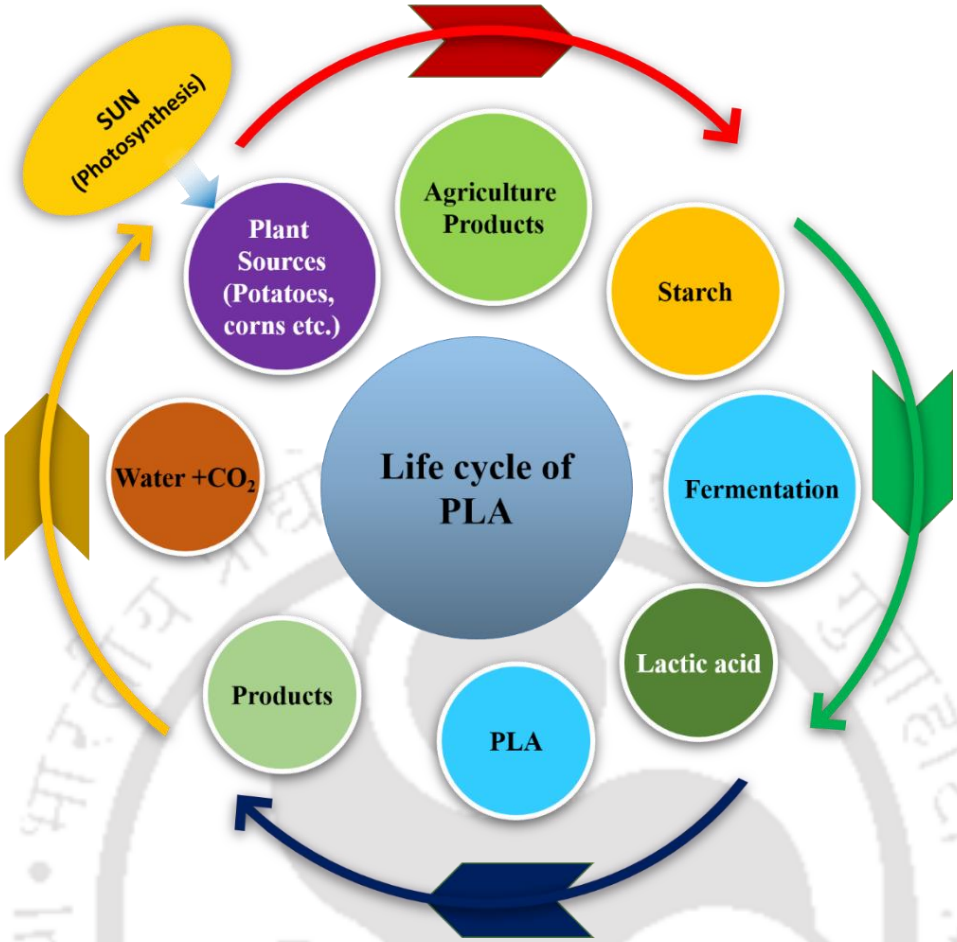

Figure 1.16: The cycle of PLA in nature

Figure 1.17: Characteristic properties of PLA

Figure 1.18: Application of PLA in various areas.

1.16 Literature Review

1.16.1 Literature review of internal fixation devices

Initially, internal fixation devices were made of metals such as titanium, molybdenum, cobalt and chromium based alloys. It was observed that these metallic fixation devices are having limitation like stress shielding, stress palpability, leaching of metallic ions and most difficult resurgery after healing of fractured bone [73]. Thus degradable metals come into an application like magnesium alloys, but it was observed that after long durations the similar problems arise. Now a day's bioabsorbable polymers come into the application, but it was seen that the mechanical strength and tuning of degradation is the

main challenges. Researchers have utilized these bioabsorbable polymers along with ceramics nano filler so that the desired properties could be achieved. This section deals with various literature available, where materials have been targeted for orthopedic fixations.

Moser et al. [74] evaluated in vitro strength retention and polymer characteristics of plates and screw made of 70:30 poly (l-lactide-co-D, l-lactide) over a 2 year period time. The plates was made by compression molding and screw was made by injection molding. Mechanical testing was performed before and after degradation. It was observed that strength of the plates was retained 84% after 13 weeks and in case of screw, the shear strength maintained 73% after 39 weeks. Thus it was finally demonstrated excellent retention of devices fabricated from 70:30 poly (L-lactide-co-D, L-lactide) over time periods**.** Wen et al. [75] reported processing of porous Ti and Mg for manufacturing metallic foam for biomedical applications. The foam has open-cellular structure and their pore size distribution in the range of 200-500µm. The compressive strength was 35 MPa and young modulus was 5.3 GPa for Ti foams. While for Mg foams, the compressive strength was 2.33 MPa and young's modulus was 0.35 GPa. It was also observed strong enough to resist handling during implantation and finally proposed for applications as biocompatible implant materials**.** G. Huang et al. [76] discussed PLA nano composites and PDL grafted nHAp with improved interfacial adhesion for bone repair and regeneration via stereo complexation. By doing so the enhanced tensile strength and other mechanical properties were obtained and finally concluded as promoting a way to obtain material composites for load bearing bone repairing applications.

Macha et al. [77] investigated PLA /HAp composite for biomedical applications as drug delivery of key mineral to support bone repair and regeneration. The composite was in the form of films so that it can be used as desired shape and size. Prati et al. [78]

determined fatigue behavior of absorbable sutures while immersed into controlled environment and time to fracture. The fatigue was measured as a function of applied load. A change in failure mechanism was observed, at high applied loads, the failures appeared brittle and was controlled primarily by the applied stress. While at lower loads, the failures were more ductile and were controlled more by the test environment**.**

Ozan et al. [79] reported Ti-Ta-Zr-Nb (TTZN) alloys with ultra-high strength for orthopedic implants applications. The alloying of TTZN have been done via electron alloy design method. The microstructure, mechanical properties, and cyto- compatibility of TTZN alloys were compared. The modulus of resilience was in the range of 6.21 to 9.37 Mj/m3 considering to enable the design of implants with high flexibility, which would be beneficial about reduced stress shielding phenomenon. Excellent compatibility with a cell adhesion was finally observed and thus proposed as a candidate material for applications in orthopedic implants**.**

Jaiswal et al. [80] reported mechanical, corrosion and biocompatibility behavior of Mg-3Zn-HA biodegradable composite for orthopedic fixture accessories. The elastic modulus was in the range of cortical bone and the Magnesium ions after leaching does not harm the cell tissues. The HAp was prepared by wet precipitation techniques. The addition of HAp in to the Mg-Zn matrix was effective to obtain the adjustable mechanical properties and appropriate corrosion resistance.

Chen et al. [81] discussed mechanical properties and biocompatibility of the porous titanium scaffolds for bone tissue engineering to regenerate bone and bone repair. The scaffolds were produced through powder metallurgy approach. The space holder material was used with magnesium powders. Up to 50% porosity was obtained. The interconnectivity of the scaffolds helps to grow the tissues nearby. Kulkova et al. [82] reported novel methods to prepare bioactive surfaces for these composites. Surface

etching was by an excimer laser to expose bioactive glass granules embedded in the resin. They analyzed two types of bioactive surfaces, i.e. bioactive glass and HAp particles. It was observed that in cell culture the bioactive glass shows more cell adherence in comparison with HAp. The surface roughness of the surface was in the range of 100-300µm leads to attachment of cell more effective.

Islam et al. [83] reported review on bioactive calcium phosphate based glasses and ceramics and their biomedical applications. The mechanism of apatite formation on the surface of the bioactive glass and the formation of the apatite layer along with standard protocol was discussed. Tajbakhsh et al. [84] reviewed a comprehensive study on the fabrication and properties of biocomposite (PLA/ceramics) for bone tissue engineering. It was mentioned that alone PLA has some limitation like mechanical strength and due to hydrophobic nature, the cell adhesion was also limited. Thus the inclusion of HAp leads toward increment in mechanical strength as well as due to bioactive; the cell attachment was also good.

Lebre et al. [85] reported the effect of shape and size of HAp particles on inflammatory responses through implantation. This study establishes a relationship between the physical properties of HAp particles and the immune responses. It was observed that HAp particle's size and morphology influence the production of inflammatory cytokines both in vitro and in vivo. Smaller needle-shaped HAp particles generated a prolonged inflammatory response compared to spherical shaped nanoparticles and larger sized spherical HAp particles, which suggested that these might be good tools in promoting successful tissue remodeling and thus to modulate the immune cell response and signals to surrounding tissues. Zhang et al.[86] reported a simple approach to prepare injectable macro porous calcium phosphate cement for bone repair. The material contains viscous hydrophilic polymeric solution. The polymeric solution selected was silanized-

hydroxypropylmethyl cellulose (Si-HPMC) as a foaming agent. The mechanical properties of the same were in the range of cancellous bone. The prepared polymeric solution has a good injectability, good cohesion, contain hierarchical macro pores in order to improve the porous composite that should promote both an osteoconductivity and resorption process.

Bartolome et al. [87] evaluated *In vitro* and *In vivo* evaluation of zirconia/niobium bio cermet for hard tissue replacement. The biological tolerance of the proposed cermet was investigated with both in vivo and in vitro approaches. The biocermet showed higher cell proliferation than niobium metal and finally concluded as an application to use in orthopedic and dental applications.

Inzana et al. [88] reported biomaterials approach to treating implants associated with osteomyelitis (chronic bone infections). Treatment of these chronic bone infections often involves combinations of antibiotics given systematically and locally to the affected site via biomaterial spacer. So for this application PMMA was considered as the gold standard, but it consists many limitations include antibiotic release, incompatibility with many antimicrobial agents and the need for follow up surgeries till the surgical reconstruction of the lost bone. Antimicrobial implant coatings are very important and need to go through the class of biomaterials. Future experimental designs should pay special attention wherever animal models are employed to evaluate biomaterial delivery systems.

Yang et al. [89] investigated growth, *In vitro* biodegradation and cyto-compatibility properties of nHAp coatings on biodegradable magnesium alloys. Since earlier magnesium alloys were considered as promising degradable materials for orthopedic applications, but the limitation such as rapid degradation rate makes it difficult to sustain. HAp coating on magnesium substrate improves its cyto-compatibility for

orthopedic applications. The coating was done through a simple hydrothermal deposition method which further improved corrosion resistance and also from rapid degradation of the magnesium based implants.

Medeiros et al. [90] evaluated in vitro mechanical analysis of different techniques of internal fixation of combined mandibular angle and body fractures. Twenty five polyurethane mandibles were used as the substrate, fixed with 2mm fixation systems and divided in to 5 groups. It was observed that the group, which was fixed with locking plates, offered no greater mechanical resistance in the displacement of 1 mm than group II. It was concluded that among the groups, fixations of bilateral mandibular fracture involving the mandibular angle and body with two plates in the region of the mandibular body and one plate in the tension zone in the region of the mandibular angle were the technique that provides better mechanical resistance.

Bellini et al. [91] reported PLA grafting of collagen chains for tendon regeneration with improved mechanical properties. The collagen based materials were prepared via heterogeneous phase derivatization of type I collagen sponges using PLA. Compared with untreated collagen, the functionalised sponge (Coll-PLA) was characterized by higher tensile properties and lower swelling capabilities. The reason is due to an increased hydrophobic character of the collagen matrix due to the presence of the PLA matrix. The hydrophobic PLA chains, grafted onto the collagen backbone using a reaction carried out in heterogeneous phase, led to the formation of a biomaterial with interesting mechanical properties and resistance to large deformations, lower water uptake capability and higher enzymatic resistance. Kaavessina et al. [92] studies the characterization of PLA/HAp composite prepared from solvent blending technique. It was observed that storage modulus, loss modulus, complex viscosity, thermal stability and degree of crystallinity increases with increase in HAp loading.

Takayama et al. [93] discussed mechanical properties of bioabsorbable PLA/PGA fibre reinforced composite prepared by melt mixing. It was observed that the flexural strength of the PLA was enhanced due to the nucleating effect of PGA fibres, which restrain the deformation at the same stress condition. The dispersion of PGA increased flexural strength.Hassan et al. [94] fabricated nHAp/PCL composite microfibers using the electrospining technique for tissue engineering applications especially for scaffold preparations. The incorporation of nHAp leads to increase the cell growth and finally concluded to use it as bone binding ability or tissue engineering applications.

Arifin et al. [95] discussed material processing of HAp/Ti as implant material using powder metallurgy for bone replacement implants. Because of light weight, high specific strength, and bio inertness, Titanium is widely used and preferred as a potential candidate. In this review, it was mentioned that the sintering parameter are the critical factor in determining the phase of two material formed during the diffusion process.

Wu et al. [96] reported improved mechanical properties of HAp in the form of whisker reinforced PLA by surface modification of HAp. The surface of the HAp whisker was modified with γ- amono propyl triethoxysilane to improve the interface between HAp whisker and PLA. It was observed that the mechanical properties were improved. Both the compressive strength and compressive modulus were increased with the weight ratio of modified HAp whiskers up to 30 wt. %, but only up to15 wt. % for non-modified HAp whiskers.

Perrone et al. [97] reported use of silk based devices for fracture fixations. The silk based screws and plates were for craniofacial devices made through solvent casting followed by mechanical machining. In vivo study was also conducted in the rat. Total 28 nos. of screws were inserted, it was observed no failure of the screw during insertion.it was observed that silk based screw was well tolerated and initiated the typical bone

remodeling process. After 4 and eight weeks' time points in vivo, there was early resorption of the screw. The silk screws in this study exhibited comparative shear properties to resorbable PLGA materials. It was also suggested the screws and plates might also need to be tuned to degrade in a shorter time frame to allow for the dynamic transfer of the load back to the healing bone.

Wang et al. [98] reviewed bone tissue engineering via nano structured calcium phosphate biomaterials and stem cells. It was discussed that an ideal orthopedic repair material is more than just fillers for bone defects. It also serves as a scaffold to provide chemical, mechanical and topographical cues to regulate cell behavior. The nano structure biomaterials promoted the process for bone regeneration by supporting cell adhesion, spreading, proliferation and differentiation. It was finally concluded that the nano structures CaP biomaterials and scaffold mimic natural bone, and have high surface to volume ratios, improved wettability and mechanical properties, and increased protein adsorption and other desirable properties, compared to conventional counterparts.

Abdal-Hay et al. [99] reported HAp doped PLA porous film coating on AZ31 Mg alloy for enhanced bioactivity and corrosion behavior. The magnesium alloys could be distinctly improved by this process. Formation of the apatite layer was observed when the samples were kept in simulated body fluid. The mechanical properties of the coated samples were satisfactory. Thus coating on magnesium alloys concluded as a promising strategy to obtain biologically active and safe implants with acceptable corrosion rates which allow sufficient time for healing and promote cell attachment, cell growth, and cell proliferation. Huang et al. [100] investigated in vitro degradation of PLA/nHAp ceramics composites for bone tissue repair materials. The composite was made through melt blending. In vitro degradation studies was conducted in PBS for 20 weeks. It was discussed that the ions released from the dissolution of nHAp in the PLLA/nHAp

composite material are basic and can neutralize the acidic degradable substances generated during the PLLA degradation process. The autocatalytic degradation effect of acids on the polymeric material can be alleviated, thus slowing down the degradation rate. The mechanical strength was also investigated before and after degradation studies.

Felfel et al. [101] fabricated bio resorbable screws reinforced with phosphate glass fiber. The screw was manufactured, and mechanical properties were characterized. The composites were made through compression molding at 210 ° C and 300 kPa. The screw was manufactured by forging composite bar. Various mechanical test as per ASTM standards was performed, and comparative properties were evaluated. It was observed that the mechanical properties associated with bio resorbable polymers were inadequate for load bearing applications. Thus fiber reinforcement is essential to improve their mechanical strength and stiffness. Felfel et al. [102] reported *In vitro* degradation, flexural, compressive and shear properties of fully bio resorbable composite rods. The rods of the composites were manufactured through compression molding at 100° C using phosphate glass fiber to reinforce PLA with appropriate fiber volume fraction. The degradation studies were conducted in PBS. The mechanical properties were evaluated before and after degradation studies. It was observed that the mechanical properties were reduced after immersion in PBS as a result of the plasticization effect of water within the composite and degradation of the fibers. The composite rods themselves becomes porous structure after degradation which was the main reason suggested for their decrease in mechanical properties and mass. Roeder et al.[103] reported HAp reinforced polymer biocomposites for synthetic bone substitutes which offer the ability to tailor the composite's elastic modulus to match with the limit of natural bone. HAp powder reinforced HDPE were s improved the mechanical strength with molecular orientation in the polymer matrix. Collagen and bone mineral were coupled by non-collagenous proteins

which bind to apatite via carboxy ligands. Hydroxyapatite and thermoplastics (HDPE, UHMWPE, PLLA, and PAEK) have little or no chemical bonding at the interface and are limited to mechanical interlock due to friction and residual stresses. Thus it was finally concluded that HAp reinforced polymer biocomposite offer a robust system to engineer synthetic bone substitute for orthopedic implant fixations.

Russias et al.[104] reported fabrication of PLA/HAp composites based on casting cum hot pressing and its *In vitro* studies. Materials with HAp content was close to 80% weight and mechanical properties were matched with the properties of bone. It was observed that the microstructure of these materials formed by ceramic particles distributed in the polymer matrix makes them quite susceptible to environmental degradation.

Chaya et al.[105] reported application of degradable magnesium alloys could provide an ideal combination of strength and degradation, facilitating fracture fixation and healing while eliminating the need for implant removal surgery. Fixation plates and screws were machined from 99.9% pure magnesium and compared with titanium devices in a rabbit ulnar fracture model. Magnesium device degradation and the effect on fracture healing and bone formation were assessed after four weeks. The 2-dimensional micro-computed tomography slices and histologic staining showed that magnesium degradation did not inhibit fracture healing or bone formation. Histomorphology showed no difference in bone-bridging fractures fixed with magnesium and titanium devices. Interestingly, abundant new bone was formed around magnesium devices, suggesting a connection between magnesium degradation and bone formation. Thus it shows potential for magnesium fixation devices in a loaded fracture environment.

Bostman et al. [106] studied about cost analysis saving after using absorbable polyester pins and screws for the internal fixation of small fragment fractures. The current cost analysis includes costs of medical care plus costs of lost time from work. The study

was based on 994 fracture patients treated with absorbable internal fixation devices and 1173 patients operated on using conventional metallic devices. The fracture types studied were uni and trimalleolar fractures of the ankle, fractures of the olecranon, and metacarpal fractures. When the costs for an implant removal procedure after metallic fixation were included, the average cost saved per patient by using absorbable implants varied from $410 in fractures of the olecranon to $903 in unimalleolar fractures. The breakeven point was attained at a removal rate of 19% for metacarpal fractures, 21% for unimalleolar fractures, 46% for fractures of the olecranon, and 54% for trimalleolar fractures**.**

Bergsma et al.[107] reported patients with fractures of the cheek bone were treated with high molecular weight PLLA bone plates and screws. Three years after implantation four patients returned with a swelling at the site of implantation. Crystal-like PLLA material internalized by various cells. The results of this investigation suggest that the PLLA material slowly degrades into particles with a high crystallinity.

Fan et al.[108] reported about the application of PLLA cushion while using an internal plate fixation. The reason behind was osteoporosis under the plate was often found, and refracture might occur after the plate removal. Animal models of internal fixation for tibia diaphyseal fracture with the placement of the PLLA cushion between the plate and the bone were established. To evaluate these models, histological investigations and three-dimensional finite element models were used to compare the stress distribution of the bone tissue with and without application degradable cushions. The reduction of stress shielding was observed in the initial and 50% healing process. Thus concluded as an alternative method for the improvement of the fracture healing process.

Zheng et al. [109] reported bovine bone screw and biodegradable interference screw for anterior cruciate ligament fixations. The screws were used for tibial fixation in each pair. Cyclic testing protocol with varying magnitude and orientation of the loading

was developed. Fifteen out of 20 reconstructions fixed and bovine bone screws and 17 of 20 fixed with biodegradable screws reached 5000 cycles with a peak force of 200N applied to the graft. Survival rate and pull out the strength of the both were compared. The tension drop was obtained ~19.7±13 N for bovine bone and ~18.9 N±16 for the biodegradable screw. It was concluded that bovine bone screws provide more stability during fixations. Sukegawa et al. [110] discussed unsintered HAp and PLLA based composite plates and screws, which were inserted in the patient. After five years, the resorption properties were observed. It was seen that at the place of the resorbed plate and screw the neo bone generation had taken place. It was also concluded that to facilitate uncompromised revision surgery; a complete osseous replacement should occur within a 2-3 year time frame. Furthermore, *In vivo* long-term studies are necessary, with follow-up until implant remains have disappeared and a new bone replacement has taken place.

1.16.2 Gaps observed in the prior art

Based on the prior art on bioabsorbable internal fixation devices, major gaps observed are:-

- Researchers developed polymer composite for biomedical applications, but the application of biopolymers for especially orthopedic fixations as per standard dimension has not been developed.
- Not much attention is paid on bioabsorbable internal fixation devices (IFDs) fabrication with the help of the injection molding process.
- Limited literature is available on the fabrication of the nHAp from natural bio wastes optimization and detailed parametric studies to fabricate nHAp formation still needs to be done.
- No such application of this fabricated biomaterials from bio waste is used to blend with the bioabsorbable polymer in order to produce IFDs.

- ❖ No researcher has attempted to test bioabsorbable IFDs mechanically as per available ASTM standards. Generally, researchers have fabricated the composite materials and analyses the general test.
- ❖ Various mechanical testing fixtures have been fabricated in order to test the fabricated IFDs realistically.
- ❖ Extensive *In vitro* hydrolytic degradation and mechanical properties as per ASTM standards are characterized and optimized in order to target the bioabsorbable IFDs for various age group peoples.

1.16.3 Motivation and objectives of the present work

- The main motivation of the present work is to develop cost effective bioabsorbable polymeric IFDs that can able to rich every needy person. To develop and explore its full potential, the following are the broad objectives of the current research work:
- Synthesis, characterization and optimization of nHAp from natural bio waste.
- Purification of commercially available PLA and parametric optimization of the extrusion cum injection molding process.
- Fabrication of various fixtures in order to fix the fabricated IFDs for mechanical testing as per ASTM standards.
- To study the *In vitro* hydrolytic degradation of each fabricated IFDs and optimization in order to conclude for application for various age group peoples.
- Bioactivity test of the fabricated IFDs as per available standards protocols.
- To develop the affordable bioabsorbable IFDs having sufficient mechanical strength, resorption rate, bioactive and biocompatible in order to match the healing of fractured bones and degradation of nearby IFDs.

1.16.4 Hypothesis

Current research is to develop nHAp based bioabsorbable polymeric IFDs, which could be cost effective without compromising its mechanical strength, bioactivity and biodegradability. Already metallic internal fixations devices are there, but it has lots of problems, which is discussed in the previous sections. Since alone PLA polymers could not provide so much mechanical strength thus nano fillers from renewable sources like fish scale bio waste has processed successfully in order to extract nano powders, which is bioactive bio ceramics and encourages neo bone regenerations.

1.16.5 The objective of the research

The objective of the research is as follows

- Fabrication and characterization of nHAp from fish scale bio waste.
- Purification of commercial available PLA in order to use for biomedical applications.
- Development of various types of molds and fixtures for production of widely used IFDs.
- Parametric optimisation of inputs values of extrusion cum injection molding process and after optimization, evaluation of mechanical strength as per available ASTM standards.
- *In vitro* degradation and bioactivity studies of the prepared IFDs as per standard protocol.
- Evaluation of mechanical strength of each fabricated IFDs during *In vitro* hydrolytic degradation.
- To examine the dimensional deviation of IFDs from their standard geometry.

Figure 1.19 summarizes the proposed objectives of the research work.

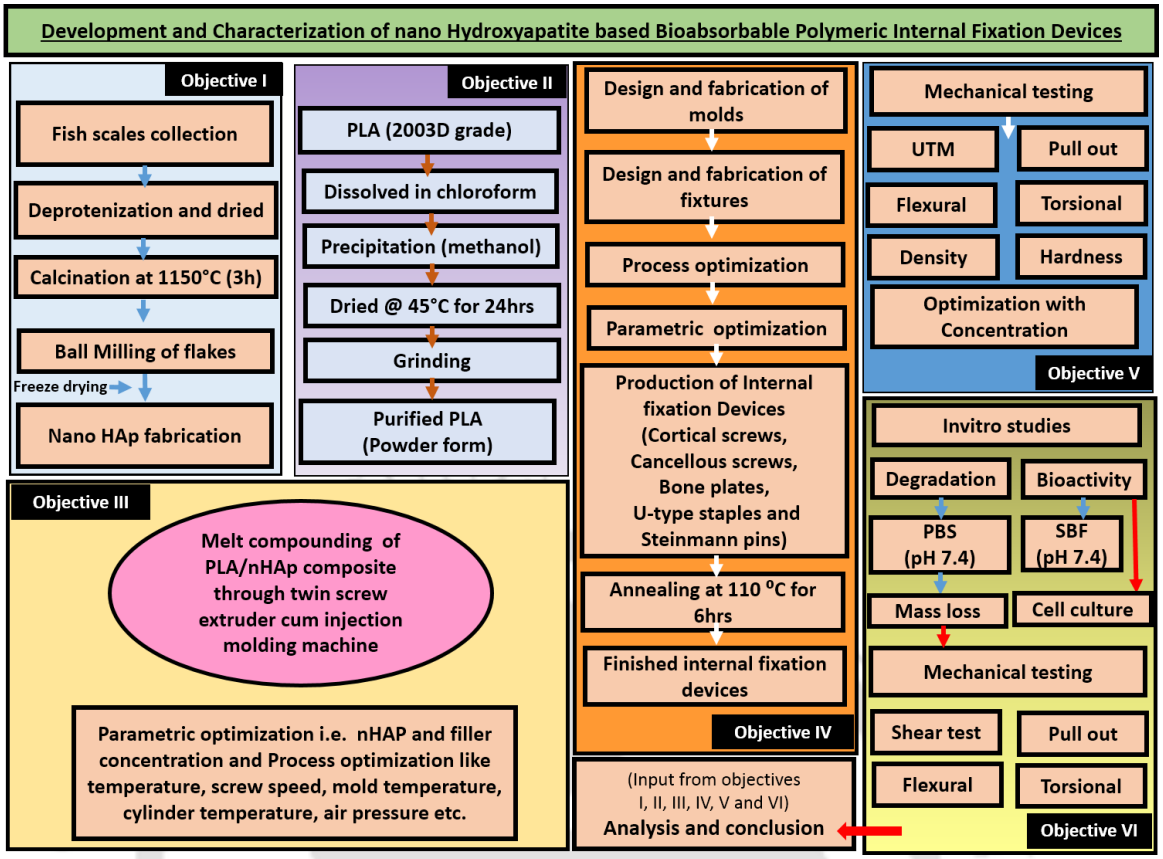

Figure 1.19: Summary of the proposed objectives for the research work.

1.16.6 Organization of thesis

Current thesis is organized into seven chapters with references at the end. **Chapter 1** discusses the need for bioabsorbable internal fixation devices and existing various traditional or metallic internal fixation devices. The shortcomings of the metallic internal fixations led to many disadvantages like stress shielding, stress palpation, ions leaching, and resurgery after fracture healing, leads to extreme pain or discomfort to the patients. Application of bioabsorbable IFDs could minimize it. Relevant literature on bioabsorbable polymer application as IFDs in biomedical applications is discussed.

Chapter 2 presents processing of nano-bio fillers to the base materials with varying concentration and exhaustive characterization of fabricated biomaterials and bio composites. Optimization of process parameters such as extrusion temperature, injection

molding temperature, cylinder temperature, mold temperature, residence time, holding time, screw speed and air pressure has been carried out for the PLA/nHAp combinations. Various analytical instruments like X-ray diffraction studies, Field emission scanning electron microscopic studies, Energy dispersive X-ray spectroscopy, Fourier transform infrared spectroscopies, Transmission electron microscopic studies, Universal tensile testing, Differential scanning calorimetric studies, Thermo gravimetric studies, polarized optical microscopies studies, Density measurement, surface wettability, water absorption, bioactivity and *In vitro* hydrolytic degradation studies were conducted to optimize the optimum concentration of filler to base material ratios. The cortical screws fabrication and its related molds and fixtures have been discussed in **Chapter 3**. It also includes various characterization such as axial pull out test, torsion test, flexural test and double shear test as per the ASTM standards. Fabrication of molds and fixtures for cancellous screws and its related characterizations is presented in **Chapter 4**. Fabrication of bone plate molds and related fixtures for conduction of bone plate test has been discussed and characterized in **Chapter 5**. Similarly *In vitro* hydrolytic degradation studies was carried out as per the ASTM standard.

In **Chapter 6**, fabrication and characterization of Steinmann pins and bone staples has been discussed. The related design of molds and fixtures is presented in this chapter. In vitro hydrolytic degradation studies and mechanical strength during hydrolytic degradation has been explored in this chapter. **Chapter 7** represents the main findings of the present work, important conclusions and future scope in the field of bioabsorbable IFDs. The outcome of the present work in the form of Patents, Journal papers, awards and conferences is reported. References are added in the last.

ABSTRACT

This chapter deals with the fabrication and characterization of PLA and nHAp based bio composites. The detailed information of materials and fabrication methods followed by characterization by distinct analytical methods. The optimization of machine process parameters for extrusion process has been done. After making the composites, mechanical studies, *In vitro* hydrolytic degradation and bioactivity studies have been performed through phosphate buffer solution (PBS) and simulated body fluid (SBF) solution respectively as per the standard protocols. During *In vitro* hydrolytic degradation, mass loss has also been analyzed in order to know the rate of degradation for a specific period.

GRAPHICAL ABSTRACT

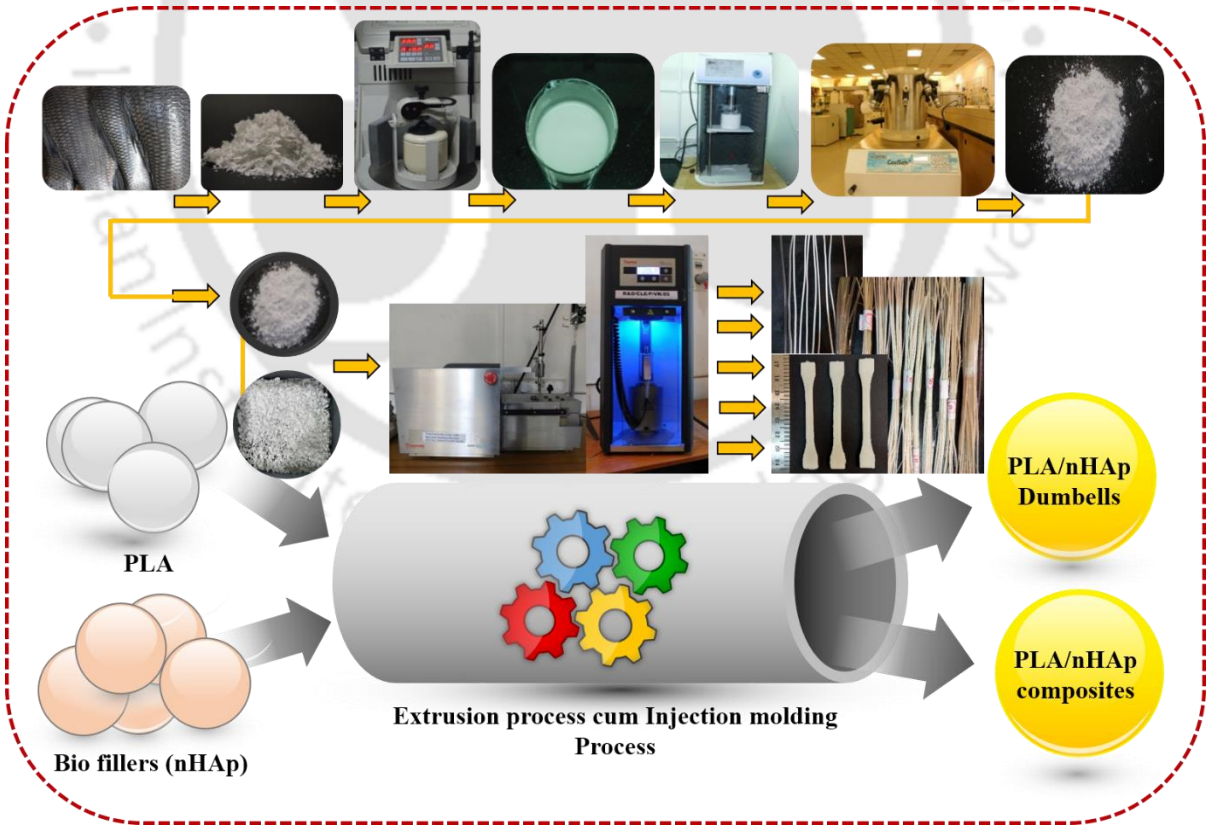

Chapter 2

2 *Poly Lactic acid and nano-Hydroxyapatite based Bio composites*

2.1 Introduction

The use of bio absorbable polymers is increasing in biomedical field especially for orthopedic fracture fixation devices and get more attention to overcome the existing limitations of metals in applications as internal fixation devices (IFDs). The selection of materials is a very important factor, particularly for its specific functions. Many metals such as magnesium [111], titanium [112], cobalt chromium alloys [113] etc. are used and many other biopolymers such as PLA, PGA, PCL, Phosphate glass etc. are processed through various methods in order to fabricate IFDs [114]. The most important parameter is the selection of materials, and its fabrication process, which revolves around the mechanical properties, sustainability during processing and their stability towards performances. Many times, it was observed that the bioabsorbable polymeric materials, which was used as IFDs are not sufficiently carrying the bearing loads and in an early stage, it degrades while the healing of the bone fractures does not happen [115]. PLA is a bio based, an aliphatic polyester polymer and has been widely used for various applications such as food packaging applications [116], automobile, wound healing applications [117] and other commodity applications [118]. In order to get the desired property, various fillers are utilized in order to enhance its effectiveness [119]. It has outstanding advantages over other polymers. As early as the 1970s, PLA products have been approved by the US Food and Drug Administration (FDA) for direct contact with biological fluids. Four of its most attractive advantages are renewability, biocompatibility, process

ability, and energy saving. PLA and its degradation products, namely H_2O and CO_2, are neither toxic nor carcinogenic to the human body, hence making it an excellent material for biomedical applications including sutures, clips, and drug delivery systems [120]. Figure 2.1 explains the cycle of PLA in nature.

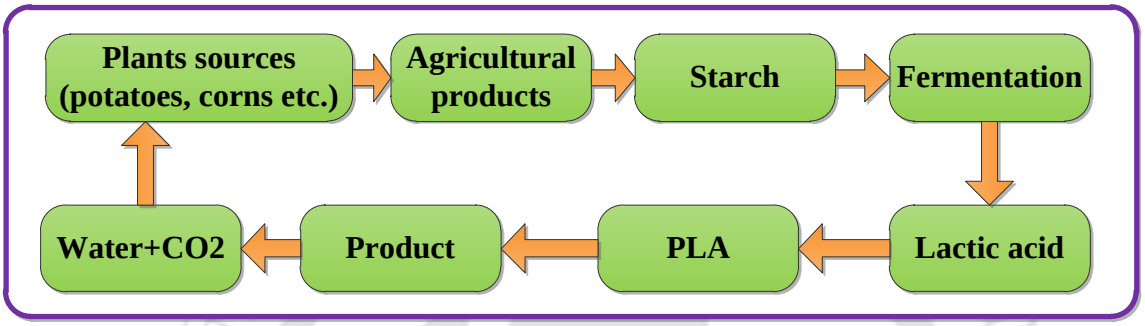

Figure 2.1: The cycle of PLA in nature.

In biomedical fields, various fillers like HAp, chitosan, silver, copper etc. are widely used to get some additional properties like load bearing capabilities, enhance its bio activeness, anti-microbial and anti-inflammatory and other also [121]. It was also observed that alone bioabsorbable polymers are having limitations like less mechanical strength, thermal stability, and uncontrolled degradation profiles. To overcome this, filler materials play a vital role. The nHAp has been widely used as filler materials for bone fixation devices. It has capabilities to attract neo bone tissue regeneration, promotes good cell adhesion and enhances the bioactivity process [122].

The combination of PLA and nHAp mimics the natural bone to some extent. Since bone is also composed of inorganic and organic components, in which inorganic part (nHAp) provides strength and stiffness to the structure, and organic part (PLA) provides flexibility, toughness and resorbability to the structures. Inorganic-organic composite is aiming to mimic the composite nature of real bone by combining the toughness of the polymer phase with the

compressive strength of an inorganic one to generate bioactive material with improved mechanical properties and degradation profiles [123]. For such composites, the alkalinity of the inorganic particles such as Hydroxyapatite neutralizes acidic autocatalytic degradation of polymers such as PLA, exploiting bioactive functions [124]. In this chapter, PLA has been selected as a base material and nHAp as filler materials. The nHAp powders have been prepared in our lab from fish scales (biowaste), and commercial PLA has been purified, after that the effect of nHAp loading on various characterization has been studied in detail.

2.2 Materials and Methodology

2.2.1 Poly lactic acid

Poly lactic acid (2003 D), (D-lactic acid: 1.4%, L-lactic acid: 98.6%, granules form, density of 1.24 g/cm^3, melt flow index: 0.73g/min at 210°C) with number average molecular weight (Mn) of ~150,000 Da and weight average (Mw) of ~2,00,000 Da, respectively was supplied by Nature works, USA. This commercial PLA (2003D) granules were purified with the help of reprecipitation with methanol in terms of catalyst removal through continuous cleaning with methanol (Finar, India). Initially, 50 gram PLA granules were dissolved in 250 mL of chloroform (Merck, India) at room temperature. The dissolved PLA was precipitated in 1000mL methanol (Finar, India). Precipitated PLA was dried in hot air oven at 55°C for 24 hours. After that, obtained fibrous PLA was grinded with high speed universal disintegrator (make: Huanghua, Model: FW100) at 24,000 rpm in order to make in powder form.

2.2.2 Hydroxyapatite

The synthesis of pure and biocompatible nHAp was fabricated from a fish scale (natural bio waste) in a cost effective way. Hydroxyapatite is widely used for bone fixation as it encourages the neo bone generation near the fractured bone sites. In the process of fabrication

of Hydroxyapatite. The fish scales were collected from the local market, Amingaon, India. The collected fish scale was repeatedly cleaned and processed through chemical treatment in NaOH (1M) and HCl (1M) in order to deproteinise it. After cleaning with running water, the cleaned fish scales were dried in hot air oven at 50°C for ~4-5 hours. The dried fish scales were further calcinated in a muffle furnace (Make: Metatherm, model: 887) at 1150°C for 3 hours in order to get calcinated HAp flakes. The calcinated HAp flakes were further milled into ball milling machine (Planetary Mono Mill PULVERISETTE 6 classic line, Fritsch Germany) for 3 hours at 290 revolutions per minute (rpm) in wet condition at room temperature. Before wet milling, the calcinated scales were mixed with deionized water to make a slurry, and the zirconia balls (08-1.0 mm diameter) were added in 10:1 weight ratio.

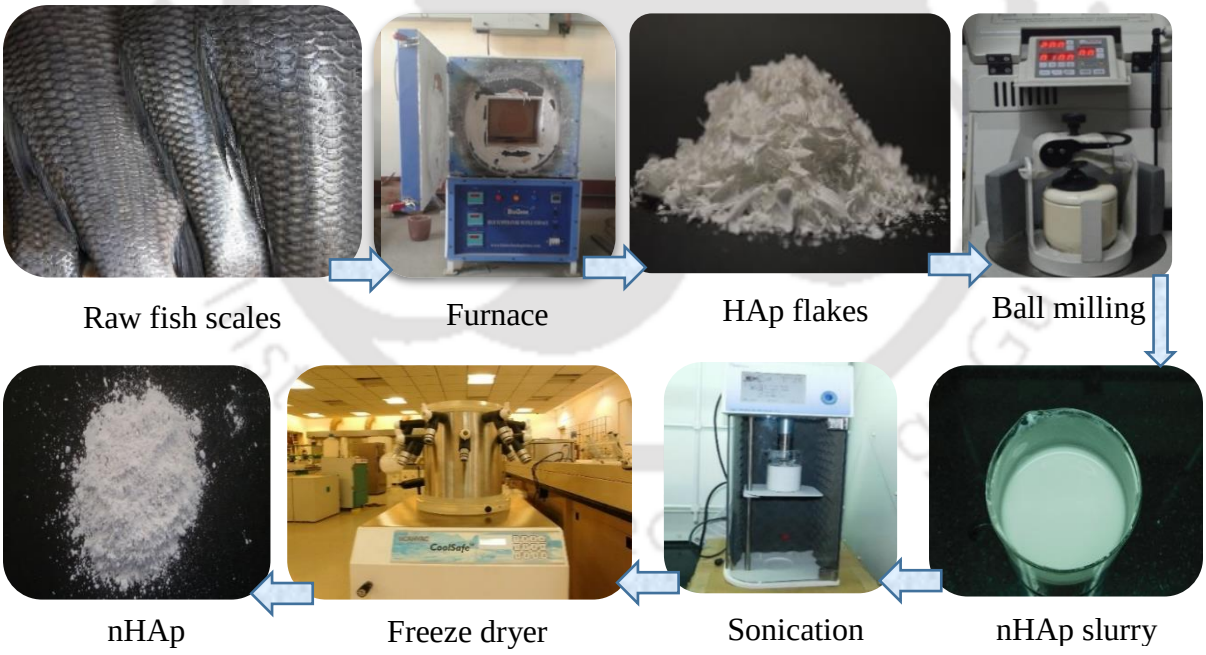

Figure 2.2: Stepwise process for the synthesis of nHAp powders.

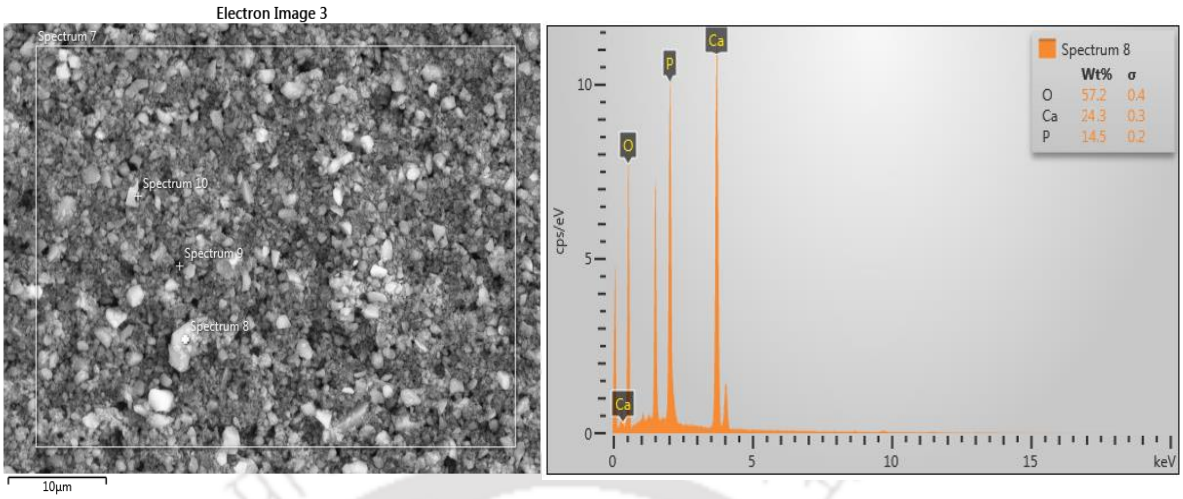

Figure 2.3: EDX analysis of nHAp particles

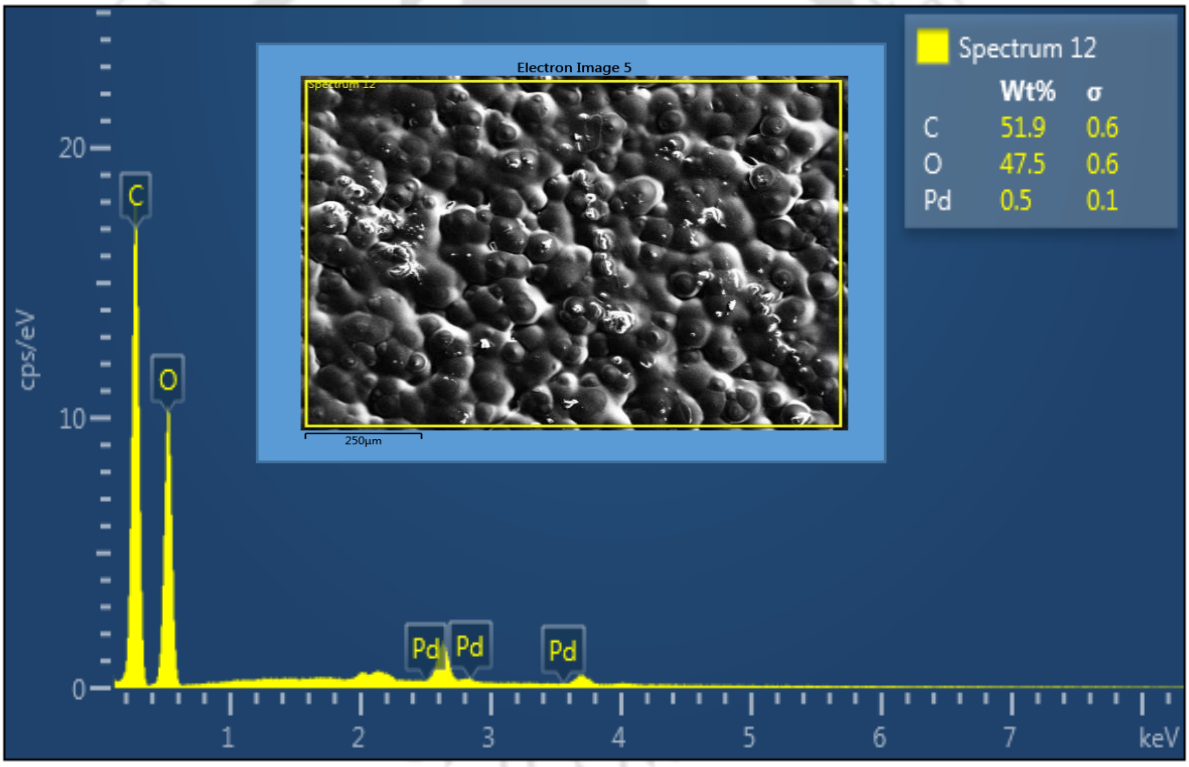

Figure 2.4: EDX analysis of commercial PLA.

After removing the zirconia balls by filtration, homogenization was done by a homogenizer (Digital Homogenizer, IKA) with 6000 rpm at 5° C for 15 min and the obtained slurry was freeze dried (LaboGene^{TM}, SCANVAC) for 72 hours at -95°C to obtain nano size particles

of HAp. Figure 2.2 explains about the stepwise procedure in order to make the nHAp. Figure 2.3 shows the EDX profile of the fabricated nHAp. Figure 2.4 and Figure 2.5 corresponds to commercial PLA and purified fibrous PLA. It can be observed that in Figure 2.5, the catalyst (Pd) is missing owing to metal catalyst free PLA polymers leads to the development of purified PLA.

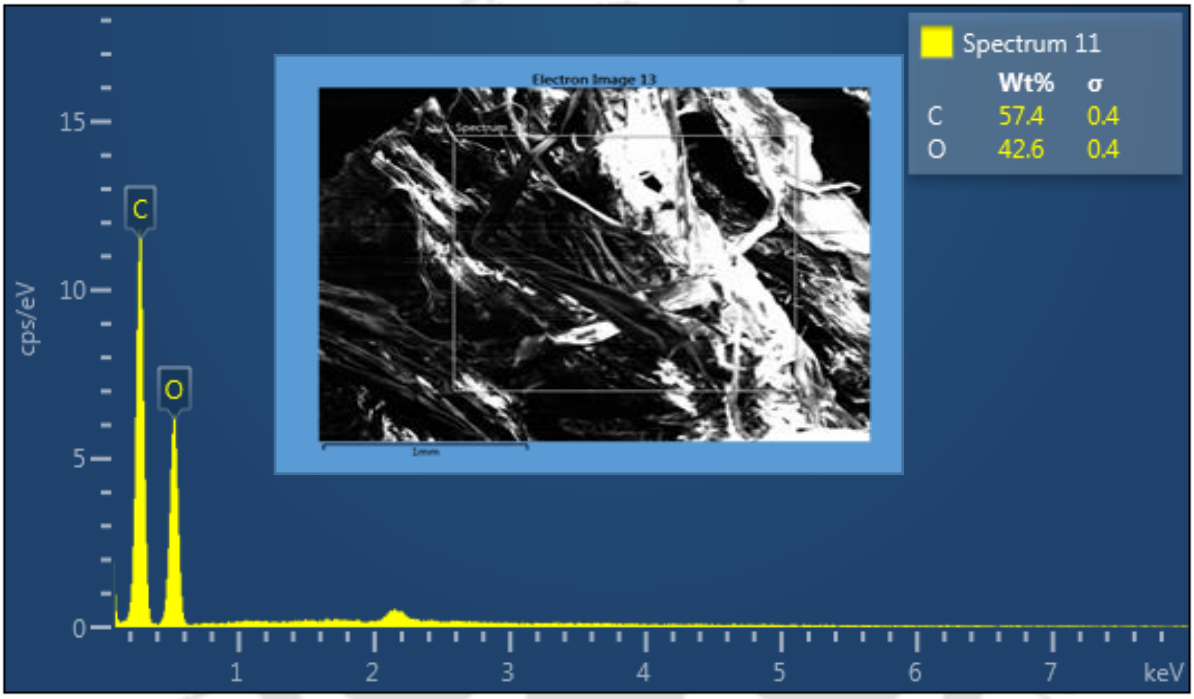

Figure 2.5: EDX analysis of purified fibrous PLA.

2.3 Processing of PLA/nHAp bio composites

In order to fabricate the PLA/nHAp bio composite. The fibrous form of PLA was initially dried at 40°C in a hot air oven for 8-10 hours to eliminate the residual moisture content. Subsequently, the freeze dried nHAp was manually mixed in varying concentration with previously dried PLA. After that, each batch of specific proportion was melt extruded in a co-rotating twin screw extruder (Haake, Minilab II, ThermoFischer Scientific) at a processing temperature of 190°C and a screw speed of ~100 rpm. The residence time kept inside the

twin screw extruder machine was maintained 1 minute. Neat PLA and PLA/nHAp bio composite were received in the form of long strips of dimension ~5 x 0.5 (width x thickness) as products. The dumbbells shape was also fabricated as per ISO527-1BA using injection molding machine (Haake, Minijet Pro, Thermo Fischer Scientific) at 190°C and feeding pressure of 50 bar. The mold temperature was maintained at 90°C. The prepared samples were stored in desiccators for further analysis. Figure 2.6 explains about the scheme of the process utilized for PLA/Hap composites.

Table 2.1: Parameters for extrusion of PLA/nHAp biocomposite dumbbells and strips.

Parameters		
1.	Processing temperature	190°C
2.	Residence time	1min
3.	Twin screw speed	100 rpm
4.	Compressed air pressure	50 bar
5.	Extrusion die (Strip: width 5mm)	Flat type

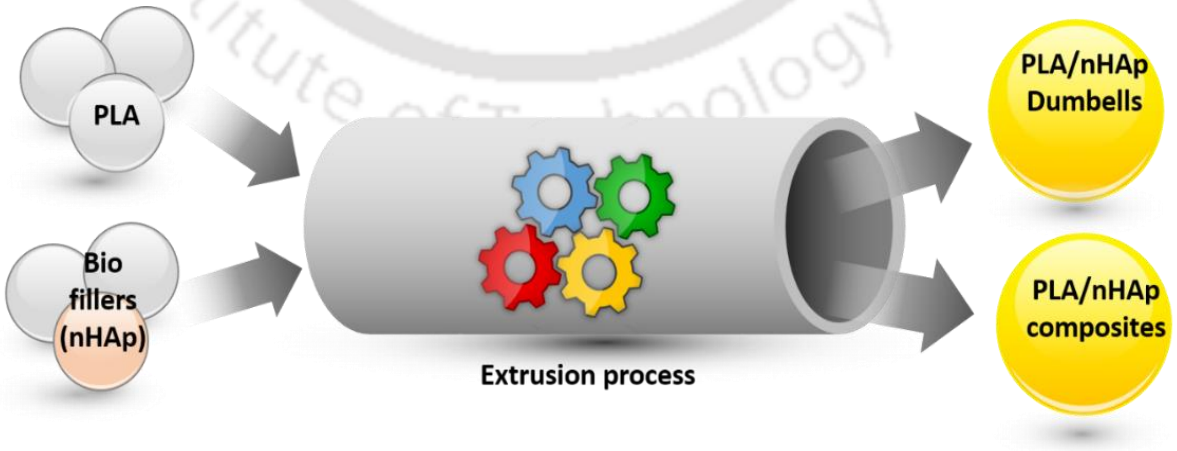

Figure 2.6: Schematics of PLA/nHAp biocomposite production.

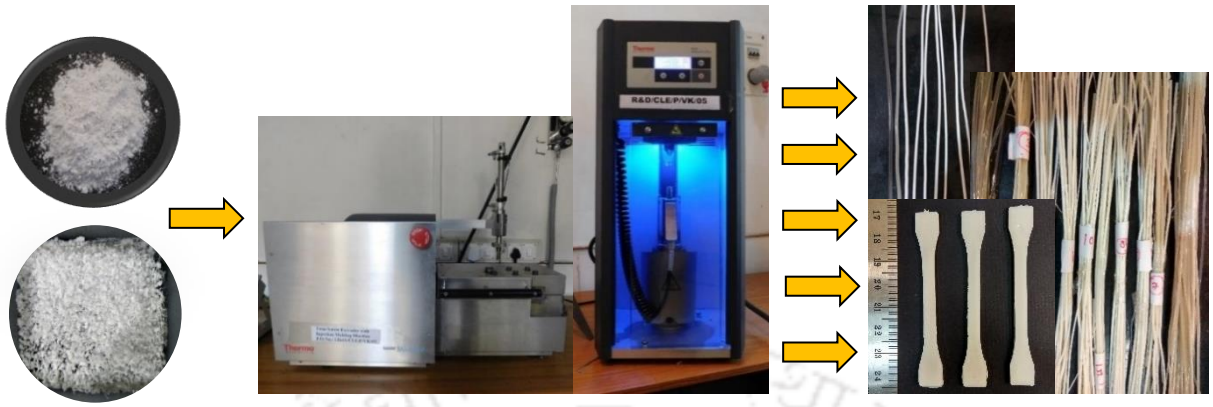

Figure 2.7: Schematics of extrusion cum injection molding process

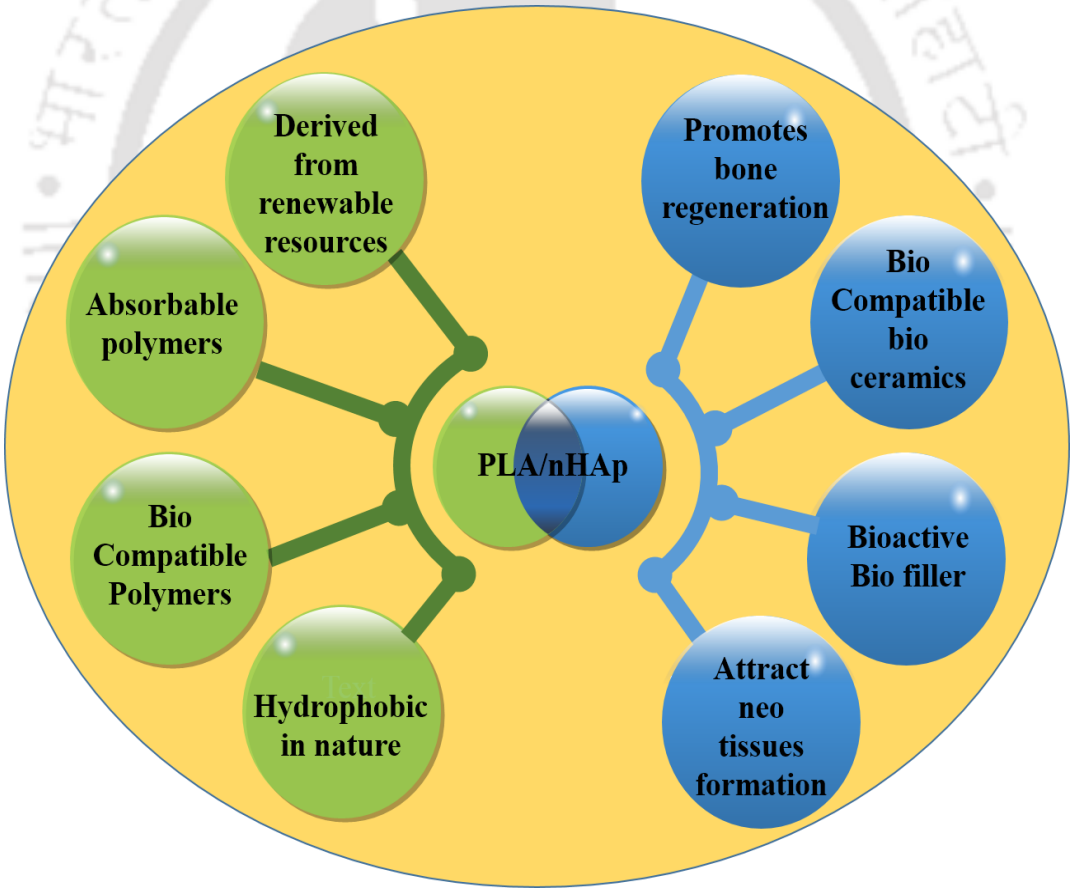

Figure 2.8: Properties of PLA and nHAp for suitable application

Table 2.1 shows the parameters followed during the extrusion process. Figure 2.7 shows the pictorial steps of extrusion cum injection molding for the production of dumbbells and PLA/nHAp composites. The media used during the extrusion process is compressed air of pressure in the range of 50-100 bar. Figure 2.8 shows the characteristics features of PLA and nHAp biocomposites in context with biomedical applications.

2.4 Characterization of PLA/nHAp bio composites

The extruded PLA/nHAp bio composites were characterized by various analytical studies like X-ray diffraction studies (XRD), thermal studies through differential scanning calorimeter (DSC) and thermogravimetric analysis (TGA), functional group identification through Fourier transform infrared spectroscopy (FTIR) and mechanical testing through universal tensile testing machine (UTM). Surface wettability measurement through contact angle analysis. The surface morphological studies were done through field emission scanning electron microscope (FESEM) and transmission electron microscope (TEM). The total sizes of batches were selected as neat PLA, 3% nHAp, 5% nHAp, 7% nHAp, and 10% nHAp, weight (wt.) of nHAp mixed into PLA. The degradation studies were performed as per ASTM F1635-11. The bioactivity studies were performed in simulated body fluid (SBF) at 37.5°C maintained at pH 7.4.

2.5 Results and Discussion

2.5.1 Field emission scanning electron microscopy (FESEM)

The surface morphology of the nHAp, PLA and extruded PLA/nHAp composite was analyzed by FESEM (Sigma, Zeiss). A small amount of nHAp powders and a small piece of strips samples was mounted on aluminum stubs over double sided carbon tape. Sputter coater

(SC7620, Quorum) was used to coat the samples under vacuum conditions. The analysis was performed at 2kV for nHAp powders and 3kV for PLA and PLA/nHAp composites with ~6 mm working distance. It was observed that from Figure 2.9 (a) and (b) the nHAp powders were in the size of 40-60nm and was uniformly shaped. While Figure 2.9 (c), (d) shows the surface micrograph of fractured neat PLA and PLA/nHAp composites.

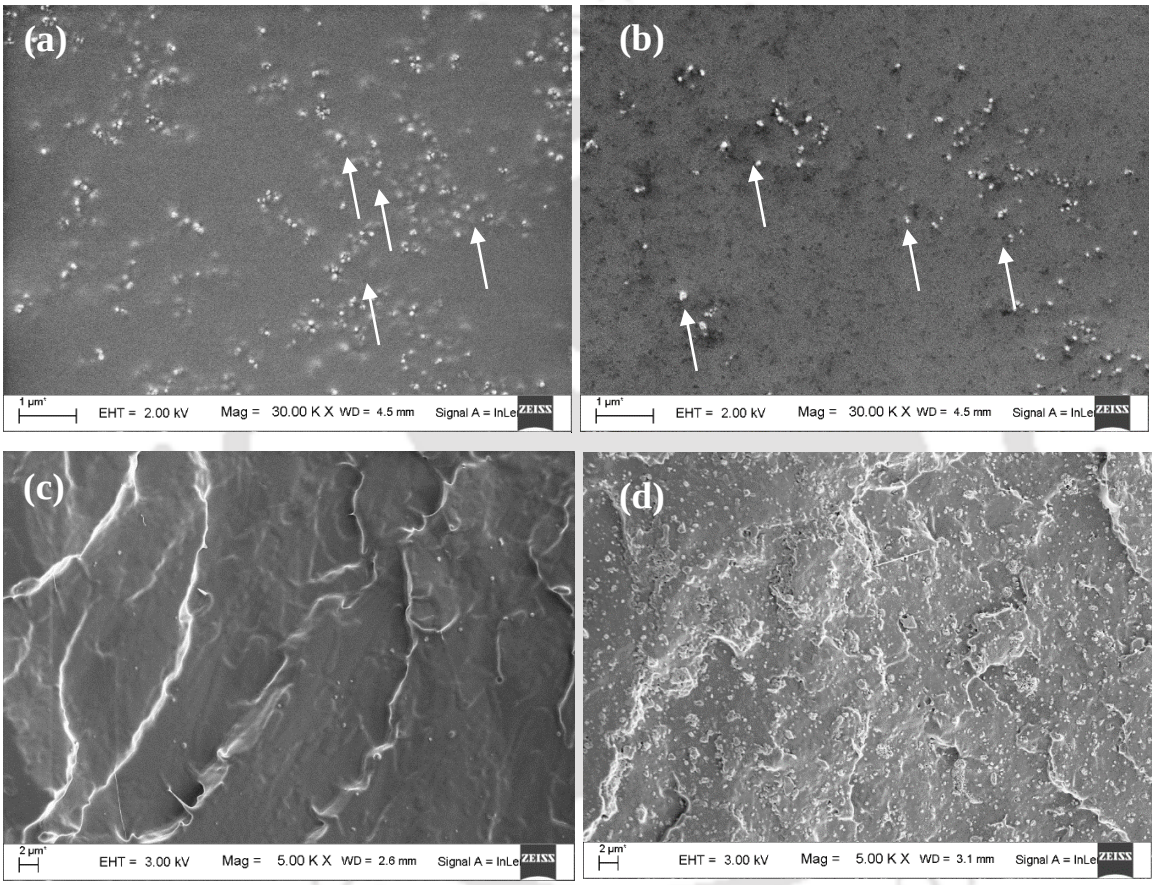

Figure 2.9: (a) and (b) The Surface micrograph of nHAp powders, (c) The crossectional surface micrograph of neat PLA and (d) The crossectional surface micrograph of PLA/nHAp composite

2.5.2 Transmission electron microscope (TEM)

The morphological investigation of nHAp powder was also carried out using field emission transmission electron microscope (JEM-2100, JEOL, U.S.A.) at 200 kV. The samples were dissolved in ethanol followed by stirring the solution for 2 hours for uniform dispersion. The

solution was drop casted on carbon coated TEM grids (Pacific, U.S.A.) and dried overnight at 50 °C before the analysis.

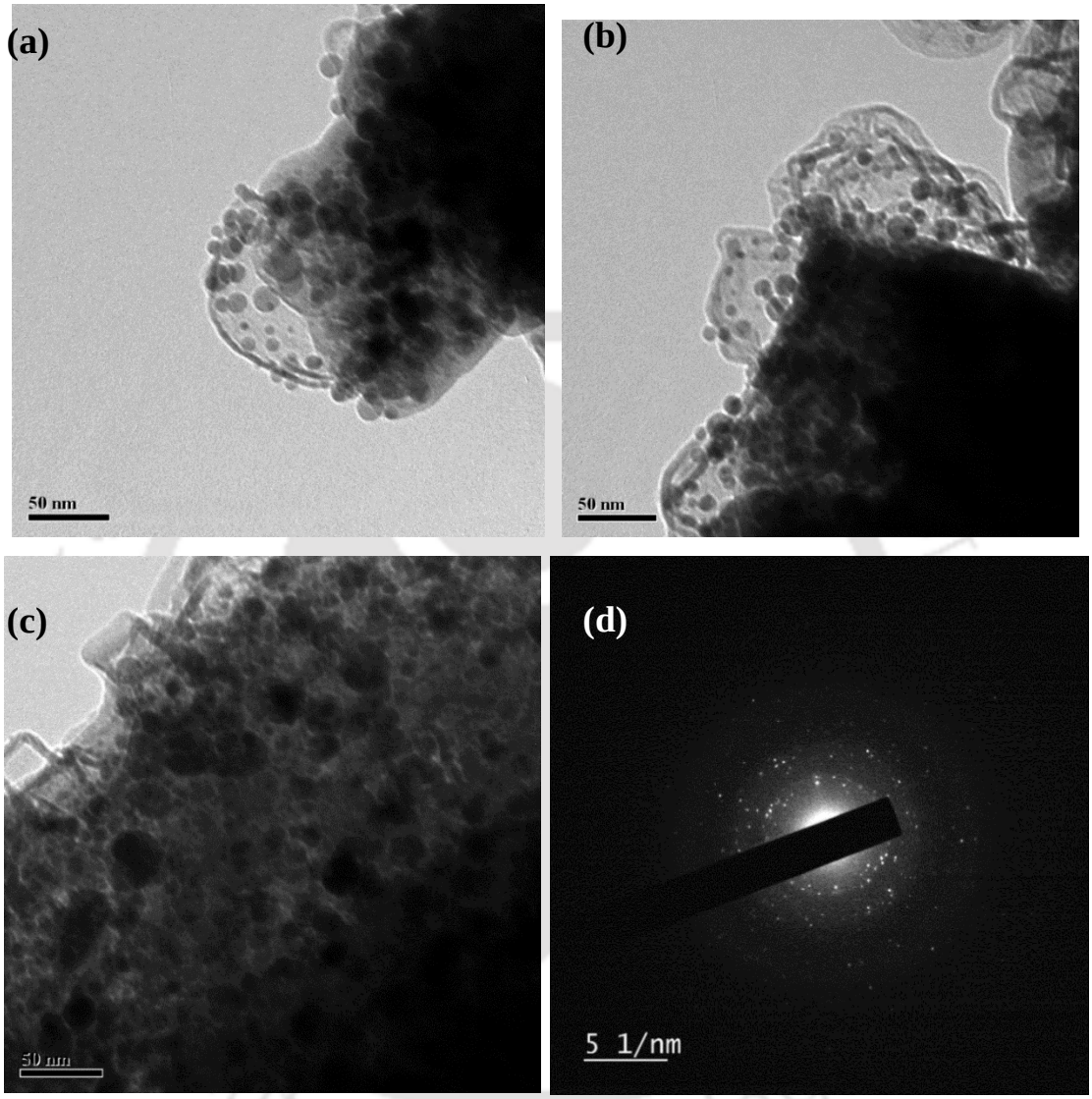

Figure 2.10: Field emission transmission electron microscope image of nHAp (b) SAED pattern of nHAp

The Figure 2.10 (a), (b) and (c) shows the morphology of nHAp powders, whereas the Figure 2.10 (d) shows the selected area diffraction pattern (SAED) of the nHAp powders. It is also observed that there is a uniform distribution of nHAp particles taking which further leads to giving better results. The main reason behind getting the uniform distribution may be due to

a fibrous form of PLA and the size of the nHAp. The measured size of the nHAp powder was in the range of 20-80 nm.

2.5.3 X-ray diffraction studies (XRD)

XRD analysis was analyzed by X-ray diffractometer (D8 Advance, Bruker, Germany) equipped with a goniometer and Ni-filtered Cu-Kα radiation (λ = 1.54 Å). The operating conditions of diverging and receiving slits were at 40 kV and 40 mA. The relative intensity was recorded in the 2θ range of 10° to 50° with a continuous increment and scan speed of 0.05°/sec and two sec/step, respectively. All the samples were annealed at 60°C for two h before the analysis. Figure 2.11 shows the profile of XRD of the fabricated nHAp and PLA/nHAp bio composites. The characteristics peak of highest intensity for nHAp was obtained at 2Θ of 31° corresponding to 211 planes. In the case of PLA/nHAp, the sharp crystallization peak at 2Θ =16.2° is observed from (2, 0, 0) reflection for PLA [125]. The crystallographic analysis of the PLA shows sharp crystalline peaks at 16.2° (2, 0, 0) which correspond to α crystalline form of the PLA. The spectra of PLA also shows two more (203) and (015) reflection peaks at 19.2 and 25.7° respectively. These reflection peaks also correspond to the combined effect of α and β crystalline forms. Hence it is confirmed from the above discussion that extruded strips are semi crystalline in nature. PLA/nHAp composite and nHAp exhibit more peak at 31.5 and 31.8 and 32.7 with more intensity as compared to PLA. It is also noted that the number of crystalline phases is increasing as an increase in loading concentration. The plane (105), (211), and (300) corresponding to Hydroxyapatite phase [125]. The slight increment in 2Θ value as in the case of 7% nHAp and 10% nHAp concludes that some of the nHAp particles intercalated in the PLA matrix and increased in interlayer spacing. After more loading of nHAp, a number of peaks appear in the XRD spectra of PLA/nHAp, which signifies the increment in crystalline nature. Hence, the XRD results

illustrate that PLA/nHAp biocomposite is semi crystalline in nature and loading of nHAp leads to an increase in crystallinity of the composites.

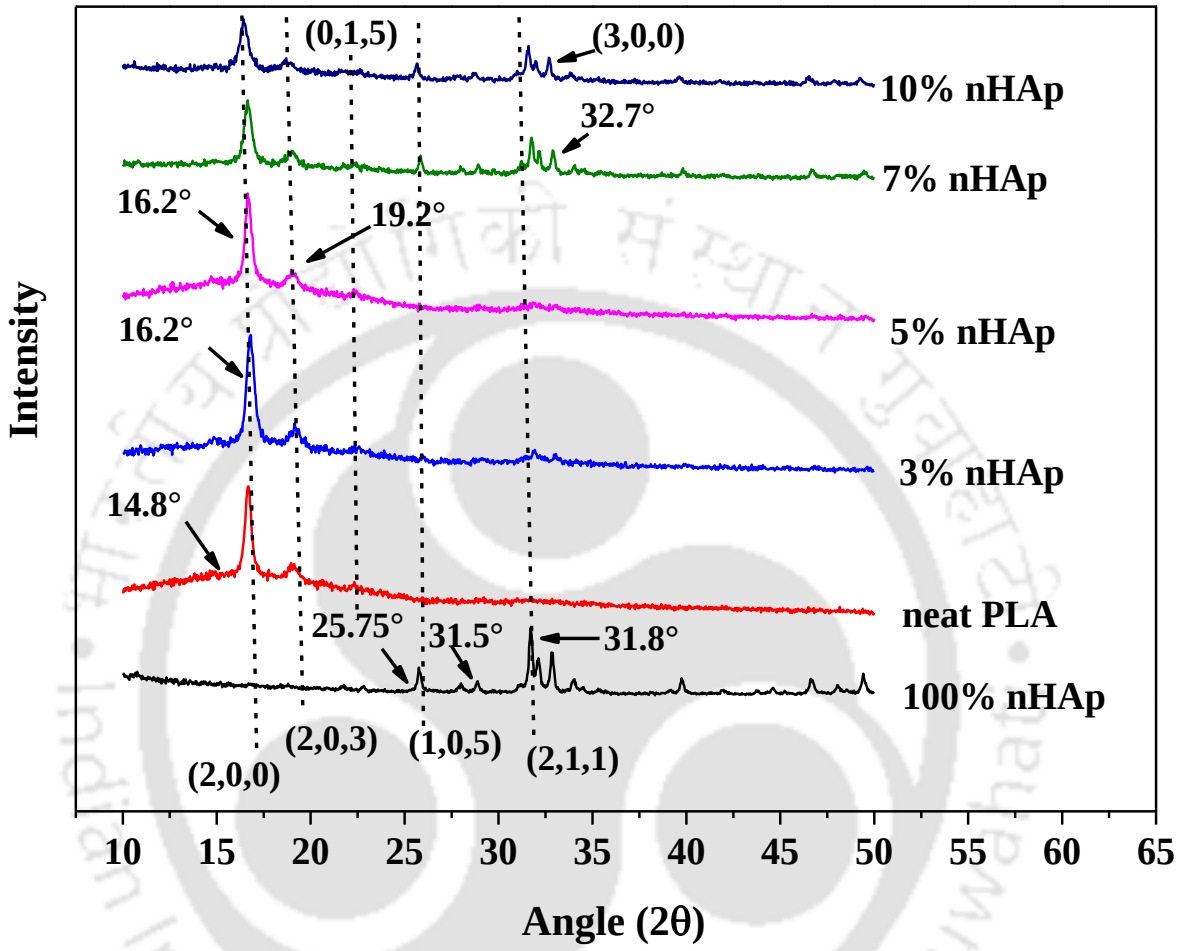

Figure 2.11: XRD diffractographs of the fabricated nHAp and PLA/nHAp composites.

2.5.4 Thermogravimetric analysis (TGA)

The thermal stability of the fabricated PLA and PLA/nHAp composite was analyzed through TGA studies. The samples (~6-7 mg) of the PLA and PLA/nHAp composites was placed in the thermo gravimetric analyzer (TGA-4000, PerkinElmer, U.S.A.) under a nitrogen atmosphere with a flow rate of 60 mL/min. The samples were placed in the alumina crucible at a temperature range from 30° C to 700 °C at a heating rate of 10° C/min. The Nitrogen gas was used to create an inert atmosphere inside the crucible chamber. Figure 2.12 shows the

TGA profile of PLA/nHAp biocomposites. It was observed that most thermal degradation had taken place in the range of 340°C - 400° C. This weight loss is responsible for material degradation. Maximum thermal stability has been observed in 10% nHAp, which reduces with a reduction in filler concentration which may be attributed as sharing of heat to the nearby nHAp particles. The other reasons for degradation may be due to the transesterification process. It was also observed that initial slight degradation due to evaporation of absorbed moisture due to the hydrophilic nature of nHAp. The temperature at which more degradation happens is at 335°C in case of neat PLA, which enhances continuously up to 20° C with an increase in filler loading up to 3% nHAp. After this when the loading of nHAp was more, then the peak temperature was reduced. The reason may be due to the loading of nHAp filler leads to create shorter polymer chains, which need less thermal energy to degrade it. The DTG curve shown in Figure 2.13, which gives the information about the temperature which the maximum degradation of PLA and PLA/nHAp composite occurs.

Table 2.2: Thermal behavior of PLA and PLA/nHAp biocomposites.

Sample name	nHAp loading	TGA		
		T onset (°C)	T max (°C)	T offset (°C)
PLA	-	315	335	365
PLA/nHAp	3	325	353	372
PLA/nHAp	5	341	355	376
PLA/nHAp	7	320	346	372
PLA/nHAp	10	318	343	362

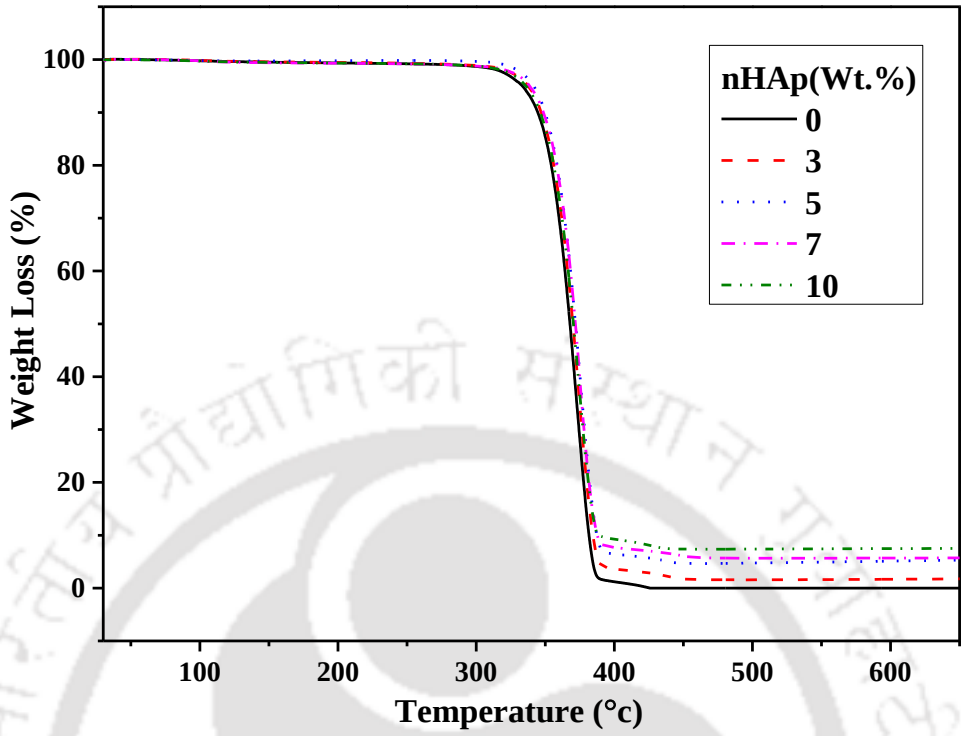

Figure 2.12: TGA thermo gram of the fabricated PLA and PLA/nHAp composites.

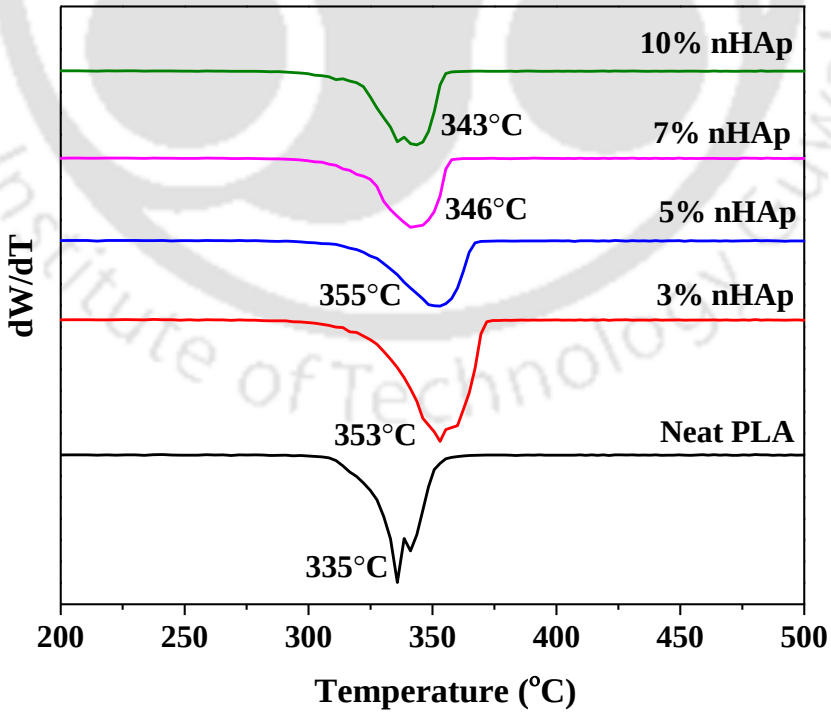

Figure 2.13: DTG profile of PLA and PLA/nHAp composites.

The reason for the main degradation is due to breakage of longer chain into a shorter chain in the presence of more loading of nHAp fillers [126]. Hence for the lower loading, nHAp filler promotes the thermal stability of the composite, and when the loading of nHAp filler was more, this same filler promoted thermal degradation of the PLA. The value of onset degradation temperature and the offset degradation temperature of the biocomposite is shown in Table 2.2.

2.5.5 Gel permeation chromatography (GPC)

The molecular weights (number average molecular weight (Mn), weight average molecular weight (Mw)) and polydispersity index (PDI) of PLA and PLA/nHAp bio composite were evaluated using gel permeation chromatography techniques (Shimadzu LC-20A system, Shimadzu, Japan). It is fitted with two PL gel 5µm mixed D columns (Agilent, U. K) in series, which was working with an eluent (HPLC grade chloroform) at 1 mL/min and sample injection volume of ~40 mL.

Table 2.3: Molecular weight of PLA and PLA/nHAp biocomposites.

Composites	**M_w**	**M_n**	**PDI(M_w/ M_n)**	**Area (%)**
Neat PLA	1,38,516	76,251	1.81	100
3% nHAp	1,08,698	63,460	1.71	100
5% nHAp	98,798	55,704	1.77	100
7% nHAp	92,856	51,387	1.80	97.4
10% nHAp	91,953	50,735	1.81	97.6

The system was calibrated with a wide molecular weight range of polystyrene (PS) standards. The samples (~30 mg) were solubilized in HPLC grade chloroform (~1 mL) followed by filtration using PTFE syringe filter (0.25um) before analysis. The Table 2.3 shows the value of Mw and Mn of PLA and PLA/nHAp composites. It is observed that up to 5% nHAp, the molecular weight was observed increasing and later on when the concentration of nHAp filler loading was increased, the value of Mw gets reduced. The reason may be due to the formation of larger chains of the polymer into smaller chains [127].

2.5.6 Differential scanning calorimetry (DSC)

The thermal behavior of extruded PLA/nHAp samples (~6−7 mg) was examined through differential scanning calorimeter (Make: NETZCH, model: Phoenix 204) under a nitrogen atmosphere with a flow rate of 60 mL/min. Two thermal cycles were applied for analysis in which the first cycle was from 30 to 200 °C at a scanning rate of 10 °C/min, followed by the isothermal condition for 2 min at 200 °C and further cooling from 220 °C to 30 °C with the same scan rate.

The second cycle was repeated the same as that of the first cycle to erase the thermal history. Further, the sample was cooled down up to 30 °C at 10°C/min and the temperature maintained for one hour to ensure the completion of the crystallization phenomena. Finally, the sample was cooled up to 30 °C at a rate of 10 °C/min. The curve was plotted to form the data obtained by second cycles. Figure 2.14 shows the thermograph obtained through DSC. It was conducted to know the melting and crystallization behavior of the samples with two heating and cooling cycles. The purpose of first heating was to remove the physically and chemically bounded moisture from the extruded PLA/nHAp bio composites. The glass transition temperature is decreasing concerning adding filler loading due to the plasticizing effect. A small reduction is seen in the cold crystallization temperature of the PLA bio

composite with an increase in loading of nHAp filler. It may be due to the presence of deformed shape and size of some of the crystal in the PLA matrix.

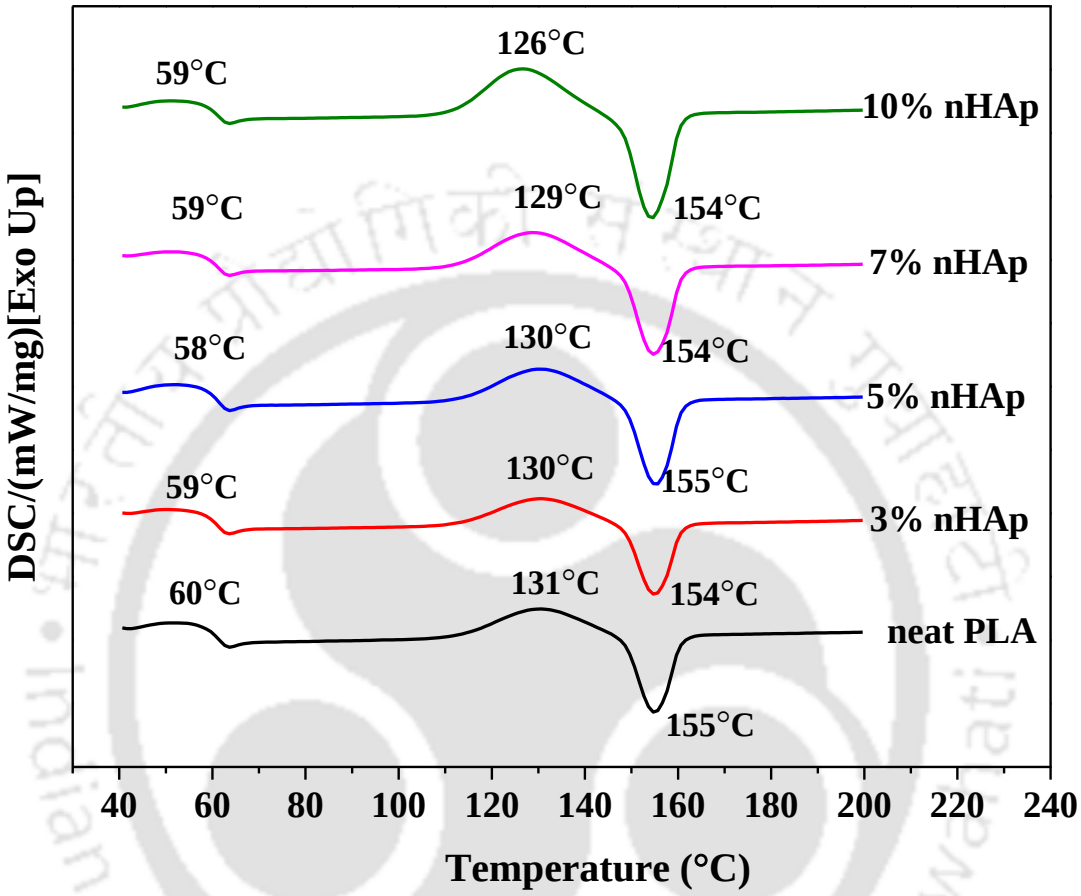

Figure 2.14: DSC profile of PLA and PLA/nHAp composites.

The melting peak was also observed decreasing with the increase in loading; it may be due to the heterogeneous distribution of crystals as well as no uniform crystal thickness. Single glass transition temperature (T_g) has been seen in the thermograph, which suggests uniform distribution for each combination of PLA/nHAp bio composite. Hence no phase separation has occurred.

2.5.7 Fourier transform infrared spectroscopy (FTIR)

The identification of various functional groups presents in nHAp, neat PLA and PLA/nHAp biocomposites are confirmed by FTIR analysis as shown in Figure 2.15. The FTIR spectra of the biocomposites were measured by attenuated total reflection (ATR) mode in Frontier FTIR spectrometer (Perkin Elmer, USA) at room temperature. The spectra were recorded after 16 scans from the wave number 4000 cm^{-1} to 550 cm^{-1}.

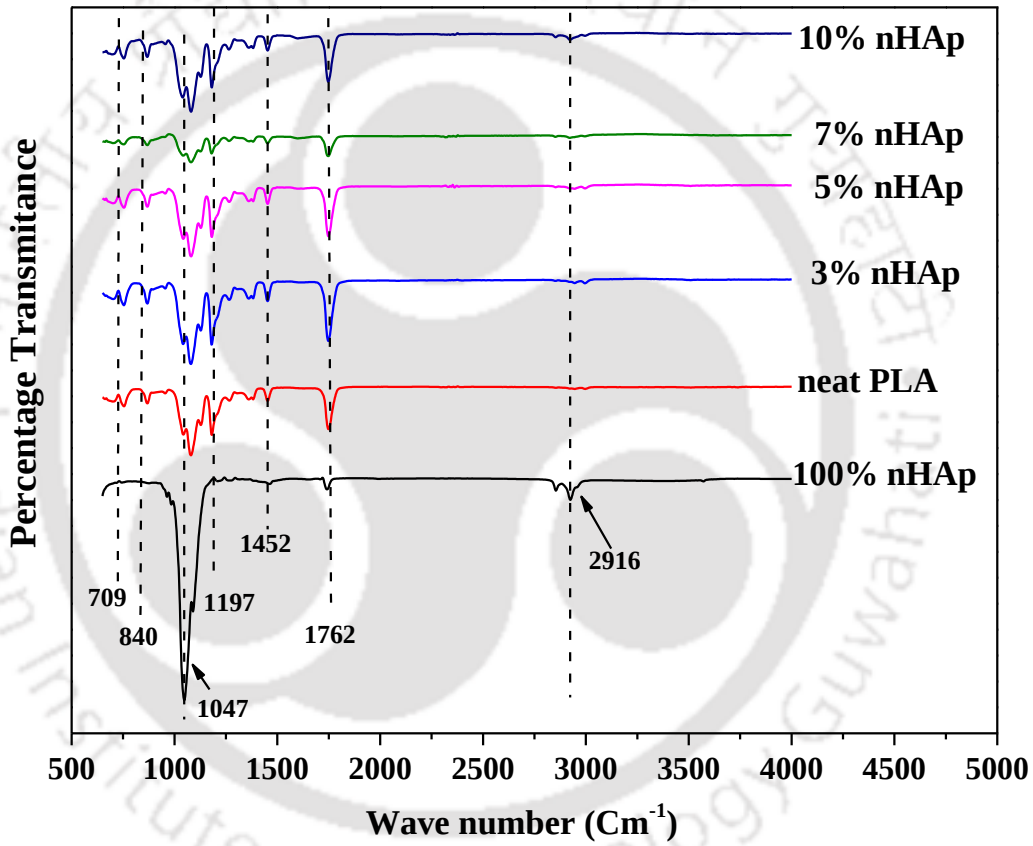

Figure 2.15: FTIR spectroscopy profile of the nHAp and PLA/nHAp composites.

The prepared biocomposite was directly analyzed, and the spectra were recorded. The absorption band at ~840 cm^{-1} corresponds to -c-c-c- stretching of the backbone of the PLA molecule. The absorption band at 1452 cm^{-1} corresponds to the bending of the methyl group. The absorption band at 1762 cm^{-1} corresponds to C=O of the PLA. Whereas the band at 2916

cm^{-1} corresponds to C-H bonding of PLA. In case of nHAp powder, the broadband centered at about 1000-1100 cm^{-1} for P-O bond of phosphate group was observed. The major peaks at ~1047 cm^{-1} and ~1097 cm^{-1} identified as symmetric vibration of PO_4 group and is the most intensified peak among the other phosphate group. The bands at 960-968 cm^{-1} and 568-620 cm^{-1} are due to symmetric P-O stretching vibrations of the PO_4 group respectively.

The band assigned to the stretching mode of a hydroxyl group (O-H) in the nHAp was observed at ~2750 cm^{-1} and ~3000 cm^{-1}. It was also observed that shifting of the peaks was present at ~1047 cm^{-1}, which indicates that the concentration of nHAp was increasing [128].

2.5.8 Mechanical Properties

The uniaxial mechanical properties of injection molded PLA and PLA/nHAp bio composite dumbbells were measured using the universal testing machine (Kalpak Instruments and controls, KIC-2-050-C), equipped with 500 N load cell with a cross head speed of 1mm/min at room temperature. The dimension of the dumbbell shaped samples was prepared and tested as per ASTM D638 standards. The pre analysis conditioning of test samples was done at 24 ± 5 °C and 60 ± 5% relative humidity (RH) for 48 hours. The ultimate tensile strength was calculated by the ratio of the peak load and cross-sectional area of the samples. The elongation at break was calculated by the ratio of the elongation at the fracture point and the initial length of the specimen followed by multiplication by 100. The values of young's modulus were determined from the slope of the stress strain curve. Three samples of each combination were tested, analyzed and reported the average values with standard deviation. Figure 2.16 shows the value of elastic modulus of the PLA with varying concentration of nHAp. It was observed that the loading of nHAp leads to increment in the value of elastic modulus. The value of elastic modulus was calculated and plotted in Figure 2.16, it was observed that for neat PLA, the value was about 2.79±0.30 GPa and when the loading of

nHAp was increased then in case of 3% nHAp, the value becomes 3.54±0.57 GPa and in case of 10 % nHAp it was 3.93±0.33GPa, i.e. 40.86% increase with respect to neat PLA. The value of elastic modulus is coming in the range of the various literature available [129-130].

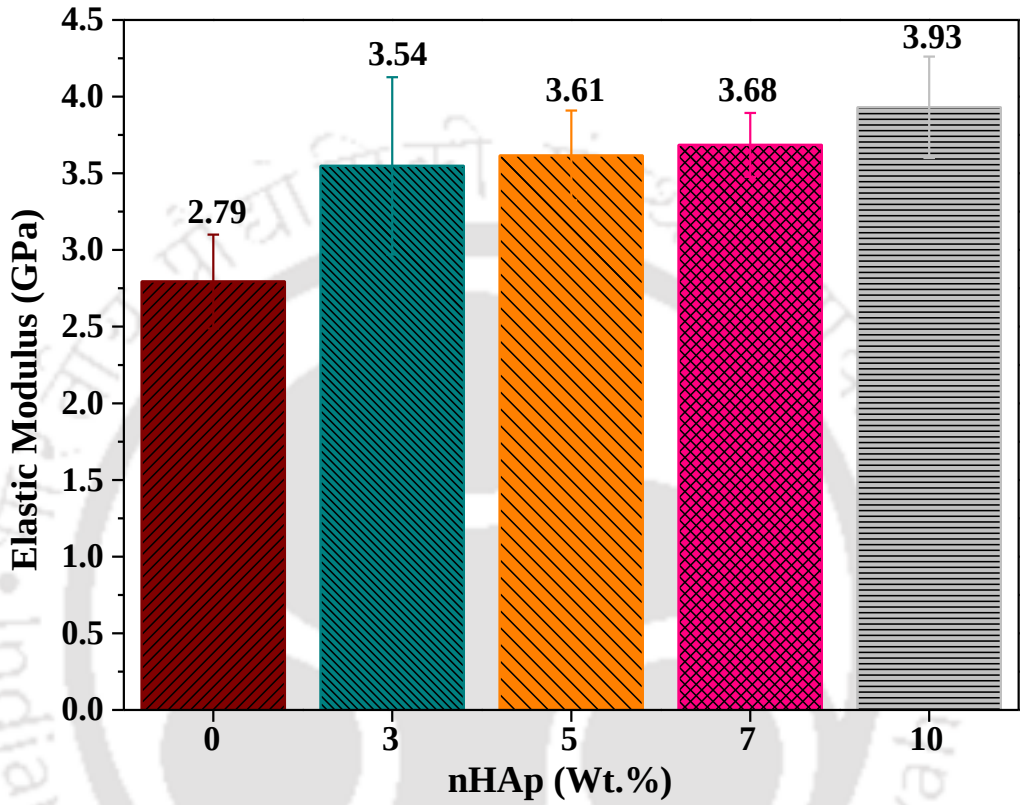

Figure 2.16: Value of Elastic modulus of the PLA with varying concentration of nHAp.

The reason may be due to the enhancement in the entanglement of the polymer chain. The nHAp act like the entangling agent and also provide the more surface area which has a good interaction with the PLA chains and thus the entangling of the chain occurs.

Figure 2.17 shows the value of percentage elongation with varying the concentration of nHAp. The value of percentage elongation was calculated 11.56 ±2.09 in case of neat PLA while for 3% nHAp, it was decreased to 11.28 ±1.27 and the same trends were observed after

loading of nHAp filler. The reduction observed from 11.56 ± 2.09 to 8.95 ± 1.24 which is equal to ~22% reduction. The associated reason may be due to the brittle nature of nHAp.

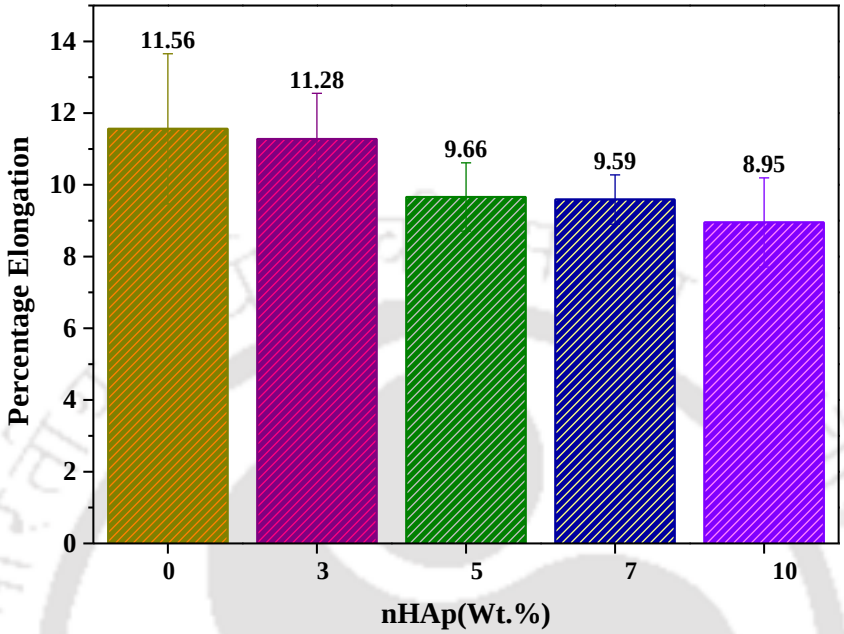

Figure 2.17: Values of percentage elongation of the PLA with varying concentration of nHAp.

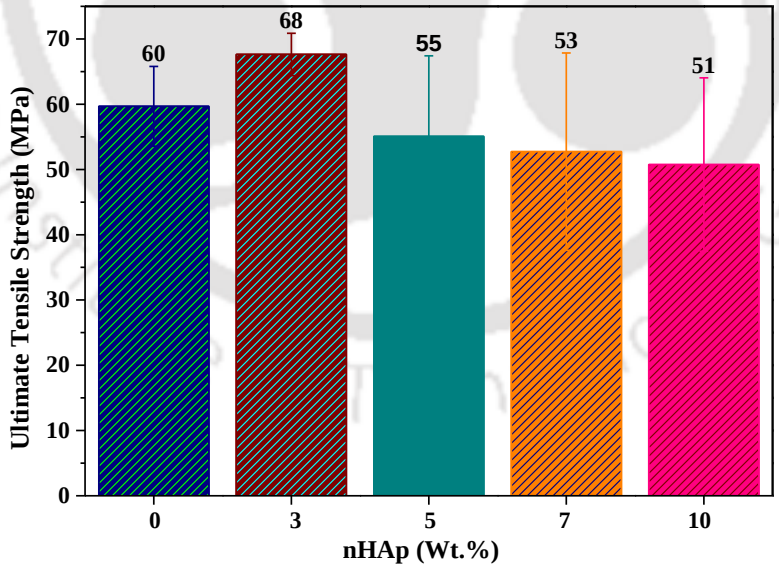

Figure 2.18: Values of ultimate tensile strength of the PLA with varying concentration of nHAp.

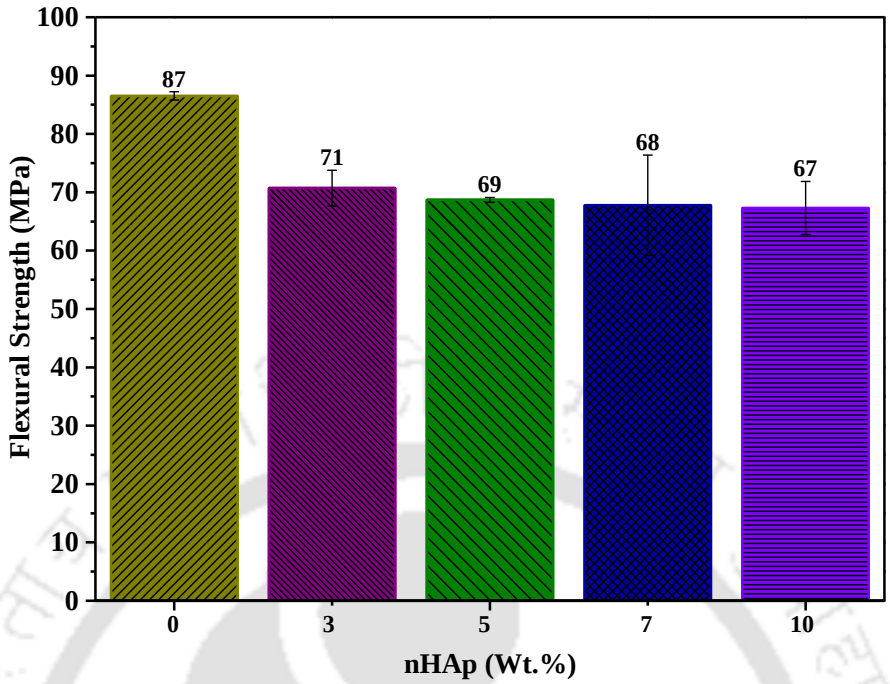

Figure 2.19: Values of flexural strength of the PLA with varying concentration of nHAp.

Figure 2.18 shows the value of the ultimate tensile strength of the PLA and PLA/nHAp composites. It was observed that in the case of neat PLA, the UTS value was 60±6.10 MPa in case of neat PLA, at a lower concentration the increment was observed to 67.62±3.24 MPa, i.e. ~12% increment. However, at more loading of nHAp, the UTS value was reduced, the reason may be due to the presence of nHAp in PLA matrix, which breaks the longer chain of PLA in to shorter chains, and when under the application of tensile load, these smaller chains align themselves and create less entanglement. Which results in a reduction of UTS values. The reduction was observed ~51±13.28 MPa (~14% reduction) in the case of 10% nHAp concerning neat PLA.

The flexural strength was also observed reducing at higher concentration nHAp filler. The value of flexural strength was calculated through a three point bend test. The flexural strength was calculated using the equation 2.1.

$$\sigma = \frac{3FL}{2bd^2} \quad \text{.....} \quad 2.1$$

Where σ = flexural strength, F = load (N), L= Span length, b = width and d = thickness of the sample. The test was conducted as per ASTM D790. It was observed that from Figure 2.19, the value of the flexural strength was reduced from 87±0.7 MPa (neat PLA) to 67.29±4.54 MPa (10% nHAp) i.e. ~23% reduction. The reason associated may due to weak intermolecular hydrogen bonding between PLA chains and nHAp crystals. The other reasons may be due to agglomeration of nHAp particles, which leads to the development of brittle fracture since the nHAp filler are brittle in nature.

2.5.9 Hardness Test

The shore hardness of the melt blended PLA and PLA/nHAp biocomposite dumbbells were carried out using Durometer (GGR-30, Hiroshima) based on ASTM D2240 at atmospheric conditions. The average hardness value was reported by measuring five different positions in each composition. The hardness value for neat PLA was about ~77.6 ± 4.7 shore D (Figure 2.20), it was observed increasing when the concentration of nHAp filler was increased. The more presence of nHAp mobilise the polymer chain to a lesser extent thus, increasing the hardness.

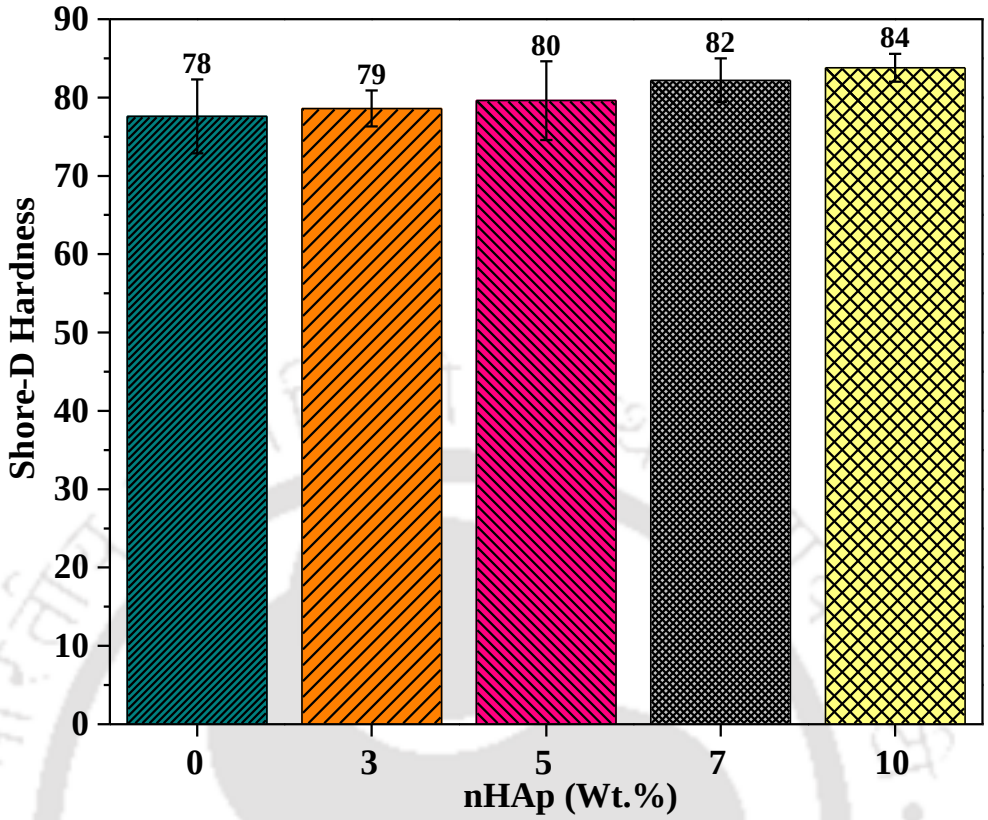

Figure 2.20: Values of the hardness of the PLA with varying concentration of nHAp.

2.5.10 Density measurement

The density of the PLA/nHAp composite was determined by a density measurement (make: Analytical Instruments, India) apparatus. Archimedes's principle is applied for determining the specific gravity of samples. A polymer sample immersed in a liquid (water) was exposed to the force of buoyancy. The value of this force was the same as that of the weight of the water displaced by the volume of the polymer sample. With a hydrostatic balance, which enables one to weigh the polymer sample in the air as well as in water, it is possible to determine the specific gravity of the polymer sample, if the density of the water is known using the equation 2.2.

$$\rho = \left(\frac{Wa}{Wa-WL}\right)\rho L \ldots\ldots\ldots\ldots\ldots\ldots\ldots\ldots\ldots\ldots 2.2$$

Where ρ is the specific gravity of the PLA/nHAp composite. ρL is the density of the liquid, Wa is the weight of the polymer in the air, WL is the weight of the polymer in liquid. For each sample, five measurements were performed, and average values with standard deviation are reported.

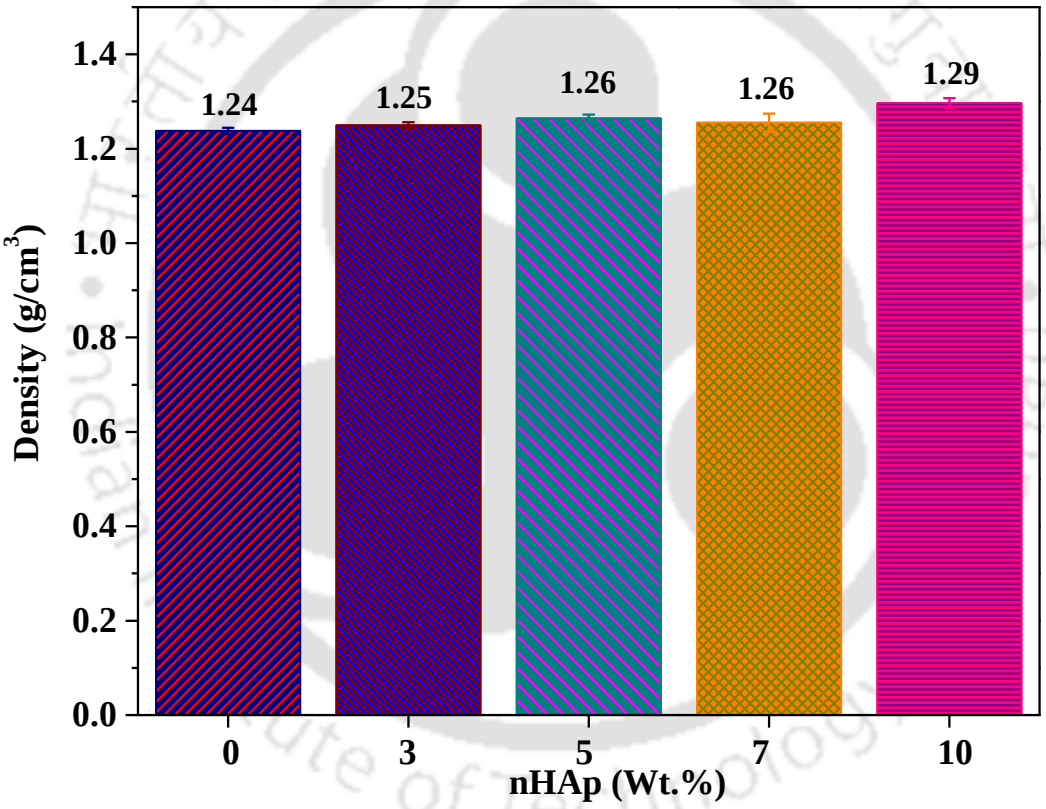

Figure 2.21: Values of the density of the PLA with varying concentration of nHAp.

Figure 2.21 shows the value of the density of neat PLA and PLA/nHAp biocomposites towards an increase in filler concentration. It was observed that the density was continuously increasing as the filler concentration was increased. In the case of neat PLA, the density

calculated was 1.23±0.006 g/cm3, while in the case of 10% nHAp, density was calculated 1.33±0.04 g/cm3, i.e. increment of ~8 %. The increasing trends of density may be due to the mass of nHAp per unit volume was increased.

2.5.11 Surface wettability

The contact angle measurement of the fabricated nHAp and PLA/nHAp composites was done using contact angle measurement system (KRUSS, DSA25, Germany) with ~4µL drop volume of Millipore water at 27° C by a sessile drop method. The liquid drop was injected on the samples by the syringe (fitted above the sample holder). The samples were prepared by dissolving the polymer in chloroform solvent and poured the solution on a glass slide. Further, the samples were dried overnight at ~50° C in a vacuum oven. During analysis, the droplet geometry was captured with the help of a camera, fitted in the front of the sample holder. The surface wettability of PLA and PLA/nHAp composite has vital importance in the application in biomedical applications. The contact angle were measured only after the stabilization of the droplet on the samples and the measurement was replicated for five times (for each measurement a new spot was selected) and the average values were reported with standard deviation. It is also known that the contact angle of the samples also depends on polymer structure, surface roughness, chemical functionality, crystallinity and charges on the surfaces including the process of sample preparation. Figure 2.22 (a-f) shows the contact angle images captured by the contact angle measuring instrument. Figure 2.23 shows the value of contact angle of nHAp, PLA and PLA/nHAp composites. The contact angle values of neat PLA is measured as ~84.8, which is the closest value of the available literature. The value for nHAp was observed ~62.8. As the concentration of nHAp was increased, the contact angle value gets decreased, which signifies that materials are tending towards hydrophilic.

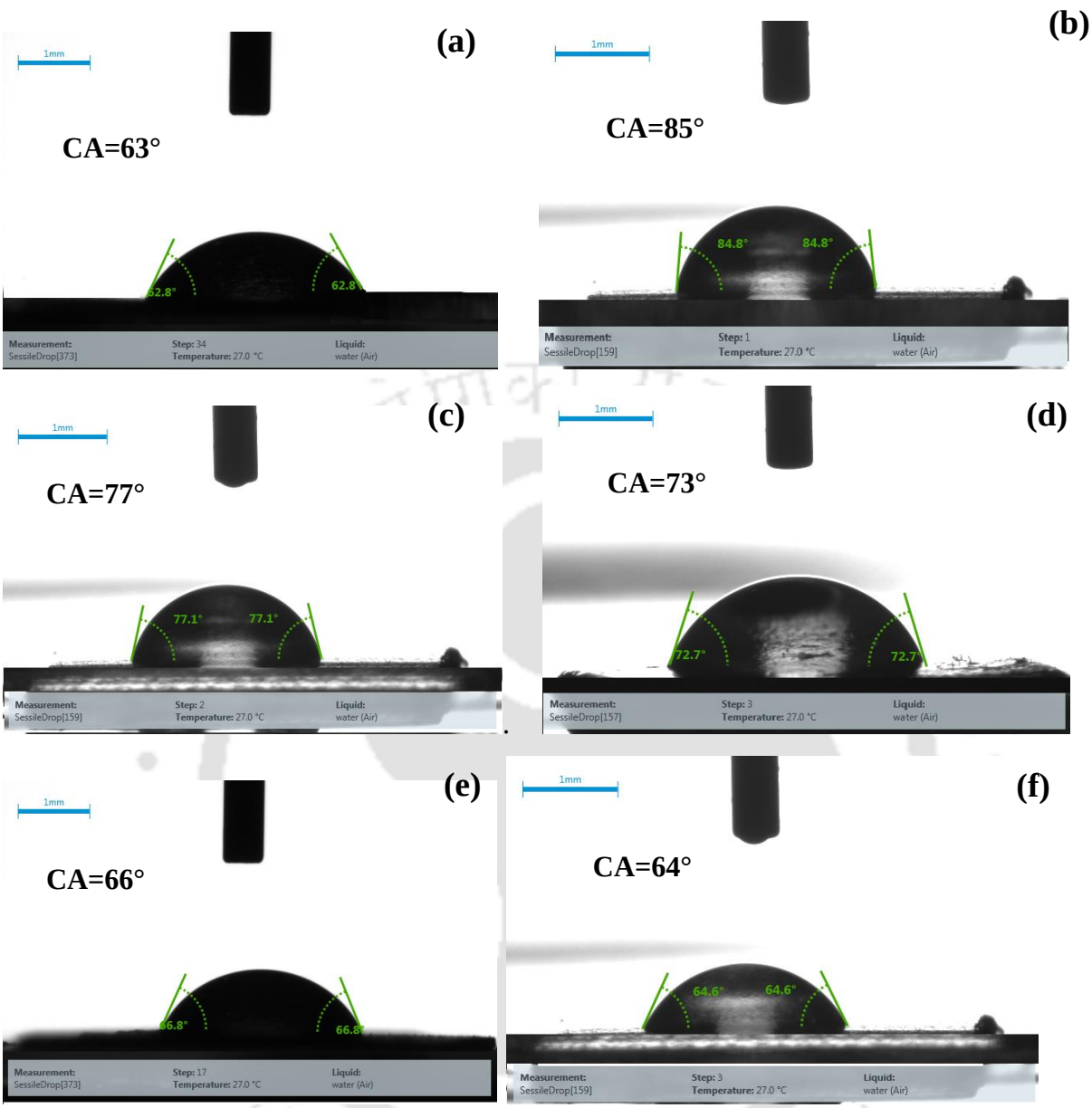

Figure 2.22: contact angle measurement of (a) nHAp, (b) Neat PLA, (c) 3% nHAp, (d) 5% nHAp, (e) 7% nHAp, (f) 10% nHAp biocomposite strips.

The 10% nHAp composite, the angle value was ~64.6°. The presence of a nHAp particle on the surface of the PLA matrix makes the surface rough, and it is also known that nHAp is hydrophilic; thus the increment in concentration results in an increment in hydrophilicity. The enhancement in surface wettability properties is good for cell proliferation and cells

attachment for a particular application of this type for applications as internal fixation devices.

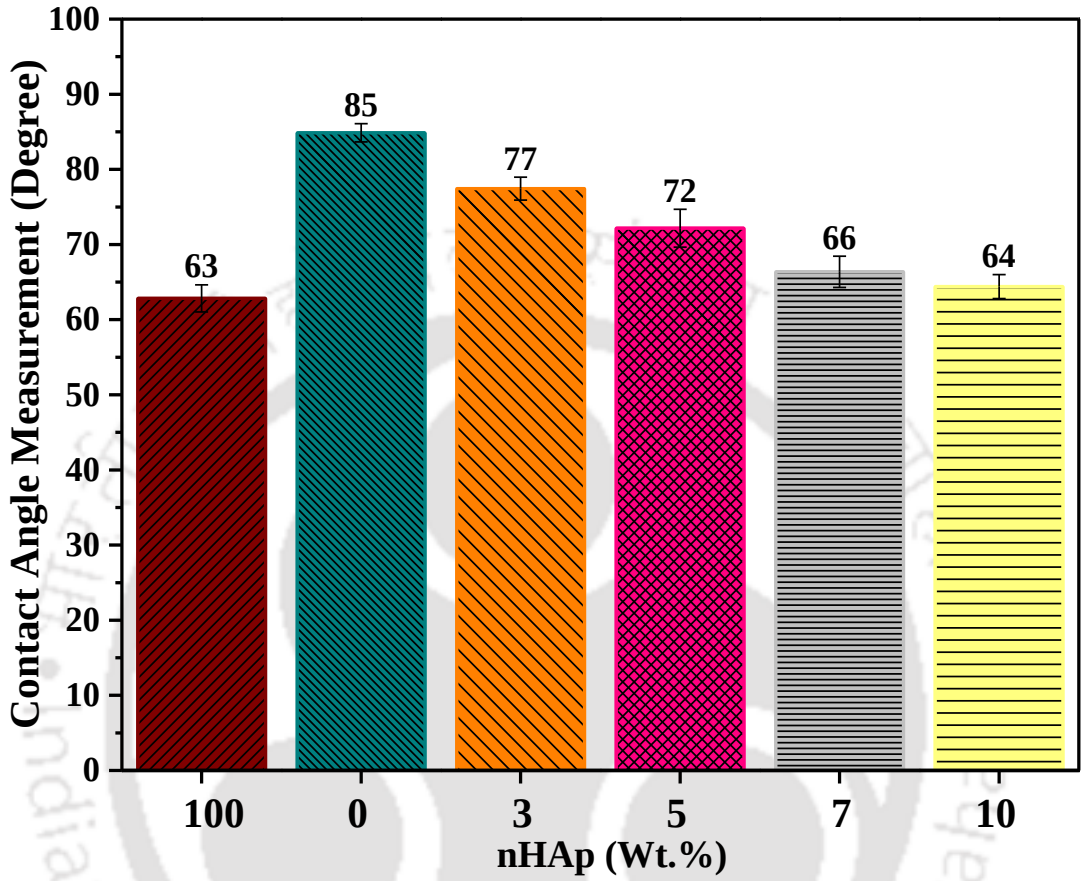

Figure 2.23: Contact angle value of nHAp, PLA and PLA/nHAp composites.

2.5.12 Polarized optical microscopic studies

The spherulite morphology, growth rate and nucleation in melt extruded PLA and PLA/nHAp biocomposite strips were measured using polarized optical microscope (Eclipse) LV 100N POL. Nikon Co., Japan) equipped with Linkam TST350 hot stage (Linkam Scientific Instrument) at the isothermal condition. The sample (~2mg) was sandwiched between two cover slides and melted at 190°C for two minutes to obtain a thin space. The slice was transferred to the hot stage and heated up to 200° C at a heating rate of 20 °C /min followed by the isothermal condition for 3 min to erase the thermal and mechanical history.

Afterwards, the samples were cooled to 110°C at a heating rate of 20°C /min followed by the isothermal condition for 1 hour (until complete crystallization).

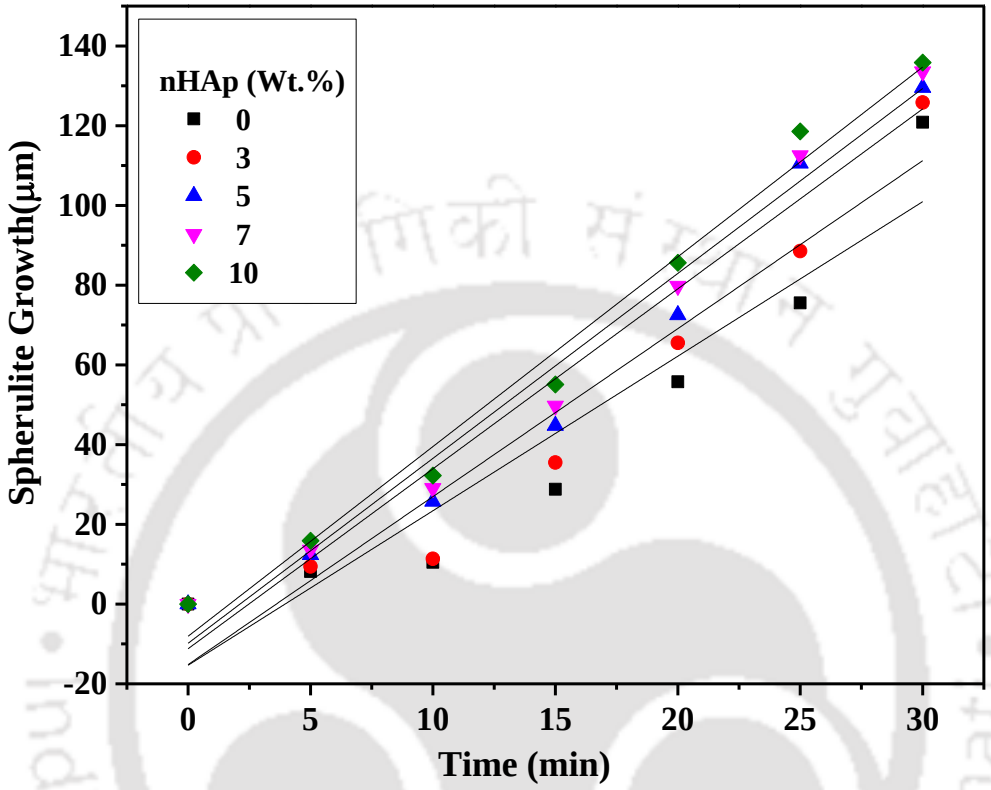

Figure 2.24: Radial growth of spherulite of the PLA and PLA/nHAp biocomposite.

The spherulite morphology was recorded in the crystallization process using an attached stationary digital camera. Figure 2.24 shows the growth of spherulite concerning time. It was observed that as time was increased, the radius of the spherulite also increased.

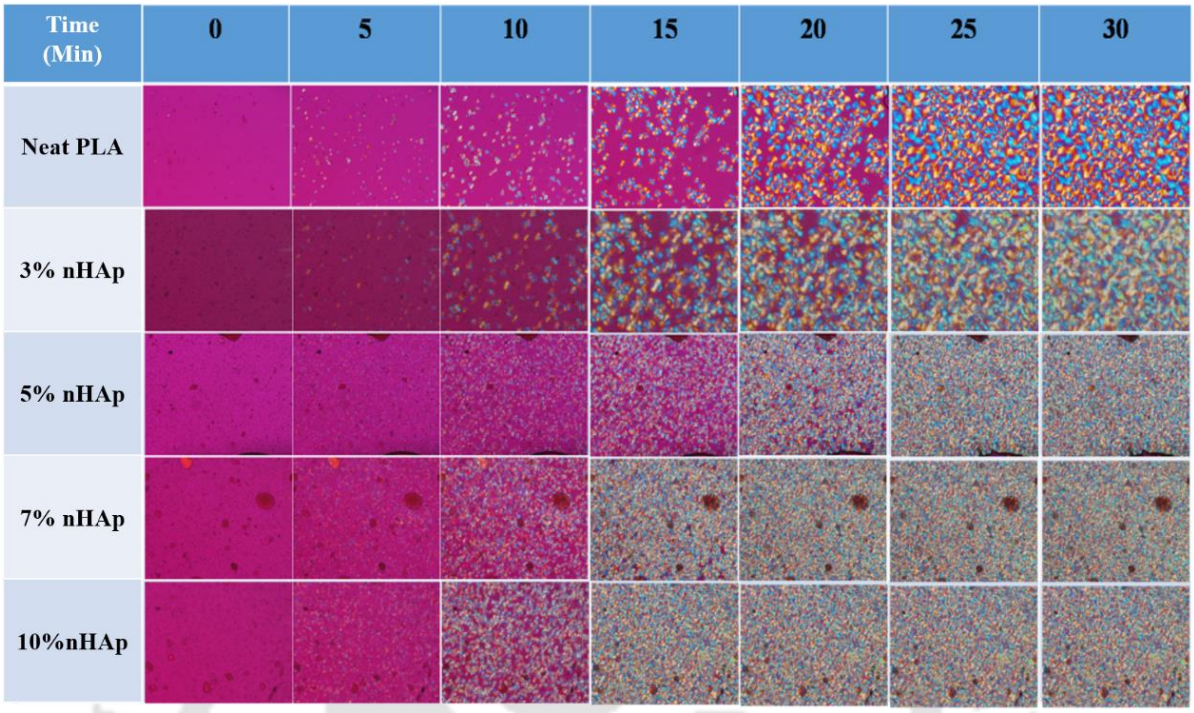

Figure 2.25: Polarized optical micrograph of neat PLA, and PLA/nHAp composites at a particular time interval.

Table 2.4: Value of density and Spherulite growth rate for PLA and PLA/nHAp composites.

Samples	Density (No. of Spherulite/mm^2)	Spherulite Growth Rate (μm/min)
Neat PLA	0.1066	3.87±0.55
3% nHAp	0.0871	4.21±0.49
5% nHAp	0.0864	4.51±0.37
7% nHAp	0.0758	4.63±0.30
10% nHAp	0.0721	4.75±0.26

Figure 2.25 shows the spherulite growth at particular time duration for PLA and PLA/nHAp composites. It is observed that as the loading of the nHAp was increased, the growth of crystals was happens at early stages. This suggests that nHAp help the growth of spherulite of the PLA matrix. The value of density and spherulite growth rate is shown in Table 2.4. It

is observed that the growth rate of neat PLA was ~ 3.87 µm/min while in case of 10% nHAp ~23% increment, i.e. 4.75 µm/min was observed.

2.5.13 Bioactivity studies

In this studies, neat PLA and nHAp reinforced PLA, i.e. PLA/nHAp composites were investigated bioactivity of the samples in the lab made simulated body fluid (SBF). The samples were in the size of 10x10x5 mm^3, respectively. First, all the specimens were dried in a hot air oven at 50° C and then allowed to normalize at room temperature in a desiccator. The samples were immersed in a glass container containing SBF (pH 7.4) at a constant temperature of 37° C for nine weeks. The samples were taken out from the glass jar after every week and pH were also measured during taking out samples. The SBF solution were made as per the available literature [131].

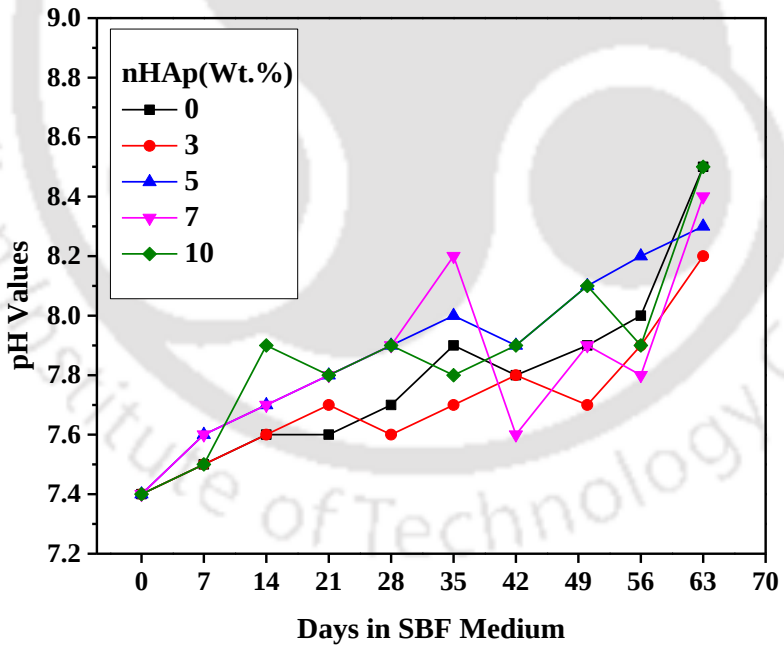

Figure 2.26: Profile of pH value concerning a number of immersion day in SBF.

When the samples were incubated in SBF. The formation of apatite layer on the surface of the pellet goes through a sequence of a chemical reaction like spontaneous precipitation,

nucleation and growth of calcium phosphate [132-133]. In this whole process, surface chemistry plays a vital role and even the functional group of the materials have the larger effect on the bone bonding properties. It is known that nHAp structure consists of $CaPO_4$ and OH groups closely packed together.

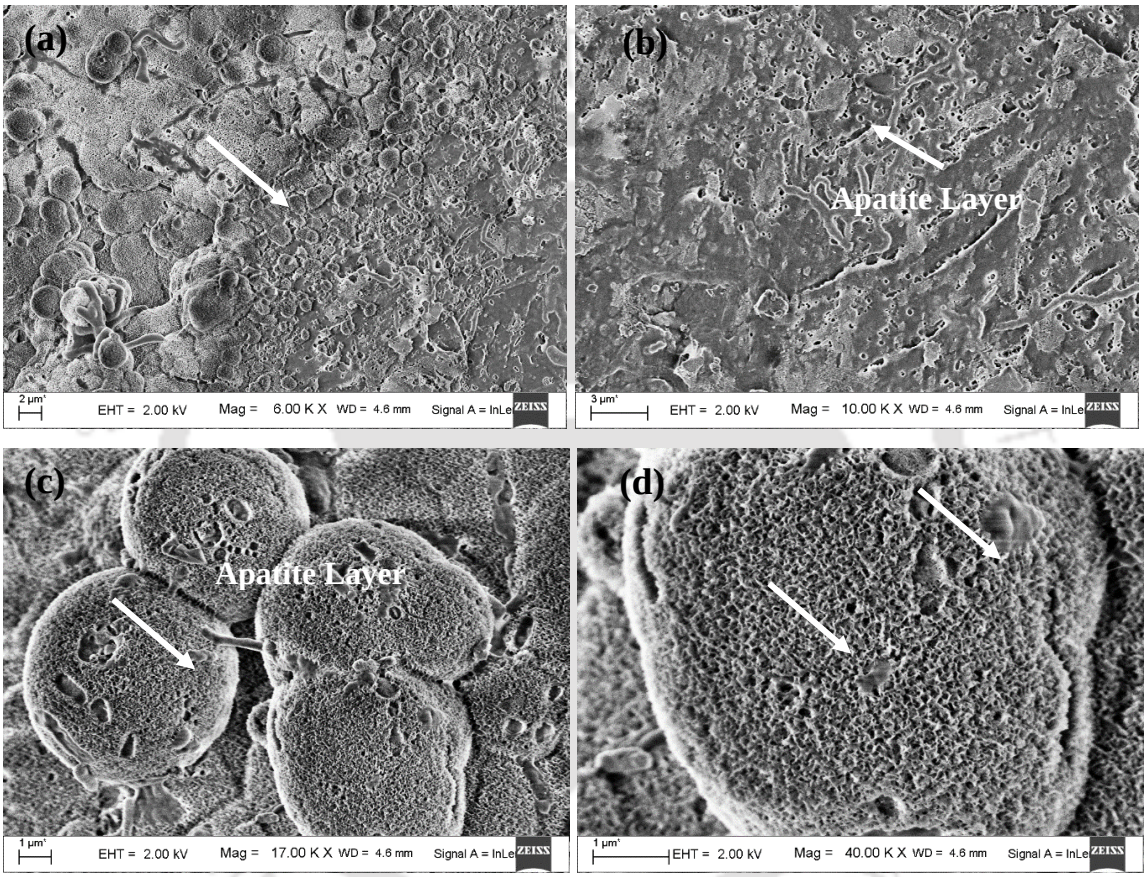

Figure 2.27: Formation of apatite layer on the surface of PLA/nHAp composites after five weeks.

The OH^- and PO_4^{3-} groups are responsible for the negativity of nHAp surface and Ca^{2+} from the positive charge on the nHAp surface. Therefore the surface gains the positive charge with respect to the surrounding SBF and further attracts the negatively charged OH^- and PO_4^{3-} ions from the SBF [134]. This leads to the formation of the apatite layer.

Figure 2.26 shows the profile of pH with respect to immersion days of samples.it was observed that as the days were immersion days were increasing the value of the pH were also increasing. This suggests that some interaction between PLA and nearby SBF was occurring. The Figure 2.27 (a-d) shows the images from FESEM showing the formation of apatite layer on the surface. The EDX analysis of the apatite layer formed on PLA/nHAp composites is shown in Figure 2.28.

2.5.14 Hydrolytic Degradation studies

The *In vitro* hydrolytic degradation studies were carried out by ASTM F1635-11 (Standard Test Method for *In vitro* Degradation Testing of Hydrolytically Degradable Polymer Resins and Fabricated Forms for Surgical Implants) in phosphate buffer saline solutions (0.1M) (KH_2PO_4 and K_2HPO_4). The corresponding pH of the PBS was maintained at 7.4 at 37° C, respectively. Samples were placed in small bottles containing 200 ml of buffer solution and maintained at 37° C in orbital incubator. Samples were periodically removed, washed with distilled water, and placed between filter paper to remove the surface water. The samples were weighed again after drying for 6 hours in a vacuum oven at 60° C. Figure 2.29 shows the profile of the pH of the samples during *In vitro* hydrolytic degradation studies. It was observed that pH was almost maintained constant, equivalent to 7.4. Figure 2.30 shows the mass loss of the samples concerning some days in PBS. In the case of neat PLA, after nine weeks, the mass loss was approx. 12%. While as the nHAp filler introduced, then for the same duration the mass loss was reduced to 10% in the case of 10% nHAp. It was also cleared that for the same duration when the filler introduced the rate of mass loss was reduced. Thus it is noteworthy to mention that by tuning with varying concentration of nHAp, the degradation rate may be varied. Generally, degradation of PLA and PLA/nHAp composites

happens in four stages, in the first stages water diffusion takes place, in which water molecules interact with the surface of the polymer composites.

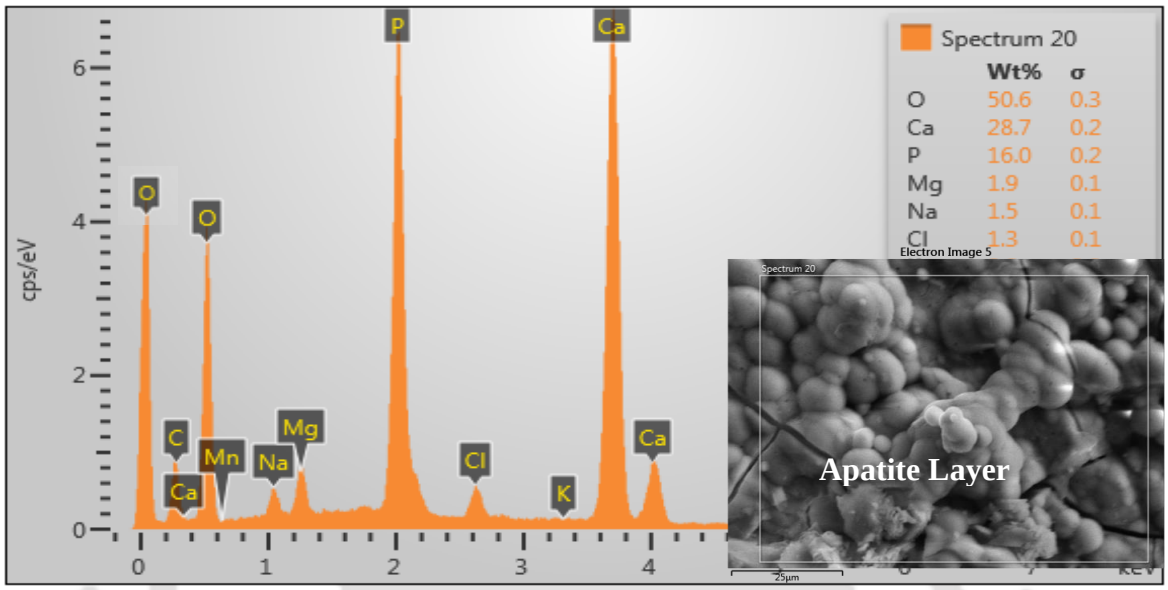

Figure 2.28: The EDX profile of apatite layer formed on PLA/nHAp composite.

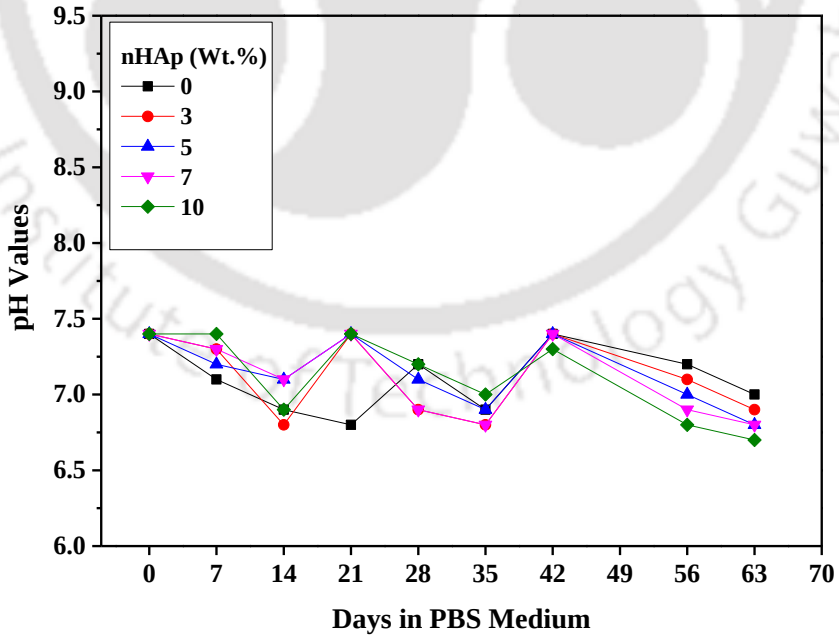

Figure 2.29: Profile of pH value concerning a number of immersion day in PBS solution.

In the second stages, acidic oligomer gets penetrated, and due to autocatalysis, little mass loss was observed, in the third stages, oligomers were diffused outside the polymer matrix composites, and ultimately in the last stages, porous structure with almost homogenous degradation takes place [135].

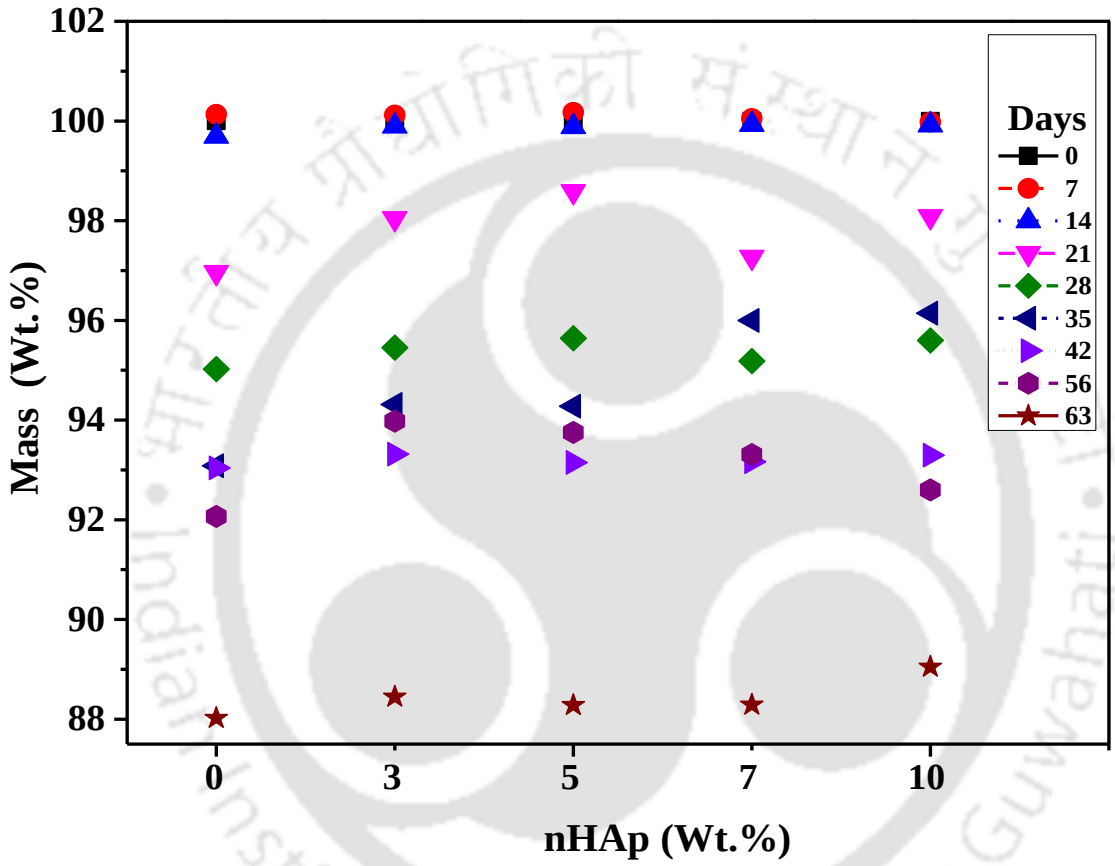

Figure 2.30: Mass loss profile of PLA and PLA/nHAp composite.

Figure 2.31 shows the surface micrograph of the PLA/nHAp composites before and after *In vitro* hydrolytic degradation. It was observed that erosion of polymeric chains takes place which further converts into crack over the surface of the composites. Sometime due to severe degradation, the cavity formation also takes place over the surface as seen in figure 2.31 (d).

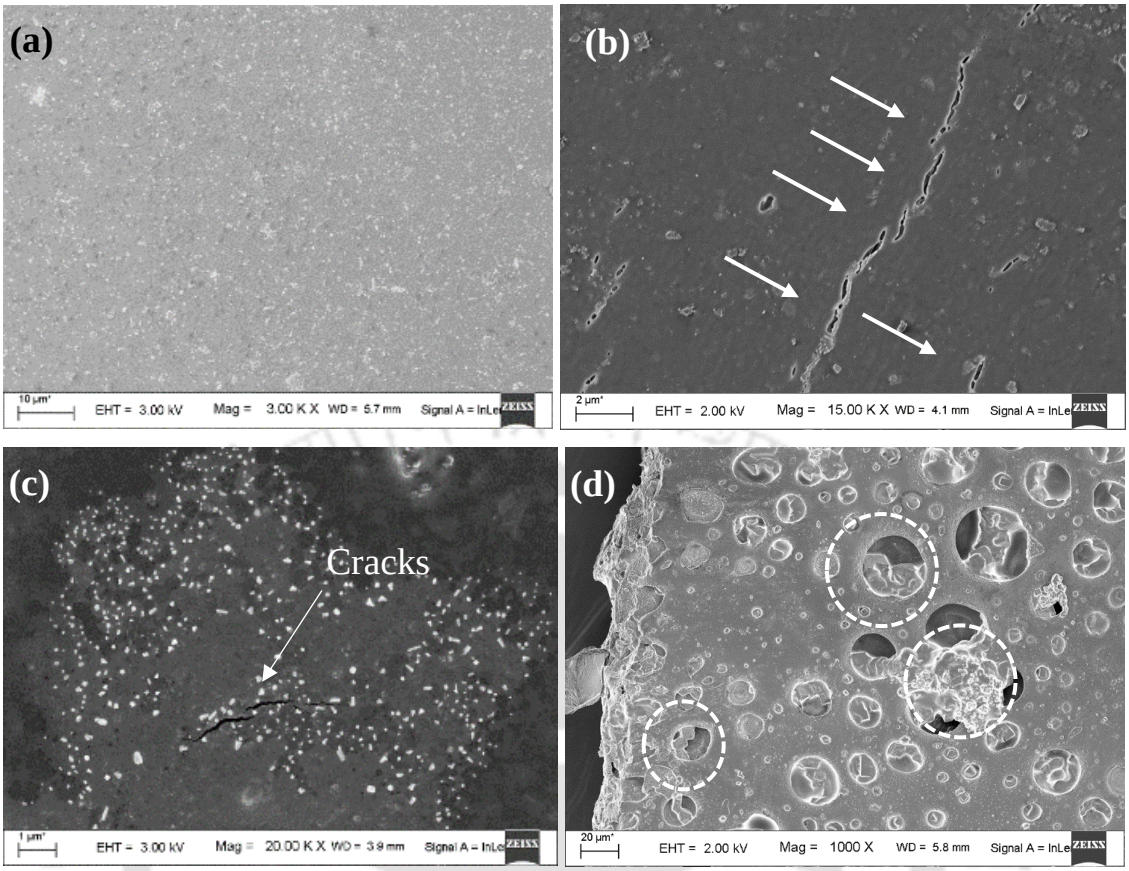

Figure 2.31: FESEM images of the surface of (a) before degradation (b), (c), (d) after the degradation of the PLA/nHAp composites.

2.5.15 Water absorption test

The effect of water absorption on nHAp reinforced PLA composites was investigated by ASTM D570-98. The samples were the size of 10x10x5 mm^3, respectively. First, all the specimens were dried in an oven at 50 °C and then were allowed them to cool to room temperature in a desiccator before weighing them in analytical weighing balance up to 0.1mg. This process was repeated until the mass of the specimens were reached constant. Water absorption tests were conducted by immersing the PLA/nHAp specimens in deionized water in a glass jar at 27 °C for eight weeks. After immersion for 24 h, the specimens were taken out from the water and water on the surface was removed with a clean, dry cloth. The

specimens were reweighed to the nearest 0.1 mg within 1 min of removing them from the water. The specimens were weighed periodically at 24 hours, 1st, 2nd, 3rd, 4th and 5th week exposure. The water absorption was calculated by the weight difference. The weight gain of the samples was measured at different time intervals was plotted as shown in Figure 2.32.

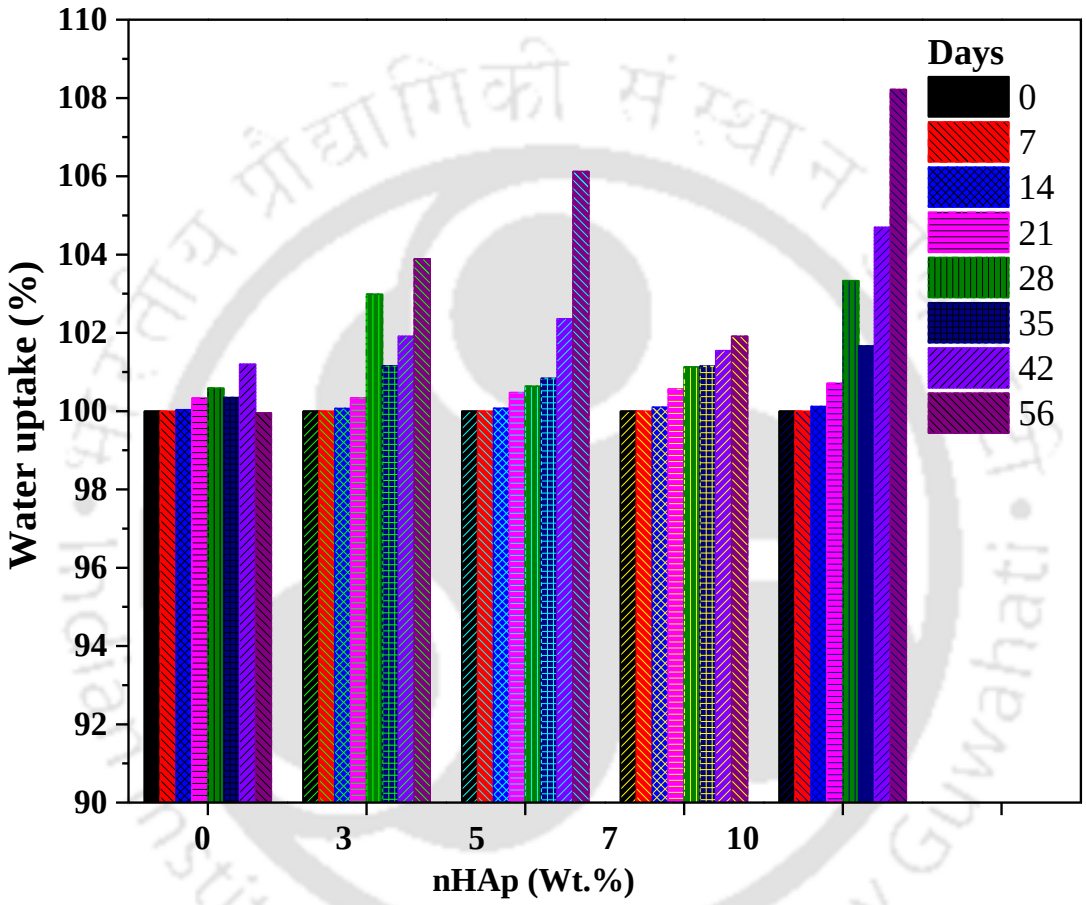

Figure 2.32: Profile of water uptake of the PLA and PLA/nHAp composite concerning a number of days.

It was observed that the PLA/nHAp composite has a water uptake more concerning neat PLA. The reason may be due to the hydrophilic nature of nHAp absorb water, and thus PLA/nHAp composite has more water absorption capability. In the case of 10% nHAp, after 56 days, the water absorption capacity was 8% higher with compared to neat PLA.

2.6 Summary

Thus from this chapter, it is summarized that nHAp was successfully fabricated form the fish scales bio waste. The fabricated nHAp was melt mixed with purified PLA in order to melt mixing cum extrusion and injection molding to make PLA/nHAp composites. The prepared dumbbells and strips of PLA/nHAp was having a uniform thickness, which was further analyzed through various characterization such as thermal, surface, mechanical, bioactivity and biodegradability properties. The XRD analysis confirms about nature of composite as semi crystalline. In FTIR analysis, all the belonging major peaks were observed at their positions for neat PLA and PLA/nHAp composites. Due to agglomeration, the flexural strength were reduced while other mechanical properties such as elastic modulus, ultimate tensile strength were observed increasing due to strong intermolecular hydrogen bonding between PLA and nHAp particles. Surface wettability shows the hydrophilicity nature as the loading of nHAp was increased. The spherulite growth also increased towards the radial direction which was confirmed by polarized optical microscopic studies. From these studies, it was also observed that the rate of degradation was less in the case of PLA/nHAp composites as compared with neat PLA. The bioactivity studies confirm the formation of apatite layer on the surface of the PLA/nHAp composites, which confirms by EDX analysis and FESEM images of the surface of the PLA/nHAp composites.

ABSTRACT

This chapter explains the development and characterization of cortical screws for fixations of fractured cortical bones and to support the bone plates. Various mechanical fixture for testing the fabricated cortical screws was made. The characterization includes mechanical testing as per the ASTM standards for the fabricated cortical screws. The optimization of the properties of the cortical screws was based on consisting superior mechanical properties. After the optimized combination of PLA and nHAp filler, the optimized cortical screw was passed through *In vitro* hydrolytic degradation studies. After this, mechanical test was also repeated so that the mechanical properties during degradation could be accessed.

GRAPHICAL ABSTRACT

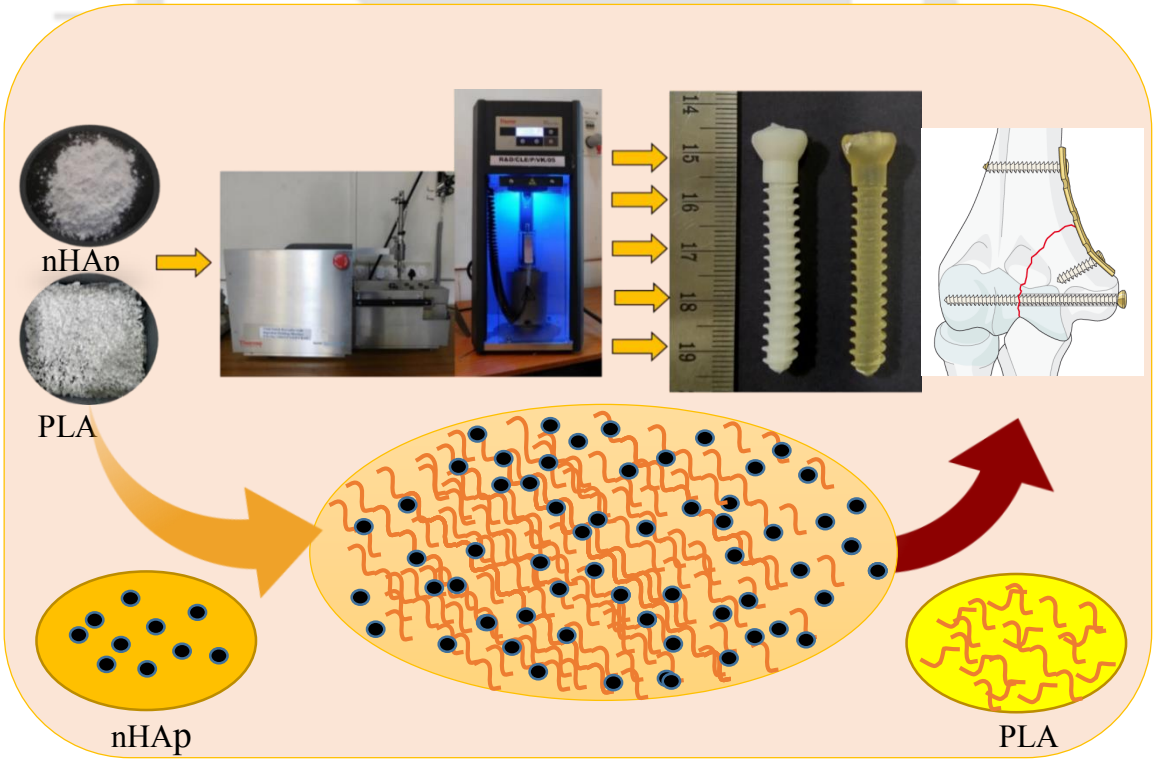

Chapter 3

3 Fabrication and characterization of cortical screws

3.1 Introduction

The orthopedic fracture is increasing day by day. The major reason may be due to trauma or poor living style. Deficiency in intake of the calcium rich foods also leads to weakening of bone and at the moment of a sudden jerk, the fracture of bone usually happens. As already discussed in the previous chapters that, metallic fixation has many limitations like stress shielding, MRI interferences and underlying bone damages. Generally, screws were fixed to support the bone plate to fix the fractured bone or inserted directly into the bone to join the fracture. Various types of screws were used to fix the fractured bone, cortical screws are also one of it, which is usually used to join the cortical part of the bone. The cortical screw is a cylinder with spiral threads running on its outer surface. It converts torsional forces into compression. The primary functional objective in the design of a screw is to dissipate and distribute the mechanical load [136]. The classification of the bone screws is like conventional screws, locking screws, headless screws, and cannulated screws etc. Most of the materials for the screws are Titanium, stainless steel and bioabsorbable polymers. The size comes in the form of 3.5 mm, 4 mm, 4.5 mm, and 6.5 mm outer diameter as standard sizes. The characteristics can be classified as self-tapping, none self-tapping, self-drilling and self-tapping cum self-drilling. Based on its characteristic features, the design of the screws is of conventional, locking, headless and cannulated types [137]. The cortical screw is having of the smaller pitch, number of threads, thread diameter to core diameter ratio is less, designed to better fix in cortical bone and threads are covered fully on the surface. The main advantages

of using bioabsorbable cortical screws are that the cortical screw does not interfere with MRI, does not interfere with future revision surgery if needed and also does not need to remove from the fixations site [138]. Major disadvantages include the breakage of the screws while insertion; it may be due to low mechanical strength. The rate of tuning degradation is also one of the challenges [139]. Various researchers have fabricated cortical screws, but the size was not standard. It was fabricated for demonstration either or craniofacial surgeries [140]. Mostly the researchers have investigated on the material composition side and proposed those composite materials for fabrication of internal fixation devices. Hughes et al. [141] reported both the tensile and torsional strength of screws are critically dependent on the core diameter, and any departures from specified dimensions result in a marked change in strength.

As a consequence, considerable increases in screw strength could be obtained by an increase of core diameter, say to 3.4 mm, this would give an increase in torque strength of about 50 per cent over the current 4 mm (major diameter) screws. Mageed et al. [142] reported internal fixation of proximal fractures of the 2^{nd} and 4^{th} metacarpal and metatarsal bone by the application of bioabsorbable screws. The screws were made of Polylactic acid, and the studies were recorded on the basis of the medical record, diagnostic images, and outcomes between the year 2014 and 2015. The implantation was done in horses. The result showed that eight horses met the inclusion criteria. There were no complications encountered during screw placement or post operatively. On follow up radiographs for 12 months postoperatively, the screws were not completely absorbed.it was also observed that some part of the screws were replaced by nearby bone tissues. Thus it was concluded to be a safe and feasible approach to use as a screw.

Kim et al. [143] reported biocompatibility and efficiency of biodegradable magnesium based plates and screws in the facial fracture model of beagles. In this study, a biodegradable magnesium alloy system was developed as a substitute for conventional plates and screws for facial fractures. The materials for fixations was consist of magnesium alloy mixed with calcium and zinc and an absorbable polymer. The mechanical test showed greater ultimate loads and structural stiffness in the experimental group. Through histological analysis, the void area and bone regeneration area were increased; thus it was concluded that magnesium based biodegradable screws showed good biocompatibility and proposed for application for fixations of cranio-maxillofacial fixations in humans. Yu et al. [144] evaluated *In vitro* and *In vivo* studies of biodegradable Mg-Ag-Y (magnesium-argentum-yttrium) alloys for use as resorbable bone fixation implants. It was observed that one wt. % Ag and one wt. % Y, provider better elastic modulus, tensile and compressive stress than pure mg. it showed close mechanical properties which were matching with the natural bone. Cell toxicity studies confirm that no cytotoxicity effect, and its degraded material was also not harming to the experimental animals. Thus it was suggested as potential clinical applications for use as a resorbable bone fixation implants. Lai et al. [145] reported the effect of pedicle screw diameter on screw fixation efficacy in human osteoporotic thoracic vertebrae. The screw rod type spinal instrumentation is widely used in the treatment of spinal column instability disorder which leads to the loosening of the screws. In this investigation, two sizes of poly axial screws were chosen and randomly implanted into each pedicle of vertebrae. This studies provided a quantitative biomechanical insight in determining the optimal size of pedicle screws for osteoporotic vertebrae based on the utilization of pull out strength testing. The results also indicate that a larger diameter screw achieved superior pull out strength

immediately after the implantation. Schumacher et al. [146] reported HAp based screw like device for anterior cruciate ligament reconstructions. The general procedure to fix the ACL reconstruction requires a graft fixation using interference screws. The alone materials like HAp are having a low strength of such materials. Thus in this study, evaluation of novel geometry for a fixation device made of Hap for ACL reconstruction has been done. The optimization was done by finite element analysis and for experimental in vivo test was done. The multiple threads with a large thread pitch. The novel design enabled the insertion of the screw into bone without the application of an external torque or a screwdriver. In turn, it also allowed for the use of low-strength and high-bioactivity materials, like hydroxyapatite. In vivo tests showed that the novel screw could sustain pull-out forces up to 476 N, which is comparable to that of the commercially available screws. Varghese et al. [147] reported the effect of various factors on the pull out strength of pedicle screw in normal and osteoporotic cancellous bone models. The materials for cancellous bone selected was polyurethane. It was mentioned that the pull out force increases with an increase in density and insertion depth, whereas it decreases with an increase in insertion angle. Thus it was finally concluded that the density in pedicle screw contribute highest towards insertion techniques (82%), pull out strength (76%), stiffness (46%) and strain energy (85%). In the case of osteoporotic bone, the insertion angle did not affect the pull out force. Insertion angle also had no significant effect on insertion torque and is based on the material property of the bone and screw engagement length. Thus finally this studies will play a vital role for planning preoperative development of new implants. Charles et al. [148] reported pull out characteristics of percutaneous pedicle screws with different cement augmentation methods in elderly spines. In these studies, six human specimens (82-100 years) were instrumented percutaneously by non-augmented

screws, vertebroplasty augmentation and fenestrated screws. The screws were oriented at 45° to the horizontal plane. The median pull out forces was 488.5 N for non-augmented screws, 643.5 N for vertebroplasty augmentation and 943.5 N for fenestrated screws. A proximal cement bolus leads to higher pull-out resistance and fracture of the vertebral body before screw pull-out. Downey et al. [149] reported the effect of shear through stiffness and failure strength of a fully threaded versus partially threaded screws. Thirty six synthetic saw bone blocks were used to test screw fixations. Based upon that the construct was made and mechanically tested by applying a shear by compressing each construct at an axial displacement of 0.5 mm/s. it was observed that the fully threaded screw has significantly greater initial stiffness and failure strength than the partially threaded screw when testing shear using compression of axial displacement. The torsion and bending strength of cancellous screws are 30% to 42% lower than those of a cortical screw which was attributed to the smaller core diameter. Thus it was finally concluded as fully threaded screw biomechanically outperformed the partially threaded screw in shear and proved superior in the initial stiffness and failure strength. Perrone et al. [150] reported use of silk based devices for fracture fixation. To avoid stress shielding, silk based material was fabricated in forms of small screws through casting cum mechanical machining methods. Due to the viscosity of high concentration silk solutions, the molding of the silk screw blank was challenging; the high viscosity did not permit uniform flow and settling of the solution in to the molds, resulting into the weld lines where different flow met. In vivo biocompatibility of the screw was also conducted into left hand limb of rats. After 4-8 week time points in vivo, there was early resorption of the silk screw. It was also suggested to include bioactive materials to play with the mechanical strength and degradation rates. Ferretti et al. [151] reported trial of

PLA/PGA screw for fixation of mandibular fractures. Based on the clinical and radiographic examination, internal fixation was achieved with PLLA/PGA screws, which were inserted in 31 patients. Patient were followed up to 1st week, 6 week, 3months, 6 and 12 months post-surgery and evaluated clinically for swelling, pain, mucosal discoloration and occlusal relation. Out of 29, 20 had an uncomplicated post-operative period resulting in the complete bone union. There was no case of non- union at the end of the fixation period. Costi et al. [152] reported comparison of torsional strength of bioabsorbable screws for anterior cruciate ligament reconstruction. The study evaluated the torsional strength and modes of failure in commercially available bioabsorbable interference screws and to test the effect of screw diameter on torsional strength when screw become jammed during insertion. The reason behind the 8 mm diameter screw had a greater failure torque overall is primarily because of the superior strength of the screw in both its design and material. The material was poly-(D, L-lactide) and appears to be more resilient than the poly-(L-lactide) used in most other screws. Chapman et al. [153] reported about factors affecting the pull-out strength of cancellous bone screws. Screws were embedded in porous materials pullout by shearing the internal threads. Experimental pullout force was correlated to the predicted shear failure force which controlled by the major diameter, the length of engagement, the shear strength of the material into which the screw is embedded, and a thread shape factor (TSF) which accounts for screw thread depth and pitch. It was observed that the average TSF for cannulated screws was 17 percent lower than that of non-cannulated cancellous screws, and the pullout force was correspondingly less. Thus from the above literatures, the various researchers were developed the combination of materials and proposed to use as a bone screw, some of them have studied about various mechanical properties and the factors responsible for their failure

and strength. Many researchers from the biomedical side, based upon the radiographic examination, the effectiveness of the screw were studies. But there is a requirement of the bioabsorbable screw which could be used in the conventional plate as well as new bioabsorbable plate available in the standard geometry. In this work, **t**he cortical screws were fabricated through the melt blending cum extrusion through twin screw extruder cum injection molding machine (make: Thermo scientific, model: Hake mini jet). The pressure maintained was in the range of 710-740 bar under compressed air environment. The holding time for injection molding was 5 seconds. In the melt blending process, the fibrous PLA were uniformly mixed with nano HAp and blending was done at 120 rpm for 1 minute. After completion of 1 minute, the material was injected in to cortical screw mold, and after the process of injection, the mold was removed and the finished product were received in the form of screws. The produced cortical screws were further kept in a vacuum oven in order to anneal it. The process parameter kept for cortical screws is shown in Table 3.1. The Figure 3.1 shows the purified PLA in the form of fiber and grinded with the help of grinder to make in powder form.

Table 3.1: Parameters for cortical screws production.

Parameters		
1.	Processing temperature	190°C
2.	Mold temperature	95°C
3.	Cylinder temperature	215°C
4.	Residence time	1min
5.	Twin screw speed	120 rpm
6.	Compressed air pressure	710-740 bar
7.	Injection pressure holding time	5 sec
8.	Weight of cortical screws	1.48 g

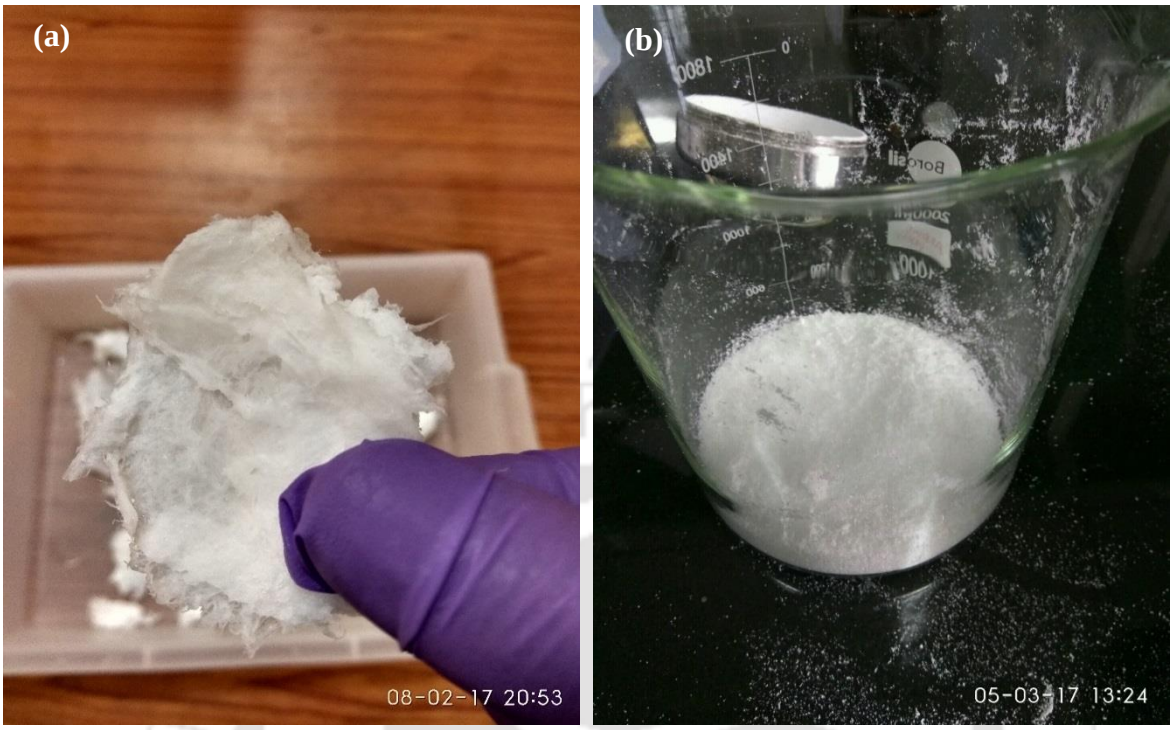

Figure 3.1: (a) Lab synthesized fibrous PLA and (b) Grinded PLA into powder form.

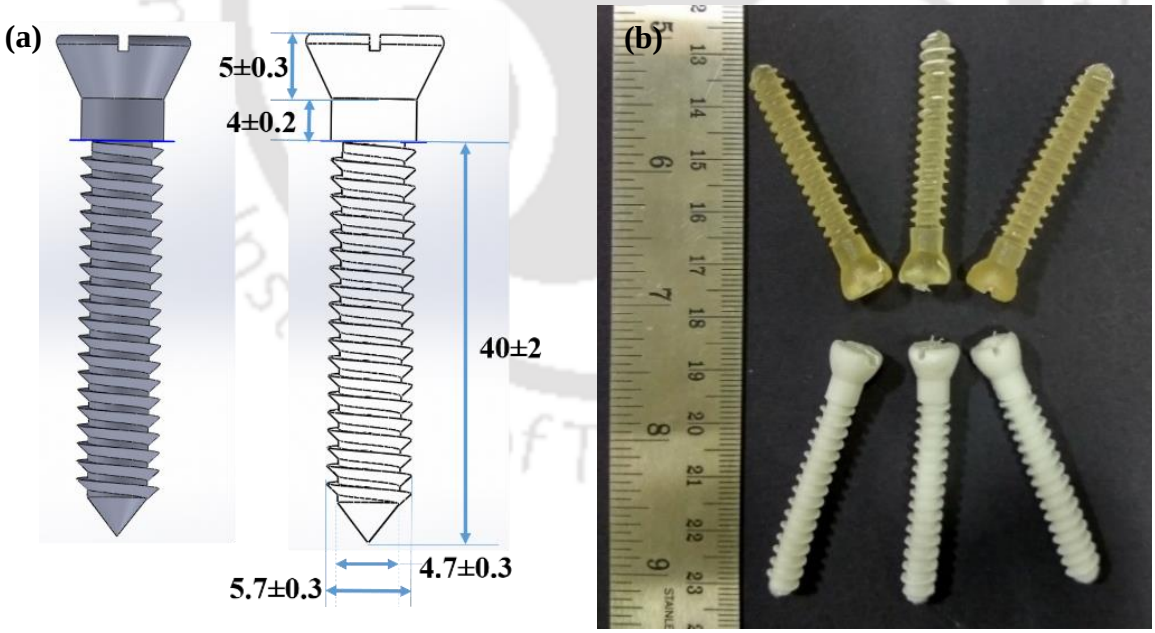

Figure 3.2: Schematic diagram of cortical screws (a) 3D line diagram of cortical screw (b) Photographic images of neat PLA (top) and PLA/nHAp (bottom) cortical screws.

Figure 3.2 (a) shows the 3 D line diagram of cortical screws, and Figure 3.2 (b) shows the photographic image of neat PLA and PLA/nHAp cortical screws.

3.2 Development of cortical screws

The cortical screw was designed in AutoCAD as per the ISO5835:1991(en) metal bone screw. The total length maintained was 47.75 mm. The threaded portion length was maintained 40±2 mm. The inner diameter and outer diameter were kept 4.7±0.3 mm and 5.7±0.3 mm respectively. The pitch maintained was ~1.75 mm. The detail dimensional diagram is shown in Figure 3.2.

3.3 Development of Molds and fixtures for cortical screws

The molds for injection molding for cortical screws (Figure 3.3) and related fixtures for its testing were initially designed in AutoCAD. After designing, The molds were manufactured using various manufacturing machines passed through various machining processs. The material choosen for making the molds was H13 (Tool Steel). H13 is a versatile chromium-molybednum hot work steel, which is widely used in hot work and cold work tooling applications.

Figure 3.4 shows three dimensional model (3D) of the fabricated cortical screw mold. The hot hardness (hot strength) of H13 metal resists thermal fatigue cracking, which occurs as a result of cyclic heating and cooling cycles in hot work tooling applications. Because of its excellent combination of high toughness and resistance to thermal fatigue cracking. H13 is used for more hot work tooling applications than any other tool steel. The high toughness and very good stability in heat treatment made this material a good choice of application to a variety of cold work tooling applications.

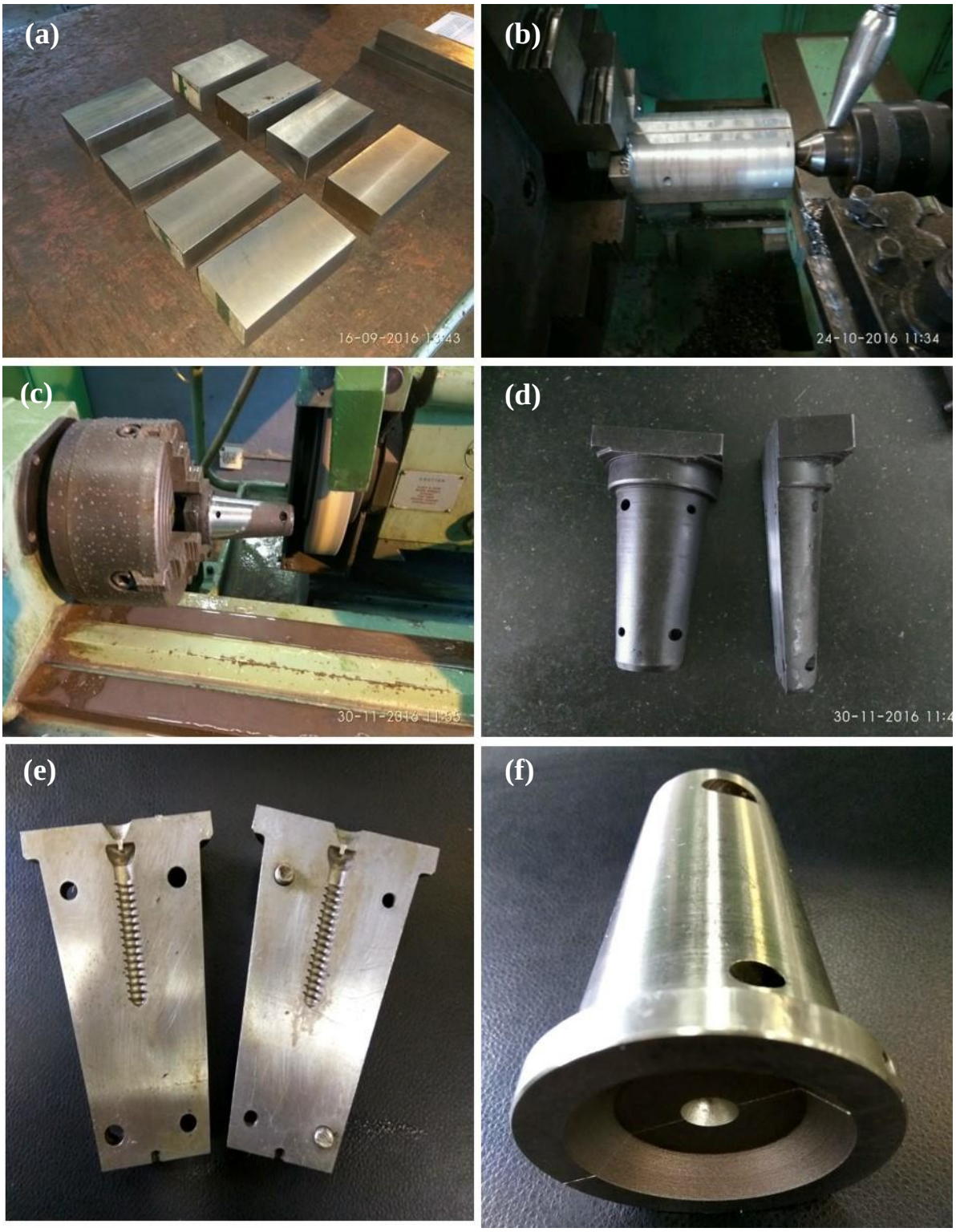

Figure 3.3: Schematic diagrams for fabrication of cortical screw molds. (a) H13 material for mold (b) machining in lathe machine (c) surface grinding (d) Heat treated mold (e) mold in final shape (f) side view of screw mold.

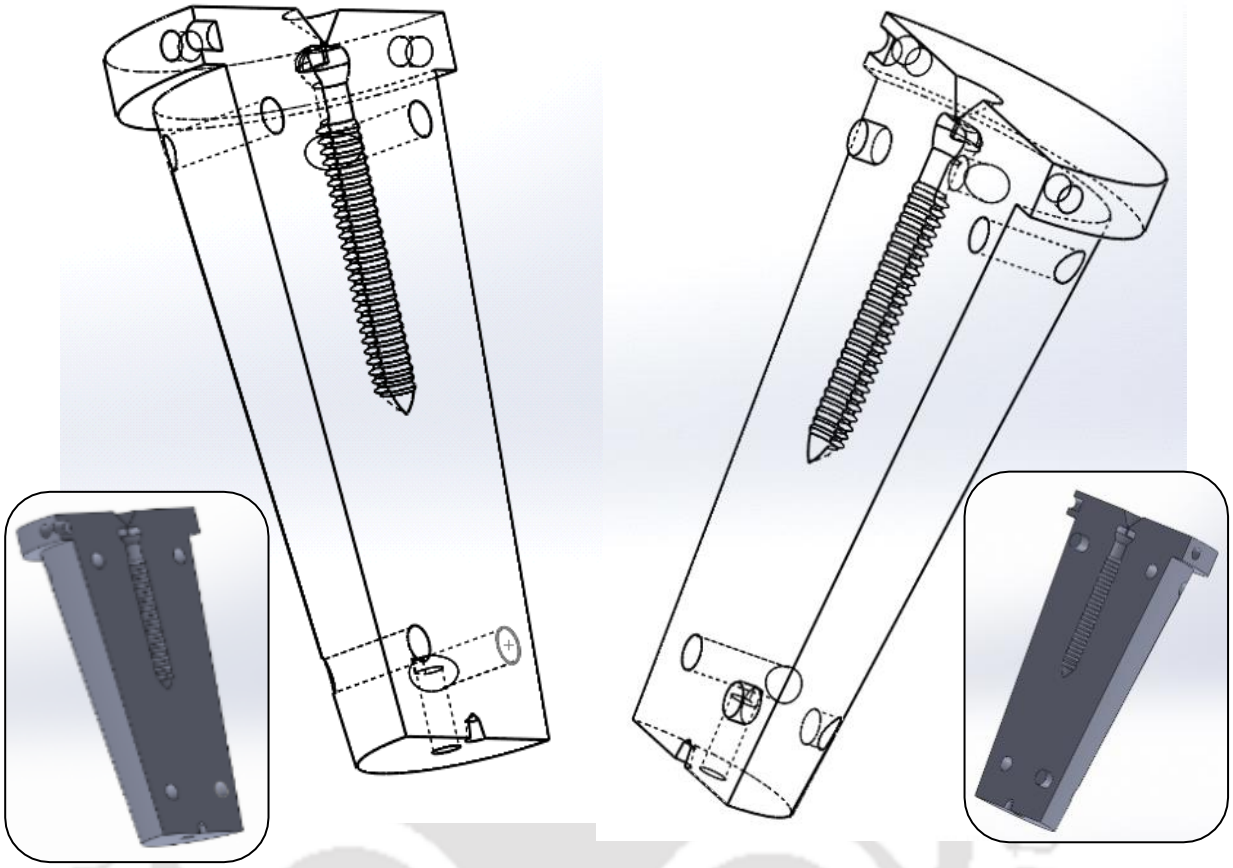

Figure 3.4: 3D model of cortical screw mold.

3.4 Mechanical Testing of Cortical screws

After production of cortical screws, the mechanical testing was done as per ASTM F2502-11 (Standard specification and test methods for Absorbable Plates and Screws for internal fixation Implants). The test was conducted on a universal tensile machine and torsion machine by attaching a customized fabricated fixtures.

3.4.1 Axial Pull out strength

The axial pullout strength was determined using the universal tensile testing machine (Kalpak Instruments, India) according to standard ASTM F 2502-11 using a fabricated pull out fixtures (Figure 3.5). The screw was inserted total depth of 15 mm of the total length of the screw thread into a previously internally threaded steel block fixture. The fixture was

perfectly aligned with the longitudinal axis of the screw and the attached load frame. A cross head speed of 1mm/min and a 5 kN load cell was used. The measurement was carried out in triplicate. The value of axial pull out strength was taken to be the maximum load reached during the test. Figure 3.7 shows the axial pull out strength concerning the various combination of PLA/nHAp of the cortical screws. It is observed that 10% nHAp is having maximum axial pull out the strength of 737N (38% increment), while lowest is about 538 N for Neat PLA The reason for an increase in axial pull out strength may be due to the transverse support provided by the nHAp powders.

The axial pull out strength value after *In vitro* hydrolytic degradation for 90 days is shown in Figure 3.8. The reduction of axial pull-out strength was observed ~3% after 30 days, ~8% after 60 days and ~38% after 90 days compared to initial axial pull-out strength. Initially, pull-out strength of the cortical screws was gradually reduced later as the time passes by, the pull-out strength decreases rapidly.

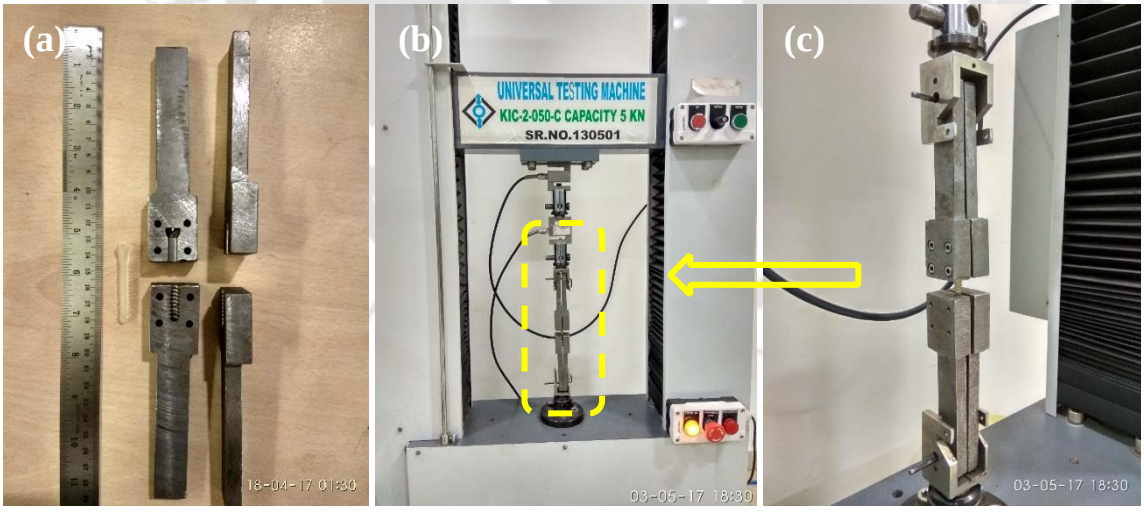

Figure 3.5: (a) Fixture for cortical screws (b) fixture setup (c) magnified the view of axial pull out test arrangement.

The reason may be due to the interaction of water molecule interacting with the surface of cortical screws leads to increase in the crystalline part of the PLA, which further increases the brittleness and thus axial pull-out reduces [154].

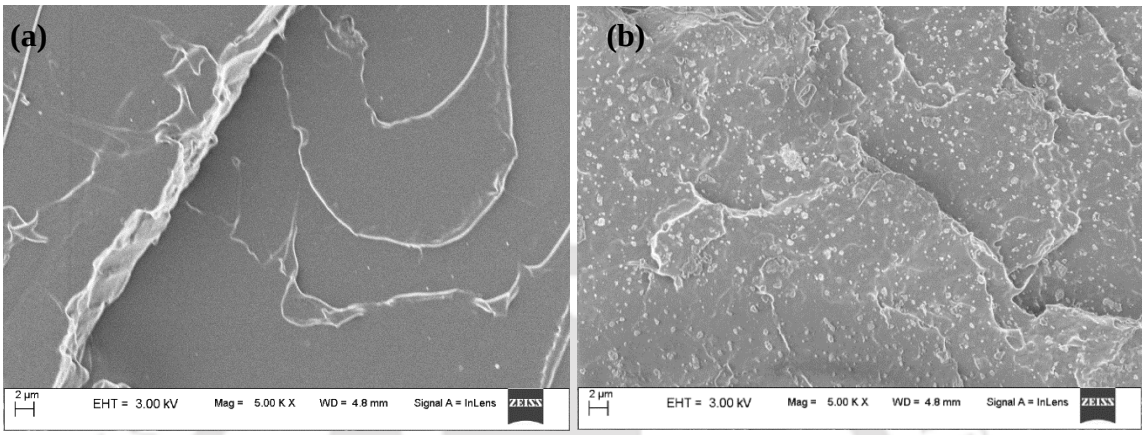

Figure 3.6: Surface micrograph from FESEM after axial pull-out test of cortical screws (a) neat PLA and (b) PLA/nHAp.

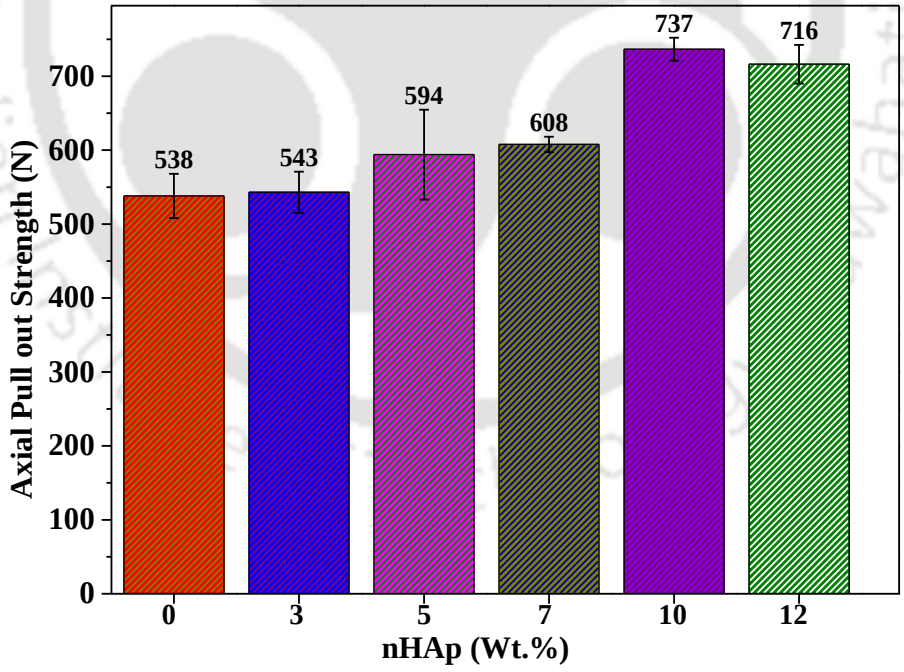

Figure 3.7: Axial pull out strength value of cortical screws with varying concentration of nHAp fillers.

In case of optimized PLA/nHAp composition (10% nHAp), reduction of axial pull-out strength observed was ~6% after 30 days, ~25% after 60 days and ~33% after 90 days. Figure 3.6 shows the fractured surface micrograph due to axial pull out strength.

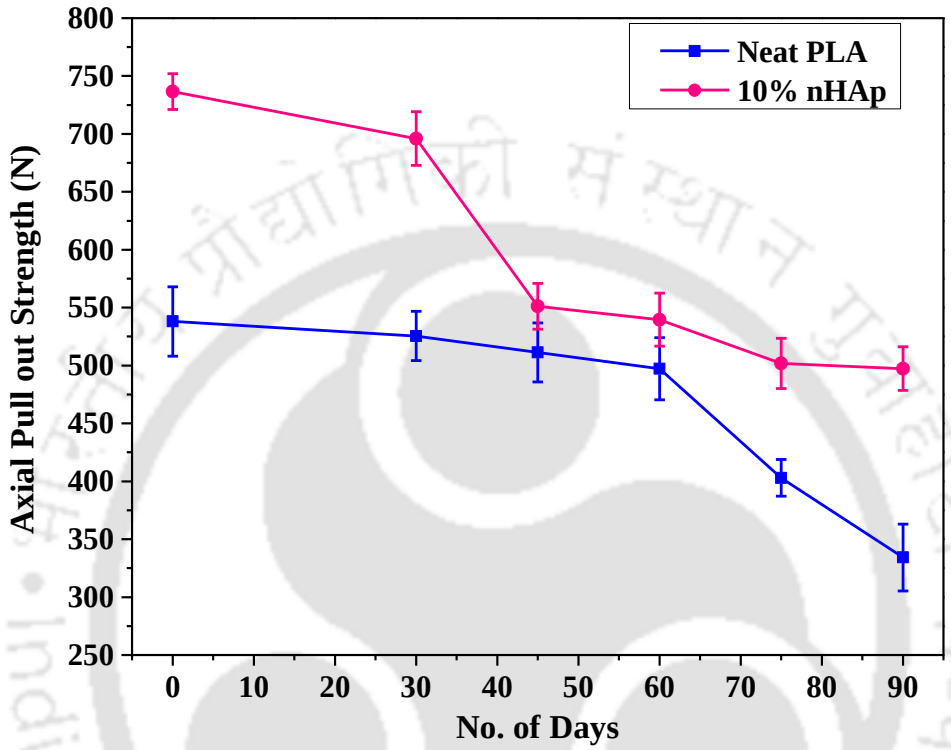

Figure 3.8: Axial pull out strength of neat PLA and 10% nHAp before and after In vitro hydrolytic degradation.

3.4.2 Torsional Strength

The maximum torque, breaking angle were measured for the cortical screw produced according to the standard ASTM F 2502-05 using fabricated torsion fixture. The measurements were done in torsion testing machine (make: Fuel instruments and equipment, India). The crosshead speed of the machine was one revolution per minute. The load cell capacity of the machine was 10kgf.m (98066.5 mili Newton meter). The gauge length was maintained about 25% of the total threaded length of the screws. The maximum torque was

represented by the highest recorded value of the torque during the test, and the breaking angle was the rotation angle at the maximum torque. The measurement was carried out in triplicate. The fixture was made of steel metal. The room temperature was maintained at 23°C. Figure 3.9 shows the fixtures arrangement during testing the torsional strength of the cortical screws. Figure 3.10 shows the values of torsional strength value concerning varying filler concentration. The increment was observed as 30% in the case of 10 % nHAp concerning neat PLA

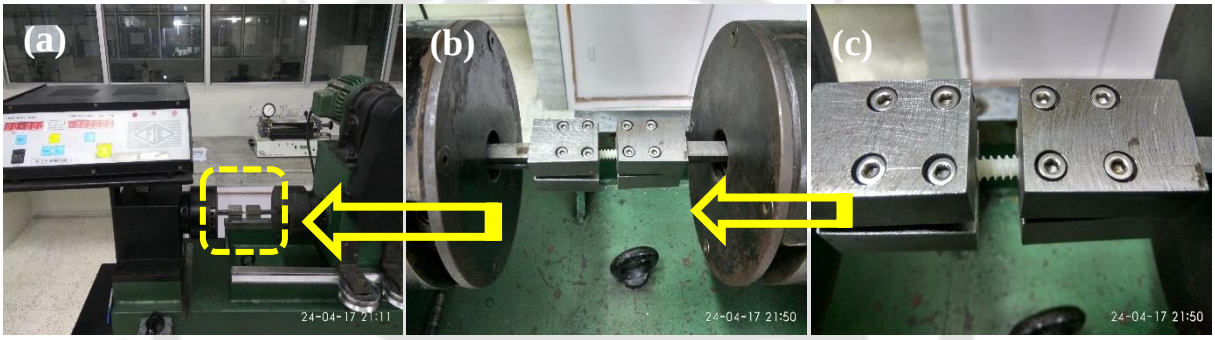

Figure 3.9: (a) Torsion test set up (b) fixation of cortical screws (c) magnified the view of cortical screw arrangement for torsion test.

It was observed that ~30% increment happened in the case of 10 % nHAp with respect to neat PLA This may be due to enhanced interfacial adhesion due to reactive extrusion process inside twin screw extruder machine, a strong shear force generated between twin screws leads to prevent from agglomeration and thus uniform dispersion of nHAp particles takes place. Strong interface bonding yields large torsion load bearing property and torsion strength. However, matrix elongation has a more important effect on torsion strength than interface bonding strength [155]. Figure 3.11 shows the values of ultimate torque after *In vitro* hydrolytic degradation studies. The torsional strength was reduced from 887 mili Newton meter (mNm) to 798 mNm (~10%) after 30 days and ~45% reduction after 90days, however

in case of 10% nHAp, the reduction was observed from 1157 mNm to 1056 mNm (~9% reduction) after 30days and 1157 mNm to 800 mNm (~31% reduction) after 90 days.

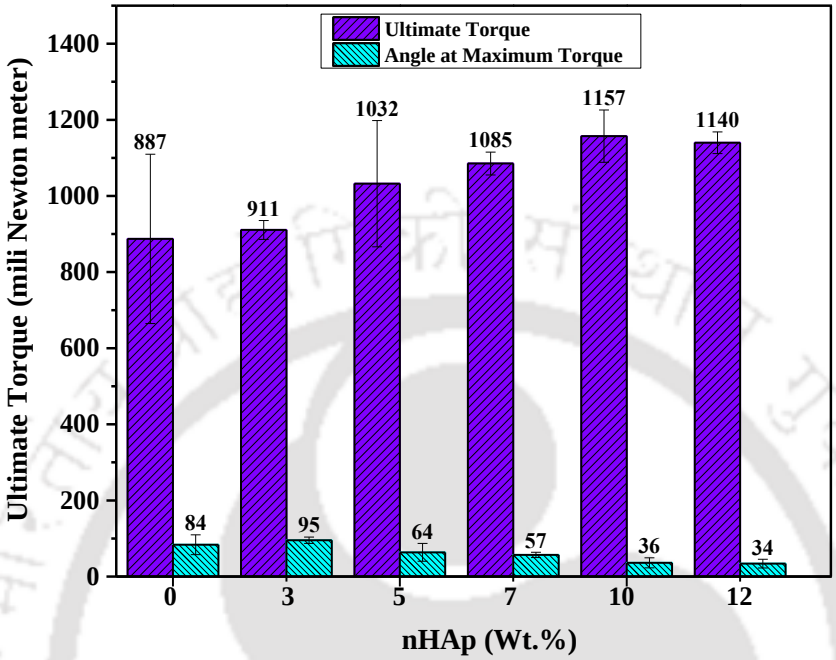

Figure 3.10: Ultimate torque and angle at maximum torque of cortical screws with respect to nHAp filler.

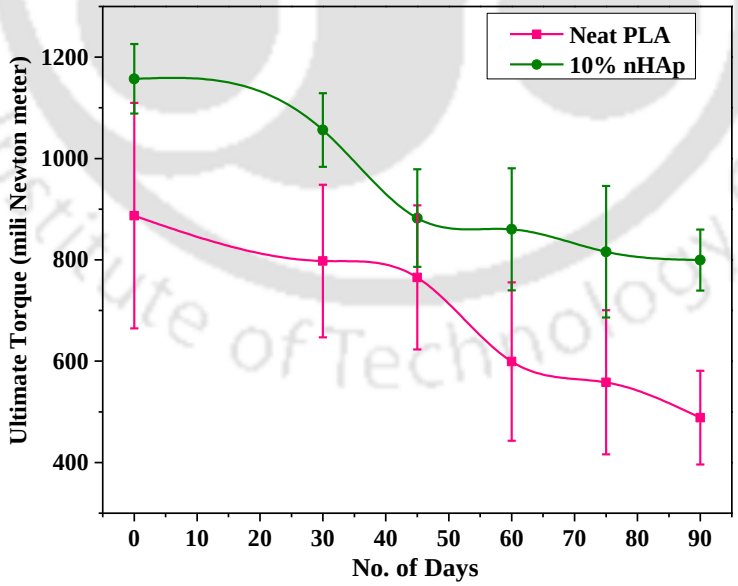

Figure 3.11: Ultimate torque value of neat PLA and 10% nHAp cortical screws before and after In vitro hydrolytic degradation.

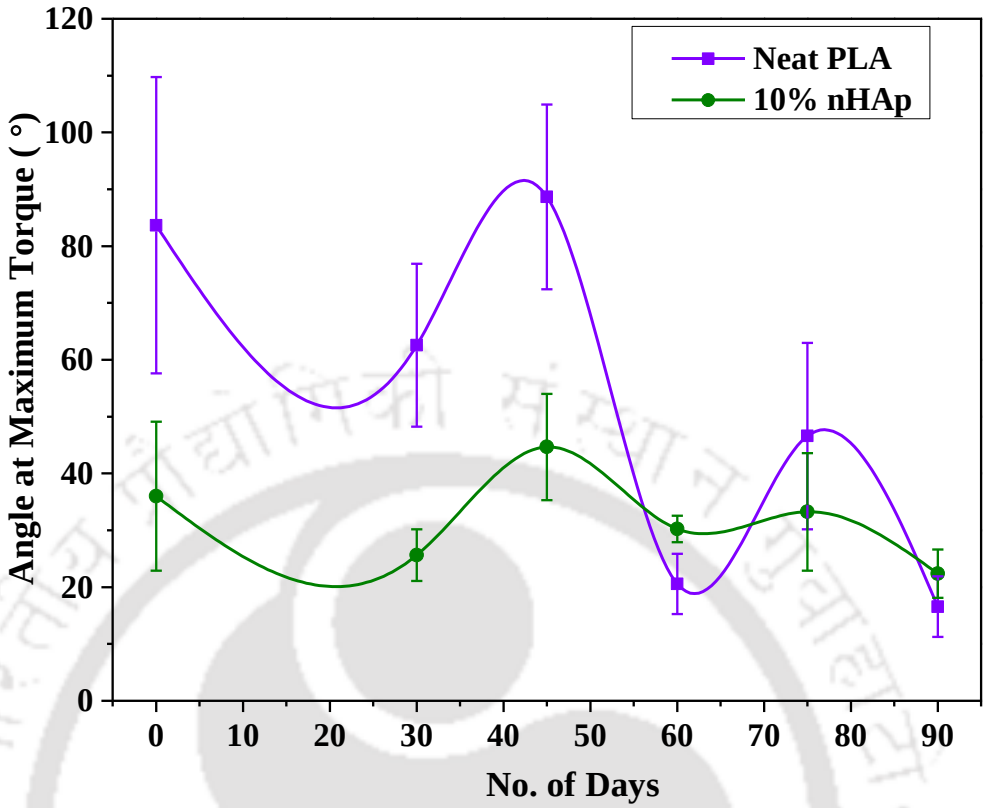

Figure 3.12: Angle at maximum torque of neat PLA and 10% nHAp cortical screws before and after In vitro hydrolytic degradation.

Figure 3.12 shows the value of twisting angle concerning the ultimate torque value obtained from torsional strength. It was observed that an increase in the concentration of nHAp particles into the PLA matrix leads to an increase in brittleness of the cortical screws which ultimately proceeds for fractures of the sample at less twisting angles.

3.4.3 Flexural testing

The maximum flexural load for the cortical screws were evaluated by flexural (3 point bend test) test using a fabricated flexural fixture at room temperature. Figure 3.13 shows the flexural set up for conducting 3 point bend test. A cross head speed of 1mm/min and a load cell of 5 kN was used.

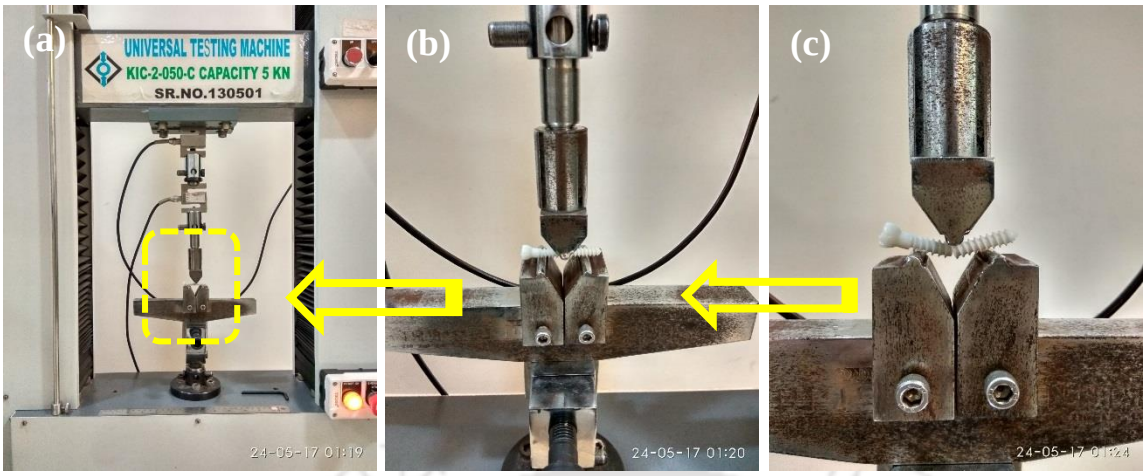

Figure 3.13: (a) Flexural test set up (b) arrangement of cortical screw for 3 point bend test (c) fracture of cortical screw during test.

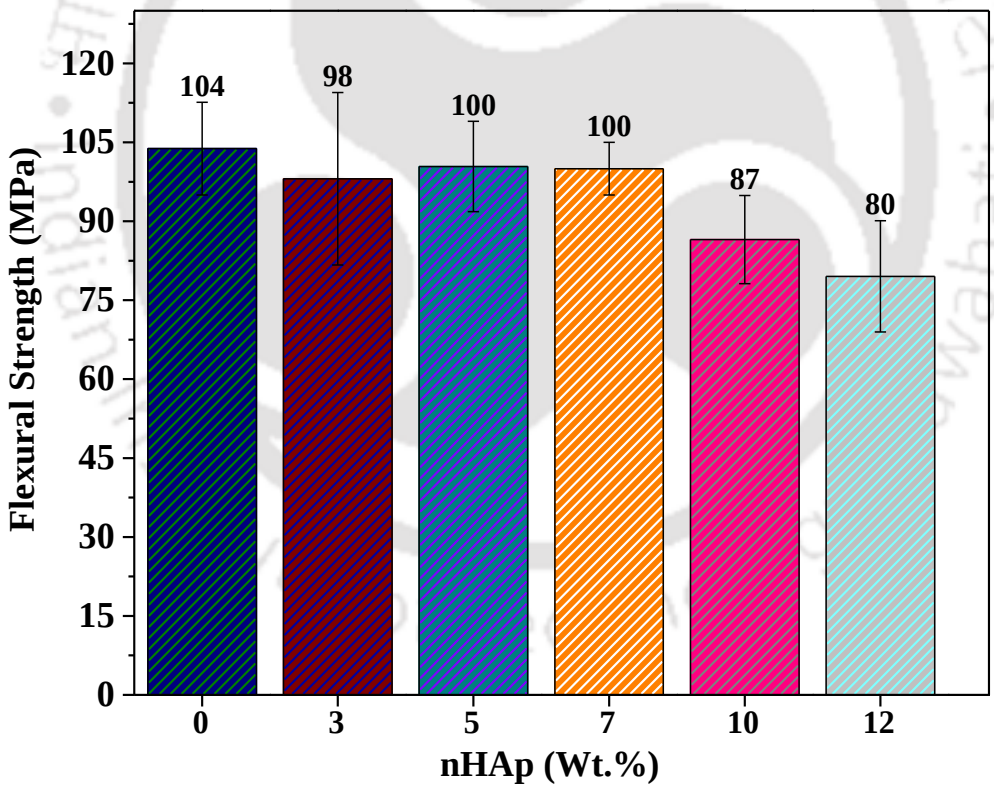

Figure 3.14: Flexural Strength value obtained through three point bend test of cortical screws concerning nHAp fillers.

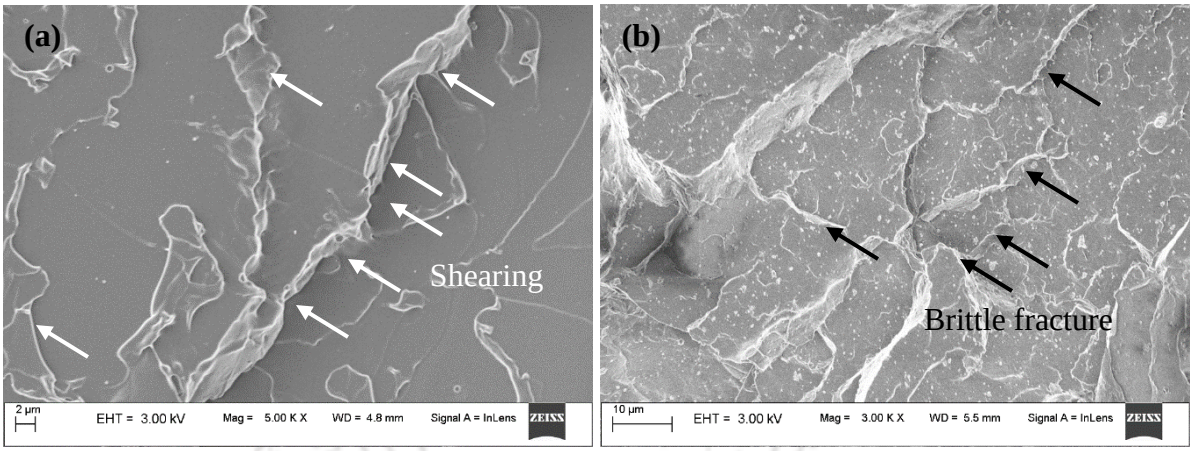

Figure 3.15: Fractured surface micrographs of a) neat PLA b) 7% nHAp from FESEM after flexural strength test.

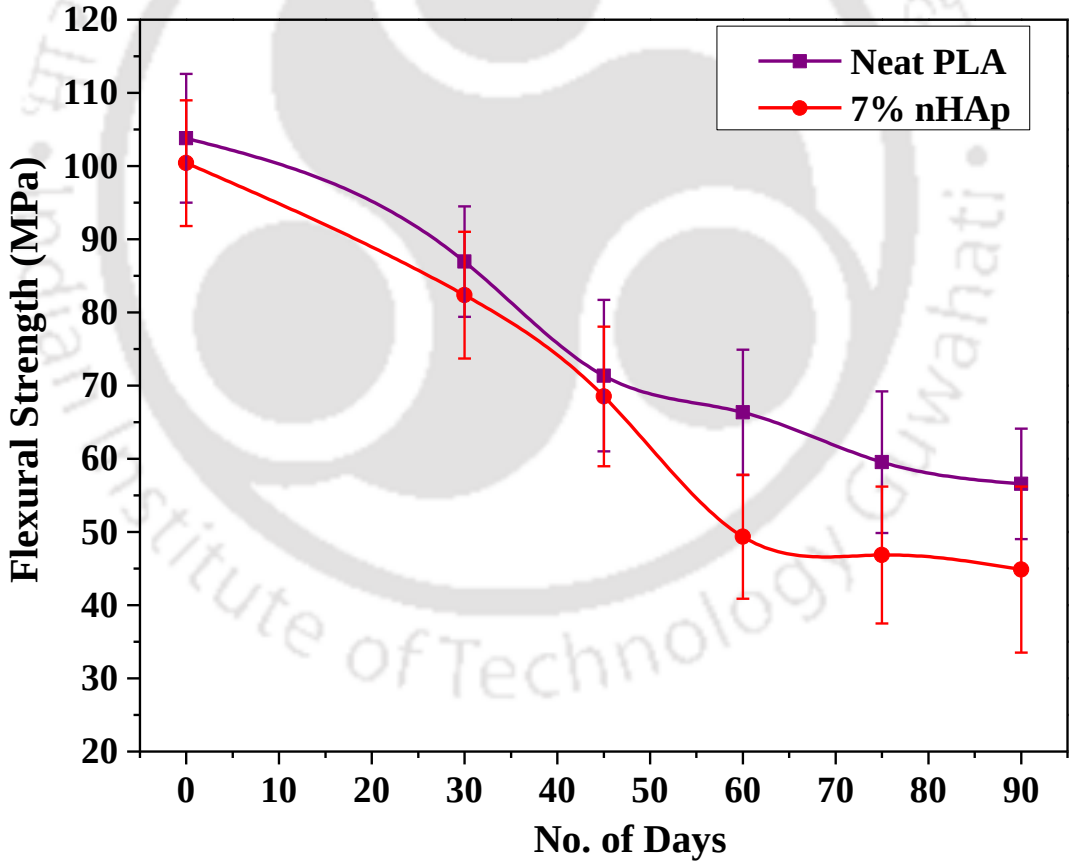

Figure 3.16: Flexural strength value of neat PLA and 7% nHAp cortical screw before and after hydrolytic degradation.

Measurement was conducted in triplicate. The support span was 20 mm, and radii for loading and supporter applicators was maintained 3mm. The flexural strength was calculate by equation no. 3.1

$$\sigma f = \frac{FL}{\pi R^3} \qquad (3.1)$$

where σf = flexural strength, F is the load applied, L is the length of the support span (mm) and R is the radius of the cortical screw..

Figure 3.14 shows the values of flexural strength with varying the filler concentration. It was also observed that flexural strength was reduced in the range of 4% to 16% concerning 3% nHAp to 12% nHAp. Figure 3.15 shows the surface micrograph of the cross-sectional area after conducting a flexural test. The flexural strength of the cortical screws was observed reduced (Figure 3.16) due to restricted crosslinking between nHAp and PLA chains. The other reason may be due to the diffusion of water into cortical screw samples act as a plasticizer and reducing the bending properties of the PLA matrix. The water from PBS solution that diffused into PLA/nHAp cortical was sufficient enough to degrade the interfaces on the cortical screw surfaces. The degradation, which results in poor stress transfer efficiency and thus leads to fracture of the screws [156-158]. From Figure 3.16, the reduction was observed from ~104 MPa to ~80 MPa (~23% reduction) with varying concentration from neat PLA to 12PLA. The cortical screw was further conducted *In vitro* hydrolytic degradation and then flexural strength were analyzed (Figure 3.16), it was observed that after 30 days, ~16% reduction, ~36% after 60 days and ~45% reduction happened in case of Neat PLA while in case of 7% nHAp, ~18% reduction was observed after 30 days and 55% reduction was after 90 days. It was also observed that for the same duration 7% nHAp has less

degradation rate as compared to neat PLA. It was observed that nHAp particles were uniformly distributed throughout the PLA matrix.

3.4.4 Double Shear Strength

The Double shear strength of the cortical screws was measured through fabricated fixtures attached in the universal tensile testing machine according to standard ASTMD7617M-11. The cross head speed of the machine was 1mm/min, and load cell capacity was taken 5kN. The maximum shear load was determined as the maximum load recorded during the test. The measurement was carried out in triplicate.

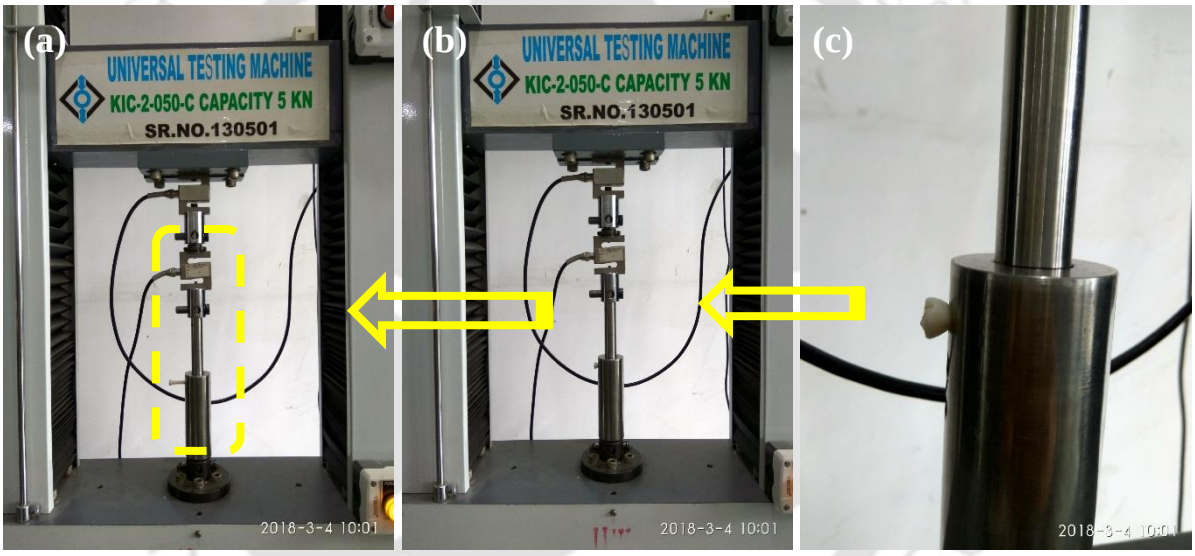

Figure 3.17: (a) Double shear strength set up (b) Arrangement of cortical screw into the fixture (c) Magnified view of cortical screws.

Figure 3.17 shows the arrangement of the fixture and the fabricated cortical screw in the universal testing machine set up. The increase of 12% was observed (Figure 3.18) in case of 10% nHAp concerning neat PLA. The double shear strength was calculated by the equation 3.2

$$\tau = \frac{P}{2A} \quad \text{.....(3.2)}$$

where τ = Double shear strength, P = applied load (N) and A = cross-sectional area (mm^2). The improvement in double shear strength may be due to reactive grafting (inside twin screw extruder) of PLA chains on the surface of nHAp leads to uniform dispersion and also enhances the interfacial adhesion between PLA chains and nHAp particles. The other reason may be due to an increase in crystallinity since nHAp particles are crystalline and thus this crystallinity leads to more intermolecular bonding and crosslinking between nHAp and PLA chains [159]. The intermolecular forces on the surface area of nHAp acts as a bridge with the PLA chains, which leads to support and elongate PLA polymeric chains and extend the fracture phenomenon. The increase of 12% was observed (Figure 3.18) in the case of 10% nHAp concerning neat PLA. *In vitro* hydrolytic degradation studies, the double shear strength of the cortical screws was shown in Figure 3.19. It was observed that in case of neat PLA, the reduction of double shear strength value from 44MPa to 31 MPa (~30% reduction) after 30 days and 44MPa to 29 MPa (~35% reduction) after 90 days happened. However, in case of optimized concentration, i.e. 10% nHAp, the reduction from 49 MPa to 39 MPa (~20% reduction) after 30 days and from 49MPa to 30MPa (~39% reduction) after 90 days observed. It was also observed that for the same duration, the degradation rate was less in the case of 10% nHAp concerning neat PLA.

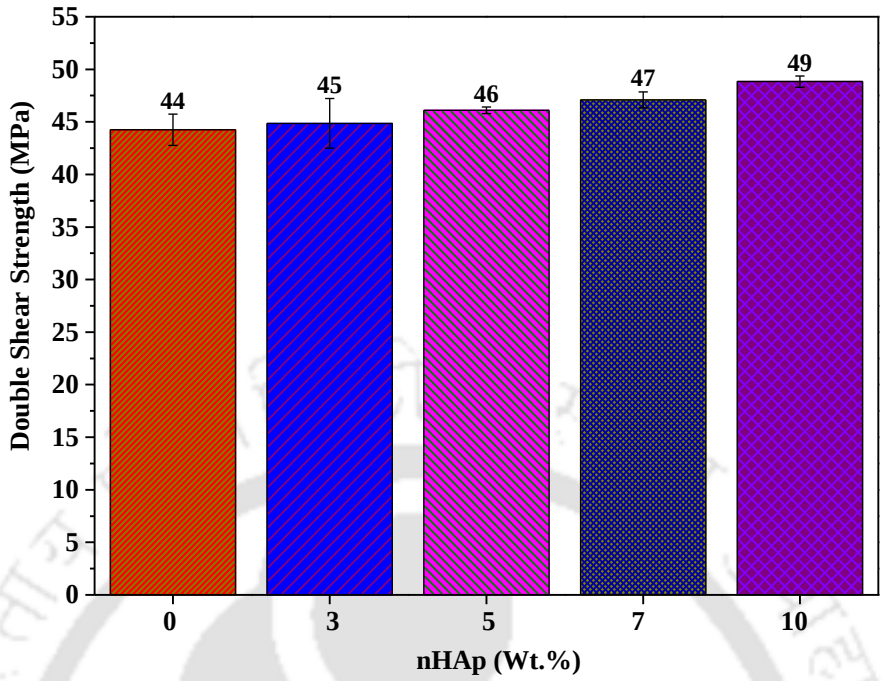

Figure 3.18: Double shear strength of cortical screws concerning variation in nHAp filler.

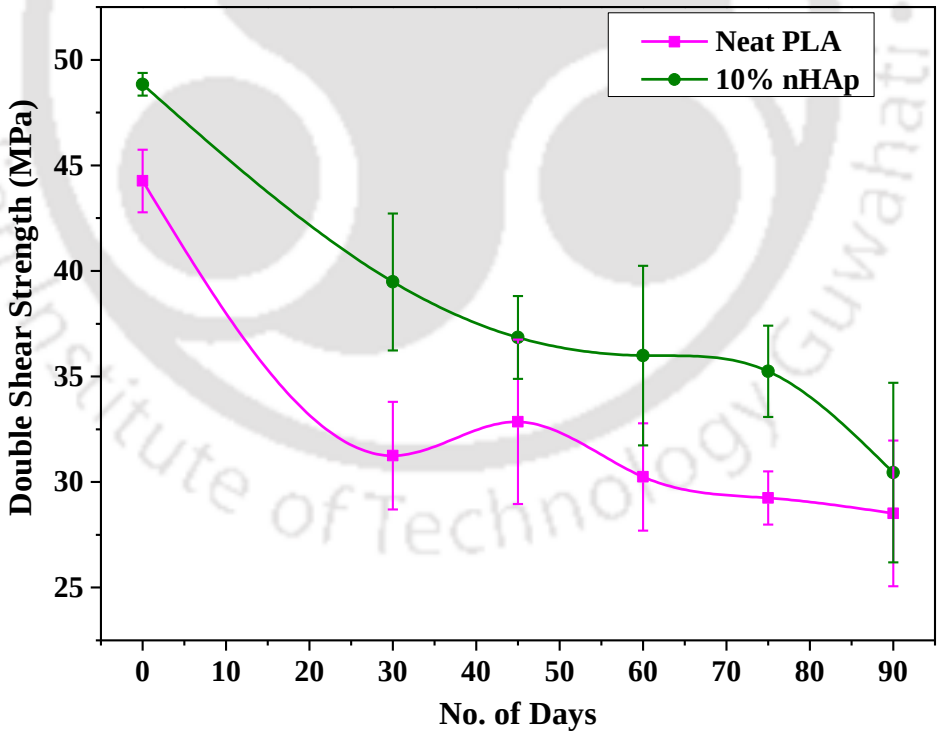

Figure 3.19: Values of double shear strength for neat PLA and 10% nHAp cortical screws before and after hydrolytic degradation.

3.5 Degradation studies

The *In vitro* hydrolytic degradation studies on fabricated cortical screw was done as per ASTM standards ASTM F1635-11. The Figure 3.20 shows the arrangement of fabricated cortical screw for the *In vitro* hydrolytic degradation studies and conducted in phosphate buffer saline solution; the cortical screw was initially dried in hot air oven after that initial weight were noted. The glass jars were cleaned properly, and synthesized PBS was poured in all the glass jar uniformly. After 30th day, 45th day, 60th day, 75thh day and 90th days, the exposed cortical screw was removed out and dried and in the form of final weight was noted. The loss of mass was calculated by subtracting the final weight from the initial weight.

Figure 3.20: (a) cortical screws in the glass jar (b) storing of glass jar in air oven (c) after drying cortical screws.

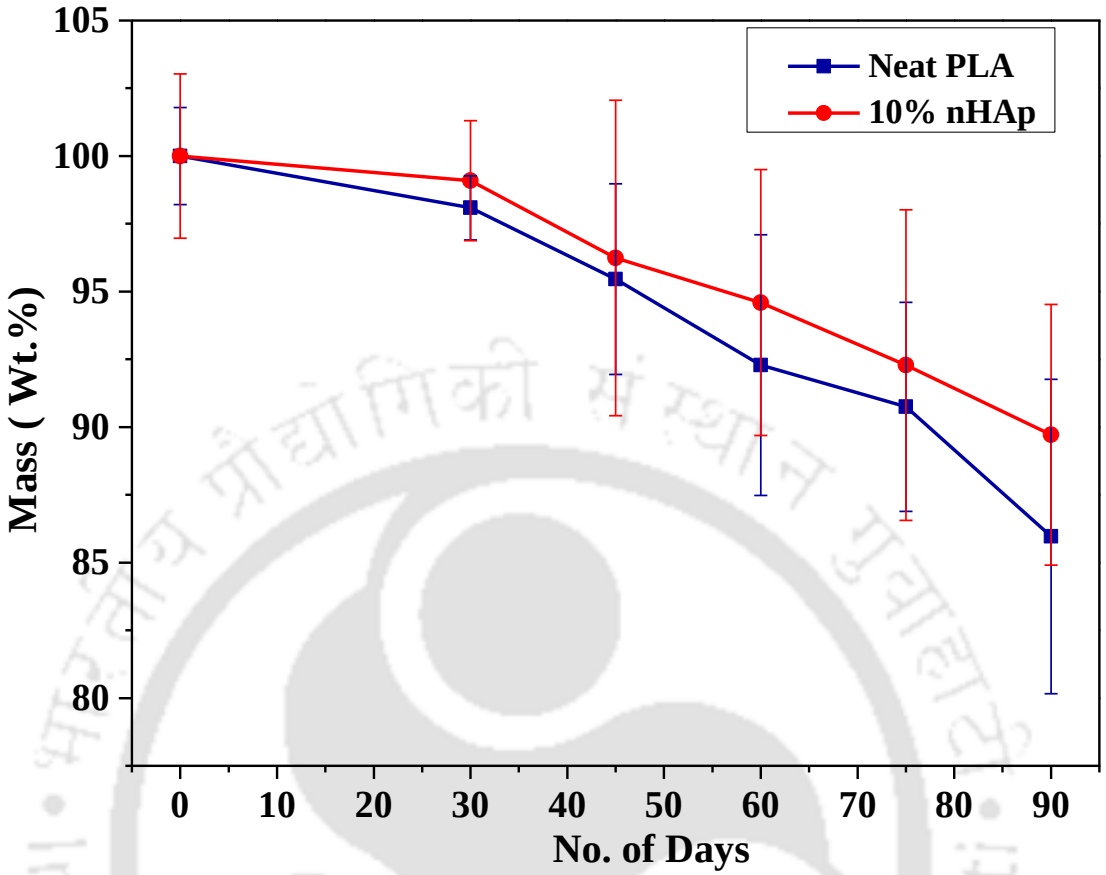

Figure 3.21: Profile of mass (wt.%) of neat PLA and 10% nHAp before and after In vitro hydrolytic degradation.

Figure 3.21 shows the loss profile of mass of the Neat PLA and 10% nHAp cortical screws exposed in PBS solution for 90 days. It was observed that ~3% reduction in mass loss after 30 days, ~11% reduction after 60 days and ~18% were the reduction in mass loss after 90 days in case of neat PLA. However, in the case of 10% nHAp, reduction of ~3% after 30days, ~7% after 60 days and ~12% after 90days mass loss were observed. It was also observed that for the same duration of exposure towards PBS solution, the rate of degradation of Neat PLA was faster as compared with 10% nHAp. This studies also reveal that 100% degradation in a mass loss would be between 9 to 12 months and healing of fracture bone also takes 8-12

months. Hence for various age group peoples, cortical screws can be tuned. Figure 3.22 shows the surface micrograph of the degraded cortical screw.

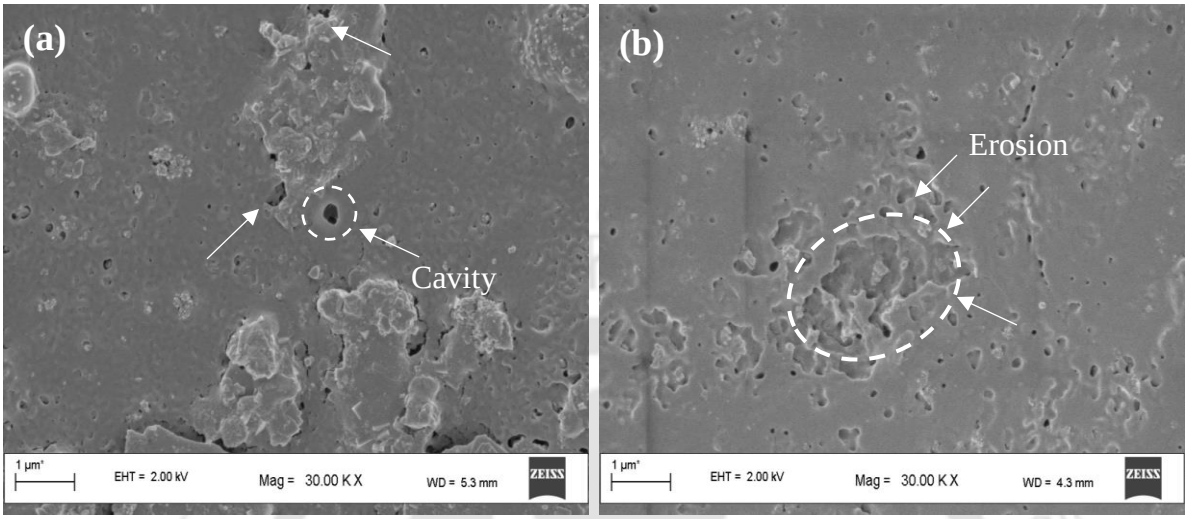

Figure 3.22: (a) The Surface profile of the degraded cortical screws. (b) The surface profile of the degraded screws after 90 days.

Figure 3.23 shows the fracture profile of the cortical screws through double shear strength test, and torsional strength and Figure 3.24 shows the flexural test and pull out test respectfully. It was observed that due to the shear strength test, most of the cortical screw was failed due to brittle fracture, ductile fracture and some were due to prolonged elongation. While in case of torsional strength test, most of the samples were failed due to gauge length shearing, shearing at screw head, shearing at the lower crest of thread and shearing cum fracture. From the Figure 3.24, most of the cortical screws were failed due to brittle and ductile fracture in case of flexural test, while in case of pull-out test, the core diameter fracture, multi zone fracture and screw thread fracture were observed [160].

Figure 3.23: Photographic images of fractured cortical screws after double shear strength and torsional strength test.

Figure 3.24: Photographic images of fractured cortical screws after flexural test and axial pull-out test.

3.6 Dimensional deviation studies

In order to know the geometrical deviation of thread pitch from the standard geometry, cortical screws were analyzed through optical surface profilometer (Optomech, vertical) at

10X (*Figure 3.26*). The corresponding samples of cortical screws were also magnified through stereomicroscope (Nikon SMZ25). The obtained images are shown in Figure 3.27. The deviation in the pitch of the fabricated cortical screw was analyzed and shown in Figure 3.25. It was observed that deviation of the samples was very less as compared with the standard dimension and later the deviated dimensions were neglected.

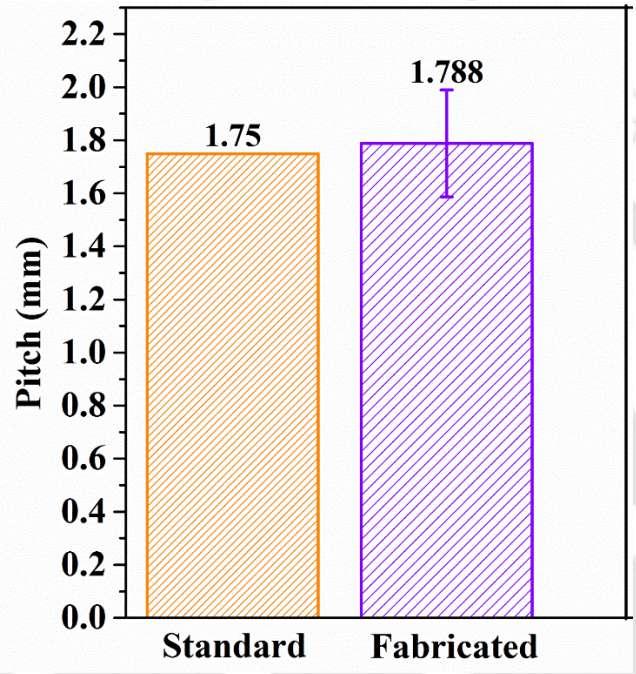

Figure 3.25: Deviation in pitch of the fabricated cortical screws.

Figure 3.26: Photographic image of surface profile optical micrograph of cortical screws

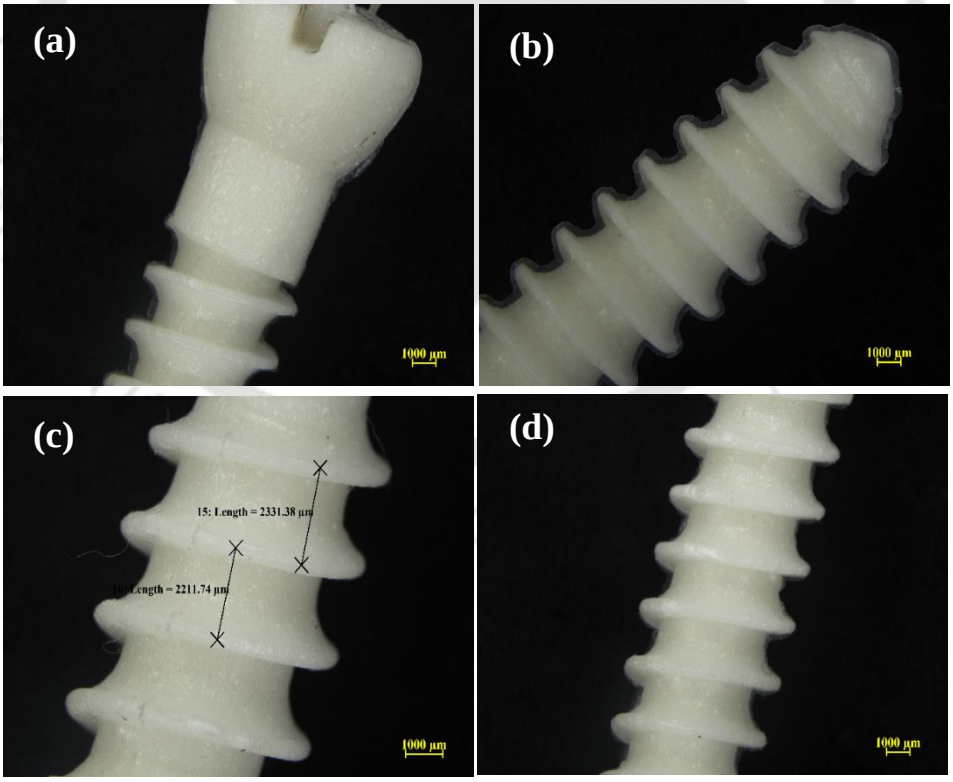

Figure 3.27: (a) Profile of cortical screw head (b) Profile of thread of cortical screw (c) Measurement of pitch in the screw (d) Threaded portion of the screw.

3.7 Summary

In this chapter, the following major points are summarized

1. The cortical screws based on purified PLA and PLA/nHAp has been successfully manufactured through extrusion cum injection molding process.
2. The process parameters have been optimized in order to produce the cortical screws
3. The design, development of the mold and related fixtures for performing mechanical testing have been discussed.
4. The mechanical test as per ASTM standards related to cortical screws has been performed.
5. The axial pull out strength of 10% nHAp gives the maximum value within the combination taken. The increment observes was about 38% as compared to neat PLA.
6. The torsional strength of cortical screws has been also conducted. The increment of 30% torsional strength was observed in the case of 10% nHAp concerning neat PLA. The corresponding breaking angle was also mentioned.
7. The flexural strength of the cortical screws was also performed as per ASTM standard. The reduction of 4% to 16% was observed with compared to neat PLA.
8. The double shear strength was also performed in the fabricated fixtures and as per ASTM standard. The maximum increase of 12% of 10% nHAp was observed within the combinations.
9. The *In vitro* hydrolytic degradation studies confirm the mass loss of the cortical screws after exposure in PBS solution. It was observed that the rate of mass loss of the neat PLA was more as compared to PLA/nHAp cortical screws.
10. The deviation in thread pitch of the fabricated cortical screws was compared with the standard cortical screw; later it was analyzed with the help of surface profilometer and stereomicroscope. The deviation was quite very less; thus the deviation result was neglected.

ABSTRACT

This chapter reveals the fabrication of the cancellous screw for orthopedic fracture fixations. The processing conditions and parameters were optimized and reported. The mechanical test was conducted from the manufactured customized molds and fixtures and the results are described in this chapter. The various mechanical test were conducted and analyzed in order to optimize the best combination of the base material and nano fillers. *In vitro* hydrolytic degradation test was conducted, and again all the mechanical test were performed so that the strength after number of days could be revealed, in thus way, the outcome properties give insights its suitable applications for various age group people. Because the bone healing efficiency also depends upon the age of the persons as well. The mechanical studies conducted for evaluating the performances was based upon the ASTM standards. Phosphate buffer saline solution was prepared in our laboratory as per the standard protocol and after that In *vitro* hydrolytic degradation studies was conducted as per ASTM standards.

GRAPHICAL ABSTRACT

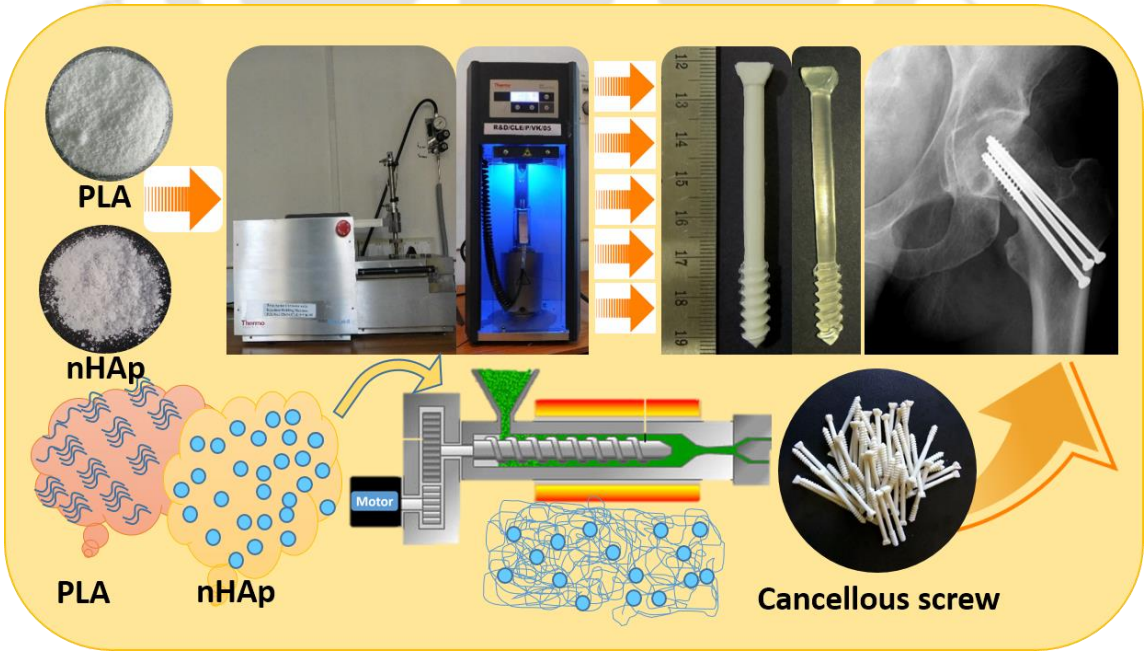

Chapter 4

4 Fabrication and characterization of cancellous screws

4.1 Introduction

The cases of bone fractures are increasing day by day. The associated reason has already been discussed in chapter 1. Since metallic internal fixation has many limitations and thus the application of the absorbable internal fixation devices takes place. The advantages of using bioabsorbable polymers to fabricate internal fixation devices have also been discussed in chapter 1. The cancellous screw is also one of the internal fixation devices which are widely used to fix the two or more objects as well as to compress object together in context with a fractured bone, prevents the sideways movement, hold the bone plate against bone, increase the grip of intramedullary nails and also allow axial displacement in some cases [161-163]. The cancellous screw threads have larger pitch, larger outer diameter and are deeper with compared to cortical screws. The diameter of the thread to the core diameter ratio is more and designed to have better purchase in the cancellous bone and are available in the form of fully or partially thread [164]. The strength of the screw mainly based on the interface between screw and bone, which generally influenced by the factors like the density of the bone, quality of the bone, the strength of screw material and area of contact of threads with the bone. The bioabsorbable screws were first introduced by Lambert et al. in 1983 using 6.5mm outer diameter after that kurosova et al. developed the concept of fully threaded interference screws [165-166]. The disadvantages of the bioabsorbable polymeric screw are the failure of the screw during insertion, which depends upon the mechanical properties. The common materials used for bioabsorbable screws are PLA, PLLA, PGA and combination of PLA and tricalcium phosphate. Since cancellous bone is much less dense than cortical bone,

the screw threads cut their path in the bone when the screw is inserted, i.e. cancellous screws are self-tapping. Partially threaded cancellous screws are often used as lag screws for metaphyseal fractures [167]. Various researchers have fabricated metallic cancellous screw, few of them has fabricated polymeric bioabsorbable screw, but it was not in the form of standard size. It was manufactured symbolically; various researchers have investigated the materials perspective to the probable application as cancellous screws. Many have compared the properties between cancellous and cortical screws. Kim et al. [168] reported cortico-cancellous bone graft versus cancellous bone graft for the management of unstable scaphoid non-union. The study was taken to determine whether cortico-cancellous bone graft and cancellous bone grafting differ in terms of their bone union rate, restoration of scaphoid anatomy and wrist function. In this study, a group of 17 patients (group A), unstable scaphoid non-union was treated with cortico-cancellous graft harvested from the iliac crest and headless compression screw and in another group of 18 patients was treated with cancellous graft harvested from the distal radius and headless compression screw. The result showed that mean time to union was significantly greater in group A. It was also observed that cancellous bone grafting leads to the earlier bone union than cortico-cancellous bone grafting with similar anatomic restoration. Furthermore, no difference in wrist function was observed between the two modalities.

Kulper et al. [169] reported novel fracture mechanics model to explain the penetration by implants. It was seen that differences in tip design affect the force required for axial penetration of similar material like cancellous bone. Ten axial penetration trial was conducted for each tip design. The steady state of stress ~4 MPA was felt in all the design of the tip. Three tip design was used like the flat, conical and elastomeric tip of 5mm diameter. It was

observed that the flat tipped implant was able to compact more than a few millimeters of material and may increase the risk of cut out. The Sharp tipped showed slow initial growth but reached as area after 4-5 mm of penetration. It may be useful in improving axial stability in cases where the bone is too strong to develop a large compaction zone during insertion or when pilot holes must be drilled. The polymer tip produced little material damage initially, as energy was absorbed into elastic compression and lateral expansion of the polymer itself. Compaction zones grew quickly beyond 2mm depth, leading this design to achieve the greatest axial stability. Thus finally it was mentioned that polymer-tipped indenters might be useful, when there is insufficient trabecular tissue to develop a stabilizing compaction zone or when implants are inserted into the bone of poor quality, such as osteoporotic bone.

Li et al. [170] investigated corrosion, mechanical properties and biocompatibility evaluation of MgF_2-coated Mg-Zn-Zr alloy as cancellous screws. It was observed that the coated cancellous screw maintain its integration in shape and high yield tensile stress after immersion in SBF for 30 days. *In vivo* experiment indicated that MgF_2 coated Mg-Zn-Zr alloy screw presented advantages in cytocompatibility, osteoconductivity and ontogenesis of cancellous bone in rabbits. Corrosion rate was also very slowly with time in long term study. The coating protected the screw substrate from degrading by the formation of new borne tissue around the coating. The coated screw was covered by compact tissue and a calcium magnesium phosphate layer after six months of implantation, which may hinder the corrosion at some degree. Roesler et al. [171] reported about torsion test methods for PDLA 70/30 anterior cruciate ligament (ACL) interference screws. Based on the screw clamping length, screw driver insertion length and the gauge length, twenty completely fabricated screw that had been submitted to different levels of hydrolytic degradation was evaluated. The result of

degradation shows a clear transition of screw mechanical behavior from ductile to brittle. The average stiffness value was about 70 Nmm/degree for virgin screw while the average value for screws after 60, 120 and 240 days degradation were 81, 73 and 54 Nmm/degree respectively. Baums et al. [172] studied intra articular migration of broken biodegradable interference screw after ACL reconstruction. In this, 29 year old female patient with a failure of biodegradable interference screw after 22 months after ACL reconstruction using bone patellar tendon bone graft was analyzed. It was observed that the screw broke and migrated into the knee joint, might be due to small diameter of the screw, poor bone quality, bone resorption and screw divergence as potential factors for inter articular migration of metallic interference screws, no specific risk factors for screw breakage and inter articular migration was reported.

Heimbach et al. [173] showed the effect of Hydroxyapatite concentration on high modulus composite for biodegradable bone fixation devices. It was mentioned that the material must have high modulus and great toughness. To get this, PLLA was utilized in combination with the matrix composed of poly caprolactane and HAp nano rods. The flexural strength of the composite was found 187 MPa. It was mentioned that PLLA fibers had a relatively small diameter, which is known to increase mechanical properties due to better alignment of the polymer chain as well as the increased surface area available for bonding to the polymer matrix. PLLA and PCL are very compatible. The main reason is due to stems from the hydrogen bonds made possible between the ketone functional group in the PCL, and the PLLA is the construction of the PCL around PLLA caused by the cooling takes place after compression molding process. It was also observed that beyond 15% volume of the nano filler, the overall composite becomes significantly more brittle. Thus finally concluded that

the fabricated composite exhibit great toughness and no brittle failure, indicated its great potential to be used as a bone fixation device. Sahoo et al. [174] reviewed nano composite for bone tissues regeneration. It was mentioned that crucial factor for nano composites is to mimic living bone tissue since no single material can mimic the composition, structure and properties of native bone. Thus nano composite is the best choice for bone tissue regenerations as they can provide the appropriate matrix environment, integrate desirable biological properties. The bone like nano composite, guided bone regenerations covers aspects of interest such as biomimetic synthesis of bone like nano composites. Niinomi et al. [175] reported biomedical titanium alloys with young's moduli mechanical properties. It was mentioned that the biocompatibility of the titanium and its alloys are superior to those of other representative metallic biomaterials. It was also mentioned that low young's modulus titanium alloys composed of nontoxic and allergy free elements are highly expected to be used in practical applications for load bearing implants such as the stem of artificial hip joints. These titanium alloys are expected to reduce adjacent segmental diseases after a spinal fusion because the rod made are flexible. However it was also suggested that the efficiency of the low young's modulus must be proven to obtain approval.

Nasution et al. [176] investigated mechanical and corrosion properties of partially degradable bone screw made of pure iron and stainless steel 316l by friction welding. The pins and screw were analyzed *In vitro*, *Ex vivo* and *In vivo* mode of studies. The maximum pull out of the screw prototype was 3800 N with a calculated failure strength by shear load equal to 22.2 kN which is higher than the strength of cortical bone. It was observed that iron ion concentration in the rat's blood slightly increased from 55 to 61 ppm without affecting the tissue recovering and healing phase. This work also demonstrated a successful friction

welding technique in joining pure iron and typed 316 stainless steel as well as prototyping of partially degradable bone screws. The slight increase of iron ion concentration in rat's blood did not affect the tissue recovering and healing phase. Thus, it has potential applicability of partially removable bone screw concept. Zhu et al**.** [177] reported novel bio resorbable phosphate glass fiber textile composite for medical applications. It was mentioned that manufactured yarn and textiles from phosphate glass fibers were twisted and coated with epoxy resin, which provided additional integrity and surface protection, making them more suitable for the weaving process. It was also explained that the mechanical properties of the composite were dependent on the fibers and polymer matrix for load bearing and the interfacial bonding between fiber and matrix for the load transfer. The flexural strength and modulus decrease with time was due to the water, which diffused into composite sample acting as a plasticizer and reducing the mechanical properties of the PLA matrix. Additionally, water that diffused into the composite samples was able to degrade the interface between the fiber and matrix, resulting in poor stress transfer efficiency and reduction of flexural properties. This phenomenon was referred to as the "wicking effect". However, the degradation rate of all the composites was faster than desired, with only~20% flexural strength and ~25% flexural modulus maintained by the 28 day time point. Moseret et al. [178] investigated pull out the strength of 2 mm cancellous and cortical screw in the synthetic bone. axial pull out and yield strength were calculated. The 2 mm cortical screw achieved lower axial pull out strength than 2 mm cancellous screw in the cancellous block. The cortical screw achieved greater pull out strength than 2 mm cancellous screw in bi cortical blocks. It was finally concluded that cancellous screw displayed superior mechanical properties in the

cancellous block and may be preferred over 2 mm cortical screw in sites with exclusively cancellous bone or cortices under 1mm of thickness.

Downey et al. [179] reported fully threaded versus partially threaded screws for determining shear in cancellous bone fixations. The 36 numbers of synthetic saw bones block were used to test screw fixations. In groups, block 1and 2 were fixed together using standard manufacturer recommended method for inserting 4 mm partially threaded stainless steel cancellous bone screws. The constructs were then mechanically tested. Shear was applied by compressing each construct at an axial displacement rate of 0.5 mm/s until failure. The fully threaded screw had a significantly greater (p ¼ .026) initial stiffness (106.4±15.8 N/mm) than the partially threaded screw (80.1 ± 27.5 N/mm). The yield load and displacement for the fully threaded group (429.4 ±11.7 N and 7.2 ± 0.35 mm) were 64% and 67% greater than those for the partially threaded screw group (261.4±26.1 N and 4.3 ± 1.03 mm), respectively. The result observed the importance of a full thread construct to prevent shear and to decrease strain at the fracture. Varghese et al. [180] investigated effect of various factors on the pull out strength of pedicle screw in the normal and osteoporotic cancellous bone. Pedicle screw is generally used for the treatment of spinal instability by spine fusion. Screw loosening is a major problem of spine fusion, contributing to delayed patient recovery. The probable factors are effects of density, insertion depth and insertion angle. It was also found that the density contributes most to pull out strength and insertion torque. The interaction effect is significant and contributes 8% to pull out strength. Axial pull out strength was 34% lower than angled pull out the strength in the osteoporotic bone model. Chapman et al. [181] discussed factors affecting the pull out the strength of cancellous bone screws. It was observed that the pull out of the screw in porous materials is governed by the factors like the major diameter, the

length of the engagement of the thread, the shear strength of the host material, thread depth and pitch. It was also mentioned that tapping decreases screw pull-out strength because the removal of material by the tap enlarges the hole considerably, in effect decreasing the depth of the internal threads.

Sideset al. [182] reported bending stiffness and pull out the strength of 6.5 mm tapered, variable pitch, cancellous screw. Generally, stabilization of fifth metatarsal jones fractures with the intramedullary screw is popular, particularly in athletes because inoperative treatment involves prolonged casting and risk of non-union and delayed union. This study was designed to compare jones fracture fixation with 6.5 mm partially threaded cancellous lag screw. The result observed no demonstrable difference in bending stiffness between metatarsal fixed with the two types of screw. The 6.5 mm screw provided significantly higher resistance to pull-out. It was concluded that headless, tapered, variable pitch compression screws of the size tested were not entirely comparable to 6.5-mm lag screws. They were effective in resisting bending but do not offer equivalent resistance to thread pull-out. Shi et al. [183] investigated silk based fixation material with mechanical properties and biocompatibility. The Gentamicin was added to make the antibacterial absorbable screw. The antibacterial activity was assessed against E. coli *In vitro* by plate cultivation. The gentamicin loaded silk based screw (GSS) showed significant bactericidal effects against E. coli. The pure silk based screw has a bending strength of 204 MPa, while the value of shear strength and young modulus were about 36 MPa and 8.3 GPa. The GSS was having a bending strength of 2.3 MPa, shear strength of 35 MPa and young modulus of 8.5 GPa. There were no significant changes occurs between them. It was finally observed that antibacterial silk based fixation material can overcome the limitations of metals and traditionally resorbable devices

with great potentials. Thus from the above literature the various researchers have used materials for the application as cancellous screws. However, for joining metaphysis part of the long bone, the cancellous screw is many essentials for it. In this work, the cancellous screws were fabricated through melt blending using twin screw extrusion cum injection molding machine as mentioned in chapter 3. Initially, the powdered form of PLA and nHAp were mixed manually into proper proportion, after that the mixture of these were fed to the extruder machine for melt blending. The melt blended mixture was further injected in the attached injection molding machine for fabricating the desired shape of cancellous screws. The parameters for the whole process is shown in Table 4.1. After the production of screws, the screws were annealed in the vacuum oven for 8hrs at 70° C so that the residual stress arises during injection molding gets normalized. After annealing, the mechanical testing were done as per ASTM F2502-11 (Standard specification and test methods for Absorbable Screws) through universal tensile test machine and torsion machines.

Table 4.1: Parameters for cancellous screws production.

Parameters		
1.	Processing temperature	190°C
2.	Mold temperature	95°C
3.	Cylinder temperature	215°C
4.	Residence time	1min
5.	Twin screw speed	120 rpm
6.	Compressed air pressure	700-710 bar
7.	Injection pressure holding time	5 sec
8.	Weight of cancellous screws	1.68 g

4.2 Development of Cancellous screws

The cancellous screw was designed in AutoCAD as per the ISO5835:1991(en). The total length maintained was ~71 mm. The threaded portion length was maintained 18.5±1 mm. The inner diameter and outer diameter were kept 4.5±0.1 mm and 6.5±0.1 mm respectively. The pitch maintained was 2.75 mm. The detail dimensional shown in Figure 4.1

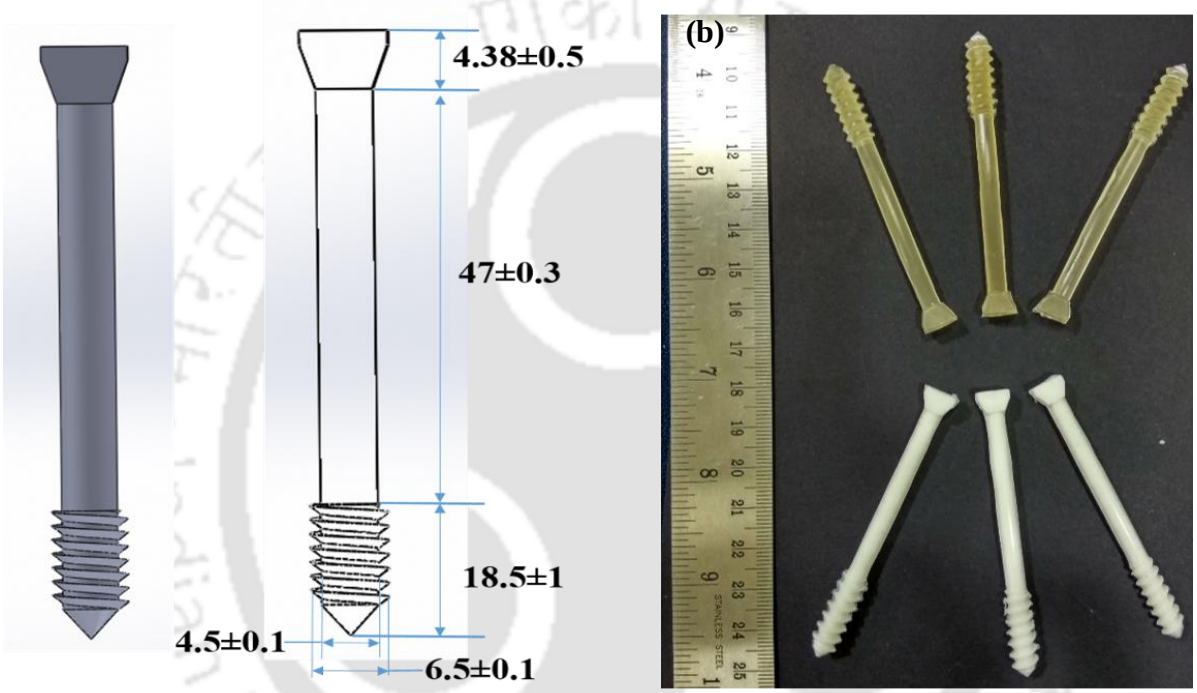

Figure 4.1: Schematic diagram of cancellous screws (a) 3D and line diagram of cancellous screws (b) Photographic images of neat PLA (top) PLA/nHAp (bottom) cancellous screws.

4.3 Development of molds and fixtures for cancellous screws

The molds for injection molding and related fixtures for its testing were initially designed in AutoCAD. After designing, the mold were manufactured using various manufacturing machines passed through various machining processs. The material choosen for making the

molds was H13 (Tool Steel) due to its excellent combination of high toughness and resistance to thermal fatigue cracking. The H13 metal was initially heat treated up to annealing temperature afterwards machined to make the mold as per the machine specifications. After machining the copper electrode were also fabricated through lathe machine in ordert to do the electric discharge machining process to get the perfect shape of the cancellous screw cavity on the fabricated molds. The Figure 4.2 shows the 3D model of the molds fabricated for cancellous screw production.

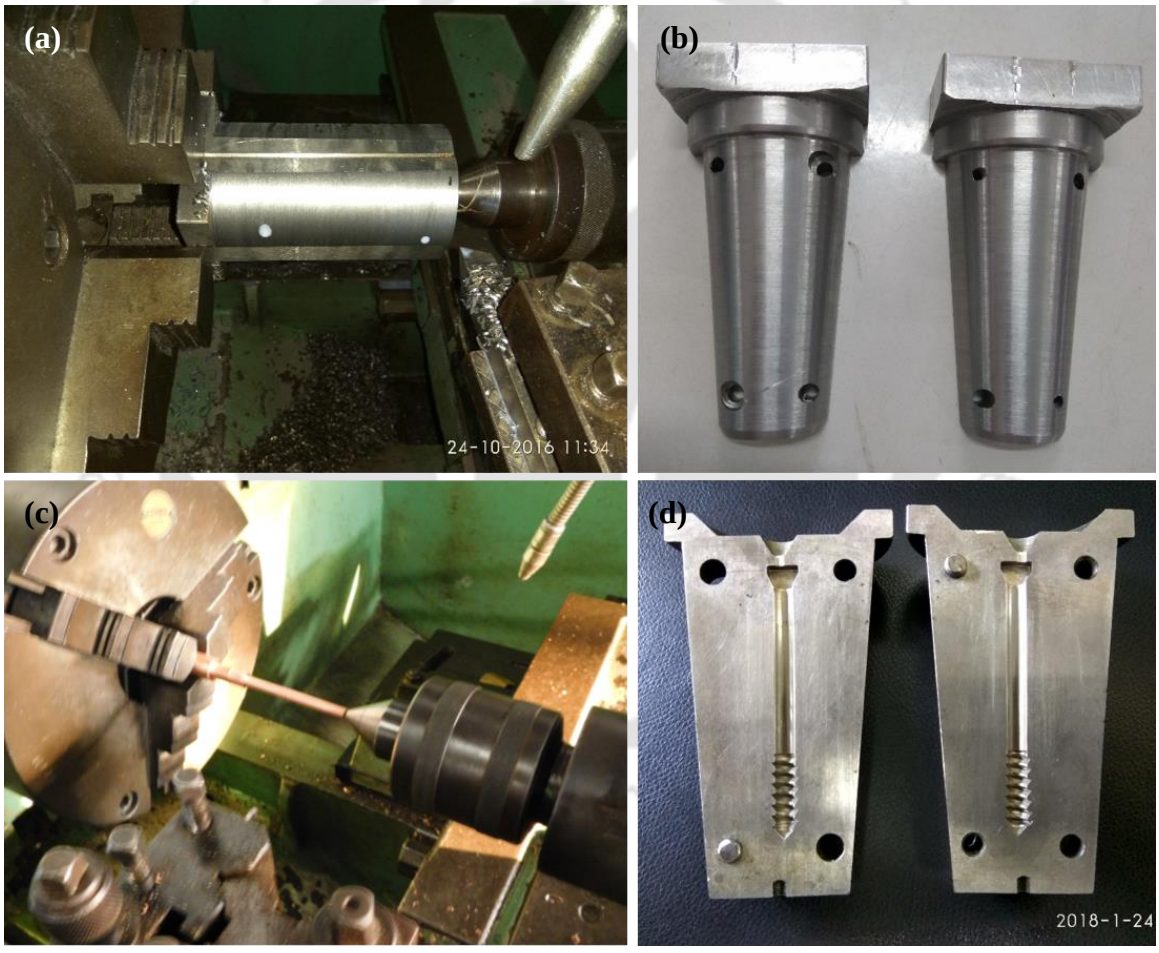

Figure 4.2: Schematic diagrams for fabrication of cancellous screw molds (a) Machining of mold (b) Mold in prefinal shape (c) fabrication of copper electrode (d) Mold in final shape after machining.

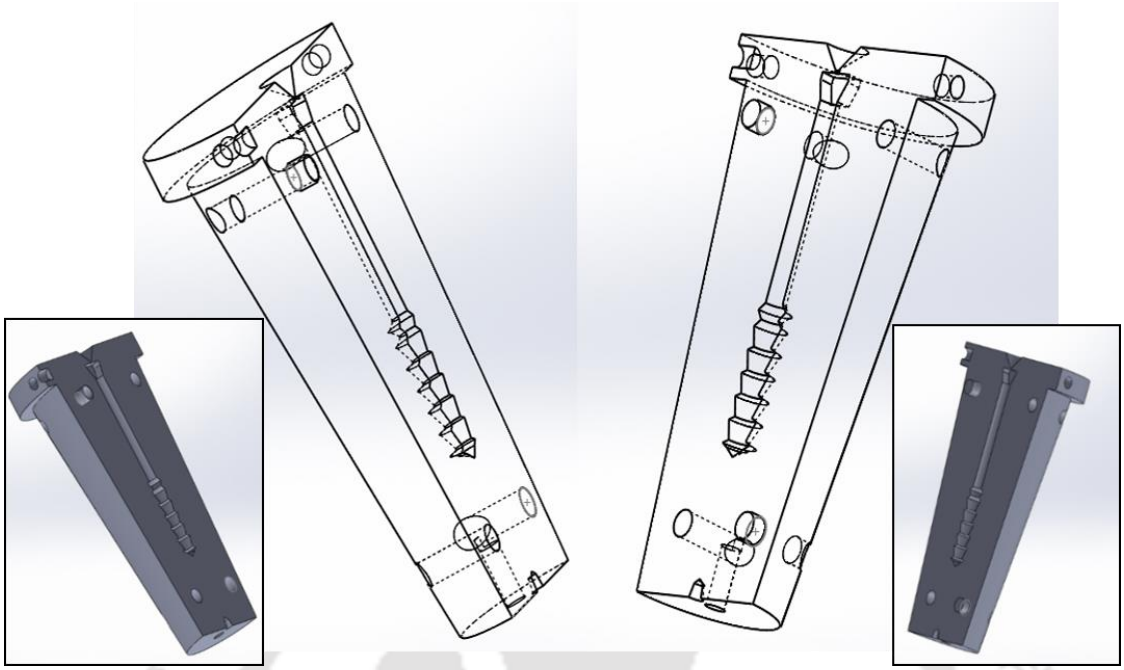

Figure 4.3: 3D solid model diagram (inset) and 3D line model diagram of fabricated cancellous screws mold.

4.4 Mechanical Testing of Cancellous screws

After production of cancellous screws, the mechanical testing was done as per ASTM F2502-11 (Standard specification and test methods for Absorbable Plates and Screws for internal fixation Implants). The test was conducted on universal tensile testing machine and torsion machine by attaching as customized fabricated fixtures. The mechanical test was conducted in both modes i.e. before the *In vitro* hydrolytic degradation and after the *In vitro* hydrolytic degradation. The degradation studies were conducted in the lab made phosphate buffer saline solution (PBS) at 37° C as per the ASTM F1635-11 standards.

4.4.1 Axial Pull out Strength

The axial pullout strength was determined using the universal testing machine (Kalpak Instrument, Pune, India) according to standard ASTM F 2502-11 using a fabricated pull out fixtures. The fixture was perfectly aligned with the longitudinal axis of the screw and the attached load frame.

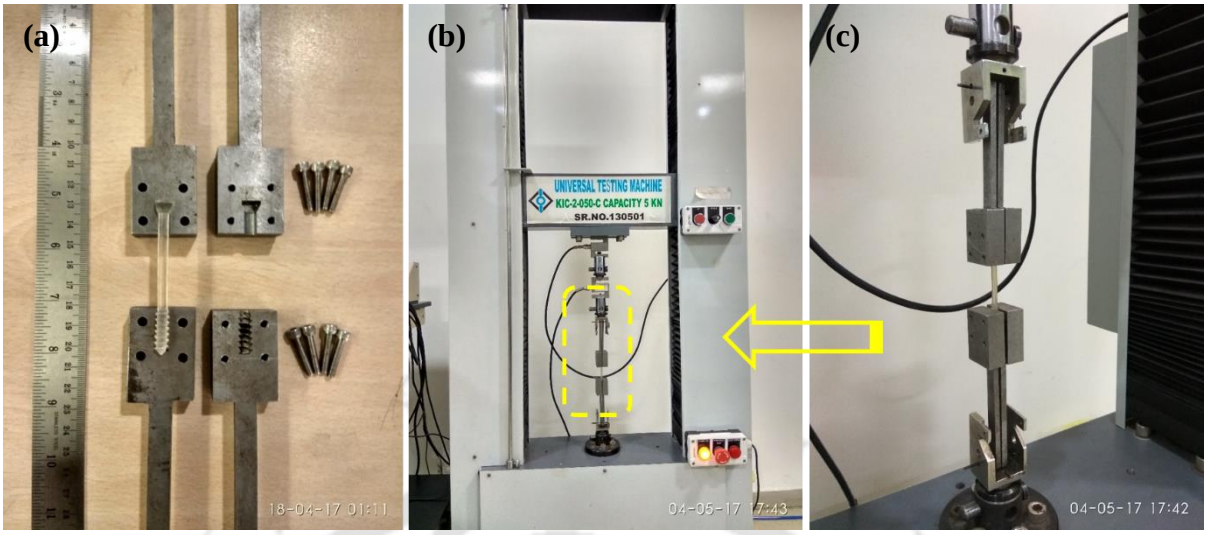

Figure 4.4: Fixtures for axial pull out the test (b) Arrangement of cancellous screw fixture in universal tensile test machine (c) Magnified pictorial images of fixture set up.

Figure 4.5 shows the value of pull-out strength of the cancellous screw concerning the varying concentration of nHAp (Wt. %) into the PLA matrix. It was observed that 10% of nHAp had ~18% increment concerning neat PLA (0 Wt. % nHAp). The value obtained was ~561 N in case of 10% nHAp while in case of neat PLA, it was 476 N.

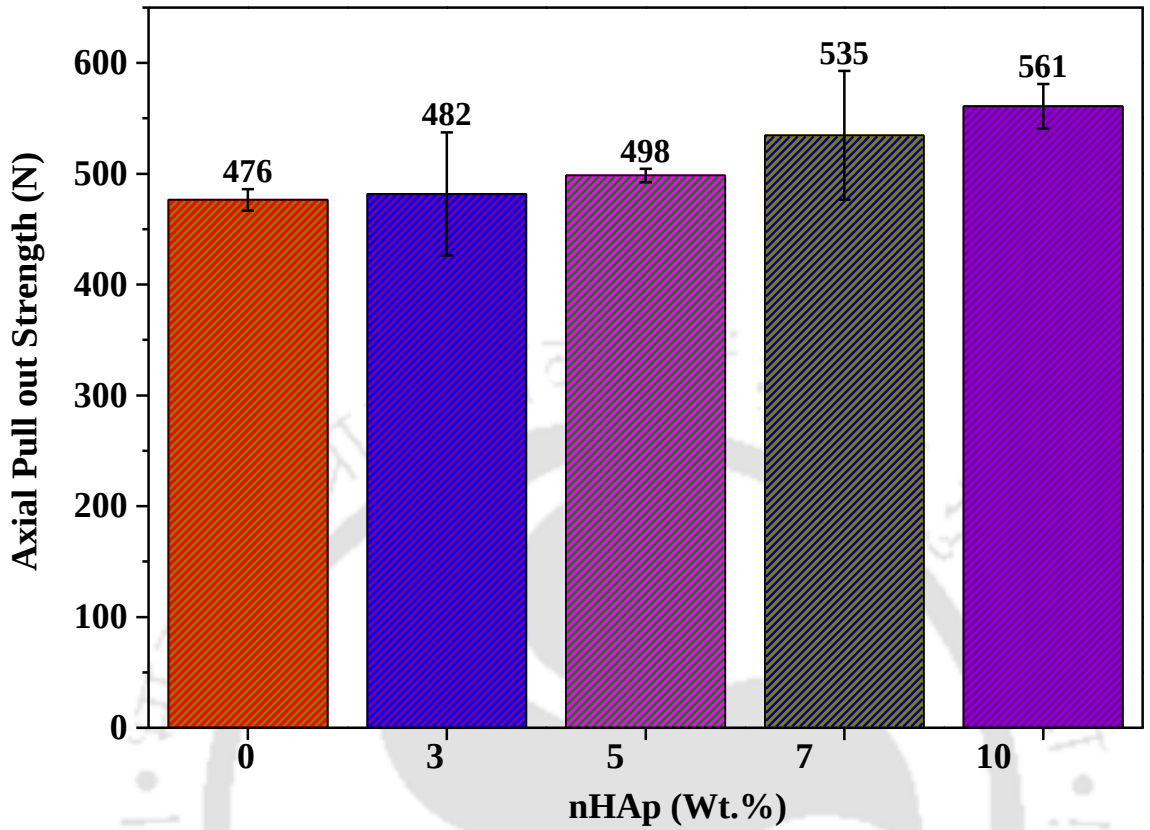

Figure 4.5: Axial pull out strength value of cancellous screws with varying concentrations.

It means that the addition of nHAp leads to enhance the pull-out strength value. The enhancement in axial pull out strength may be due to the alignment of short chains present in the polymer matrix since the polymer matrix consists of a mixture of long and short chains, these shorter chains are responsible for breaking the entangled chains under the application of the pull-out test [184]. The other reason might be the transverse support provided by the nHAp in the polymer matrix to PLA chains. Figure 4.6 shows the value of axial pull-out test before and after hydrolytic degradation studies of neat PLA and 10% nHAp. In case of neat PLA the axial pull out strength gets reduces from 476N to 423N (reduction of ~11%) after 30 days, 476 to 379N (~21% reduction) after 60 days and 334N (reduction in ~30%)

after 90 days, while in case of 10% nHAp, reduction was happening from 561N to 539N (reduction of ~4%) after 30days, to 483 (reduction of ~14%) after 60 days and 432 N (reduction of ~23%) after 90 days. It can be also observed from Figure 4.6, that for the same duration of hydrolytic degradation, the rate of reduction of mechanical strength in the case of 10% nHAp is less as compared to neat PLA.

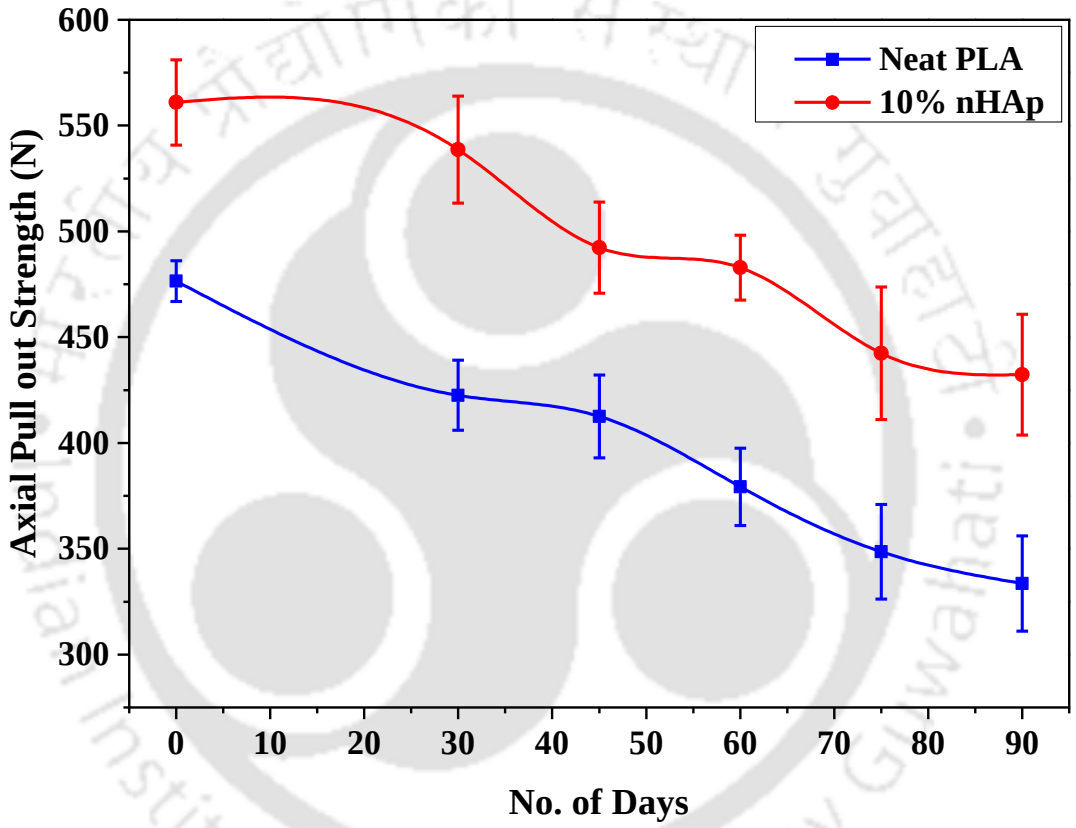

Figure 4.6: Axial pull out strength of neat PLA and 10% nHAp after In vitro hydrolytic degradation.

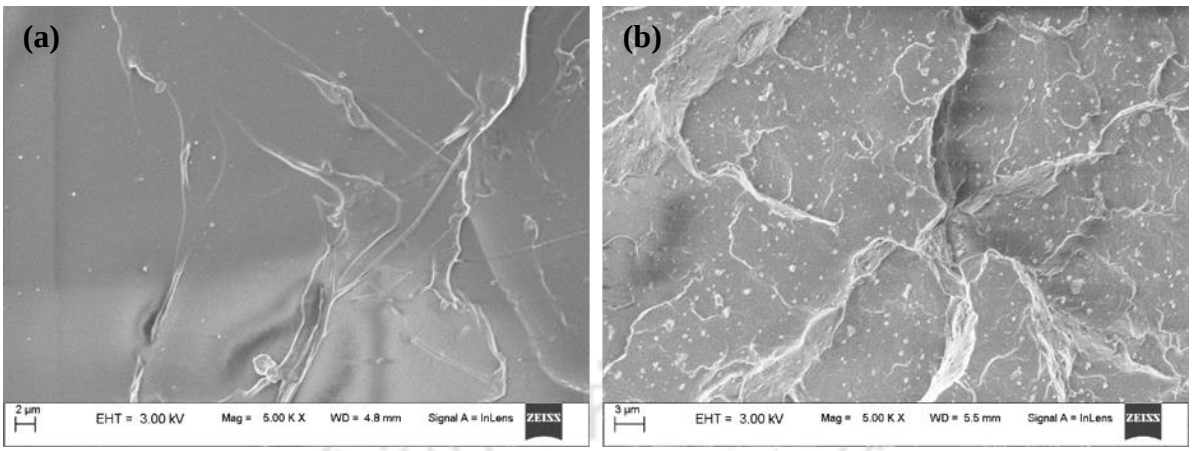

Figure 4.7: Surface micrograph from FESEM after axial pull-out test of cancellous screws (a) neat PLA and (b) PLA/nHAp.

The surface micrograph of the fractured cancellous screws after the axial pull-out test is shown in Figure 4.7. Initially, the pull-out strength of the cancellous screws was gradually reduced later as the time passes by the pull-out strength decrease rapidly. The reason may be due to the interaction of water molecule interacting with the surface of cancellous screws leads to increase in the crystalline part of the PLA, which further increases the brittleness and thus axial pull-out reduces.

4.4.2 Torsional Strength

The maximum torque, breaking angle were measured for the cancellous screw produced according to the standard ASTM F 2502-05 using fabricated torsion fixture. The measurement was done in torsion testing machine (make: Fuel instruments and equipment, India). The crosshead speed of the machine was one revolution per minute. The load cell capacity of the machine was 10kgf.m (98066.499 mili Newton meter). The gauge length was maintained about 30% of the total length of the screws. The maximum torque was represented by the highest recorded value of the torque during the test, and the breaking angle was the rotation angle at the maximum torque. The measurement was carried out in triplicate. The

fixture was made from steel metal. The arrangement of the fabricated torsional fixtures with the attached fabricated cancellous screw is shown in Figure 4.8.

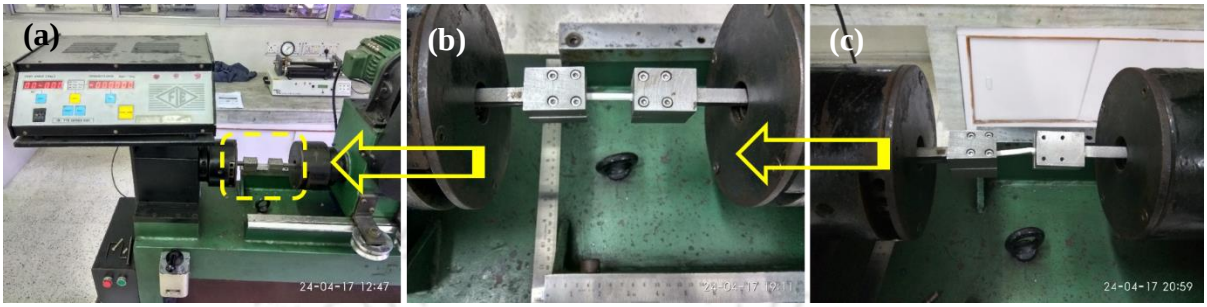

Figure 4.8: (a) Torsion machine set up (b) cancellous screw holding in the torsion set up the machine (c) After torsion testing

Figure 4.9 shows the value of torsional strength and value of twisting angle during the torsion test of the cancellous screw. It was observed that addition of nHAp enhances the torsional strength values. The increment observed was about~48% from 680 mNm (neat PLA) to 1007 (mili Newton meter) mNm (10 %nHAp). This may be due to enhanced interfacial adhesion due to reactive extrusion process inside twin screw extruder machine, a strong shear force generated between twin screws this uniform dispersion of nHAp particles between PLA chains takes place. Strong interface bonding yields large torsion load bearing property and torsion strength [185]. However, matrix elongation has a more important effect on torsion strength than interface bonding strength.

Figure 4.10 shows the values of ultimate torque after *In vitro* hydrolytic degradation studies. The studies were conducted for 30^{th} days, 45^{th} days, 60^{th} days, 75^{th} days and 90^{th} days. It was observed that torsional strength were reduced from 680 (mNm) to 575 mNm (~15%) after 30 days and to 410 mNm (~40% reduction) after 90days, however in case of 10% nHAp, the reduction was observed from 1007 mNm to 891 mNm (~12% reduction) after 30days and 1007 mNm to 717 mNm (~29% reduction) after 90 days.

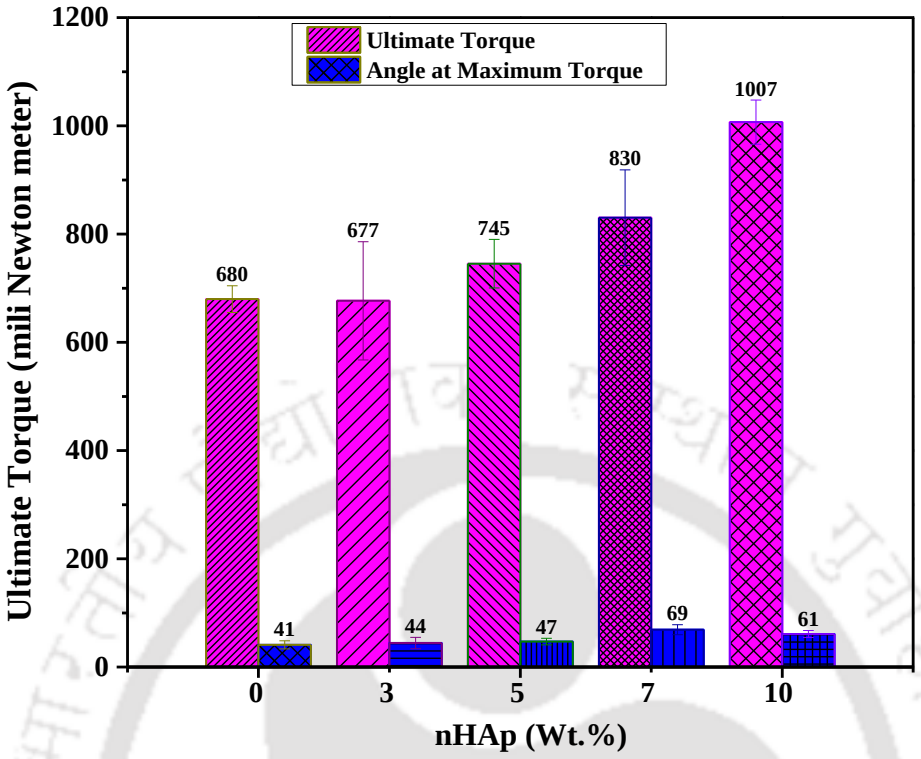

Figure 4.9: Torsional strength value and corresponding twisting angle of cancellous screws with varying concentrations.

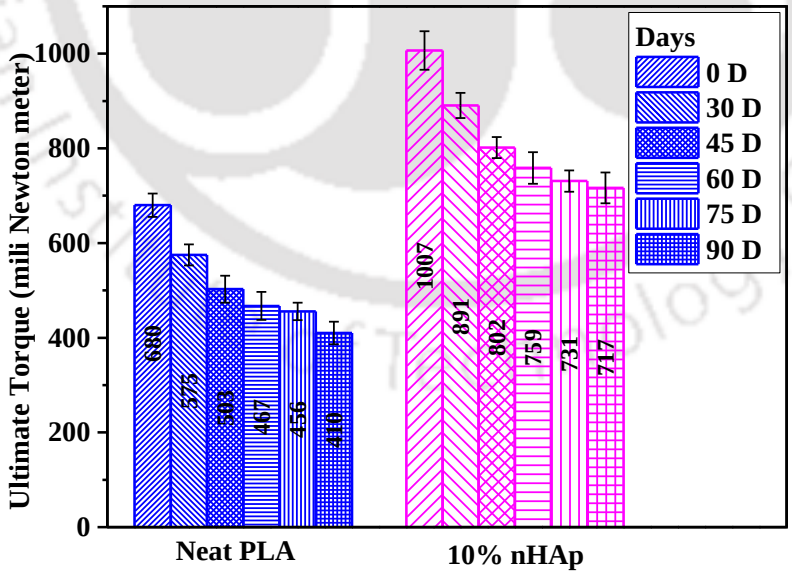

Figure 4.10: Torsional strength of neat PLA and 10%nHAp after In vitro hydrolytic degradation.

The twisting angle with respect to the ultimate torque value obtained from torsional strength is shown in

Figure 4.10.

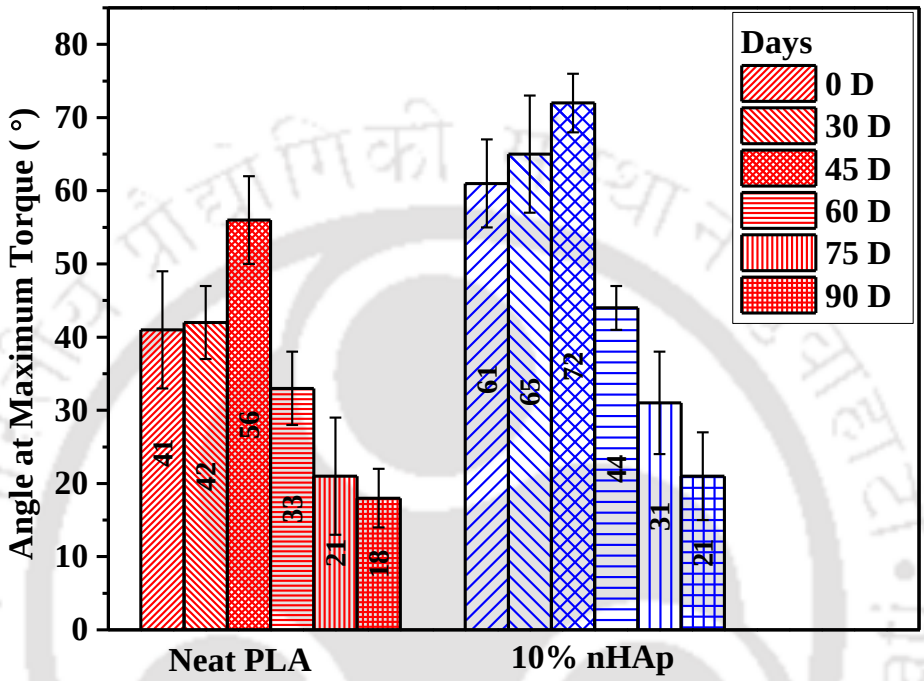

Figure 4.11: Twisting angle corresponding to the ultimate torque of neat PLA and 10 % nHAp after In vitro hydrolytic degradation.

It was observed that an increase in the concentration of nHAp particles into PLA matrix leads to an increase in brittleness of the cancellous screws which ultimately proceeds for fractures of the cancellous screw at less twisting angles. The value of the twisting angle of neat PLA and 10% nHAp cancellous screw during *In vitro* hydrolytic degradation is shown in Figure 4.11.

4.4.3 Flexural testing

The maximum flexural load for the cancellous screws were evaluated by flexural (3 point bend test) test using a fabricated flexural fixture at room temperature. A cross head speed of

1mm/min and a load cell of 5 kN was used. The support span was 40 mm, and radii for loading and supporter applicators are 3 mm. Measurement was conducted in triplicate. The fixture was made of steel metal.

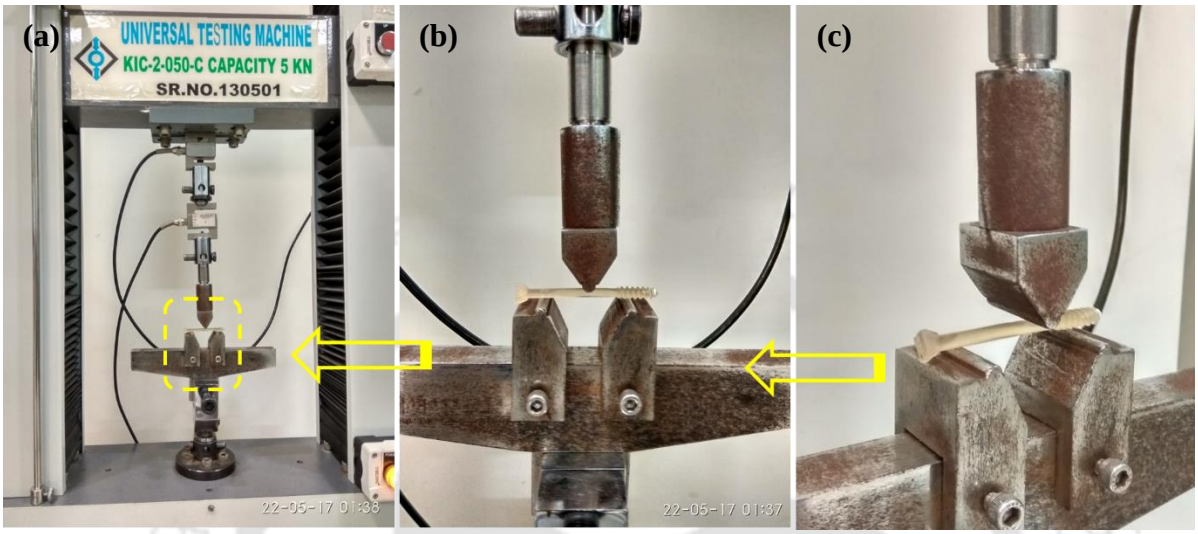

Figure 4.12: Flexural test set up for the cancellous screw (b) Magnified view of the set up (c) side view of the arrangement of the cancellous screw for flexural strength measurement.

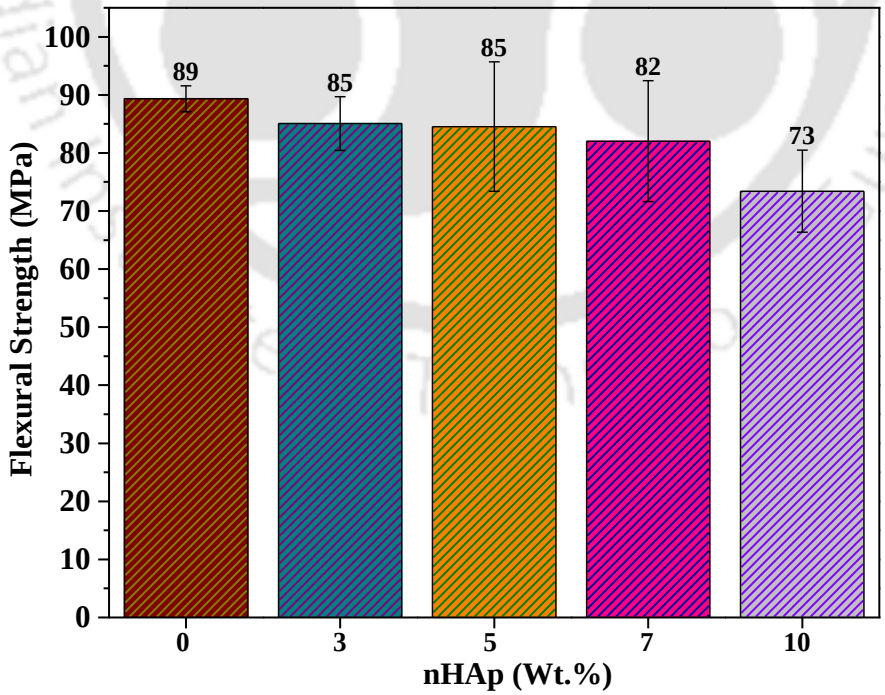

Figure 4.13: Flexural strength value of cancellous screws with varying concentrations.

Figure 4.12 shows the arrangement of three-point bend test fixture with the cancellous screw for the flexural test. The samples were tested in triplicate. Figure 4.13 shows the flexural strength value of the cancellous screw after varying the concentration of nHAp. It was observed that the reduction of strength was obtained as we increase the nHAp concentration; it may be because of restricted crosslinking of polymer chains and nHAp particles. It was observed also due to agglomeration of nHAp leads to ununiformed dispersion, which became the factors in reducing the bending properties. The other reason may be due to the diffusion of water into the cancellous screw act as a plasticizer and reducing the bending properties of the PLA matrix [186]. The water from PBS solution that diffused into PLA/nHAp cortical was sufficient enough to degrade the interfaces on the cancellous screw surfaces. The degradation which results in poor stress transfer efficiency and thus leads to fracture of the screws. From Figure 4.14, the reduction was observed from ~89 MPa to ~73 MPa (~18% reduction) with varying concentration from neat PLA to 10% nHAp. The cancellous screw were further conducted *In vitro* hydrolytic degradation, and then flexural strength were analyzed, it was observed ~12% reduction after 30 days, ~34% after 60 days and ~49% reduction after 90 days was happened in case of neat PLA, while in case of 5% nHAp, ~13% reduction was observed after 30 days and 38% reduction was after 90 days. It was also observed that for the same duration of exposure in PBS, 5% nHAp has less degradation rate as compared to neat PLA. The fractured surface micrograph is shown in Figure 4.15. It was observed that some of the nHAp particles were agglomerated which owes to the reduction of bending properties.

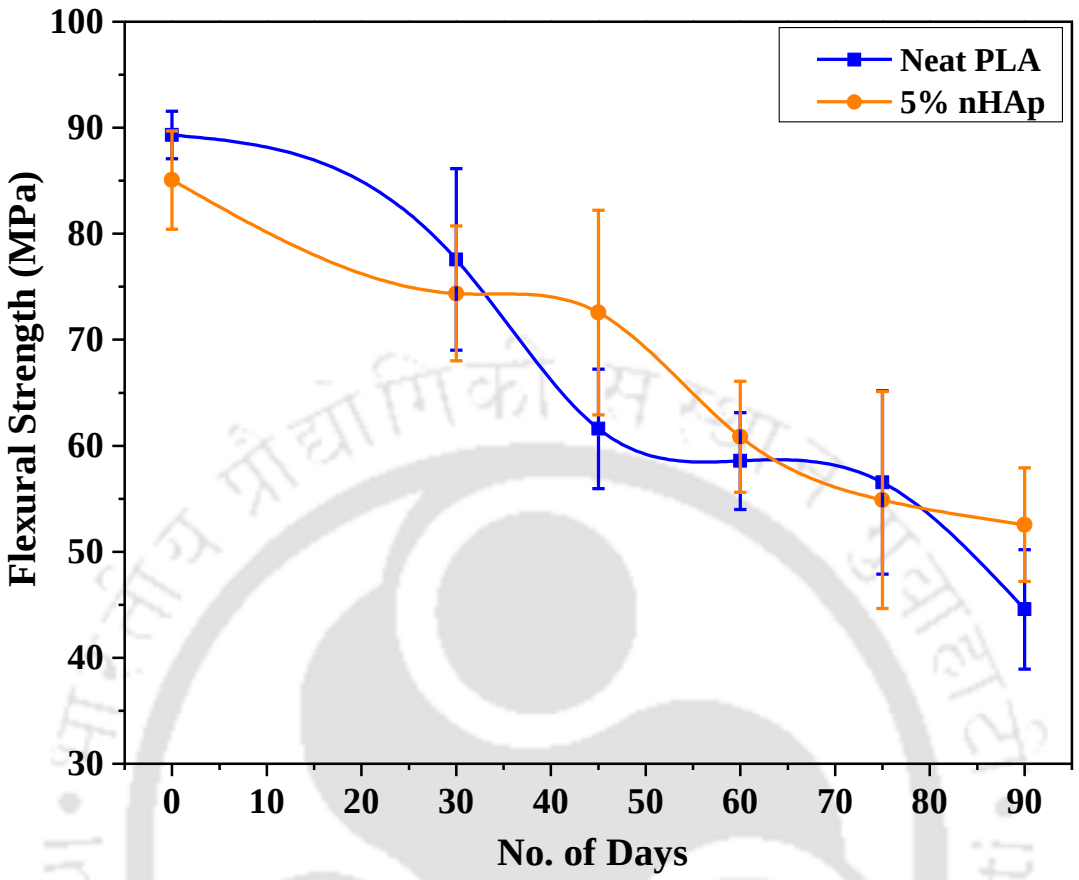

Figure 4.14: Flexural strength of neat PLA and 7% nHAp after In vitro hydrolytic degradation.

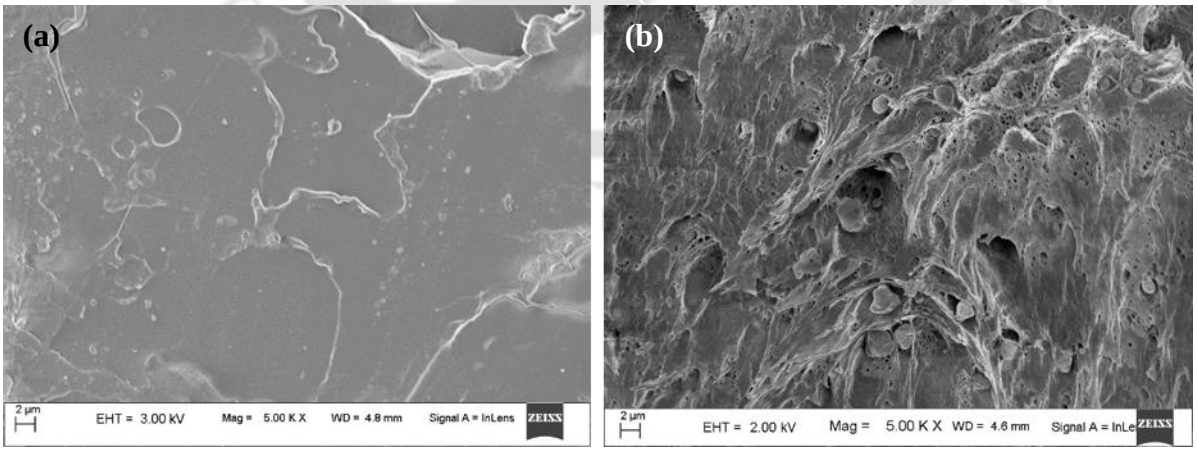

Figure 4.15: Fractured surface micrograph of (a) neat PLA and (b) PLA/nHAp from FESEM.

4.4.4 Double Shear Strength

The Double shear strength of the cancellous screws was measured through fabricated fixtures attached in the universal tensile testing machine according to standard ASTM D7617M-11. The cross head speed of the machine was 1mm/min, and load cell capacity was taken 5kN. The maximum shear load was determined as the maximum load recorded during the test. The measurement was carried out in triplicate.

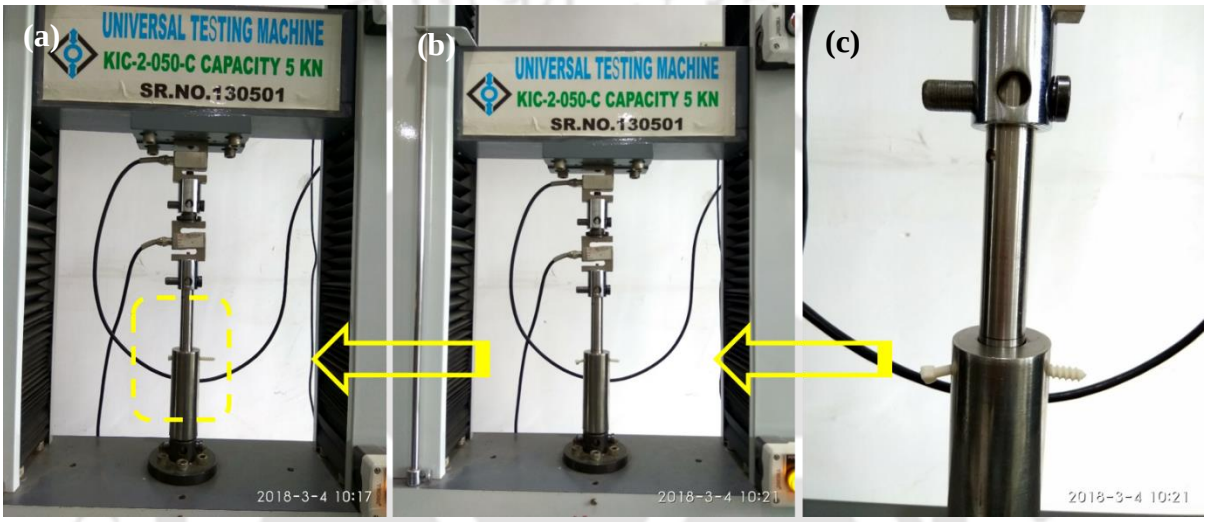

Figure 4.16: (a) Double shear strength test set up for cancellous screw (b) fixture attachment in Universal tensile test machine (c) magnified pictorial view of the cancellous screw in the fixture.

Figure 4.16 shows the attachment of the fabricated fixtures for double shear strength in the universal tensile test machine. Figure 4.17 shows the double shear strength value of cancellous screws after varying the concentration of (wt. %) of nHAp into PLA matrix. There was no much change was observed with varying the concentration. However, 10% nHAp has shown an increment of ~5% with respect with neat PLA. The improvement in double shear strength and torsional strength may be due to reactive grafting of PLA chains on the surface of nHAp leads to uniform dispersion and also enhances the interfacial adhesion between PLA chains and nHAp particles. The other reason may be due to an increase in crystallinity since

nHAp particles are crystalline and thus this crystallinity leads to more intermolecular bonding and crosslinking between nHAp and PLA chains.

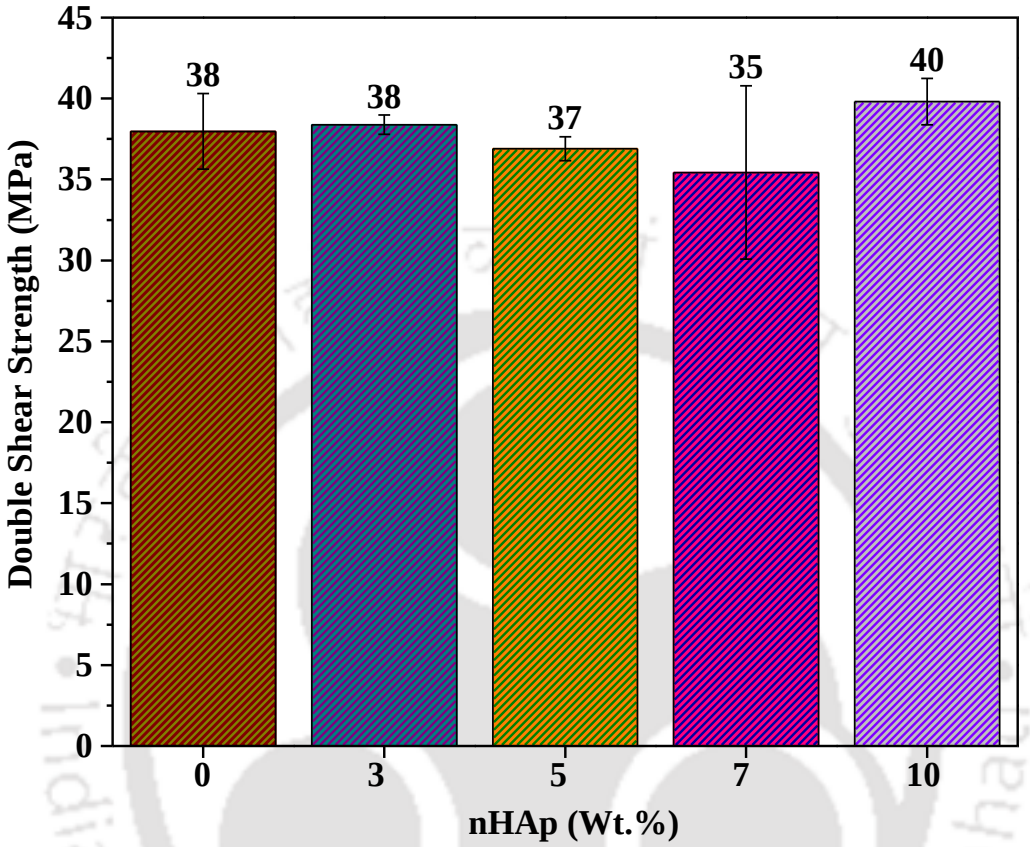

Figure 4.17: Double shear strength value of cancellous screws with varying concentrations.

The intermolecular forces on the surface area of nHAp acts as a bridge with the PLA chains which leads to support and elongate PLA polymeric chains and extend the fracture phenomenon [187-189]. During *In vitro* hydrolytic degradation studies, the double shear strength of the cancellous screws were shown in Figure 4.18. It was observed that in case of neat PLA, the reduction of double shear strength value from 38MPa to 30 MPa (~21% reduction) after 30 days and 38MPa to 19 MPa (~50% reduction) after 90 days happened. However in case of optimized concentration, i.e. 10% nHAp, the reduction from 41 MPa to 33 MPa (~20% reduction) after 30 days and from 41MPa to 22MPa (~46% reduction) after

90 days observed. It was also observed that for the same duration, the degradation rate was less in the case of 10% nHAp concerning neat PLA.

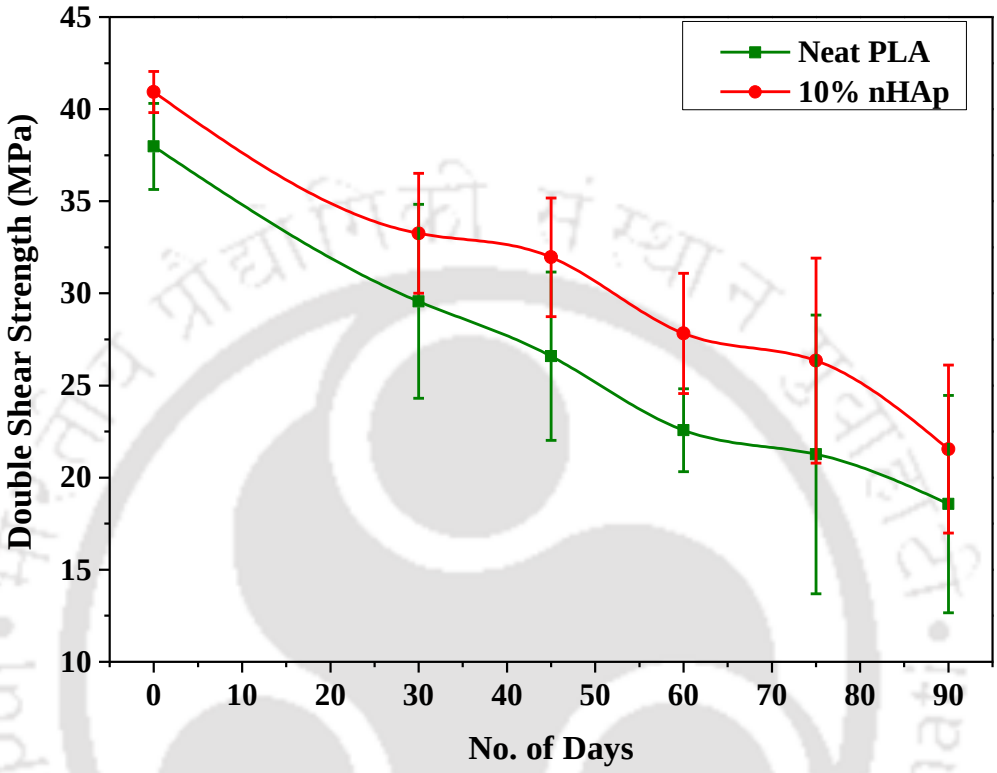

Figure 4.18: Double shear strength of neat PLA and 10% nHAp after In vitro hydrolytic degradation.

4.5 Degradation studies

Figure 4.21 shows the mass loss profile of the neat PLA cancellous screws and optimized cancellous screws (10% nHAp) exposed in PBS solution for 90 days. It was observed that ~3% reduction in mass loss after 30 days, ~11% reduction after 60 days and ~18% were a reduction in mass loss after 90 days in case of neat PLA. However, in the case of 10 % nHAp, reduction of ~3% after 30days, ~7% after 60 days and ~12% after 90days mass loss observed. It was also observed that for the same duration of exposure towards PBS solution the rate of degradation of neat PLA was faster as compared with 10% nHAp. The whole study was

conducted as per ASTM standards as shown in Figure 4.19. This studies also reveal that 100% degradation in a mass loss would be between 9 to 12 months and healing of fracture bone also takes 8-12 months. Hence for various age group peoples, cancellous screws can be tuned.

Figure 4.19: (a) In vitro hydrolytic degradation of cancellous screw arrangement in a glass jar (b) Hot air oven maintained at 37° C (c) pH measurement of PBS solution for maintaining the pH routinely.

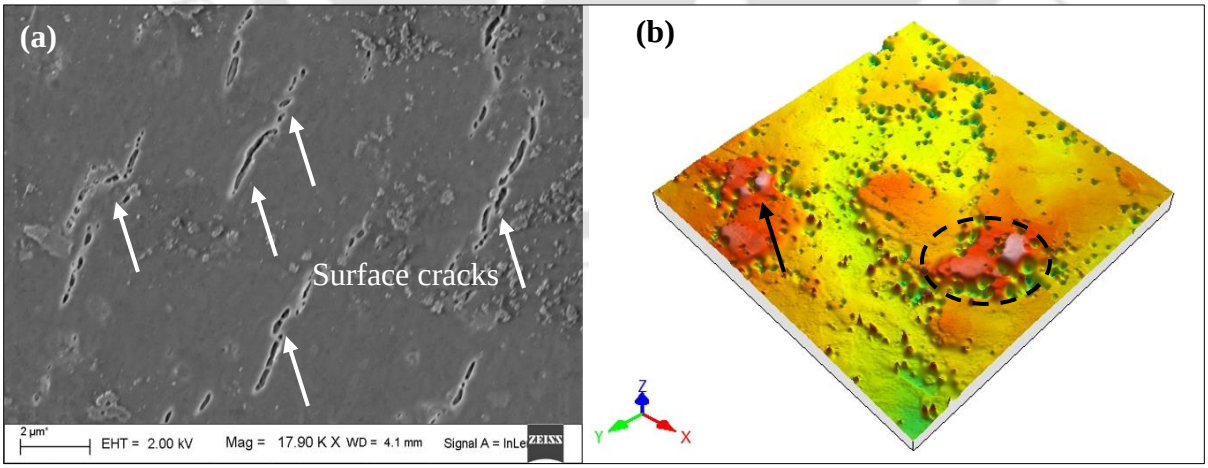

Figure 4.20: (a) Surface micrograph from FESEM after three weeks In vitro hydrolytic degradation of PLA (b) Surface Profile of the hydrolytically degraded PLA surface through surface profilometer.

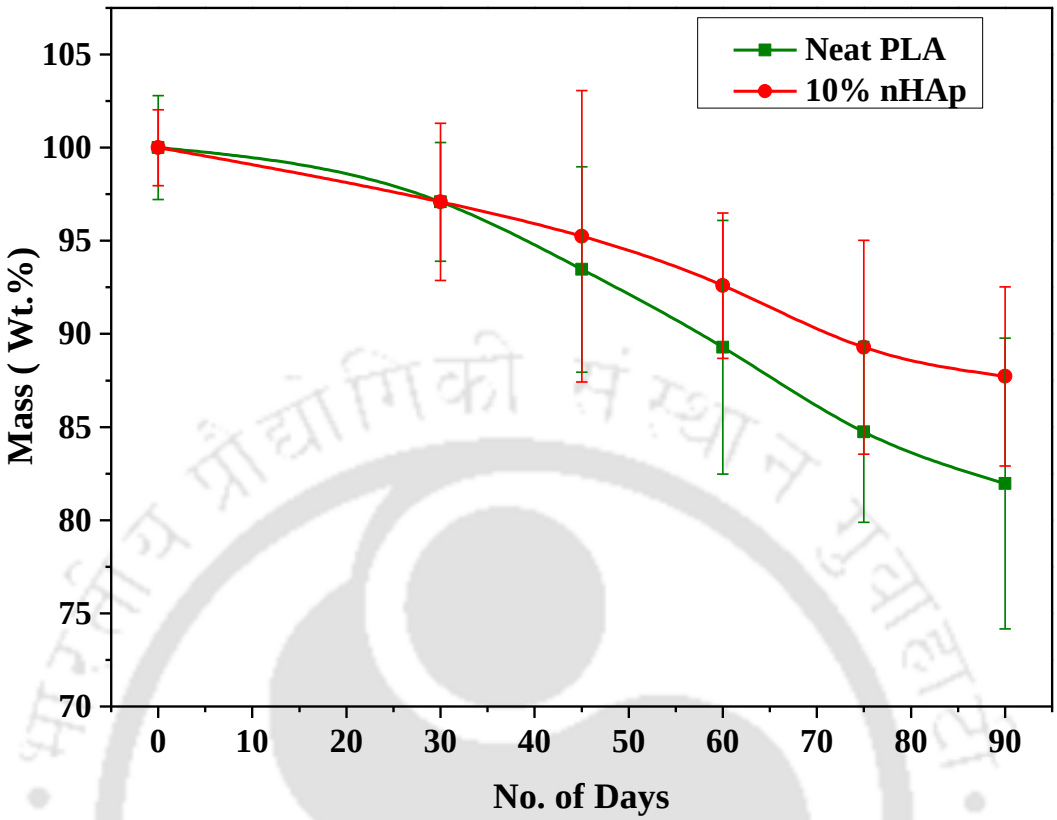

Figure 4.21: Mass loss profile of neat PLA and 10% nHAp before and after In vitro hydrolytic degradation.

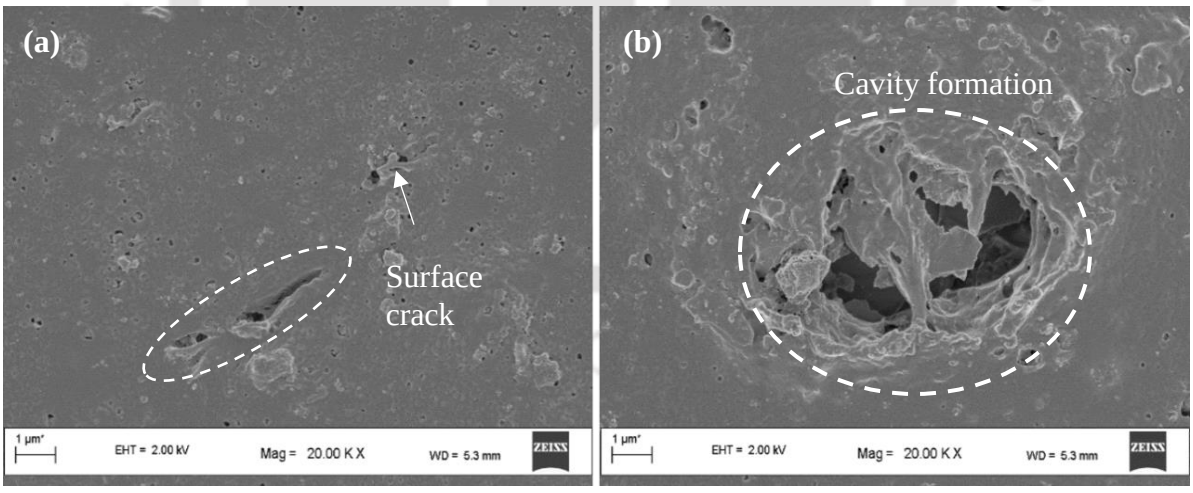

Figure 4.22: FESEM images of cancellous screw surface after 90 days In vitro hydrolytic degradation (a) Surface crack formation (b) Cavity formation due to severe degradation.

Figure 4.22 shows the surface micrograph of the degraded cancellous screw after three weeks of exposure towards PBS solution. It was observed that thee degradation of the surface starts from the surface which propagates towards inner core as the time duration increases.

Figure 4.23: Photographic images of fractured cancellous screws after torsion test and double shear strength test.

Generally PLA is semi crystalline polymeric material, the amorphous part of the PLA get direct contact with the PBS, which will lead the amorphous part out from the consolidated structure [190-192] , and the remaining crystal part would be insufficient to get the solid structure of the whole, thus leads to creation of surface crack as seen in the Figure 4.20. Figure 4.22 shows the surface micrograph of the *In vitro* hydrolytically degradaed cancellous screw surface after 90 days. Figure 4.23 shows the fracture profile of the cancellous screws through torsion test, double shear test, pull-out and flexural test. It was observed that due to the shear strength test, most of the cortical screw was failed due to brittle fracture, ductile fracture and some were due to prolonged elongation. While in case of torsional strength test,

most of the samples were failed due to gauge length shearing, shearing at screw head, shearing at the lower crest of thread and shearing cum fracture.

Figure 4.24: Photographic images of fractured cancellous screws after the pull-out test and flexural test.

From the Figure 4.24, most of the cancellous screws were failed due to brittle and ductile fracture in case of flexural test, while in case of pull-out test, the core diameter fracture, multi zone fracture and screw thread fracture were observed.

4.6 Dimensional deviation studies

In order to know the geometrical deviation of the pitch from the standard geometry, cancellous screws were analyzed through optical surface profilometer (Optomech, vertical) at 10x (Figure 4.26). The corresponding samples were also magnified through stereomicroscope (Nikon SMZ25). The obtained images are shown in Figure 4.27. The deviation in pitch profile of the fabricated cancellous screw is shown in Figure 4.25.

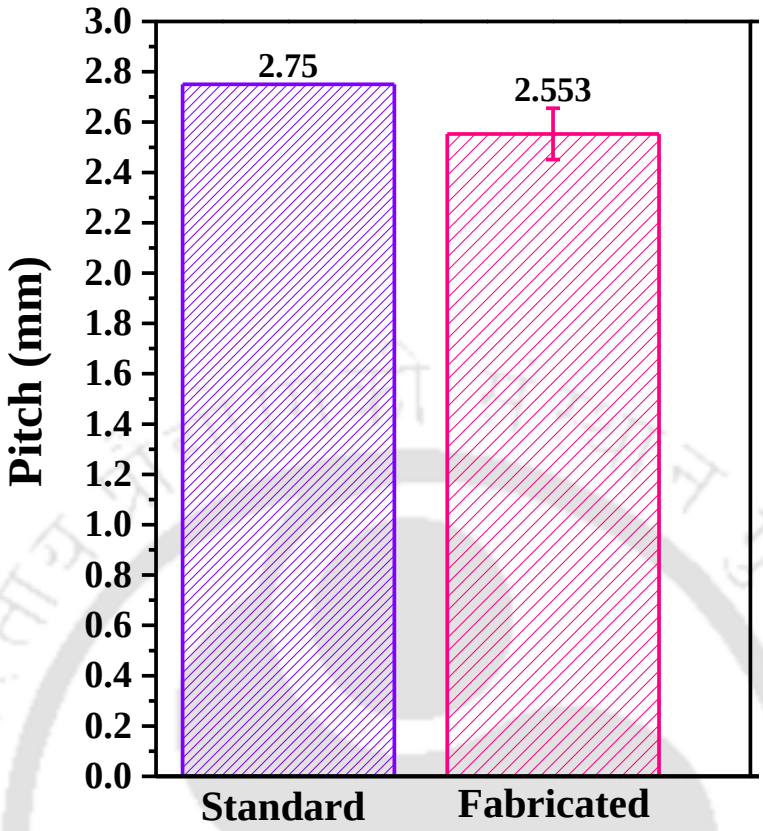

Figure 4.25: Deviation in pitch of the fabricated cancellous screw from the standard pitch.

It was observed from the Figure 4.25 that the deviation of the pitch of the cancellous screw was very less as compared with the standard dimension and later the deviated dimensions were neglected.

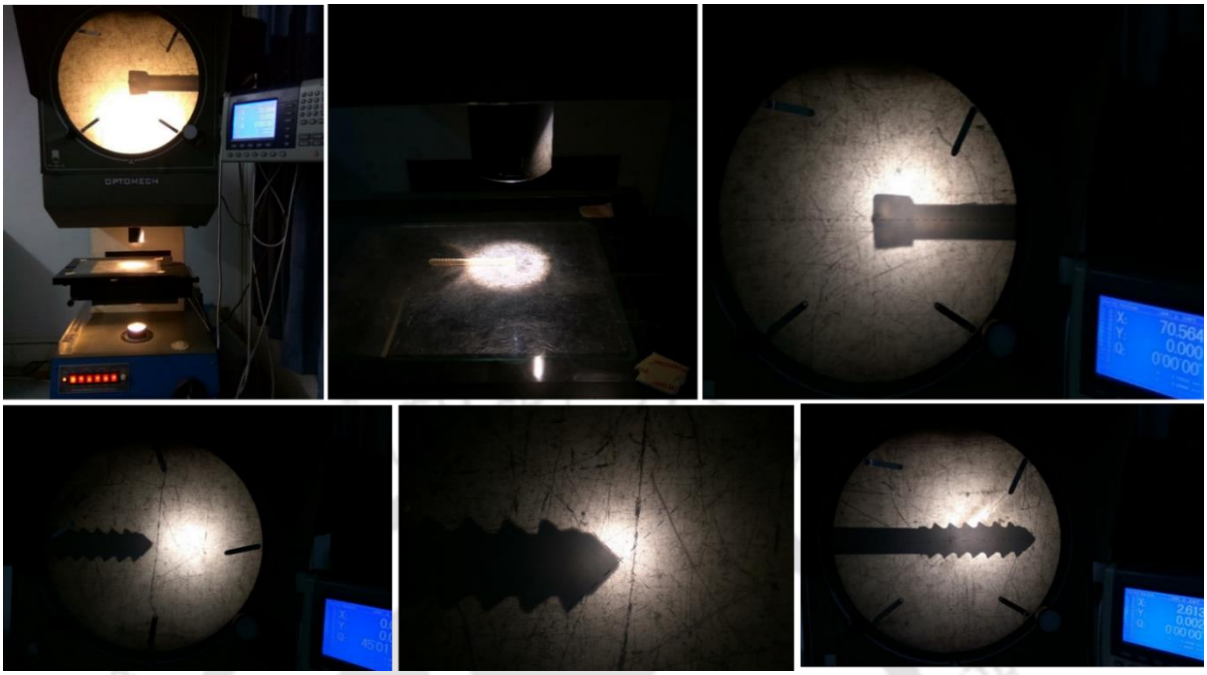

Figure 4.26: Photographic image of surface profile optical micrograph of cortical screws

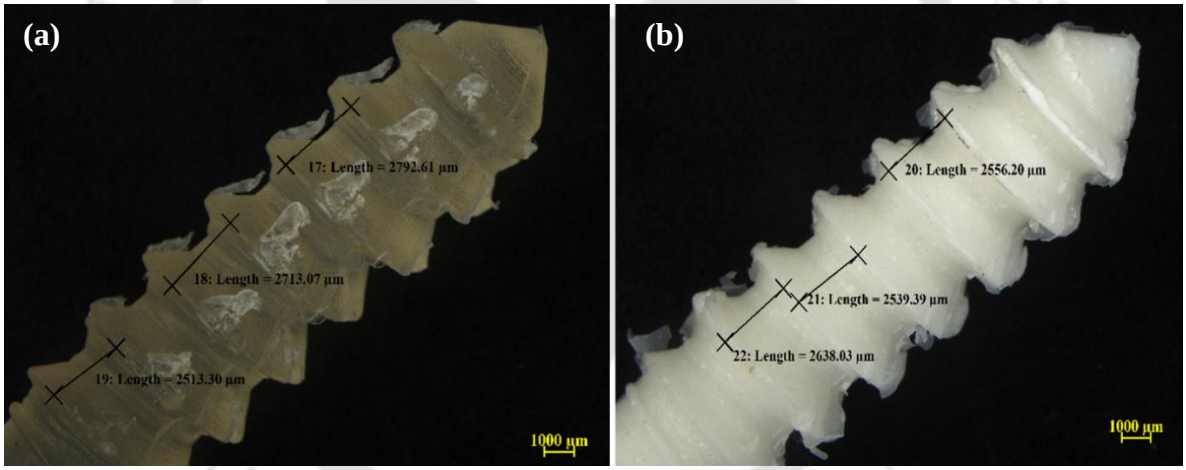

Figure 4.27: Stereomicroscopic images of cancellous screw thread (a) neat PLA cancellous screws (b) PLA/nHAp cancellous screw.

4.7 Summary

In this chapter, the following major points are summarized

1. The cancellous screws based on purified PLA and PLA/nHAp has been successfully manufactured through extrusion cum injection molding.
2. The process parameters have been optimized in order to produce the cancellous screws

3. The design, development of the mold and related fixtures for performing mechanical testing have been discussed.
4. The mechanical test as per ASTM standards related cancellous screws has been performed and discussed.
5. The axial pull out strength of 10 % nHAp gives the maximum value within the combination taken. The increment observes was about 39% as compared to neat PLA.
6. The torsional strength of cortical screws has been also done. The increment of 48% torsional strength was observed in the case of 10% nHAp concerning neat PLA. The corresponding breaking angle was also mentioned.
7. The flexural strength of the cancellous screws was also performed as per ASTM standard. The reduction of 5% to 18% was observed with compared to neat PLA.
8. The double shear strength was also performed in the fabricated fixtures and as per ASTM standard. The maximum increase of 8% of 12% nHAp was observed within the combinations.
9. In vitro, hydrolytic degradation studies were conducted successfully, and it confirms the mass loss of the cancellous screw after exposure towards PBS solution. It was also observed that the rate of mass loss of the neat PLA was more as compared to PLA/nHAp cancellous screws.
10. The deviation in the profile of thread pitch was compared with the standard pitch profile of the cancellous screw; later it was analyzed with the help of surface profilometer and stereomicroscope. The deviation was quite very less, thus the deviation result was neglected.

ABSTRACT

In this chapter, the fabrication of four combination holes bone plates has been discussed through twin screw extruder cum injection molding process. The process parameters have been optimized, and the mechanical test has been conducted as per ASTM standards. The mechanical test holding fixtures were also fabricated in order to use a universal tensile testing machine effectively to conduct the various mechanical test. The bone plates were fabricated in such a way that commercially available screw can be accommodated into it. After mechanical testing, the optimum combination of bone plate was reported. The optimized bone plate was later evaluated *In vitro* hydrolytic degradation, and then again mechanical test was evaluated after *In vitro* hydrolytic degradation for specific durations. The mechanical strength was later analyzed and concluded for its applications for various age group peoples.

GRAPHICAL ABSTRACT

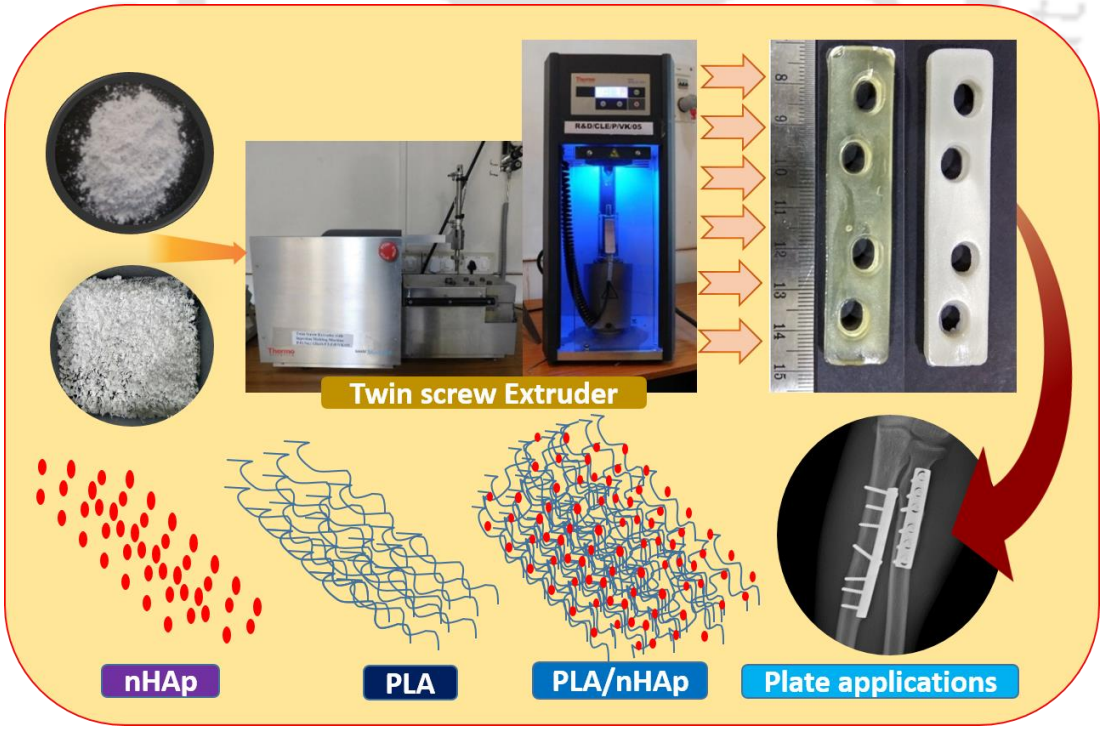

Chapter 5

5 Fabrication and characterization of Bone Plates

5.1 Introduction

Bone plates are surgical tools, which are used to assist in the healing of broken and fractured bones. The breaks are first set and then held in place using bone plates in situations where casts cannot be applied to the injured area. Bone plates are often applied to fractures occurring to facial areas such as the nose, jaw or eye sockets [193-194]. Repairs like this fall into an area of medicine known as osteosynthetis. A bone plate is a thin implant used to immobilize bone segments. It is also called as orthopedic bone plates and is used to hold the broken bones together with screws. It comes in different types like dynamic compression plate (DCP) or least contact dynamic compression plate (LCDCP). Bone plates may be left in place after healing is complete, or they may be removed in specific cases. A broken bone must be supported in order to heal the fracture in to original shape[195]. To set the bone fracture, the orthopedic surgeon repositioned the bone fragments into normal alignment, and fracture bones and bone plates are held together with the help of screw and plates. Metallic implants are made of stainless steel and Titanium, which are durable and strong, but it is also known that stiffness of metals are very much high as compared with natural bone, this mismatch in stiffness and other mechanical properties leads to the development of stress shielding phenomenon[196] . Because of stress shielding, the growth of bone tissue was shielded and in those places, which further leads to the accumulation of the tissue nearby. The underlying bone under a metallic bone plate also gets damage, and further regeneration of bone does not grow, and thus healing of the bone gets stopped.

Since metallic bone plates are conventionally used for load bearings regions, consist of the disadvantages that they usually need to be removed after 1-2 years of surgery due to stress shielding and ion releasing effects. Natural bone tissue has the remarkable ability to regenerate itself. If a fractured bone can be held together, it can regenerate the tissue and regain most of its original strength. For severe fractures, bone plates are surgically implanted to hold the bone in place. If the bone plate has more stiffness value, then the implant bears most of the load placed on the bone. Although this is favorable while the bone is weak, as the bone heals and regains strength, if the bone plate does not allow the bone to carry an increasing load, there will be a reduction of bone mass and final regained strength. The general mode of failures of implanted bone plates is due to overload, fatigue, corrosion and loosening. The location of failures due to overload and due to fatigue in bone plates are generally take place at the bone fracture site, implant screw hole, threads. The reason behind may be due to small size implants and unstable reduction. The corrosion of metallic plates is also responsible for the failure of the plate near the attached screw head, plate hole and bent area. The reasons may be due to over tightening screws, misalignment of screws, over bent etc.

Due to motion also loosening of the plates happens which also leads to failure of the bone plates. The fatigue failures of bone plates happen in the bone fracture site. The interaction between the body and the implant in case of fracture treatment depends upon the condition of the implants and its effect on soft tissue and bone healing and probable feedback on implants. If the bone plate is too weak, then non-union of the bone held and the bone plate leads to fatigue failures. If the implants are too rigid, then cortex structure of the bone gets disturbed, and loosening of the bone plates takes place. If the fixation is not stable, then the

healing of the bone gets delayed. The local relative motion responsible for fretting corrosion leads to tissues impregnation and this proceeds towards a change of pH value with oxygen depletion results in enhanced corrosion. As a bone healing progress, it is desirable to subject the bone to gradually increasing stress, thus reducing the stress shielding effect. This is possible only if the plate loses its rigidity in an *In vivo* environment. As a non resorbable polymer lack, this property resorbable polymers such as PLA should be used as a composite matrix. In order to improve its mechanical properties, this matrix should be reinforced with such non resorbable material as bio glass or carbon fibers and bioactive bioceramics [196-198]. The surgical cutting of a bone, especially to allow realignment is done by the osteotomy equipment, which is made of primarily Titanium and stainless steel. The broken bones are first surgically align into their proper position. Then a plate is screwed onto the broken bones to hold them in place, while the bone heals back together. After initially placing the plate on the break or fracture the bones are compressed together and held under some slight pressure, which helps to speed up the healing process of the bone. Unfortunately, after a couple of days, the tension provided by the steel plate is lost, and the fracture is no longer under compression, which further slows the healing process. The design of the plate must have sufficient mechanical strength so that after application of the appropriate amount of pressure to avoid break and fractures [199].

Various researchers have focused their research on the material perspective utilized for applications as bone plates. The materials for fabricating the bone plates were generally of metallic, degradable and bioabsorbable polymers along with fillers for enhancing the tissue growth. Some of the literature in this context is as follows.

Nasiri et al. [200] investigates the mechanical properties of tubular carbon/Kevlar with poly(methyl methacrylate)/graphene nano plates as used in the internal fixation of bones. Carbon fibers are good candidates for developing high-strength biomaterials, and due to better stress transfer and electrical properties, they can enhance tissue formation. Frigg et al. [201] developed the locking compression plate which is the ideal combination of two well-known anchorage concepts in one implants. As opposed to conventional osteo-synthesis plates and what is known as internal fixators, the surgeon can without having to change system decide which type of anchorage to use depending on the type of fracture, bone quality, access technique or prevalent soft tissue situations. Frigg et al. [202] reported biomechanics of plate osteo-synthesis. It was mentioned that improper design of bone plate might have the risk of delayed union and infection as well as a result of poor fixation in osteoporotic bone. The locking plate aims a flexible elastic fixation to imitate spontaneous healing including induction of callus formation. Flexible fixation allows the fracture fragments to displace about each other when the load is applied. The external load result only in reversible deformation of the splint. After unloading, the fracture fragments move back in to their former relative position. When the load result in an irreversible deformation of the splint, the fragment remains permanently displaced. Such a situation with plastic deformation of the implant is called unstable fixation. It appears likely that some flexibility of fixation is the most important mechanism triggering and inducing callus formation.

Mehboob et al. [203] Optimally designed of a functionally graded biodegradable composite bone plate by using the taguchi method and finite element analysis. Since the design of the bone plate also affects the healing of the bone fracture. The Taguchi methods were used to design the experiments to determine the influence of the design factor of a bone plate on the healing of the fractured bones. The parameters were selected four such as the average young modulus, spatial distribution of the FGM layers, the degradation rate of

the materials, and the thickness were varied to analyse to influence on healing of fractured bones. The healing performances of bone non-union were less than 20%, and most of the central calluses of non-union were filled with immature bones (*Figure 5.1*). However, the external calluses were filled with intermediate and mature bone in non-union cases.

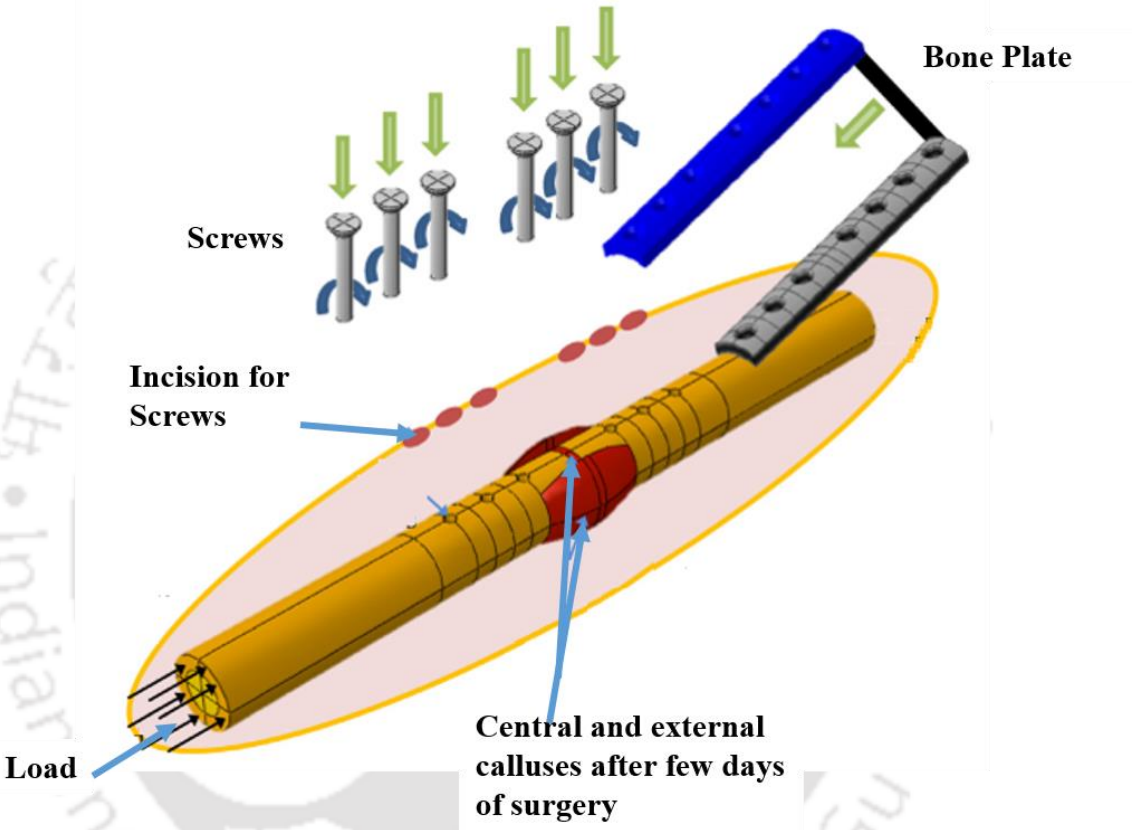

Figure 5.1: Bone plate assembly during implantation of a bone plate for fracture fixations [203].

Mehboob et al. [204] evaluated healing performance of biodegradable composite bone plate for a simulated fractured tibia model by finite element analysis. In this study, they considered the use of various composite materials such as phosphate glass fibre/ Polylactic acid composite and a carbon/epoxy composite for bone plate and estimated the healing performances of bone plate made of said materials by applying them to fracture with gaps of

1-10 mm (Figure 5.2) and oblique angles of 0-35°. The degradation rate was analysed and evaluated the healing performance of biodegradable composite bone plates for a simulated fractured tibia model by finite element analysis. The results showed that the biodegradable composite bone plates had considerably better healing performance.

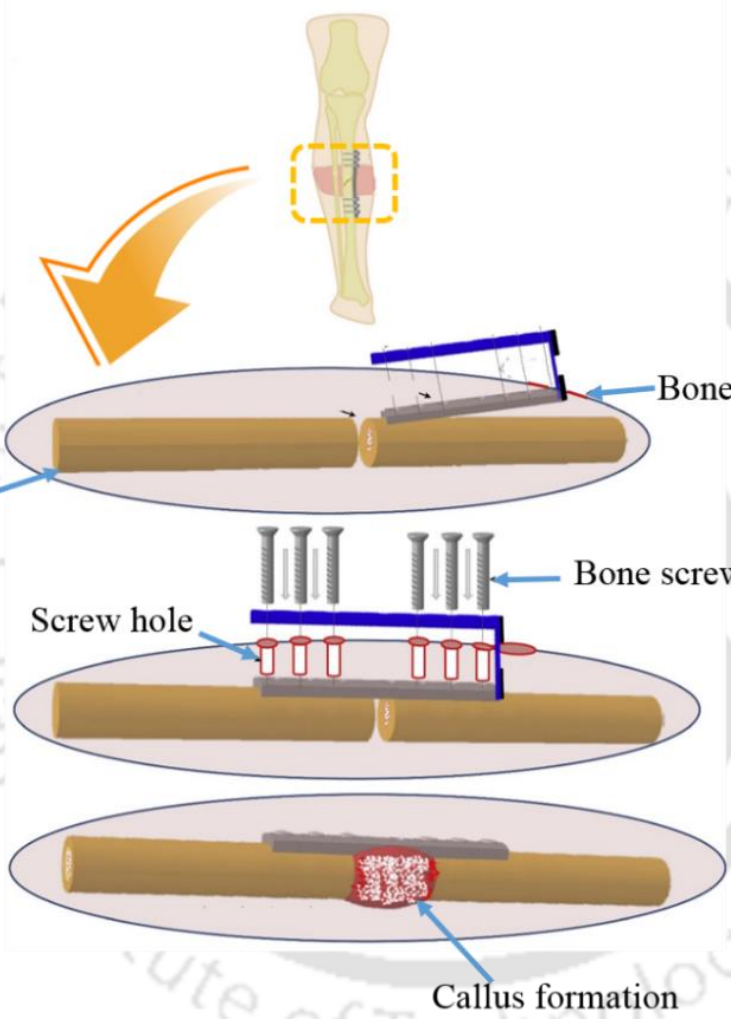

Figure 5.2: Tibia bone fracture fixations by bone plates [204].

Mehboob et al. [205] reviewed applications of composites to orthopaedic prostheses for effective bone healing as shown in Figure 5.2. Fractures occur more often in lower limb long bones than in other bones because of their high aspect ratio and exposure to impact and other dangers. The extrinsic causes of this fracture include trauma such as that from a vehicle

accident, sporting injuries and fall and sometimes the cause is intrinsic for example from muscular action or some pathology resulting in a fracture. Composite materials are getting more attention in the engineering field for the development of high performance implants to enhance the healing of bone fractures and more efficient function oriented composite materials such as resorbable/ biodegradable and bioactive composites are being developed to meet the required performance characteristics of orthopaedic prosthesis and implants. Kohal et al. [206] examined the in vitro and in vivo response of osteoblast to a novel acid etched and sandblasted zirconia surface. Hfob 1.19 cells were cultured. After 28 days, the biomechanical test showed a significantly higher value for electrochemically anodized titanium than other treated titanium surfaces. It was also observed that novel, rough zirconia surface was accepted by hFoB 1.19 cells and integrated into rat bone tissues. However, osseointegration seemed to proceed more slowly and to a lesser extent compared to a moderately roughened titanium surface.

Allgower et al. [207] Changing loads tend to produce relative movements between the fragments. Any such motion results in undesirable fragments shortening due to resorption of the bone. Relative motion at the fracture site is accompanied by the increased mechanical strength of the implants.

Huang et al. [208] reported diaphyseal fractures as shown in Figure 5.3 are generally treated using compression bone plates made of stainless steel, Cr-Co and Ti alloys. But it was also mentioned that underlying bone damaged due to more stiffness. Thermoplastic carbon/PEEK (poly-ether-ether-ketone) materials were selected due to their biocompatible nature. For the same carbon/PEEK materials system, the numerical experiments indicated that ideally, the composite bone plates made of unidirectional, angle-plied, multidirectional,

and braided fabric laminates and having a thickness comparable to that of a clinically used stainless steel plate might all satisfy the stiffness and strength requirements for applications.

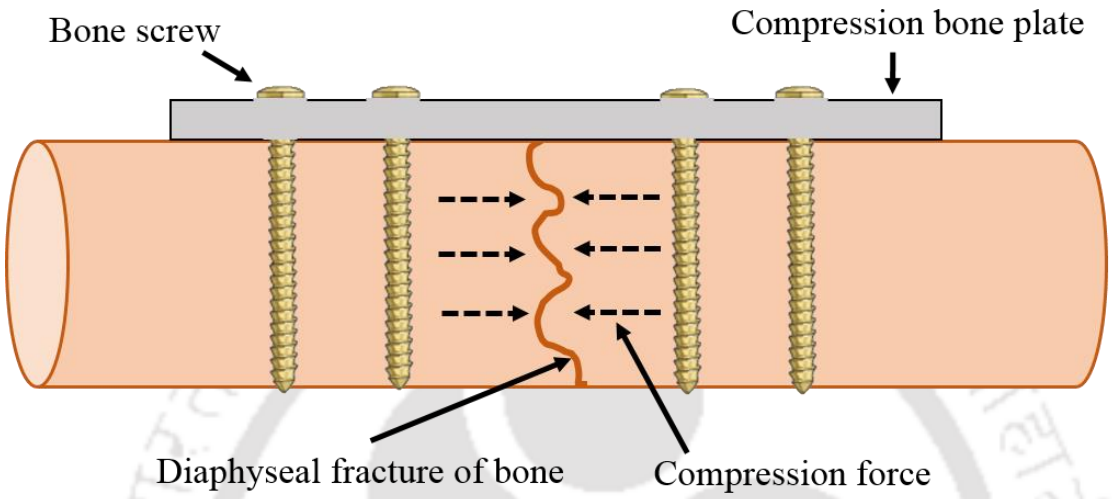

Figure 5.3: Schematic of a compression plate for bone fracture fixations

Ferretti et al. [209] investigated the performance of PLLA/PGA copolymer plates and screws in the fixation of the mandibular fracture. The implants were tested in 31 patients. Elastic maxilla mandibular fixation was maintained for four weeks and a blenderized diet for six weeks. Patients were periodically followed up and evaluated clinically for swelling, pain, mucosal, discoloration and occlusal relation. Patients who presented with a mandibular fracture less than 21 days old and who expressed the ability to return for follow up were selected. The patients were examined clinically and the diagnosis confirmed radiographically with panoramic and poster anterior mandibular views. It was mentioned that resorbable implants have minimum removal problems but exposed titanium fixation requires removal of the entire plate and all the screws, with considerable soft-tissue exposure and often requiring general anaesthesia.

Kim et al. [210] reported relationship between mechanical stimuli and curing tissue generation and development to understand the effective healing of bone fractures. Fnite element analyses were carried out to estimate the interfragmentary strain distribution at the fracture site of a tibia according to the bending stiffness and contact conditions of composite bone plates with a simplified rectangular cross-section, and polymeric porous layers at the contact area. From the analysis results, it was verified that the interfragmentary strain varies not only with bending stiffness but also with the contact condition of the bone plate.

Montufar et al. [211] reported **b**iodegradable α-tricalcium phosphate/iron (α-TCP/Fe) composites for the fabrication of temporal osteosynthesis devices. Similar to biodegradable metals, these composites can avoid implant removal after bone fracture healing, particularly in young patients. In this work, a-TCP/Fe composites are studied for the first time in a wide range of compositions, showing not only higher degradation rate in vitro than pure components, but also good cytocompatibility and mechanical properties controllable with the Fe content. Ceramic matrix composites show high specific strength and low elastic modulus, thus better fulfilling the requirements for bone fractures fixation. In vitro study showed that TCP/Fe composites have a higher degradation rate than their components, but are mechanically reliable during the time required for bone fracture healing. Furthermore, osteoblast-like cells attached and spread on the surface of the composites, presenting a similar proliferation rate. Samiezadeh et al. [212] investigated on optimization of a composite bone plate using the selective stress shielding approach. It was discussed that despite recent advancement in implant design and surgical techniques aiming to protect bone vascularity and to facilitate healing, complication is still prevalent, and include malunion, non-union, hardware failure and bone refractures. The situation can lead to a reduction in the

compressive loads. After the union, the reduction of mechanical stresses on the femur leads to bone resorption at the presence of the implants over time due to stress shielding.

Dewo et al. [213] investigated redesign of Indonesian made osteosynthesis plates to enhance their mechanical behaviour. Mechanical properties determined by fatigue strength, ductility and toughness are important measures for osteosynthesis plates in order to tolerate some load bearing situations caused by muscle contraction and weight bearing effects. The plates with shoot peening were found increased fatigue strength, and other mechanical properties can be enhanced by treatment of the surface of the implant. Dewo et al. [214] reported mechanical properties of Indonesian made narrow dynamic compression plate. It was mentioned that osteo-synthesis plates are clinically used to fixate and position a fractured bone. They should have the ability to withstand cyclic loads produced by muscle contraction and the total body weight. The mechanical properties of the Indonesian made plate were compared with the European standard AO standard plate, and its relationship to geometry, microstructural features and surface defects of the plates. It was observed that the Indonesian plate appeared to be weaker than the standard narrow DCP because they consistently failed at lower stresses. This was caused by using inferior material, the absence of strengthening plastic deformation in the production process and a poor reproducibility of the manufacturing process.

Chakladar et al. [215] investigated optimization of a composite bone plate for ulnar transverse fractures. An ulnar transverse fracture was characterised, and finite element techniques were employed to investigate the feasibility of a composite-plated fractured bone construct over a stainless-steel equivalent. Numerical models of intact and fractured bones were analysed, and the mechanical behaviour was found to agree with experimental data. The mechanical properties were tailored to produce an optimised composite plate, offering a 25%

reduction in length and 70% reduction in mass. The optimised design may help to reduce stress shielding and increase bone healing rates. Sukegawa et al. [216] investigated long term bio resorption of bone fixation devices made from a composite of unsintered hydroxyapatite particles and poly l lactides (u-HA/PLLA), because of their bioresorbability and osteoconductive properties. In this, it was observed that 3D-CT at six years after surgery, degradation of the u-HA/PLLA composite resorbable device was almost complete. However, it had been shown very small and brittle residual plate and screws in contact with the mandible, which was later on removed. The u-HA/PLLA composite resorbable device was almost completely degraded and was replaced with bone. Uhthoff et al. [217] studies on internal plate fixation of fractures. It was mentioned that initial shortcomings such as corrosion and insufficient strength had been overcome; more recent design has not solved all problems. Further research is needed to develop a plate that accelerates fracture healing while not interfering with bone physiology. Rigid plates lead to cortical porosis, delayed bridging, and refractures after plate removal.

Roeder et al. [218] studies the hydroxyapatite (HAp) reinforced polymer bio composite for synthetic bone substitutes. It was discussed that at the interface of HAp and polymer, collagen and bone minerals were coupled with non-collagenous proteins which bind it to apatite via carboxy ligands. Hydroxyapatite and thermoplastics (HDPE, UHMWPE, PLLA and PAEK) have little or no chemical bonding at the interface and were limited to mechanical interlock due to friction and residual stresses. Nourisa et al. [219] evaluated biomechanical properties of intramedullary mail and bone plate for the fixation of distal metaphyseal fractures. The study was about the advantages and disadvantages of two common fixation methods, intramedullary nails and the bone plate, for the fixation of distal

metaphyseal tibial fractures. It was shown that plate fixations bring enough flexibility for bone implants to construct and a promote a large amount of cartilage production, while intramedullary nailing causes excessive shear and low axial movement and thus prevents sufficient mechanical stimuli required for biological healing. Kharazi et al. [220] reported design of a textile composite bone plate using 3D-finite element method. In their work, a partially resorbable composite bone plate consisting of a poly l lactic acid matrix and textile bio glass fiber was used as reinforcement. The composite was modelled and analyzed using the ansys software. Results showed that for a volume fraction equal to 45%, the longitudinal modulus of elasticity and the ultimate tensile strength would be 23 GPa and 230 MPa, respectively. The bending strength and bending modulus of the plate were calculated to be about 55 MPa and 16.6 GPa, respectively and come in the range of the forearm region of the bone.

Gaball et al. [221] investigated minimally invasive bioabsorbable bone plates for rigid internal fixation of mandible fractures. This study was conducted in two analysis considered for normal post-surgical patients loads. The first analysis was about pertinent strain and stress measures within a fractured human mandibular finite element model which was fixated with a standard titanium mini plate. The second analysis used the same modelling conditions to evaluate a bioabsorbable bone plate. The bioabsorbable copolymer used in this analysis was a self-reinforced PLA (L/DL) 70/30. It was observed that it was very difficult to conduct a fatigue analysis over time when the actual mechanical strength of the bioabsorbable material will also change with time. Despite having ignored fatigue failure, gave a valuable input in the proper design of a safe, absorbable bone plate for fractures of the adult mandible.

Hur et al. [222] investigated the use of alendronate for sustained delivery to the bone for their active regeneration in the bioabsorbable bone plate. Alendronate is a drug known to inhibit osteoclast mediated bone resorption and also expedite the bone remodelling activity of osteoblasts. In this research work, the bone plates were fabricated using twin screw extrusion cum injection molding process.

Table 5.1: Extruder cum injection molding parameters for bone plate fabrication.

Parameters		
1.	Processing temperature	190°C
2.	Mold temperature	100°C
3.	Cylinder temperature	220°C
4.	Residence time	1min 30 sec
5.	Twin screw speed (rpm)	120
6.	Compressed air pressure	650-710 bar
7.	Injection pressure holding time	5 sec
8.	Weight of bone plate	6.455 g

The fabricated moulds as per the specimen of the bone plate were loaded in the injection molding machine cavity, and according to process parameter mentioned in Table 5.1, the parameters were optimized for the successful production of PLA and PLA/nHAp bone plate. After production of the bone plate, the mechanical testing was done as per ASTM F2502-11 (Standard specification and test methods for absorbable bone plates). Figure 5.4 shows the stepwise images for fabrication of bone plate moulds. The density of natural bone lies in the range of 1.3-1.8gm/cc. Thus some of the fixtures for testing the fabricated plate was made of wood as shown in Figure 5.5, since the wood density is almost similar to the natural cortical bone.

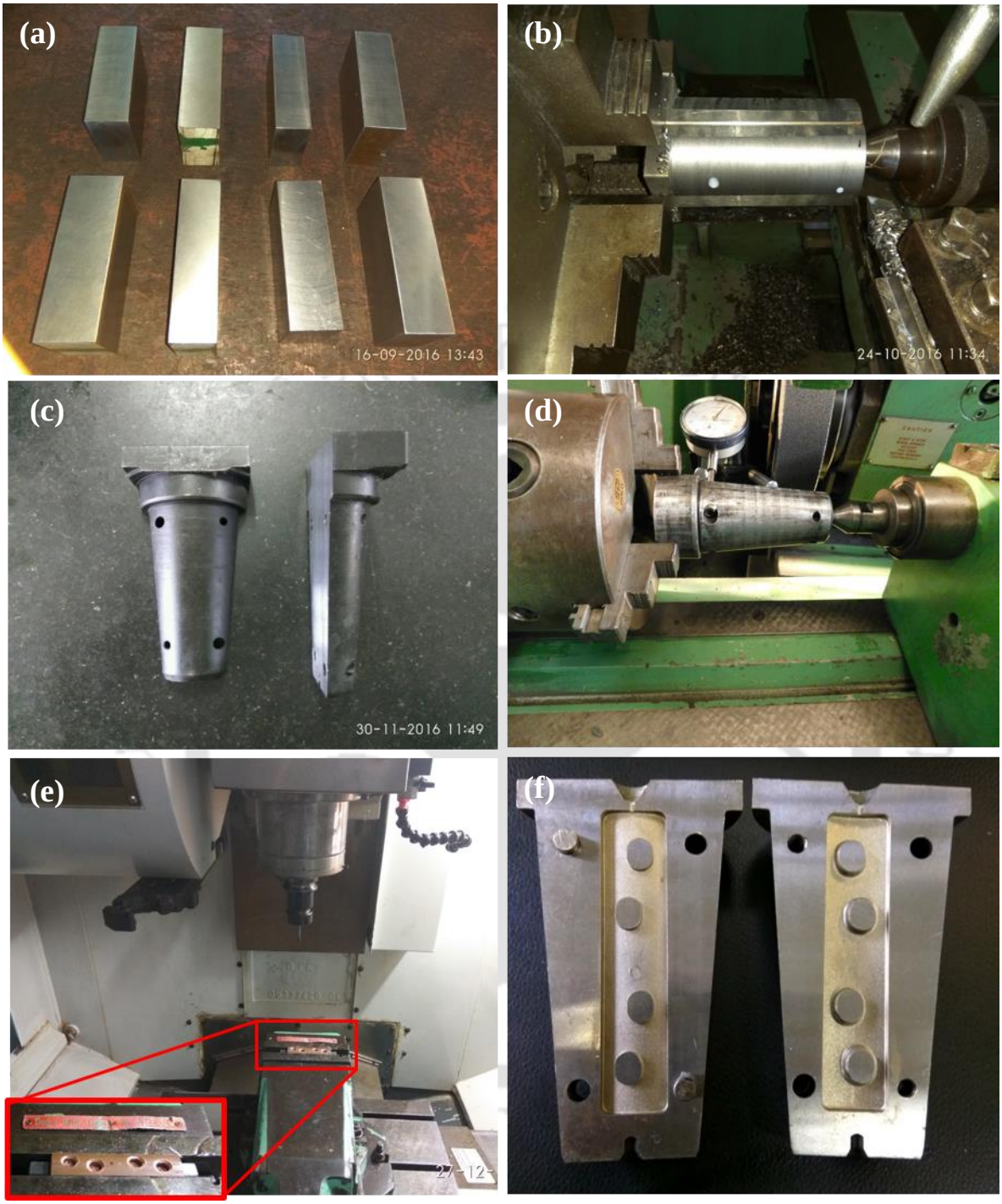

Figure 5.4: (a) H13 metals in form of raw materials (b)machining to the lathe machines for giving shapes as per the injection molding machine mold cavity (c) Heat treatment of the H13 metal (d) Cylinderical turning of the heat treated mould (e) Bone plate electrode made of copper (f) Bone plate mold in final shape.

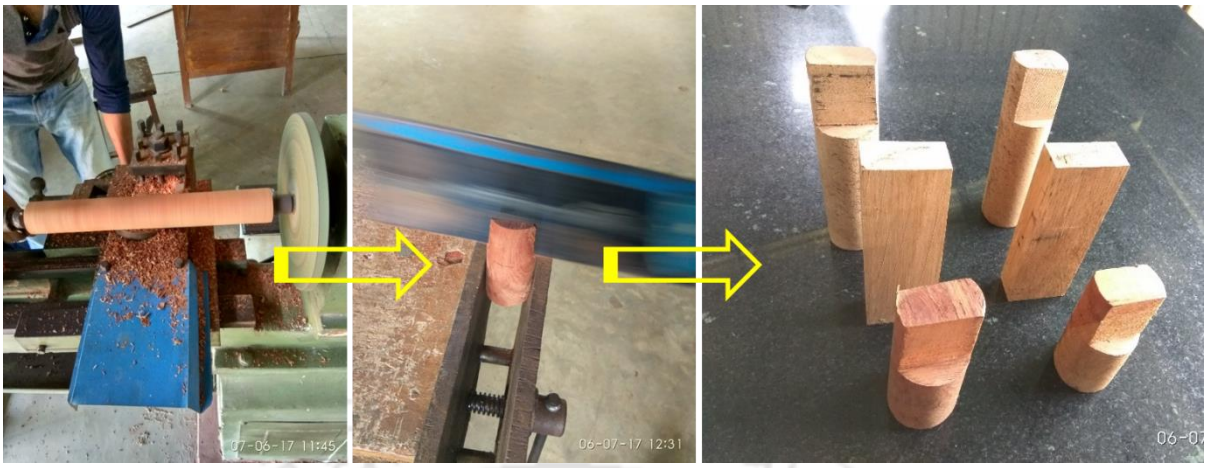

Figure 5.5: fabrication of wooden fixtures for fabricated bone plate mechanical testing

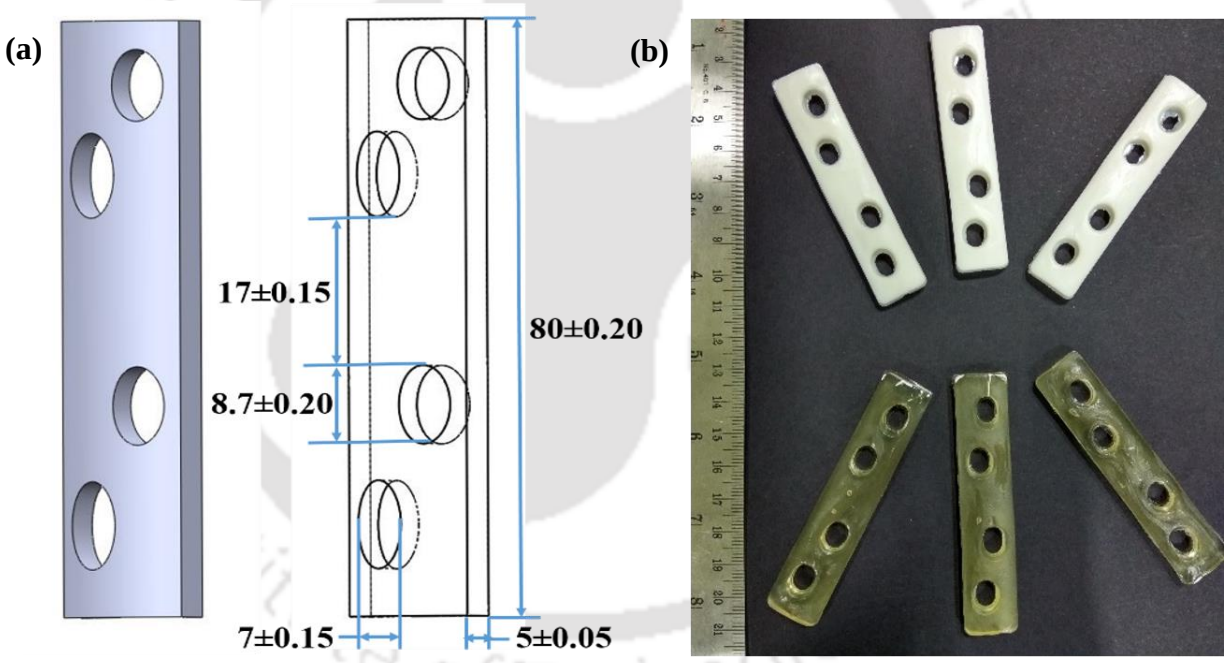

Figure 5.6: (a) 3D and line diagram of a bone plate (b) Photographic images of neat PLA (top) and PLA/nHAp (bottom) bone plate.

5.2 Development of Bone Plate

The bone plate was designed in AutoCAD as per the commercially available metal bone plate. The total length maintained was 80 mm. The width was maintained to 17±0.15 mm and thickness 5±0.05 mm. Bone plate had four combination holes throughout the plates in order

to fix the cortical and cancellous screws. The bone plate was a little bit bend in the inner circle of radius of 50mm. The detail dimension of the fabricated bone plate is shown in Figure 5.6. The material choosen for making the molds was H13 (Tool Steel) because of its excellent combination of high toughness and resistance to thermal fatigue cracking. *Figure 5.7* shows the 3D solid model for bone plates.

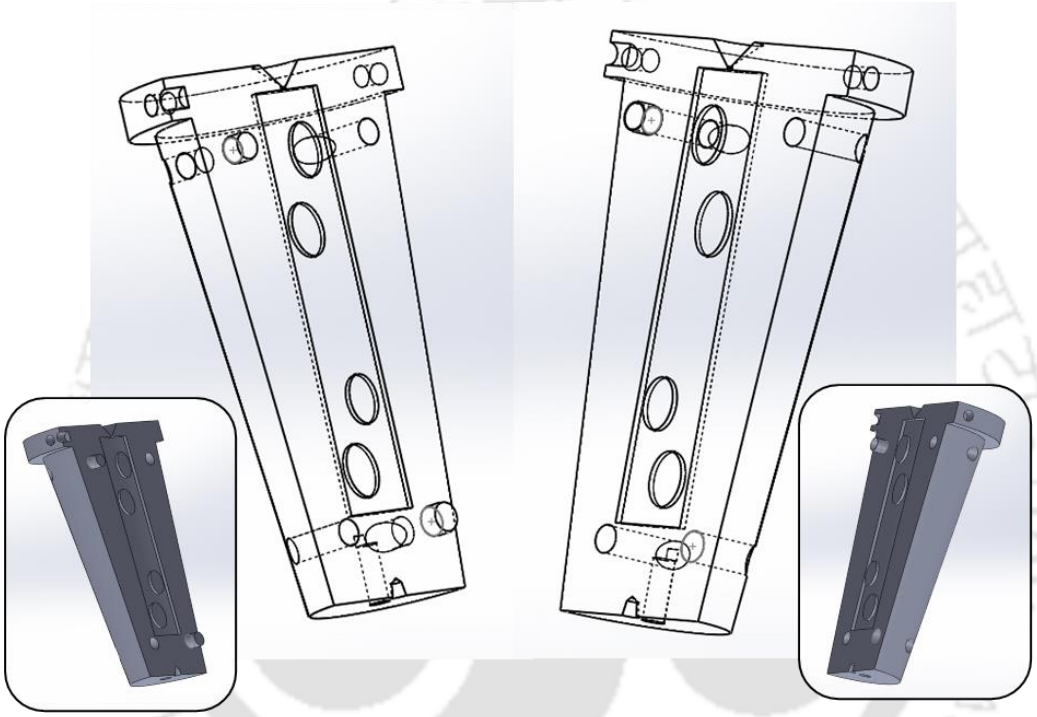

Figure 5.7: 3D solid model diagram (inset) and 3D line model diagram of fabricated bone plate mold.

5.3 Mechanical Testing of Bone Plate

After production of the bone plate, the mechanical testing was done as per ASTM F2502-11 (Standard specification and test methods for Absorbable Plates and Screws for internal fixation Implants).

5.3.1 Flexural testing

The maximum flexural load for the bone plate were evaluated by flexural (3 point bend test) test using a fabricated flexural fixture at room temperature. A cross head speed of 1mm/min and a load cell of 5 kN was used. The support span was 40 mm, and radii for loading and supporter applicators are 3mm. Measurement was conducted in triplicate. Figure 5.8 shows the arrangement of the three point bend test performed on bone plates. The Figure 5.9 shows the values of flexural strength with varying the filler concentration. It was also observed that flexural strength was reduced in the range of 4% to 8% with respect to 3% nHAp to 10% nHAp. The Figure 5.10 shows the values of flexural strength with respect to varying filler after *In vitro* hydrolytic degradation. It was observed that the reduction of ~19% after 30 days and ~35% after 90days. While in the case of 3% nHAp, reduction of ~11% observed after 30 days and ~37% after 90 days in flexural test occurred.

Figure 5.8: Arrangement of 3 point bend test performed on bone plates.

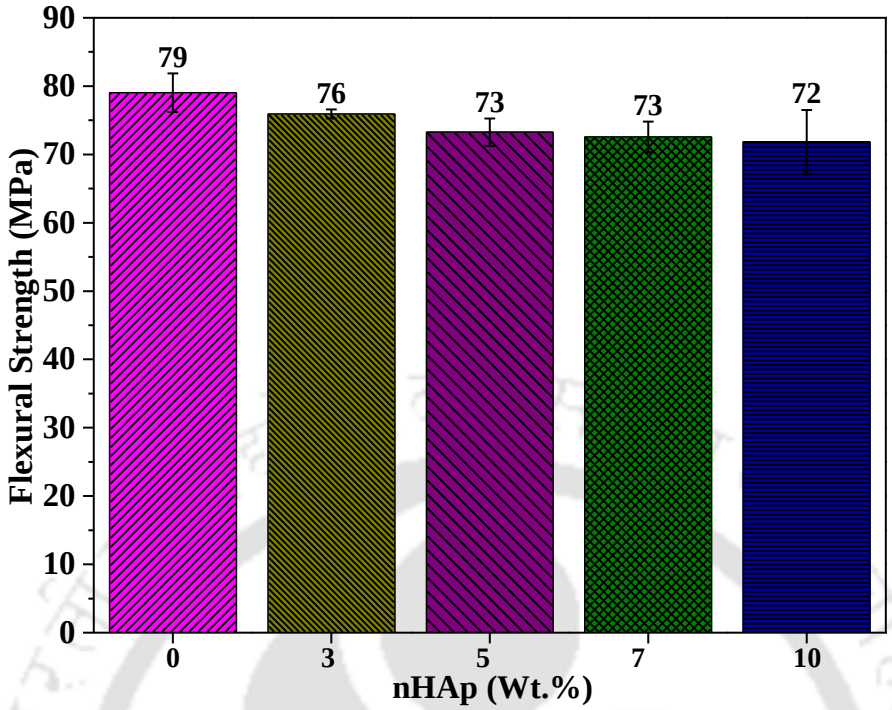

Figure 5.9: Flexural Strength value obtained through 3 point bend test of a bone plate concerning nHAp.

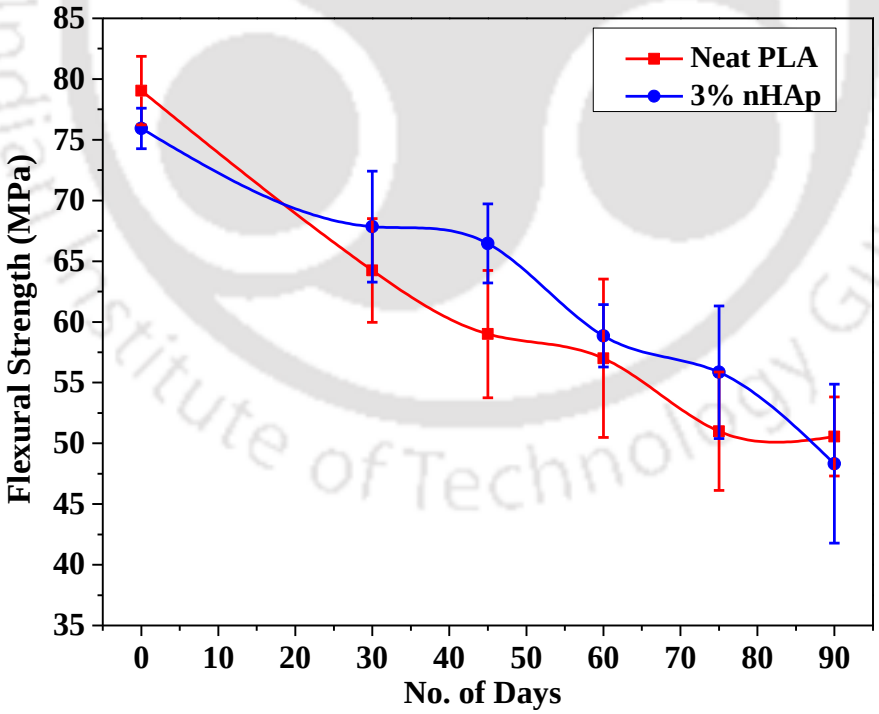

Figure 5.10: Flexural strength of neat PLA and 3% nHAp after In vitro hydrolytic degradation.

5.3.2 Torsional Strength

The maximum torque, breaking angle were measured for the bone plate using fabricated torsion fixture. The measurement was done in torsion testing machine (make: Fuel instruments and equipment, India). The crosshead speed of the machine was one revolution per minute. The load cell capacity of the machine was 10kgf.m (9806.6599 mili Newton meter). The gauge length was maintained about 20% of the total length of the plates. The maximum torque was represented by the highest recorded value of the torque during the test, and the breaking angle was the rotation angle at the maximum torque. The measurement was carried out in triplicate. The fixture was made from mild steel metal, and torsion testing machine is shown in Figure 5.11. The room temperature was maintained at 24°C.

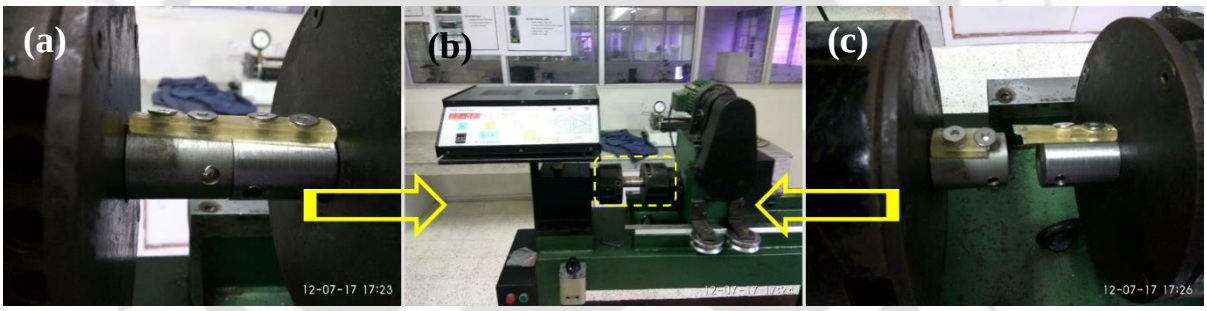

Figure 5.11: Arrangement of bone plates to the torsion machine for torsion testing (a) before fracture (b) arrangement in the machine (c) After fracture.

From Figure 5.13, Figure 5.14, Figure 5.15 and Figure 5.16. The torsional strength was reduced ~11% after 30 days and ~34% reduction after 90days, however in case of 5% nHAp, the reduction was observed ~10% reduction after 30days and ~30% reduction after 90 days. It was observed that an increase in the concentration of nHAp particles into the PLA matrix leads to an increase in brittleness of the plate, which ultimately proceeds for

fractures of the sample at lesser twisting angles [223]. Figure 5.12 shows the fractured surface micrograph of the bone plate sample after conducting torsion testing.

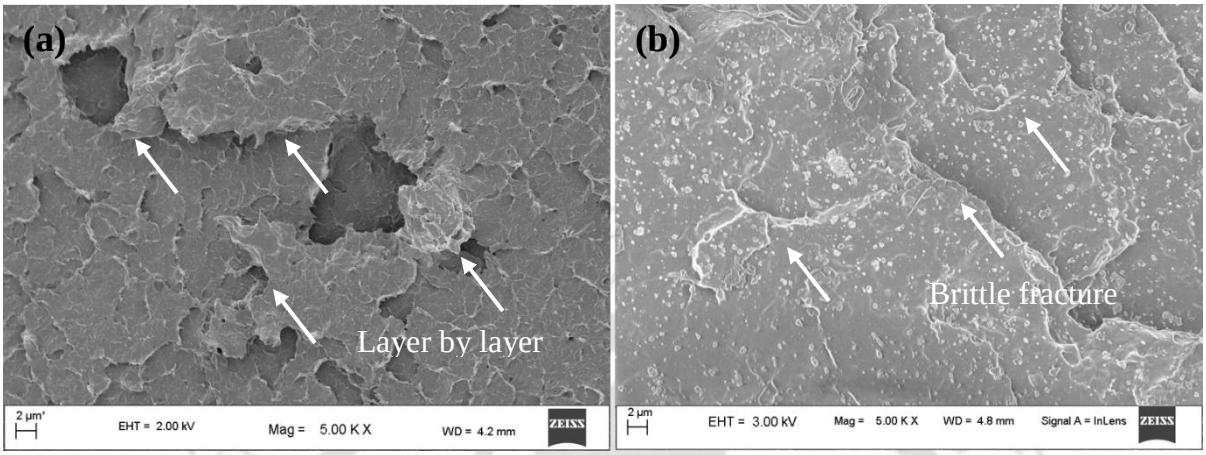

Figure 5.12: Surface micrograph of the fractured bone plates (a) neat PLA (b) PLA/nHAp after torsion testing.

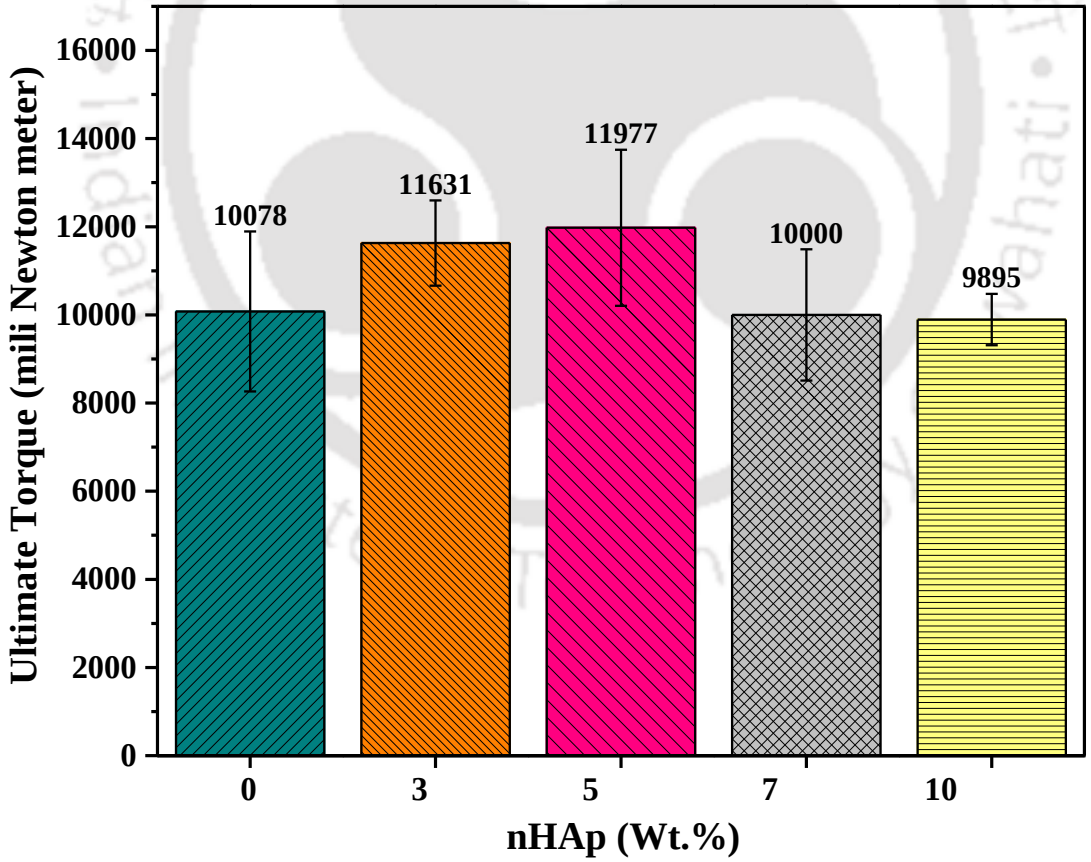

Figure 5.13: Values of ultimate torque concerning nHAp filler concentration.

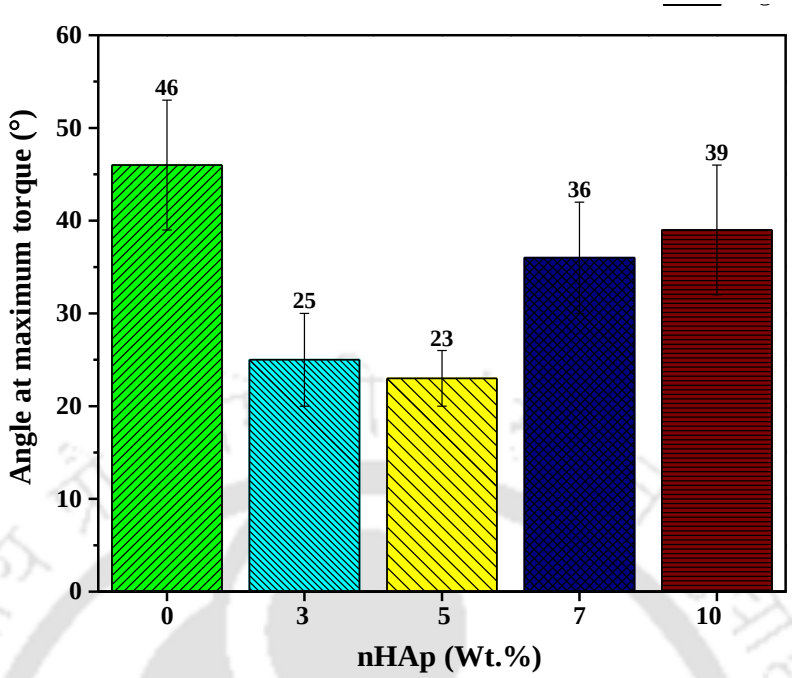

Figure 5.14: Values of the angle at which maximum torque was observed concerning nHAp filler concentration.

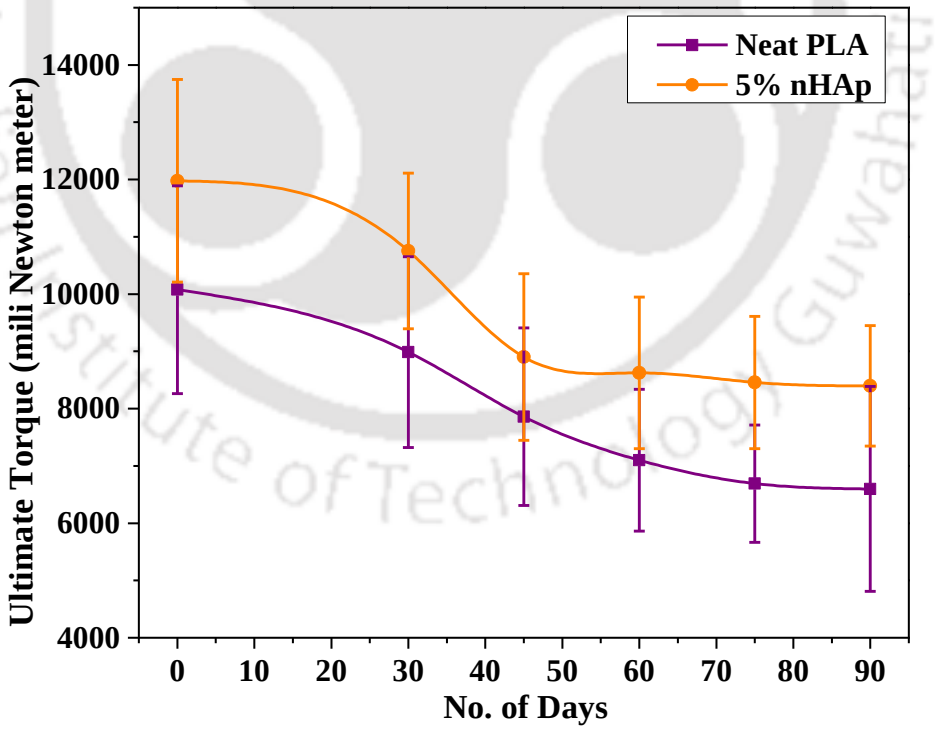

Figure 5.15: Torsional strength of neat PLA and 5% nHAp after In vitro hydrolytic degradation.

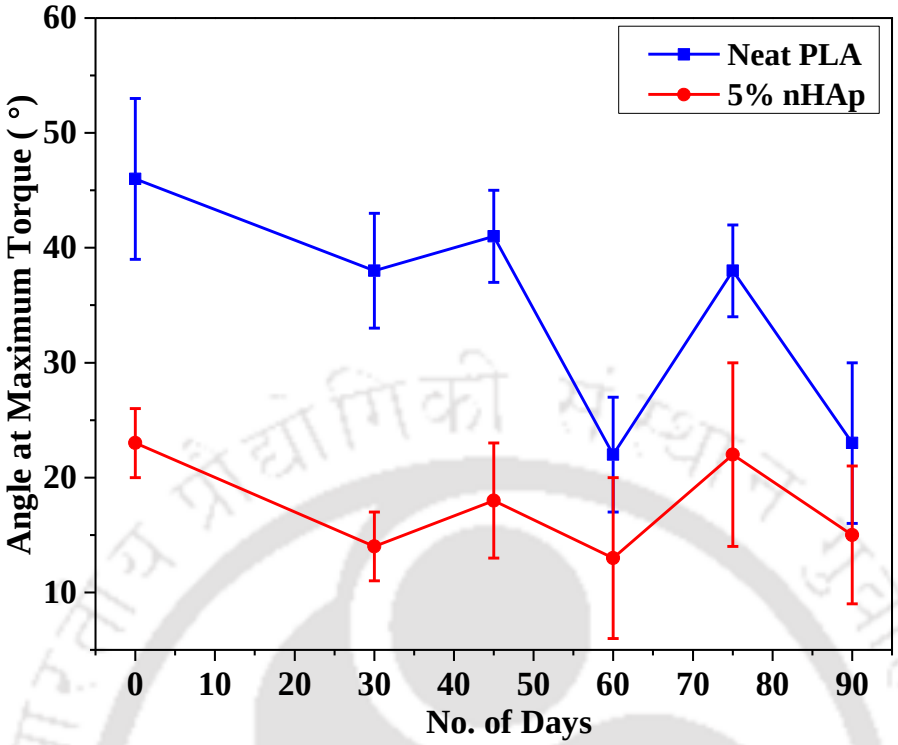

Figure 5.16: Values of corresponding twisting angle before and after in vitro hydrolytic degradation test.

5.3.3 Uniaxial single plate tensile test

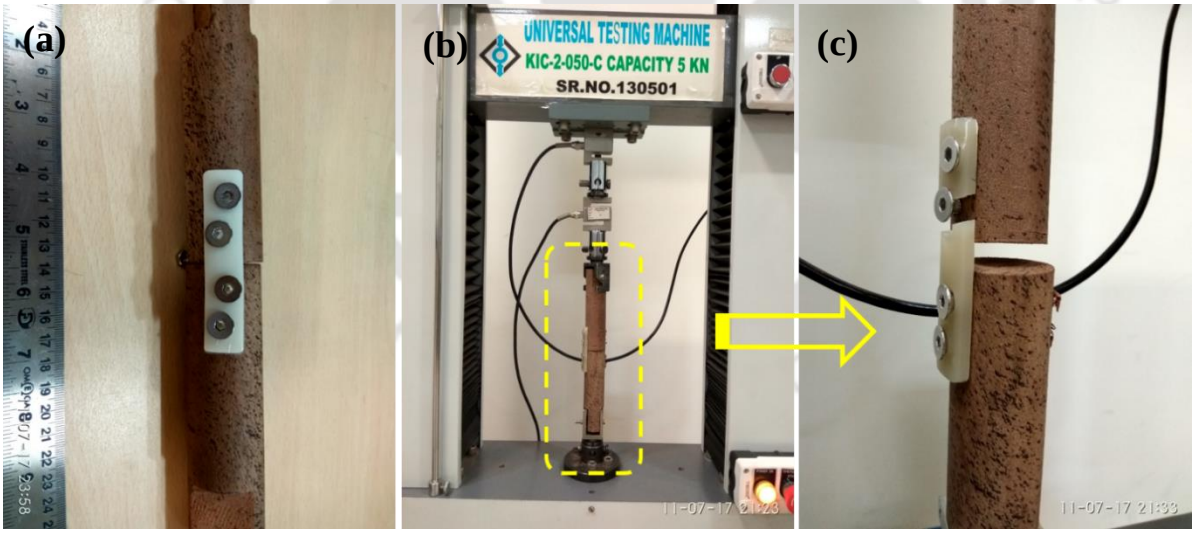

Figure 5.17: (a) Arrangement of the bone plate to the wooden fixtures (b) Bone fixtures along with bone plate arrangement in the universal tensile testing machine (c) Fractured bone plate after the axial pull out testing.

The axial pullout strength was determined using a universal testing machine (Kalpak Instrument, Pune, India) using a fabricated wooden pull out fixtures. The plates were inserted to the fixture on various holes spot throughout the total length of the plates into a previously internally threaded wood block fixtures as shown in *Figure 5.17*. The fixture was perfectly aligned with the longitudinal axis of the plate and the attached load frame. A cross head speed of 1mm/min and a 5 kN load cell was used. The measurement was carried out in triplicate. The value of uniaxial tensile strength was taken to be the maximum load reached during the test divided by its crossectional area. Figure 5.18 shows the value of uniaxial tensile strength concerning the various combination of PLA/nHAp of the bone plate. It was observed that 3% nHAp is having the uniaxial tensile strength of 16 MPa (3% increment), while lowest is about 11MPa (~27% reduction) for 10% nHAp concerning neat PLA.

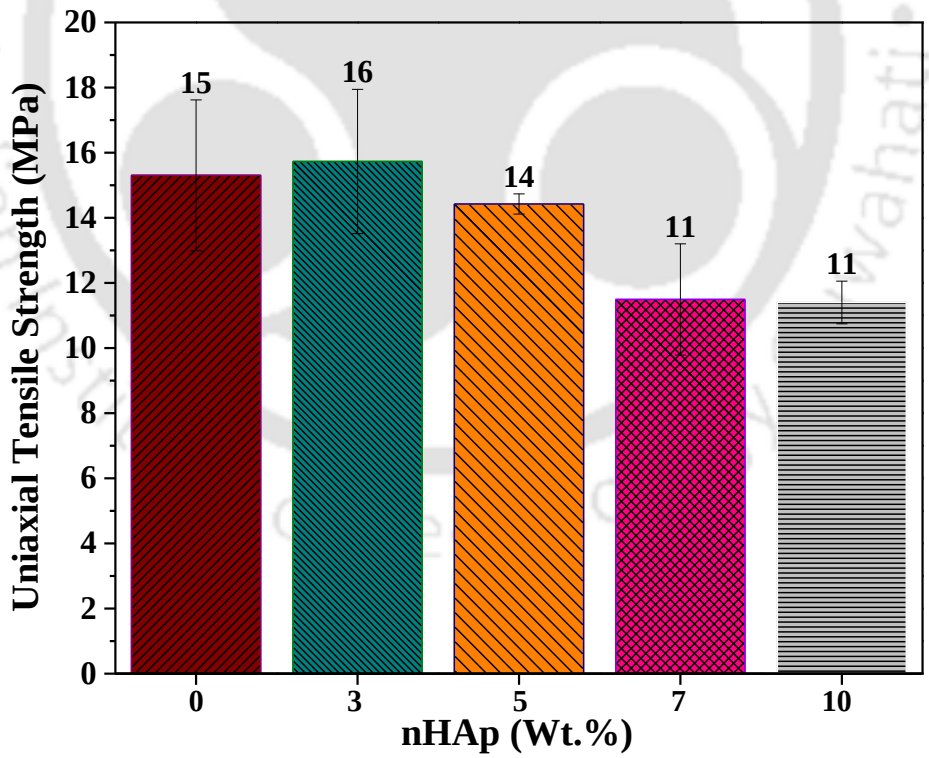

Figure 5.18: values of uniaxial tensile strength concerning varying nHAp filler concentration.

From Figure 5.19, the surface micrograph of the crossectional side of the fabricated bone plate is shown. Figure 5.19 (a) show of the surface micrograph of neat PLA bone plate and Figure 5.19 (b) shows the magnified surface micrograph of the neat PLA bone plates. Figure 5.19 (c) shows the PLA/nHAp bone plate crossectional side while Figure 5.19 (d) shows the magnified view of the PLA/nHAp fabricated bone plate crossectional side.

Figure 5.20 shows the value of uniaxial single plate tensile strength concerning the varying concentration of filler (nHAp) after *In vitro* hydrolytic degradation. It was observed that reduction of ~9% after 30 days and ~28% after 90days was noted in neat PLA based bone plate. While in the case of 3% nHAp bone plate, reduction of ~3% observed after 30 days and ~25% after 90 days in uniaxial single plate tensile strength value was observed.

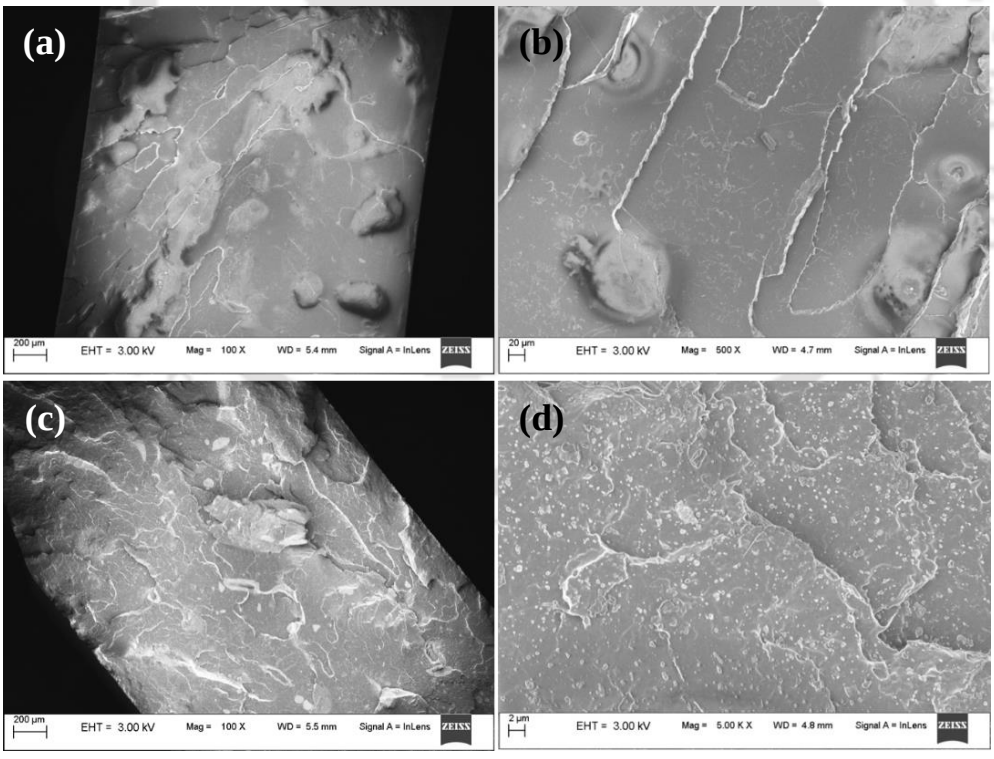

Figure 5.19: Surface micrograph of the fractured crossectional surface after uniaxial tension test (a) neat PLA (b) Magnified view of PLA (c) PLA/nHAp (d) Magnified surface micrograph of PLA/nHAp

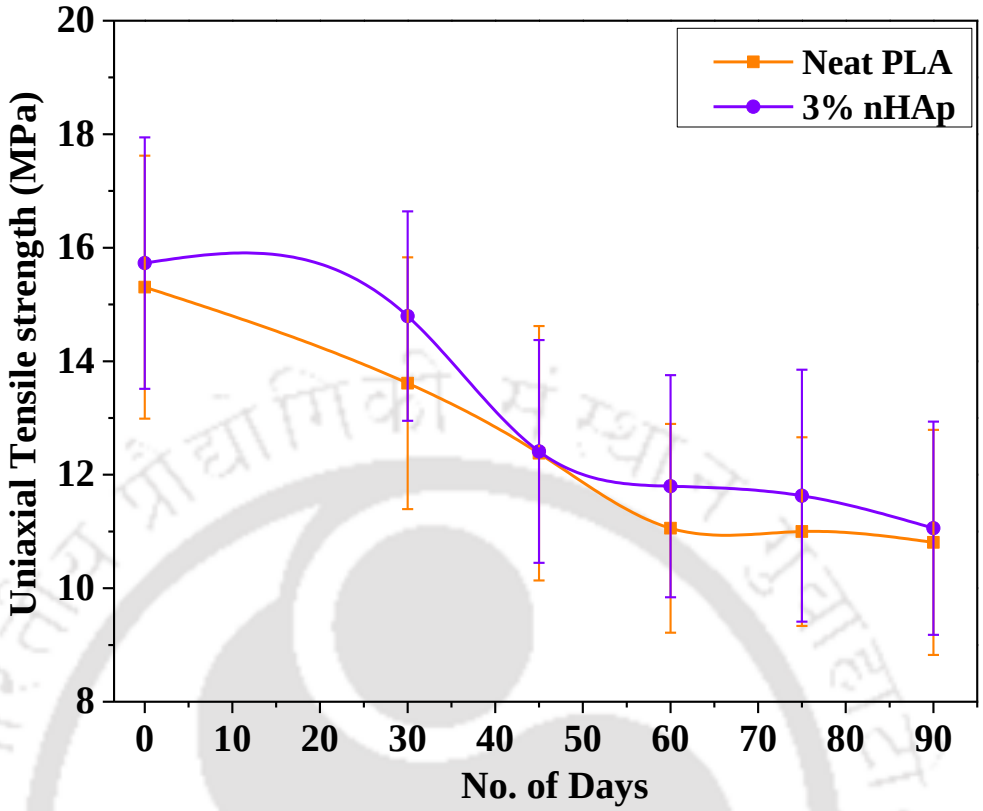

Figure 5.20: Values of uniaxial tensile strength of neat PLA and 3% nHAp before and after In vitro hydrolytic degradation.

5.3.4 Uniaxial double plate tensile strength

The uniaxial double plate tensile strength were evaluated using a universal testing machine (Kalpak Instrument, Pune, India) using a fabricated wooden pull out fixtures. The screw was inserted to a depth of 25 mm of the total length of the plate is attached into a previously internally threaded both side of the wooden block as shown in Figure 5.21 and Figure 5.22. The fixture was perfectly aligned with the longitudinal axis of the plate and the attached load frame. The plates were attached to the wooden frame in both sides through its circumference. A cross head speed of 1mm/min and a 5 kN load cell was used. The measurement was carried out in triplicate. The value of axial pull out strength was taken to be the maximum load divide by its crossectional area of the plate during the test.

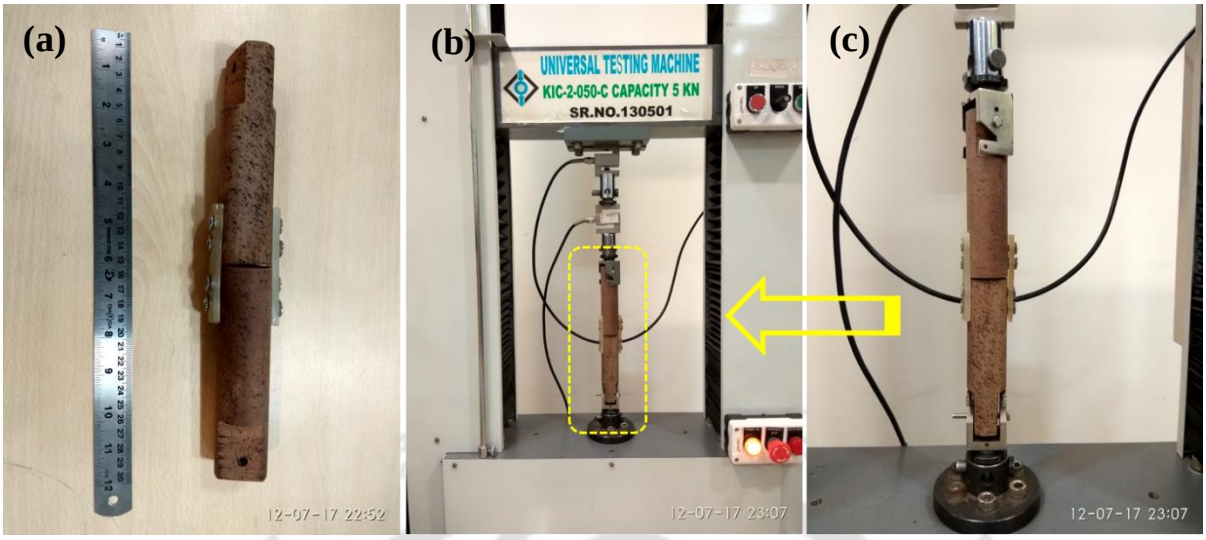

Figure 5.21: (a) Arrangement of the bone plate to the wooden fixture for the pull out test. (b) Machine set up for fixture arrangement (c) magnified view of the attached bone plate in the universal tensile testing machine for the pull out test.

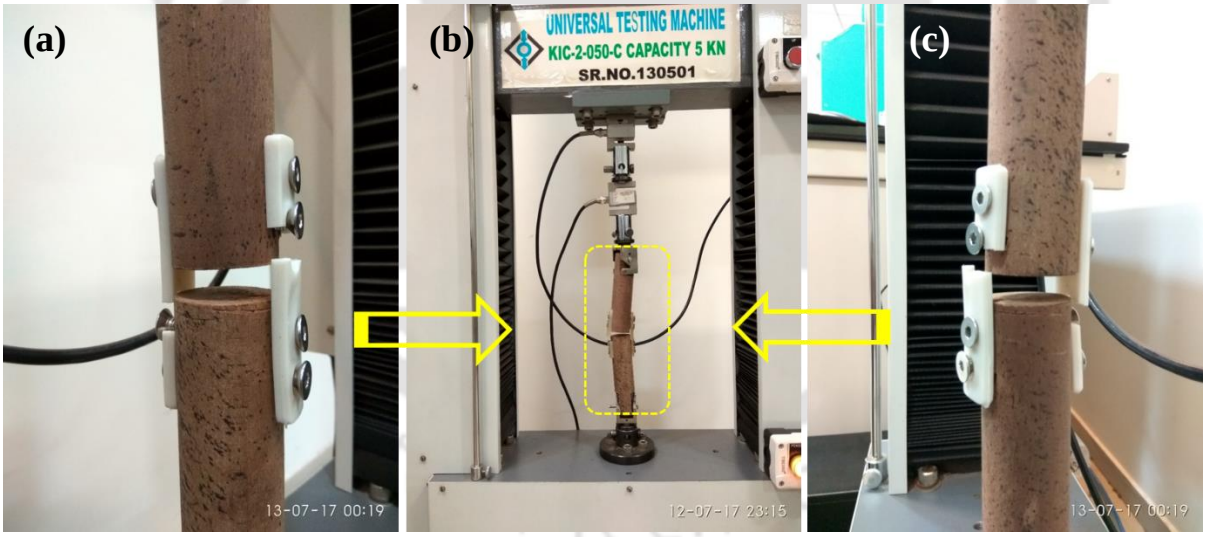

Figure 5.22: Fractured bone plates after uniaxial double plate pull out the test. (b) Attachment of fixture in the machine (c) Fractured bone plate during tension test.

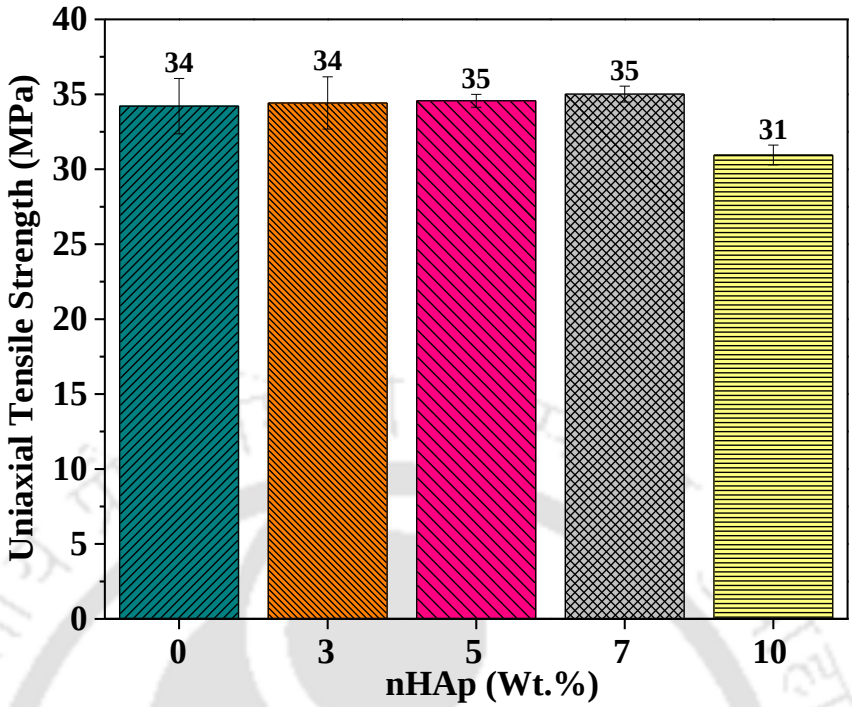

Figure 5.23: Uniaxial tensile strength values of the double plate concerning varying nHAp filler concentration.

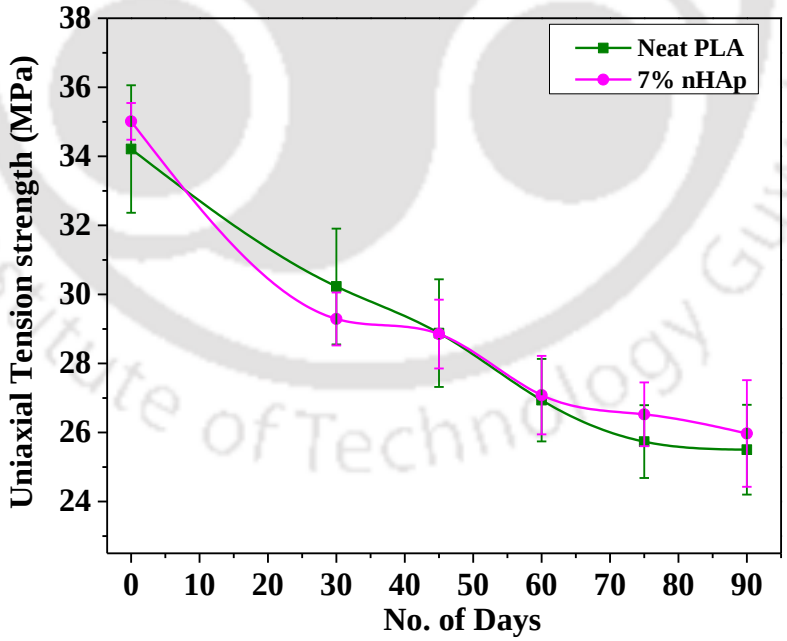

Figure 5.24: Uniaxial tension values of neat PLA and 7% nHAp after In vitro hydrolytic degradation.

Figure 5.23 shows the value of uniaxial tensile strength of double plate concerning the various combination of PLA/nHAp. It was observed that in case of neat PLA based plate, the uniaxial tensile strength value was about 34 MPa, while in case of 7% nHAp plate, the value was about 35 MPa (~3% increment) was observed. The reason for the increase in uniaxial tensile strength may be due to the transverse support provided by the addition of nHAp powders to the PLA matrix. From Figure 5.24, the uniaxial tensile strength value of double plates was observed reduction about ~12% (30 MPa) after 30days and ~24% (25 MPa) after 90 days. While in the case of 7% nHAp, the reduction was observed ~17% (29 MPa) after 30 days and ~26% (26 MPa) after 90 days.

Figure 5.25: Fractured bone plate profile after the mechanical test.

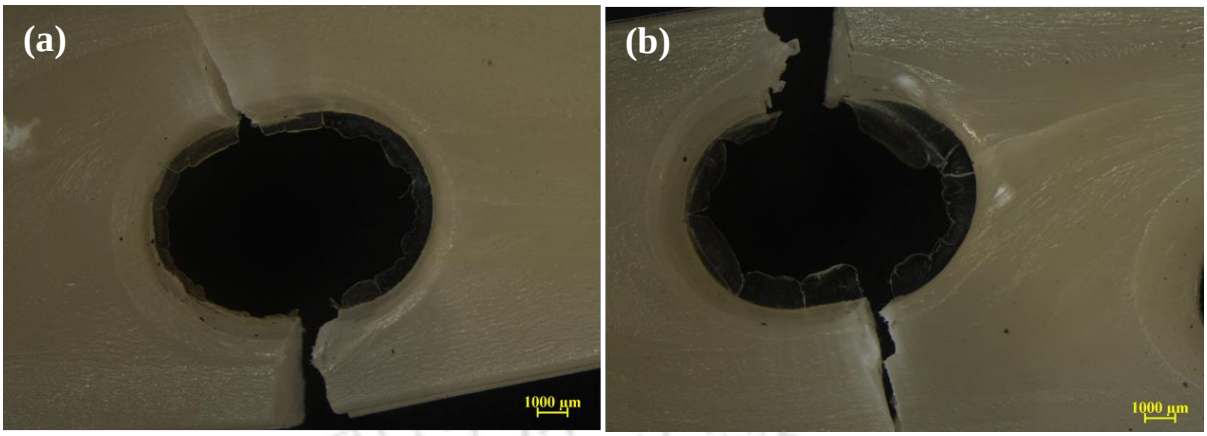

Figure 5.26: Photographic images captured by stereomicroscope (a) neat PLA bone plate at fracture site. (b) neat PLA bone plate fractured near combination holes.

5.4 Degradation studies

Figure 5.28 shows the mass loss profile of the neat PLA based bone plate and optimized bone plate (7% nHAp) exposed in PBS solution for 90 days. The In vitro hydrolytic degradation was studied as shown in Figure 5.27 in PBS solution maintaining temperature of 37.5 at pH 7.4 throughout the studies.

Figure 5.27: Glass jars used for in vitro hydrolytic degradation studies. (b) Magnified view of the bone plate kept in PBS medium (c) arrangement of PBS filled glass jar in hot air oven maintaining the temperature at 37.5°C.

It was also observed that for the same duration of exposure towards PBS solution the rate of degradation of neat PLA was faster as compared with 7% nHAp. It might also reveal that ~100% degradation in mass loss would be between ~9 to 12 months and healing of fracture bone also takes ~8-12 months. Hence for various age group peoples, bone plates can be tuned. The mass loss was also observed after exposure towards PBS solution. In case of neat PLA, mass loss was~2% after 30 days, while after 90 days, ~16% reduction was observed. While in the case of 7% nHAp, the mass loss was ~1% after 30 days and after 90 days, 14% reduction in mass was observed. The Figure 5.30 shows the surface micrograph of *In vitro* hydrolytically degraded plates.

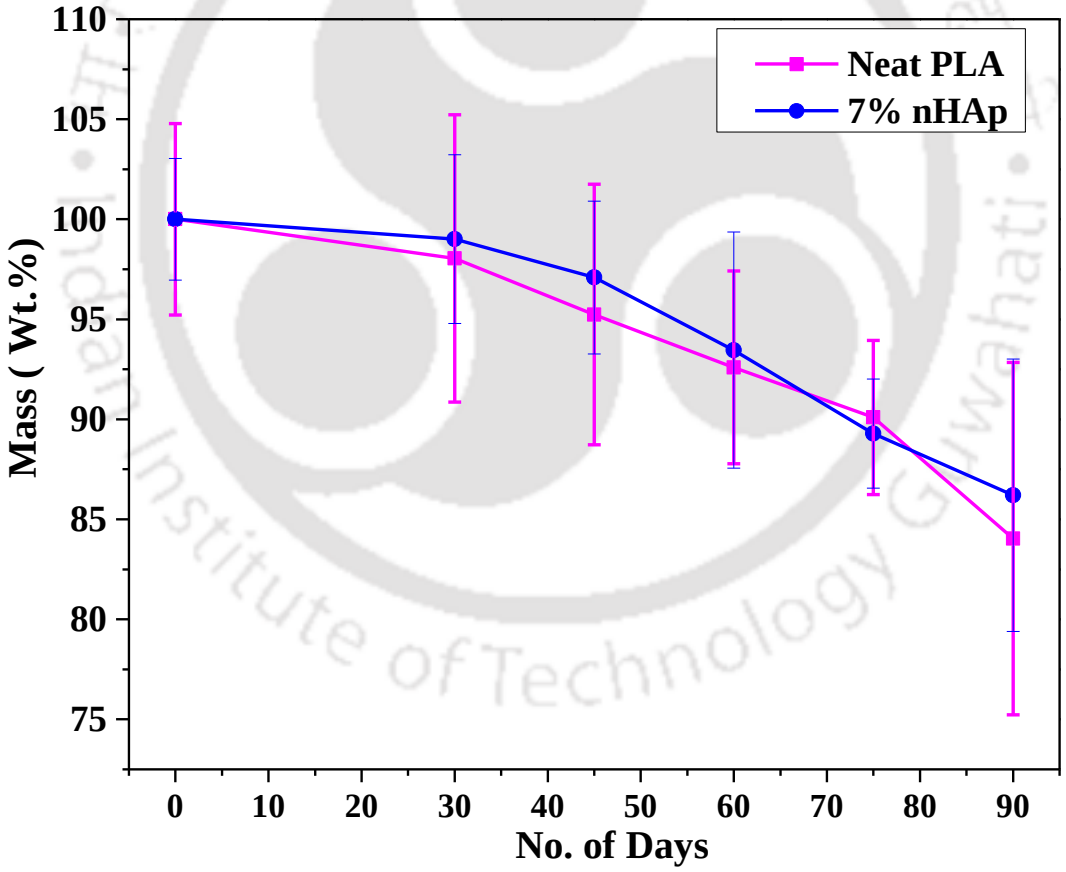

Figure 5.28: Mass loss profile of neat PLA and 7% nHAp before and after In vitro hydrolytic degradation.

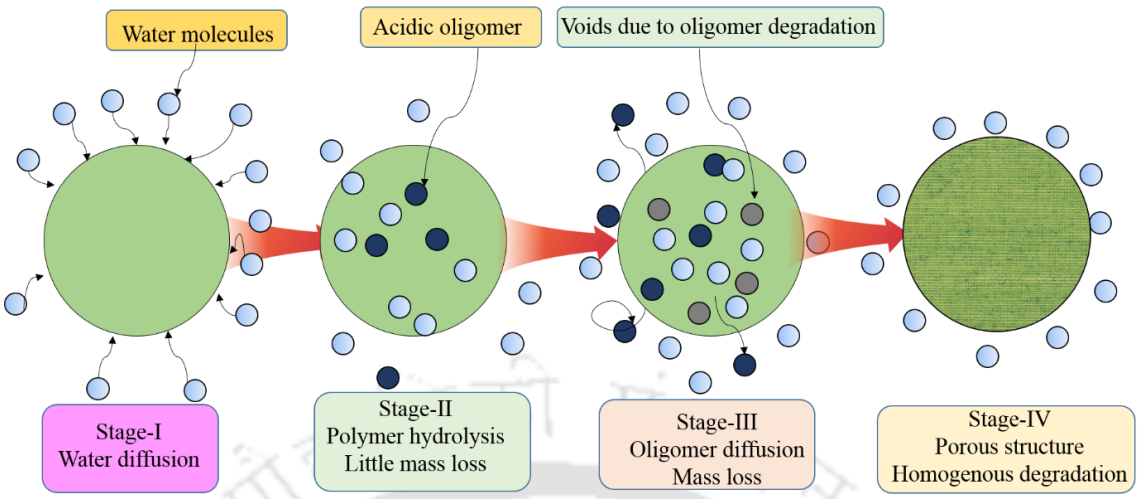

Figure 5.29: Mechanism of In vitro hydrolytic degradation of semi crystalline polymers.

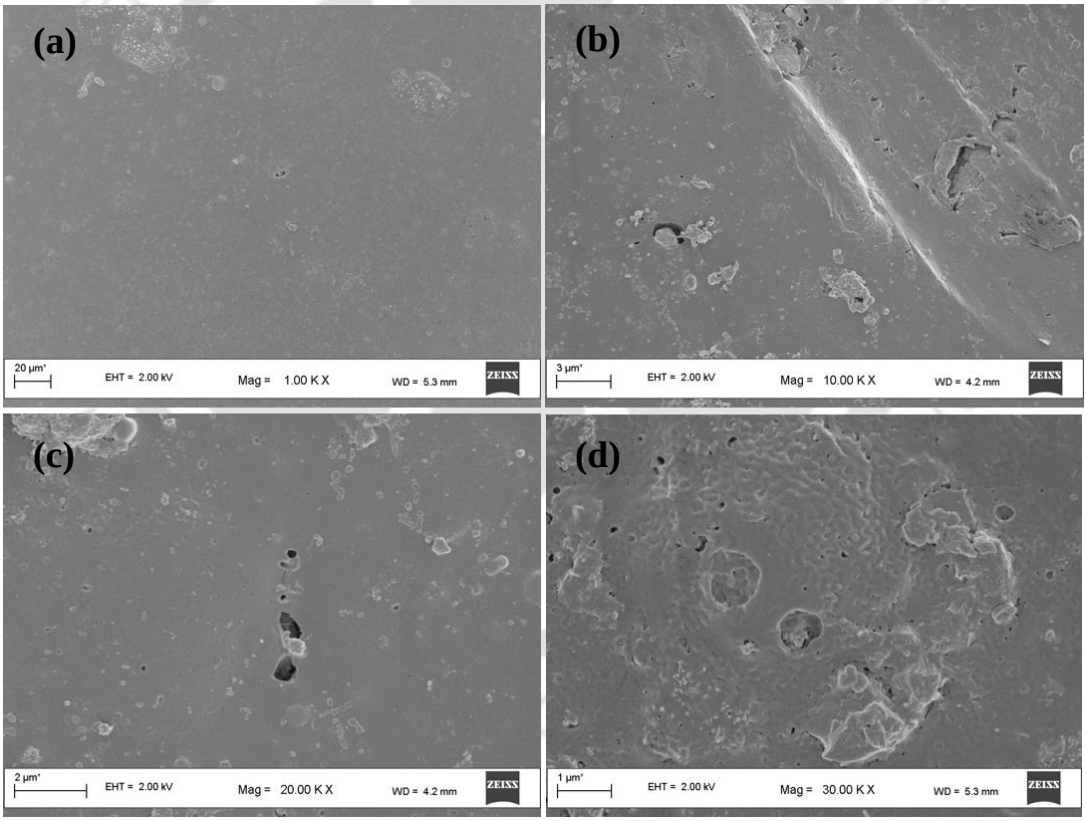

Figure 5.30: (a) surface micrograph from FESEM of In vitro hydrolytic degraded bone plate sample (b) Magnified at 10 thousand zooms (c) magnified image at the 20kX (d) magnified image at the 30kX,In vitro hydrolytic degradation of the bone plate surface exposed towards PBS for 28 days.

Figure 5.29 shows the mechanism of in vitro hydrolytic degradation of the polymer composites during exposure towards PBS solution. The whole degradation happens mainly in four stages. In stage one, the water gets diffused to the surface of the polymer composites, which leads to the hydrolysis of the polymer in which acidic oligomer gets penetrated to the polymer matrix, and during this interaction, some of the molecules come out. The outgoing molecules create a void in the polymer matrix composites, which results in a mass loss. Moreover, in the final stage four, the porous structure of the polymer matrix composite obtained with uniform degradation [224-225].

5.5 Dimensional deviation studies

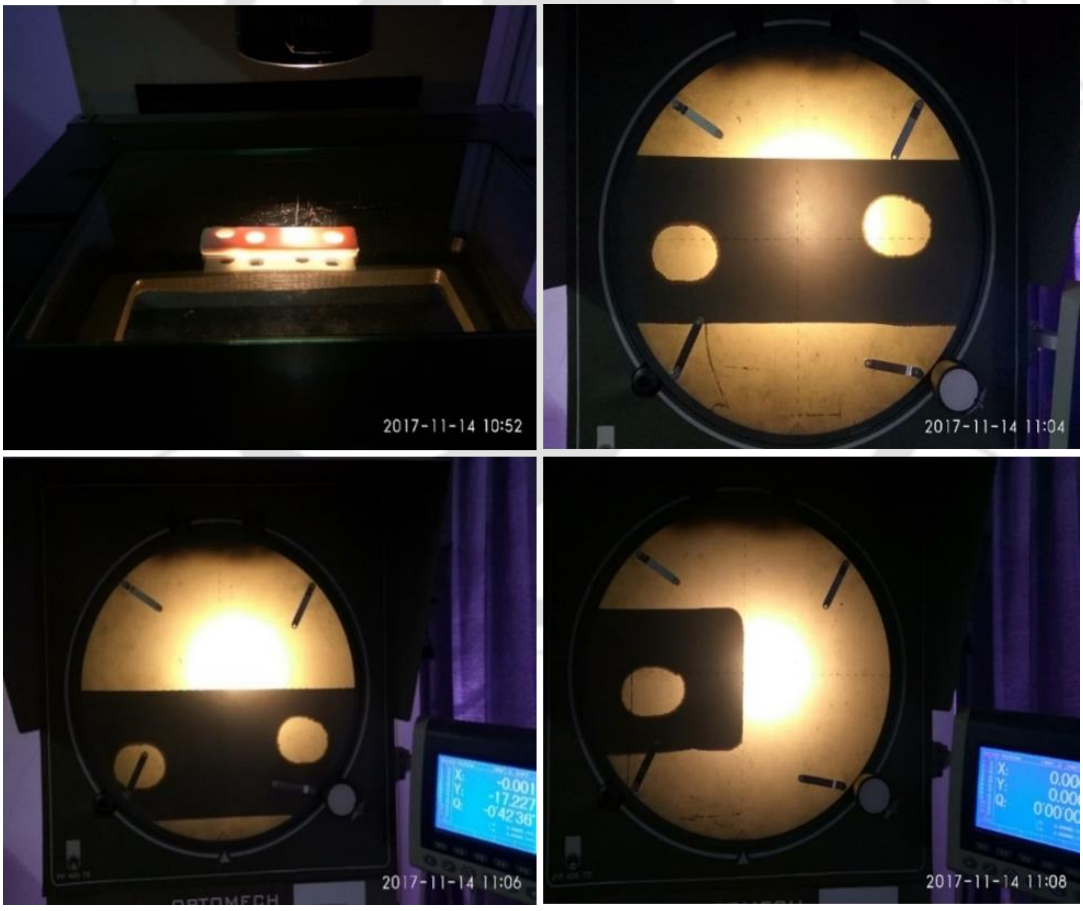

Figure 5.31: Photographic image of surface profile optical micrograph of bone plates.

In order to know the geometrical deviation from the dimension of bone plates from the standard geometry, bone plates were analyzed through optical surface profilometer (Optomech, vertical) at 10x (*Figure 5.31*). It was observed that deviation of the geometries of the bone plates was very less as compared with the standard dimension and later the deviated dimensions in their geometries were neglected.

5.6 Summary

In this chapter, following major points are summarized

1. The bioabsorbable bone plate based on neat PLA and PLA/nHAp has been fabricated through extrusion cum injection molding.
2. The process parameters related to extrusion cum injection molding has been optimized.
3. The development of the bone plate mold and related fixtures for performing mechanical test has been discussed.
4. The mechanical test as per ASTM standards related bone plates has been performed.
5. The flexural strength of the bone plate was also performed as per ASTM standard. The reduction of 4% to 8% was observed with compared to neat PLA.
6. The torsional strength of 5% nHAp gives an increment of 19% concerning neat PLA.
7. The single plate tensile strength was performed, and 3% nHAp gives 3% increment concerning neat PLA based bone plate.
8. The double plate tensile strength was also performed and 7% nHAp gives the 3% increment concerning neat PLA.
9. The mechanical test during degradation has been conducted and explained.
10. The deviation in geometries of the fabricated bone plates was found insignificant.

ABSTRACT

This chapter elucidates the fabrication and characterization of steinmann pins and U-type bone staples for interphalangeal joints, metatarsal bone fracture and to join the soft and hard tissue respectively. The Steinmann pins and bone staples were fabricated through extrusion cum injection molding process through an optimized processing parameter. The varying concentration of nHAp and neat PLA composite was injected into the respective staples and pin molds via commercially viable process, i.e. injection molding process. After development and fabrication, the staples and pins were conducted the mechanical test. The optimized staples and pins were also undergone through *In vitro* hydrolytic degradation studies, and again mechanical test was done during the degradation test. The optimized combination is reported, and fracture profile of the fixation implants has been successfully discussed.

GRAPHICAL ABSTRACT

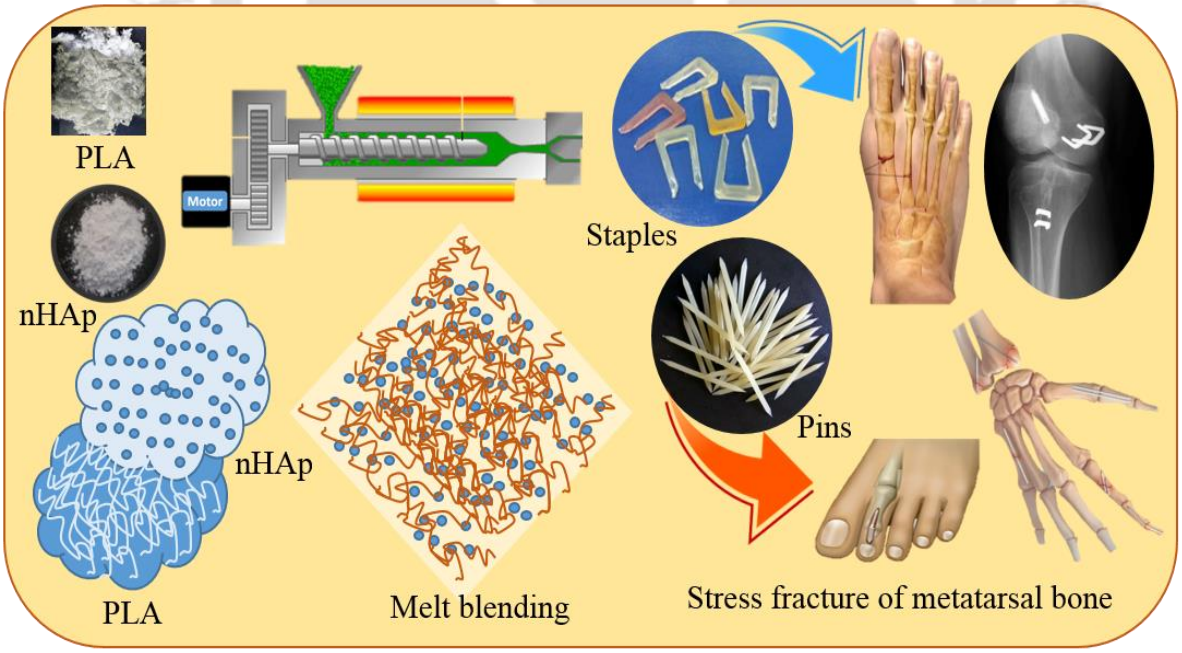

Chapter 6

6 Fabrication and characterization of Steinmann Pins and Staples

6.1 Introduction and fabrication process

Steinmann pins are often used to fix the bones back together. These are often used to hold together pieces of bone that are too small to be fixed with screws. In many cases, it is used in conjunction with other forms of internal fixation, but it can be used alone to treat fractures of small bones, such as those found in the hand or foot [226]. Steinmann Pins are generally made from implant-grade stainless steels. Steinmann pins are similar to K-wires (Kirschner wires) but typically have larger diameters [227]. These pins typically have trocar, chisel, or spherical ends with partially threaded or smooth outside diameters. Since K wire has lots of disadvantages like pin tract infection, swelling near the implant site, and infection occurs because of external fixation devices [228]. Bioabsorbable pins have many advantages like it avoids stress shielding phenomenon, no need of resurgery after fracture healing, implanted inside the body so no chances of inflammation, and to avoid pin tract infection [229]. Various researchers have proposed the pins made of various metals which were bio inert, some are a bioabsorbable copolymer based. Some of the researchers have compared the various mechanical properties of bioabsorbable pins with the stainless steel pins. Gut et al. [230] reported novel, internal fixation devices based on the human cortical bone for use in the orthopedic surgery. Pins and screws of different diameters were formed from processed human lower limb bones according to standard tissue banking procedures: freezing, defatting and radiation sterilization (35 kGy). The mechanical properties of the pins and screws were

evaluated using bending or braking tests. The results indicate potential usefulness for clinical applications. Hirvensalo et al. [231] reported absorbable polyglycolide pins in fixation of displaced fractures of the radial head. In this study, 24 patients with a displaced fracture of the radial head were treated by open reduction and internal fixation using absorbable polyglycolide pins, 2 mm in diameter. It was also observed that this study caused no difficulties; no temporary fixation was needed while preparing drill-holes or inserting the pins. Jensen et al. [232] compared biodegradable pins with kirschner wires in hand surgery. Eleven patients were allocated to biodegradable pins and 12 patients to kirschner wire group. All patients were evaluated after six months. No differences in time to union or complication rates were found. However, the number of additional operative procedures in the kirschner wire group significantly exceeded the number needed in the biodegradable pin group. It was also discussed about polydioxanone pins may provide effective fixation of fractures, anthrodeses and osteotomies in hand without adverse side effects. Weimann et al. [233] evaluated primary stability of bone patellar tendon bone (BPTB) graft fixations with biodegradable pins compared with interference screw in anterior cruciate ligaments reconstruction using bovine knees. Ten pairs of fresh bovine knees were used to simulate young human femoral density. It was observed that the mean yield load in the cross pin group was 400.2 ±122.4 N and 402.7±143.7N in the biodegradable interference group. The maximum load at the failure was ~525 N in the interference screw group. Thus it was finally concluded that fixation of a BPTB graft using two biodegradable 2.7mm pins (rigid fix) leads to primary stability comparable to fixation with biodegradable interference screws. Pietrzak et al. [234] reported bioabsorbable fixation implant for use in the proximal interphalangeal joint (Hammer Toe) Arthrodesis: Biomechanical Testing in a synthetic bone substrate.

Polymeric pin type implant was made from 82% PLA and 18% PGA to fix the synthetic bone block together in form of pins. For both bioabsorbable and k wire fixation groups, the failure mode was bending of the respective implants. Implant fracture did not occur in either group. Accelerated aging in vitro studies at an elevated temperature was performed to hydrolytically degrade the bioabsorbable polymer over a shorter time interval at 37° C. In the initial the peak load of bioabsorbable fixation was about ~8.2 MPa. While the stiffness value was about 6.48 MPa. The aging studies suggest that this implant retains strength over the equivalent of approximately six weeks. Valentin et al. [235] evaluated the incidence of pin-tract infection (PTI) during limb lengthening using external fixation in 88 patients and the effect of infection on outcomes. The rate of half pin site infection was significantly higher in half pin fixators than in hybrid fixators. It was also observed that there was a significantly higher incidence of half pin site infection than fine wire site infection. The rate of additional surgeries for treating PTI was higher for half pin site than for fine wire sites. Three of 88 cases leads to chronic osteomyelitis. Careful insertion and a simple, well defined, excellent pin care protocol can minimize PTIs.

Bellisari et al. [236] evaluated mechanical properties of cross pins used for femoral fixation of Hamstring Grafts in ACL reconstructions. The goal of their studies was to test the mechanical strength of 4 cross pins currently available for femoral fixation by loading each cross pin to failure as received and determine the effect of 1 million cycles of fatigue loading. The strength of the resorbable pins was tested after prolonged exposure to biologic conditions. Six implants each of arthotek, mitek, biomet, cortical allograft and control were tested for 3 point failure strength. During fatigue testing, Rigid Fix implant failed at ~18894 cycles. All other implant tested endured 1 million cycles of loading (50-200N) without

fracture or 1.5 mm central deformation. Neither of the bioabsorbable pins demonstrated a significant change in yield strength after prolonged exposure to water. Thus it was finally concluded that polymeric implants showed gradual enough loss of mechanical properties to achieve this goal, and the other two implants far exceed the strength needed. The mechanical properties of the bioabsorbable cross pin appear to meet clinical demands and maintain their strength for a sufficient length of time to permit biological fixations. Kembhavi et al. [237] studied a case related to the outcome of fracture fixed with biodegradable pins. Eleven patients were included in this study involving 13 fracture among which ten were children, and one was adult. Fracture fixation was performed either by open reduction or closed reduction with percutaneous fixation using 1.5 or 2 mm biodegradable pins. In the initial cases, it was observed that the biodegradable pins were loose and did not fit perfectly in their bony tunnel. The biodegradable pins were deformable and became loose in the similarly sized tunnels. This problem was avoided by drilling the initial tunnel with smaller sized K- wires. It was seen around the fracture site and implant site. Because of these changes, it was decided to continue plaster immobilization for six weeks post operatively to prevent fracture displacement. Thus it was finally concluded that biodegradable pin was an effective way of fixation for fractures that can be fixed with k wires. Singh et al. [238] reported anterior cruciate ligament (ACL) reconstruction using the femoral rigid fix and tibial bio-intrafix devices. In this study, the evaluation of clinical and functional outcomes of the knee joint after ACL reconstruction with hamstring graft fixed femoral cross pin (rigid fix) and tibial bio-intra fix devices was done. All patients between 18 and 45 years of age who were operated for their ACL deficient knee with autologous hamstring graft fixed by rigid fix device in the femoral tunnel and bio-intrafix device in the tibial tunnel were prospectively

evaluated. In the early post-operative period, the strength of the fixation of the graft is the critical point limiting aggressive rehabilitation. During graft stabilization with absorbable pins inserted perpendicular to the femoral tunnel provides a secure fixation when compared with other soft tissue fixation devices. The stiffness was ~77-17N/mm. Thus these fixation devices securely fix the graft to the tunnels until biological fixation has occurred.

Table 6.1: Parameters for Steinmann pins production.

Parameters		
1.	Processing temperature	190°C
2.	Mold temperature	100°C
3.	Cylinder temperature	220°C
4.	Residence time	1min
5.	Twin screw speed	120 rpm
6.	Compressed air pressure	680-740 bar
7.	Injection pressure holding time	5 sec
8.	Weight of steinmann pin	1.58 g

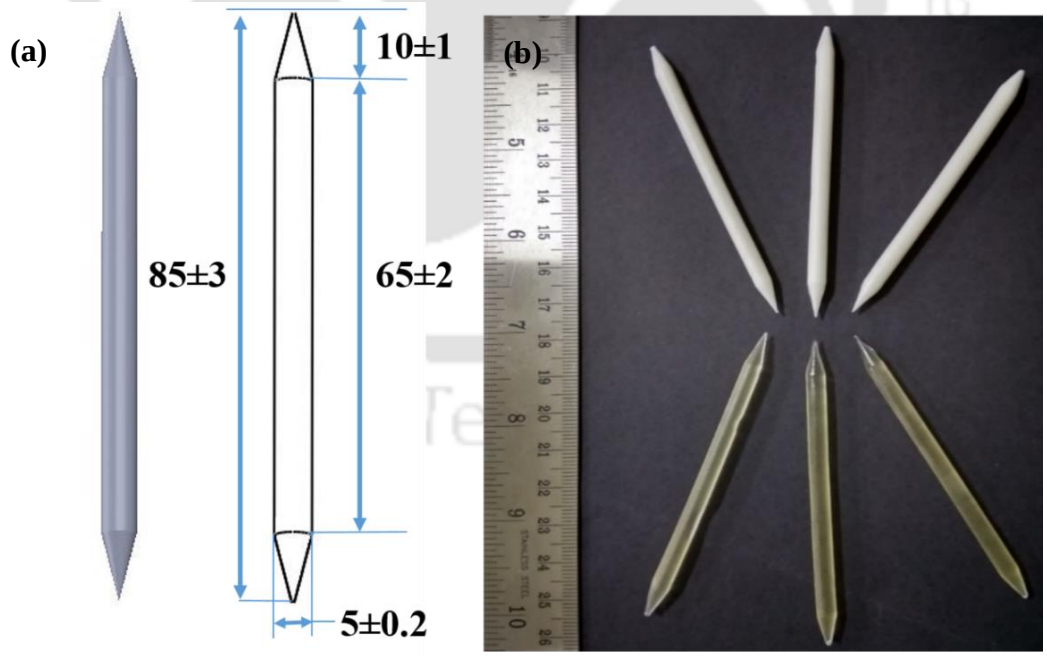

Figure 6.1: Schematic diagrams of steinmann pins (a) 3D and line diagram of pins (b) Photographic images of neat PLA (top) and PLA/nHAp (bottom) steinmann pins.

In these studies, bioabsorbable steinmann pins and U-type bone staples have been fabricated through twin screw extruder cum injection molding process. The fabricated mold as per the specimen of Steinmann pin and U-type staples were loaded in the injection molding cavity, and according to parameters mentioned in Table 6.1, the parameters were set for the successful production of PLA and PLA/nHAp Steinmann pin and U-type bone staples. After production of the Steinmann pin, the mechanical testing was done as per ASTM standards. Figure 6.1 shows the three dimensional image of the fabricated steinmann pin and its dimensional geometries.

6.2 Introduction to U-type bone staples and fabrication process

Bone staples have a shape of a hook with sharp conical or trapezoidal points. Size and shape are given by the extent of the osteotomy. Some staples have thin ribs inside. Bone staples fixate adjusted bandy or valgus deformations in upper osteotomy of the tibia. Staples are constructed in a way so that they could compress the osteotomy slit during infixing. Staples keep cutting surfaces together with required extend of bone tissue growing until complete healing. These staples can be recommended even for treatment of bandy or valgus inflammation of knee joint. A bone staple is a single fixation device made up of two or more points of entry into bone that are joined to each other. The bone staples in the market come in various design construction demonstrating various cross sectional shapes, leg lengths, bridge shapes, tip contours and the presence and absence of leg barbs. Russell et al. [240] reported design consideration for Nitinol bone staples. Generally, nitinol bone staples are inserted through a process of being chilled, opened, and inserted into predrilled holes. Upon insertion, they recover their preprogrammed shape either through spring back after removal of a constraint (using super elasticity) or thermal triggering (using thermal shape memory).

It was also mentioned about the various staples available in the commercial markets and its applications. It was observed that the factors that influence staple choice include activation control, force control, ability to stabilize the fracture and ease of use. It was finally concluded that heat activated staples that use a controlled heat source appear to have the best combination of clinical forces and procedural control. Koukoubis et al. [241] reported meniscal fixation with an absorbable staple. This study was conducted in dogs. The staples were made of a copolymer of Polyglycolic acid and Polylactic acid connected by a flexible suture made of the same absorbable material. The staples were developed for arthroscopic use, eliminating the risk of nerve or vascular injuries associated with suture fixations. It was concluded that the meniscal staple that was studied seems to be a technically feasible alternative for meniscus fixation. The staples were almost completely absorbed during the first post-operative year in the canine model appear to be due to surgical factors related to the small size of the canine meniscus rather than to the device itself. Rethnam et al. [242] investigated mechanical characteristics of three staples commonly used in foot surgery. Comparison between shape memory staples and a standard stainless steel staple has been made. In this metatarsal bone model made from tufnol tube were osteotomized and stabilized using one of three types of bone staples, two types of memory staple (memory staple and heat activated memo clip) or a standard stainless steel staple (Richards). The constructs were loaded in bending and torsion on a material testing machine. The moment and torque to achieve 10° of bending or torsion and permanent angulation of the osteotomized bones were assessed. It was observed that the Richard staple was found to provide a four times larger resistance to bending and torsion than the two memory staples. However, it was permanently deformed after bending. Thus finally it was seen that the Richards staple was stiffer, although

the permanent deformation of this staple is a disadvantage. Memo clips staples exhibit lower but adequate stiffness when compared to the standard Richard staple and are not permanently deformed after bending. The bone staples were fabricated through the melt blending cum extrusion followed by injection molding machine (make: Thermo scientific, model: Hake mini jet).

Table 6.2: Parameters for U-type bone staples production

Parameters		
1.	Processing temperature	190°C
2.	Mold temperature	100°C
3.	Cylinder temperature	215°C
4.	Residence time	1min 30 sec
5.	Twin screw speed	100 rpm
6.	Compressed air pressure	720-740 bar
7.	Injection pressure holding time	5 sec
8.	Weight of bone staples	2.90 g

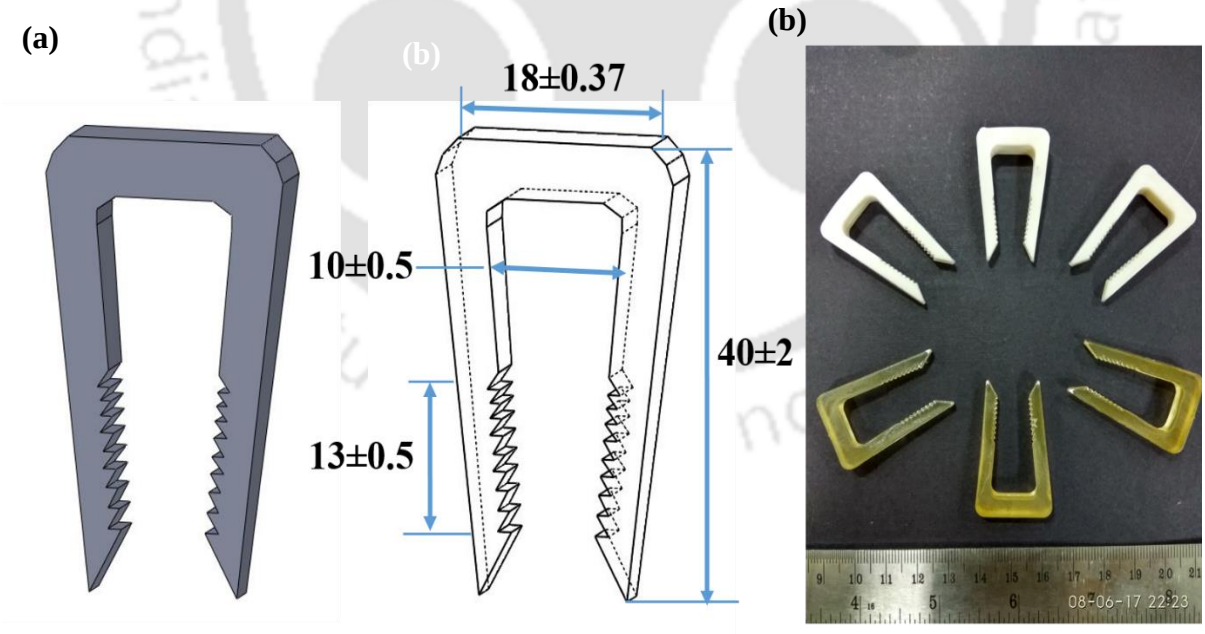

Figure 6.2: (a) 3D line diagram of U-type bone staples (b) Photographic images of neat PLA (bottom) and PLA/nHAp (top) U-type bone staples.

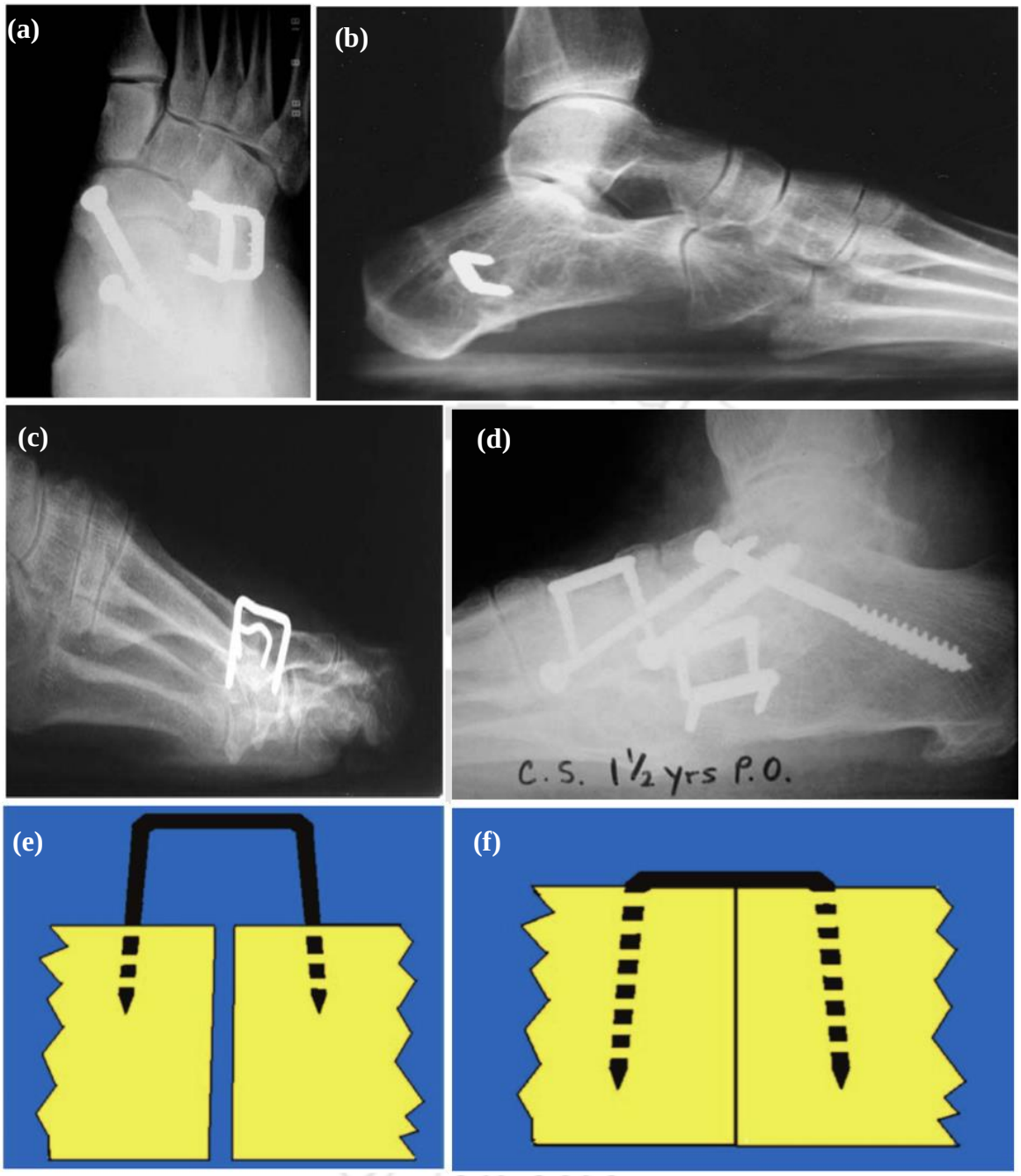

Figure 6.3: (a) Application of bone staples at foot ankle joint as compression devices. (b) Applications of bone staples in foot heel joints. (c) Hammer toe joints. (d) Combinations of internal fixation devices applications in foot bone fracture joints. (e) Bone staple before insertion and (f) Bone staples after insertion [243].

6.3 Development of Steinmann Pins and U-Type bone Staples

The Steinmann pins and U-type bone staples were designed in AutoCAD as per the commercial available metallic Steinmann pins and bone staples. In case of steinmann pins, the total length maintained was ~85 mm. The diameter was maintained to 5±0.2 mm sharp spherical edges both side 10±1 mm. Steinmann pins were having a gauge length of 65±2 mm. The detail dimension of the fabricated Steinmann pins is shown in Figure 6.1. The ASTM F564-10 was followed to fabricate the U-type bone staples. The total length in case of staples was maintained ~ 38 mm. The bridge length was maintained 18±0.37 mm. The corner tip was about 0.5 mm. The grip length maintained was 13±0.5 mm. The dimensional diagram is shown in Figure 6.2. Figure 6.3 shows the application of bone staples in fixation of various parts in our bodies.

6.4 Development of Molds and fixtures for Steinmann Pins and U-type bone Staples

The molds for injection molding and related fixtures for its mechanical testing were initially designed in AutoCAD. After designing, the mold of steinmann pins and U- type bone staples (Figure 6.4) were manufactured using various mechanical machines passed through various machining processs. The material choosen for making the molds was H13 (Tool Steel), because of its excellent combination of high toughness and resistance to hot work and cold work tooling applications. Figure 6.5 shows the three dimensional model (3D) of the fabricated steinmann pin mold and Figure 6.6 shows the bone staple mold. After making the mold, various fixtures were fabricated in order to conduct the mechanical test as per ASTM standard for the respective bone steinmann pins and U-type bone staples.

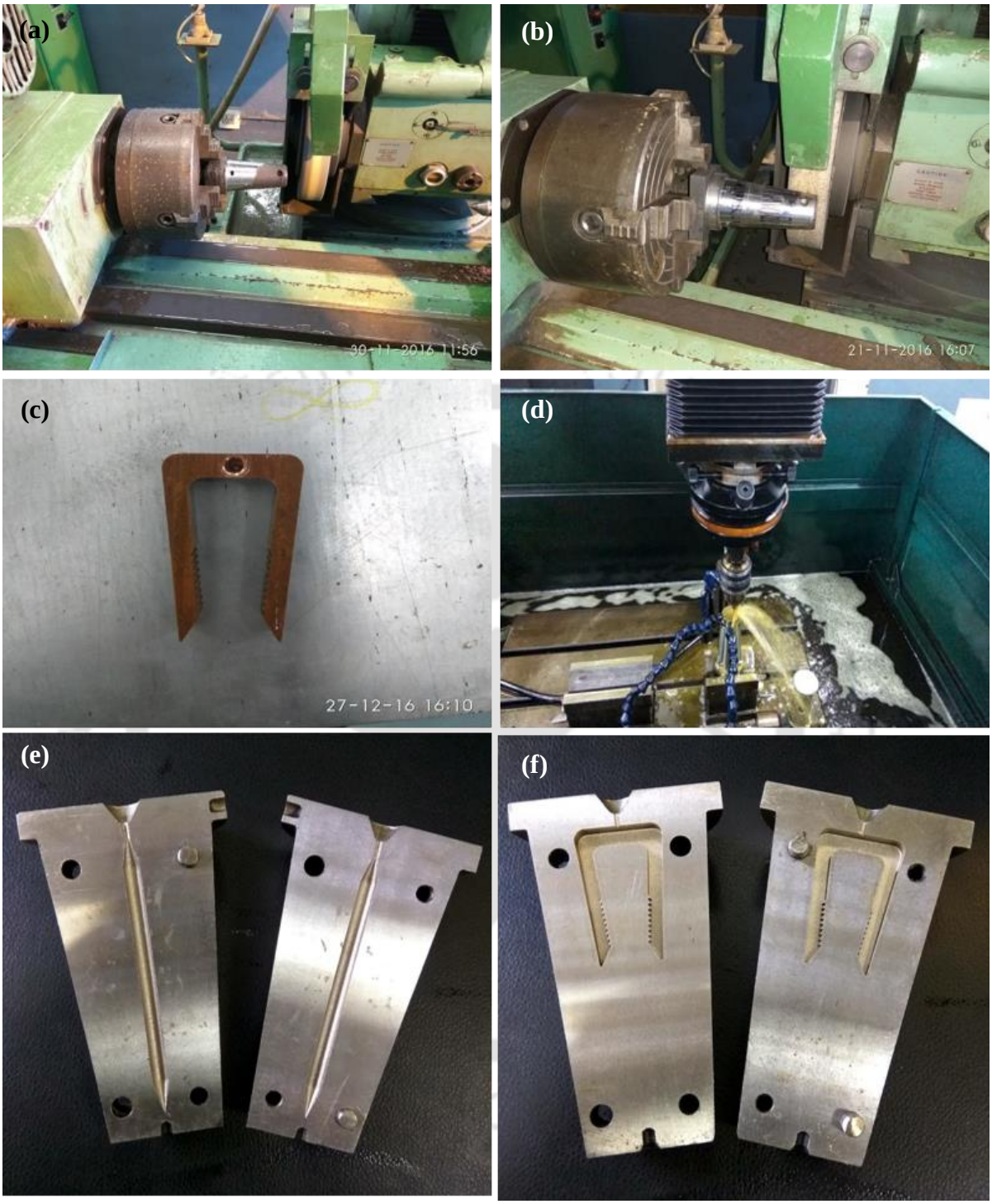

Figure 6.4: Schematic diagrams of pins and staples related to (a) Fabrication of H13 metals in form of mold cavity (b) Machining after heat treatment (c) Bone staples electrode for electric discharge machining (d) Electric discharge machining process (e) Fabricated mold of pins (f) Fabricated molds of bone staples.

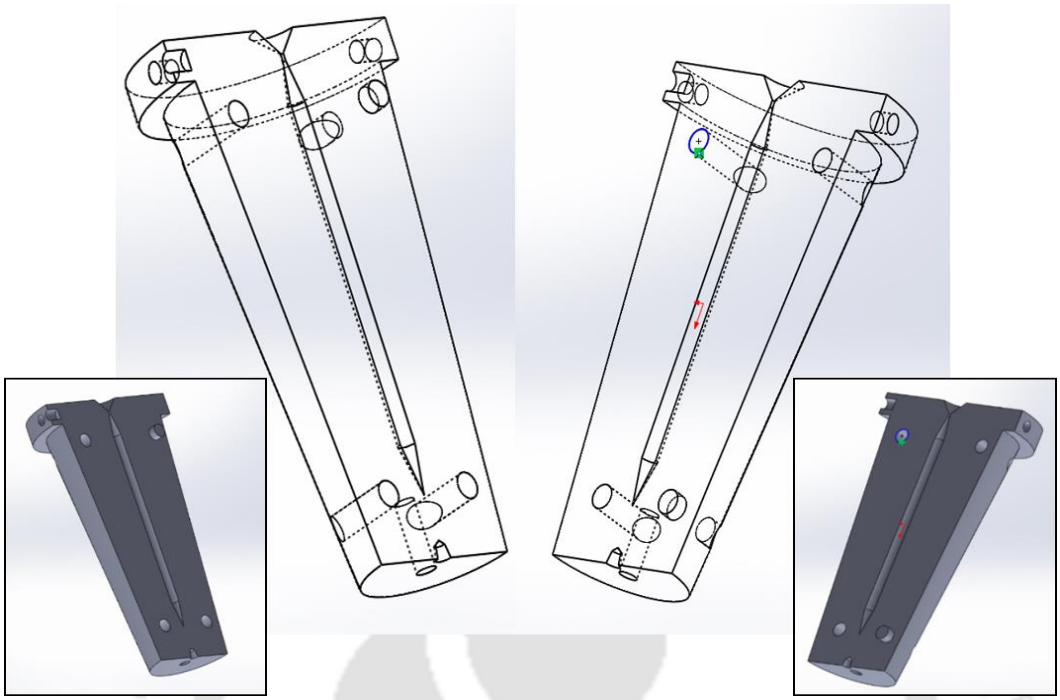

Figure 6.5:3D solid model diagram (inset) and 3D line model diagram of fabricated Steinmann pin mold.

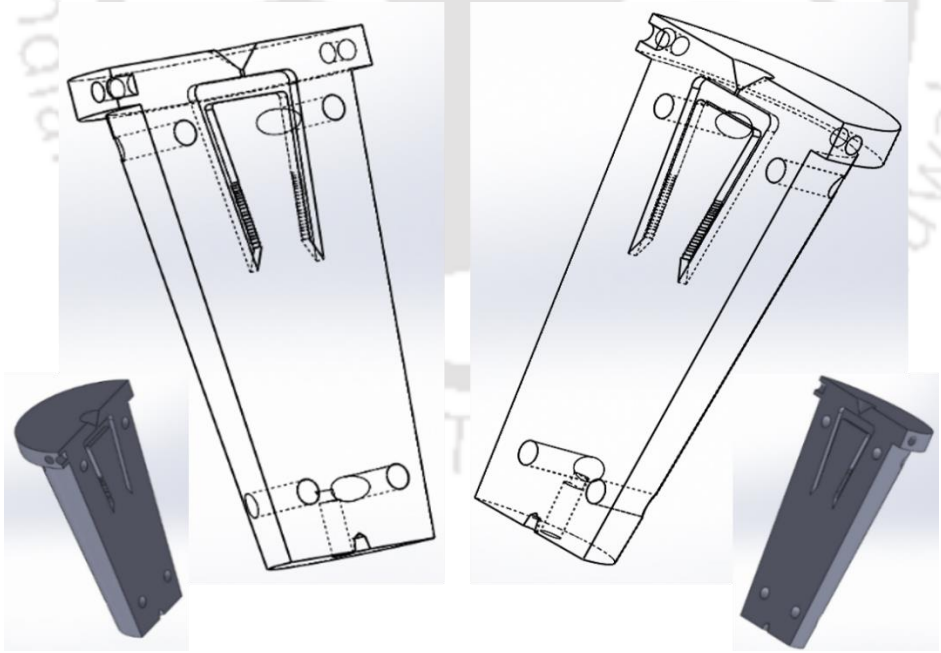

Figure 6.6: 3D solid model diagram (inset) and 3D line model diagram of fabricated U-type staples mold.

6.5 Mechanical Testing of Steinmann Pins

After production of bioabsorbable polymeric steinmann pins, the mechanical test was conducted to evaluate its bending strength (Flexural strength) and shear strength.

6.5.1 Flexural Strength

The maximum flexural load for the steinmann pins were evaluated by flexural (3 point bend test) test using a fabricated flexural fixture. A cross head speed of 1mm/min and a load cell of 5 kN was used. The support span was 40 mm, and radii for loading and support applicators are 3mm. Measurement was conducted in triplicate.

$$\sigma f = \frac{FL}{\pi R^3} \quad \text{.....(6.1)}$$

where σf = flexural strength, F is the load applied, L is the length of the support span (mm) and R is the radius of the steinmann pin.

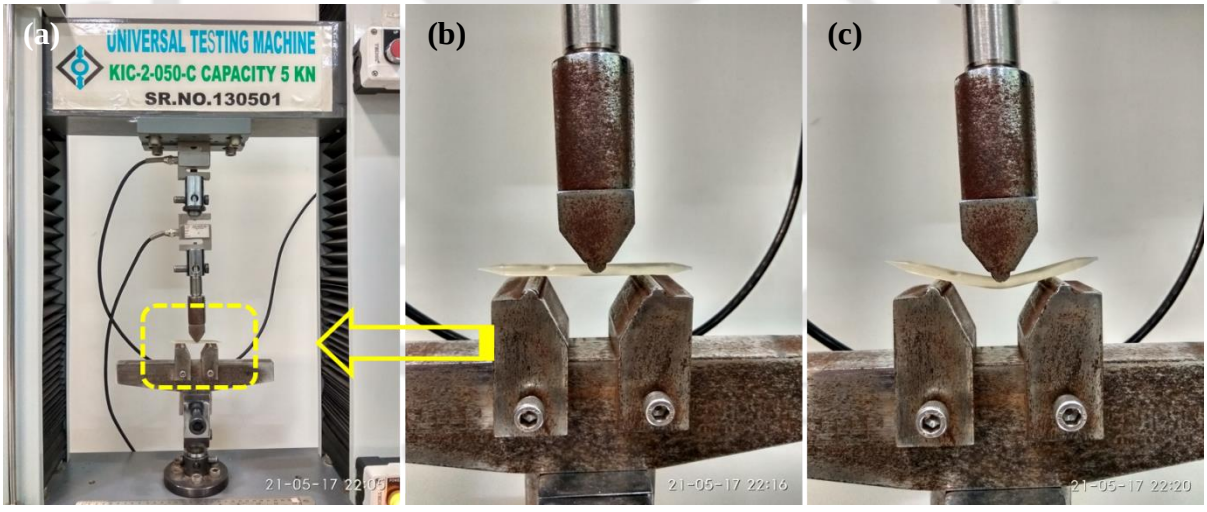

Figure 6.7: Arrangement of 3 point bend test performed on Steinmann pins (a) Universal tensile testing machine (b) Fabricated steinmann holding on the fabricated flexural molds (c) Magnified view of the 3 point bend test of the PLA pins.

Figure 6.7 shows the arrangement of 3 point test performed on Steinmann pins. During the test, the room temperature was maintained constant about 23°C. The flexural strength was calculated by the equation 6.1.

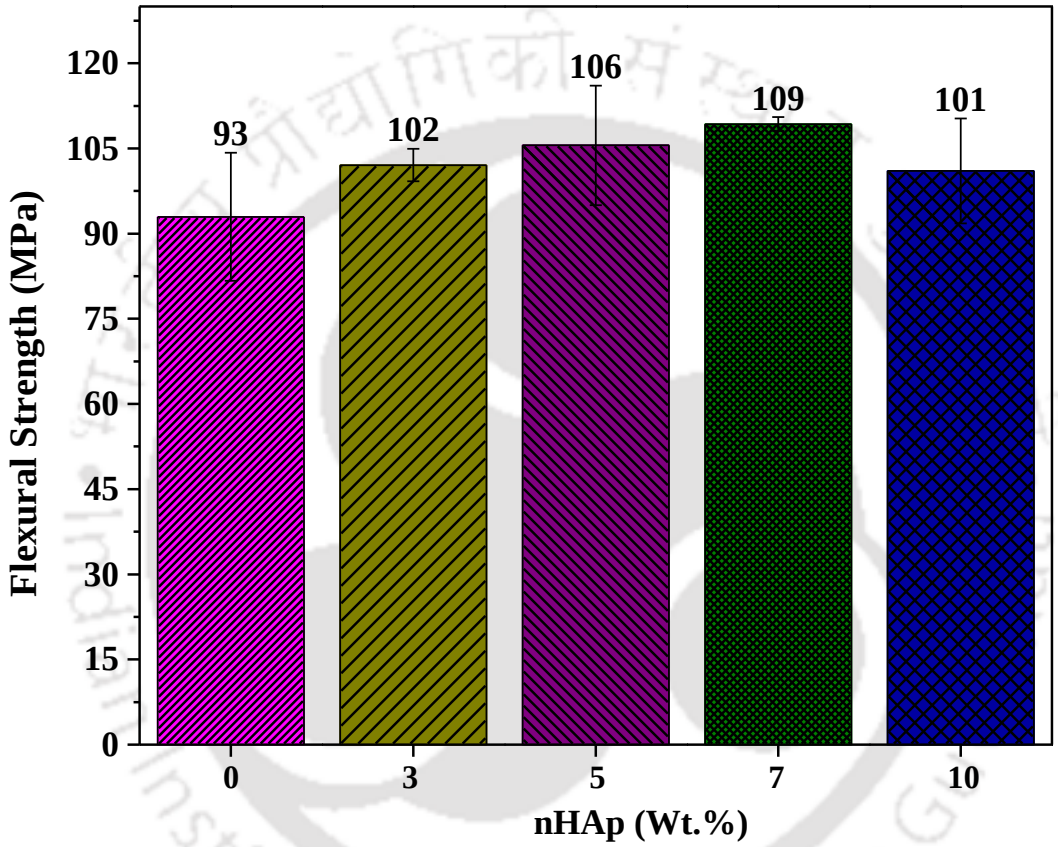

Figure 6.8: Flexural Strength value obtained through a three point bend test of Steinmann Pins concerning nHAp filler.

Figure 6.8 shows the values of flexural strength with varying filler concentration. It was observed that flexural strength was increased in the range of 9% to 17% concerning 3% nHAp to 7% nHAp. The reason may be due to agglomeration of nHAp particles.

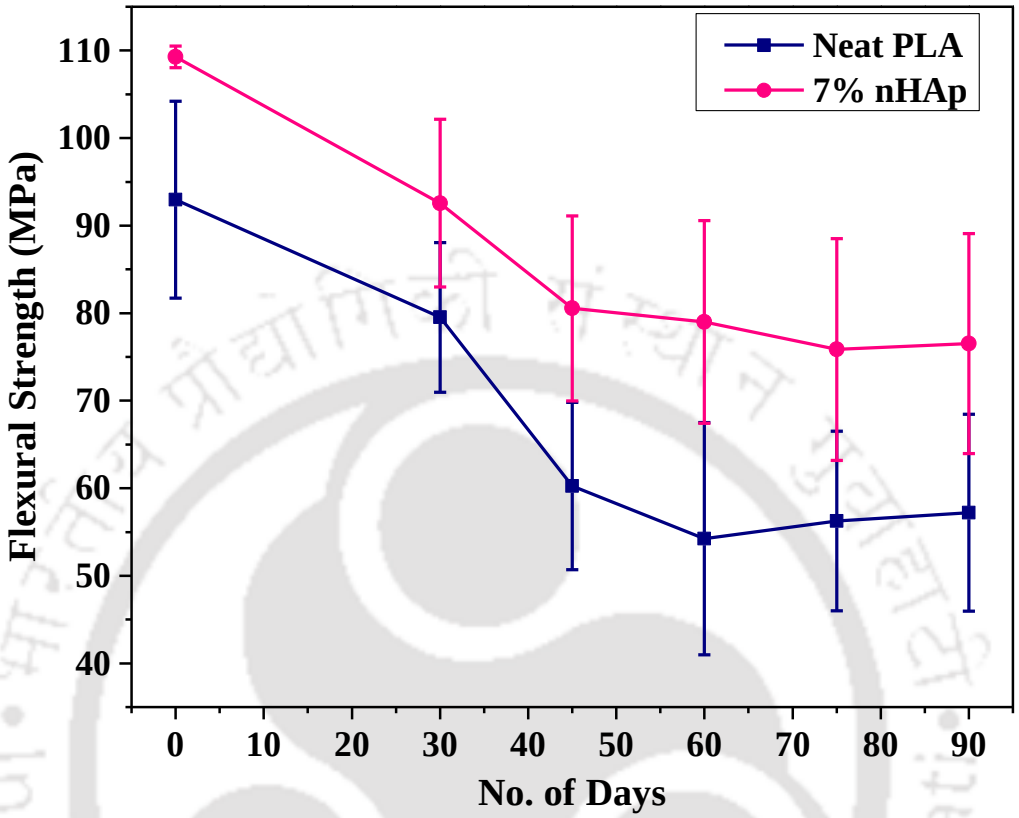

Figure 6.9: Flexural strength value of neat PLA and 7% nHAp after In vitro hydrolytic degradation.

Figure 6.9 shows the values of flexural strength after in vitro hydrolytic degradation; it was observed that the reduction of ~14% after 30 days and ~38% after 90days. While in the case of 7% nHAp, reduction of ~15% was observed after 30 days and ~30% after 90 days in flexural test happens. The reason may be due to the presence of the voids created throughout the composite for the reduction of the flexural strength, these voids wok as stress concentration centers and generally formed due to many reasons which includes agglomeration of the particles, air trapping while mixing with polymer or may be due to moisture sensitivity of the nHAp filler materials [244].

6.5.2 Double Shear Test

The Double shear strength of the Steinmann pins was measured through fabricated fixtures attached in the universal tensile testing machine according to standard ASTMD7617M-11. The cross head speed of the machine was 1mm/min, and load cell capacity was taken 5kN. The maximum shear load was determined as the maximum load recorded during the test. The measurement was carried out in triplicate. The arrangement of the test is shown in Figure 6.10. The increase of 11 % was observed in case of 10%nHAp concerning neat PLA. The double shear strength was calculated by the equation 6.2

$$\tau = \frac{P}{2A} \quad \text{.....(6.2)}$$

where τ = Double shear strength, P=applied load (N) and A=cross-sectional area (mm^2).

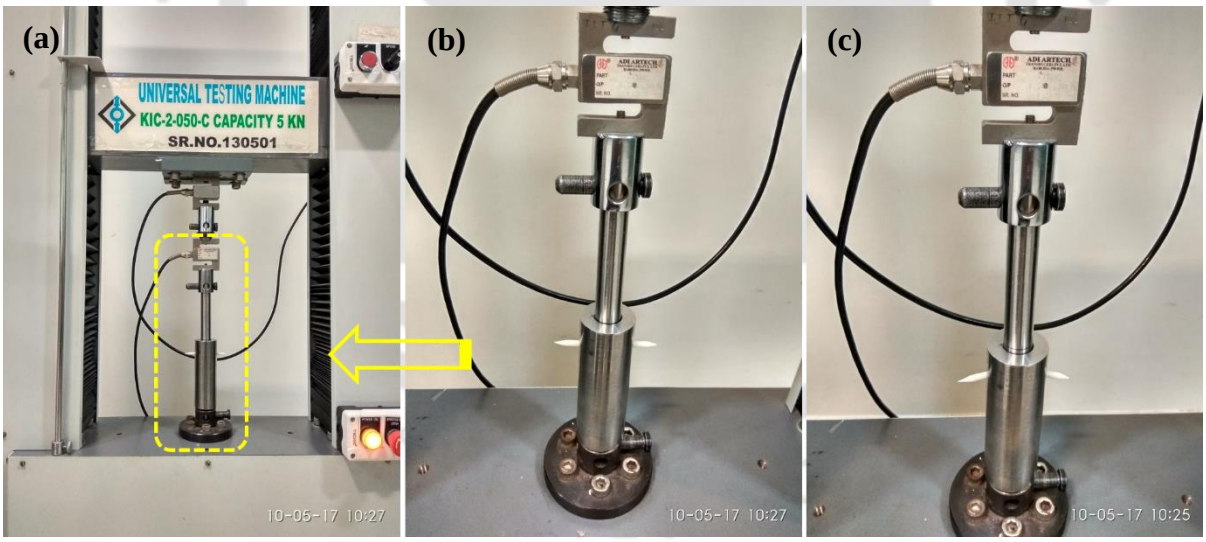

Figure 6.10: (a) universal tensile testing machine for double shear test measurement. (b) The arrangement of the steinmann pin in to the fabricated molds (c) Fabricated steinmann pins during the double shear test.

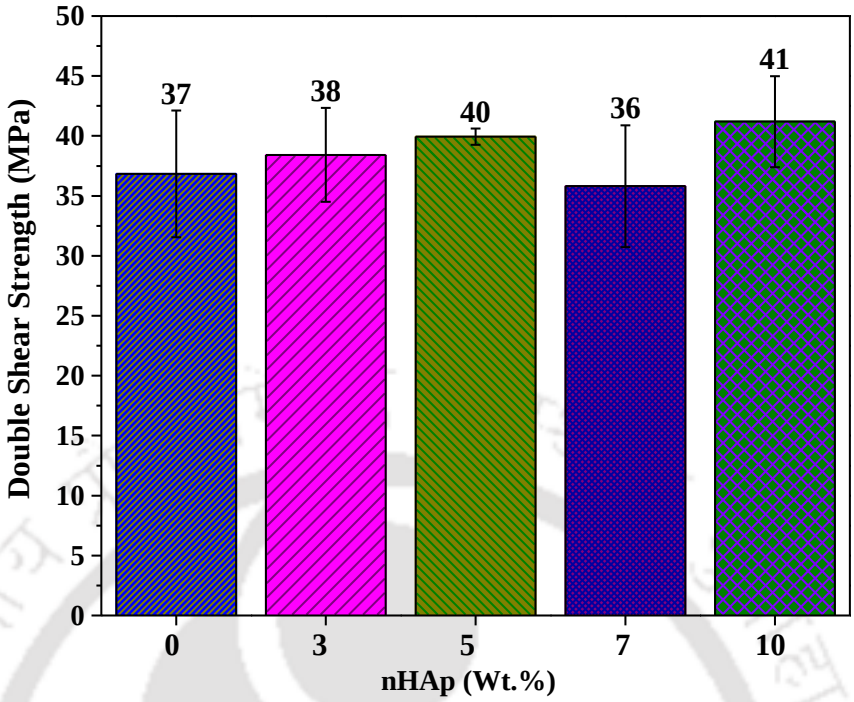

Figure 6.11: Double shear strength of Steinmann pins concerning variation in the nHAp fillers.

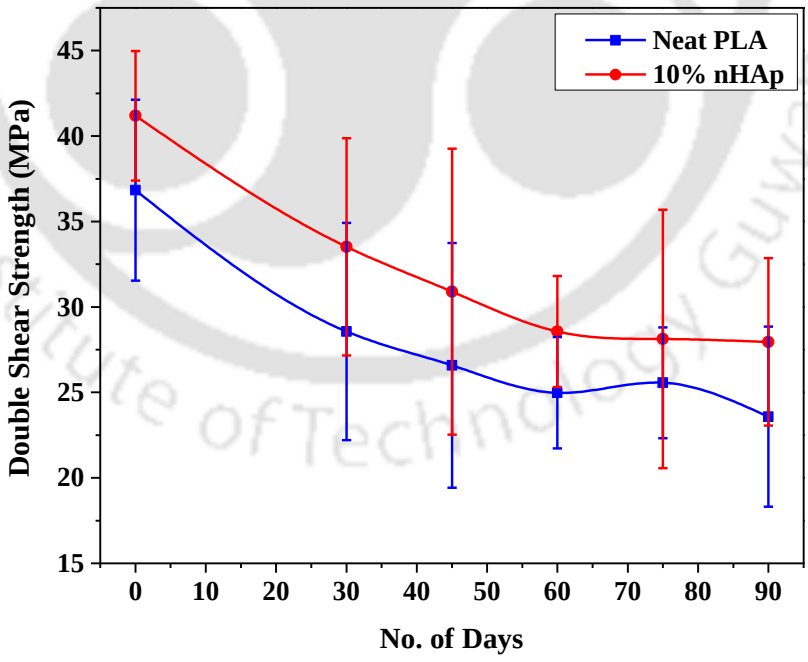

Figure 6.12: Double shear strength values of neat PLA and 10% nHAp after In vitro hydrolytic degradation.

Figure 6.11 and Figure *6.12* shows the value of double shear strength before and after In vitro hydrolytic degradation test. The pins were observed a reduction of ~21% after 30 days and ~35% after 90days in neat PLA. While in the case of 10% nHAp, reduction of ~17% observed after 30 days and ~31% after 90 days during double shear strength test of the fabricated steinmann pins. The enhancement in double shear strength may be due to the polymer chain enwrap and connect nHAp particles to form an elastic viscous structure in the PLA/nHAp mixture. Since the nHAp is hydrophobic, the formed structure would increase the bonding and interlinking forces, and decrease the void ratio of the polymer/nHAp composite. The reason for the reduction in double shear strength may be due to agglomeration of nHAp filler at higher concentration. The agglomeration of nHAp results in the formation of voids over the surface becomes the point of stress concentration which further leads to failure of the composites [245].

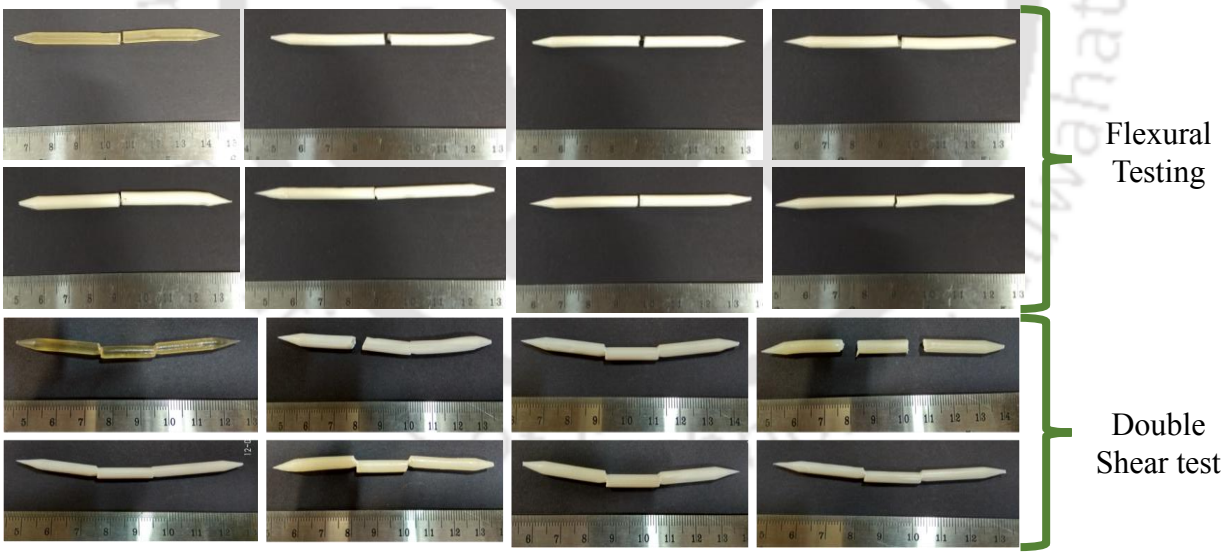

Figure 6.13: Photographic images of the fractured fabricated steinmann pins after flexural test and double shear strength.

Figure 6.13 shows the photographic images of the fractured steinmann pin through a flexural test and double shear test. It was observed that in the case of neat PLA, the fracture was

ductile but in the case of PLA/nHAp, the fracture becomes brittle. Figure 6.13 shows the stereomicroscopic images of the steinmann pins made of neat PLA and PLA/nHAp composite.

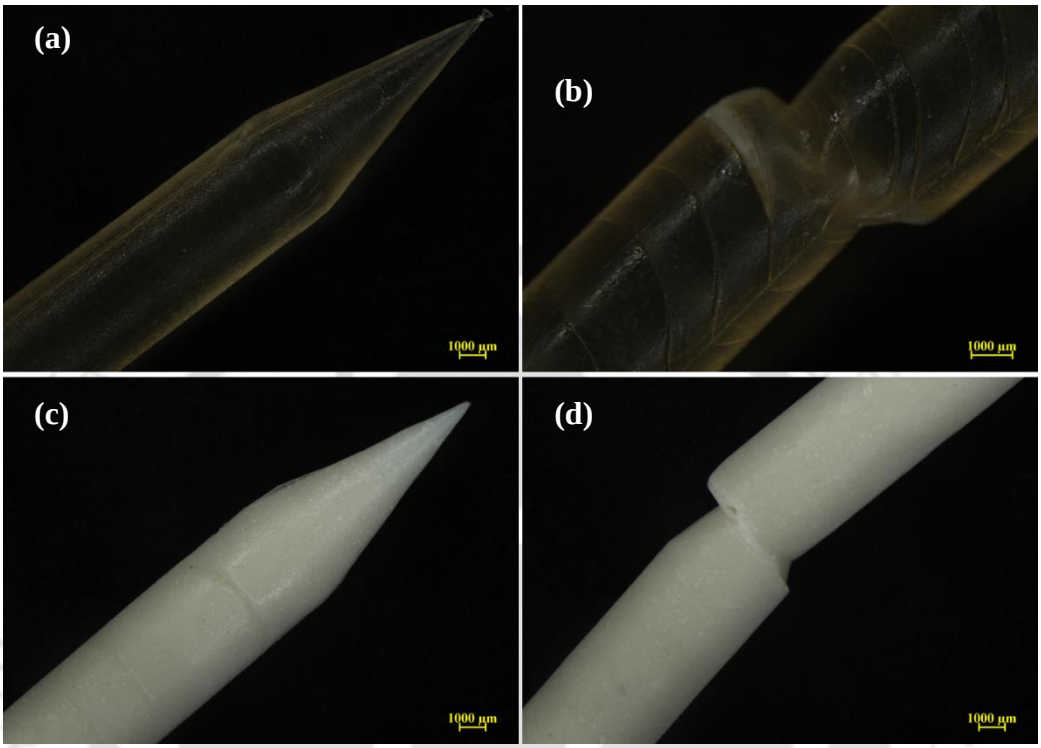

Figure 6.14: Stereomicroscopic surface images of the fabricated steinmann pins (a) neat PLA (b) Magnified view at fracture site of fabricated neat PLA (c) PLA/nHAp steinmann pins (d) magnified images at the fractured site of the PLA/nHAp steinmann pin.

6.6 Mechanical Testing of U-Type bone Staples

The injection molded bone staples were tested as per ASTM F564-10. The bone staples are tested under tension test to know the ultimate tensile strength and peak load. The torsional test corresponding to twisting angles was also conducted.

6.6.1 Ultimate tensile test

Figure 6.15 explains the arrangement done to evaluate the ultimate tensile strength of the bone staples. Figure 6.16 shows the variation of the ultimate tensile strength of the bone

staples concerning varying the concentration of nHAp fillers. The value of tensile strength is reducing towards increment in the loading of filler's concentration.

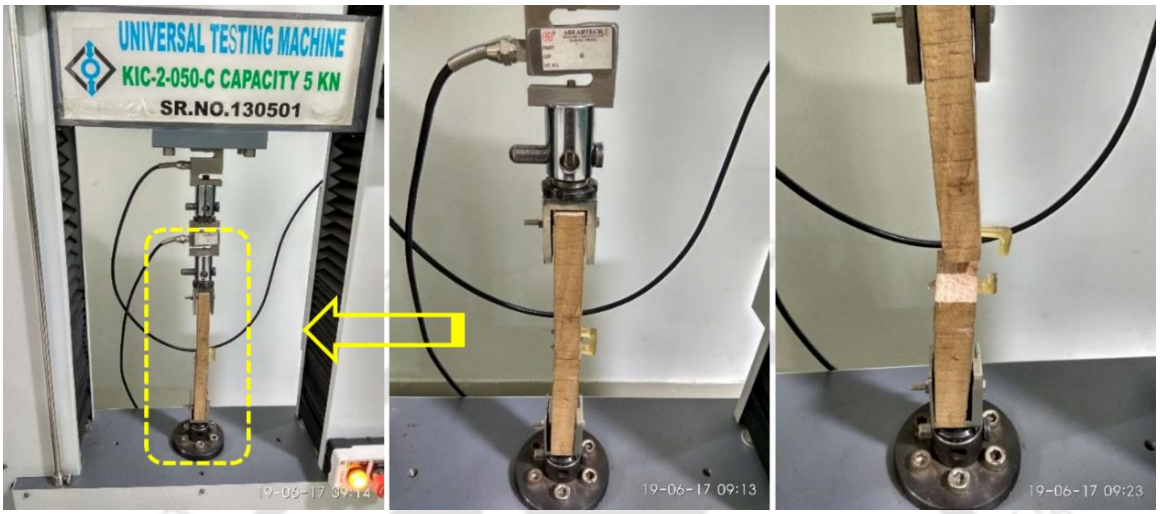

Figure 6.15: Arrangement of testing of bone staples for the tensile test.

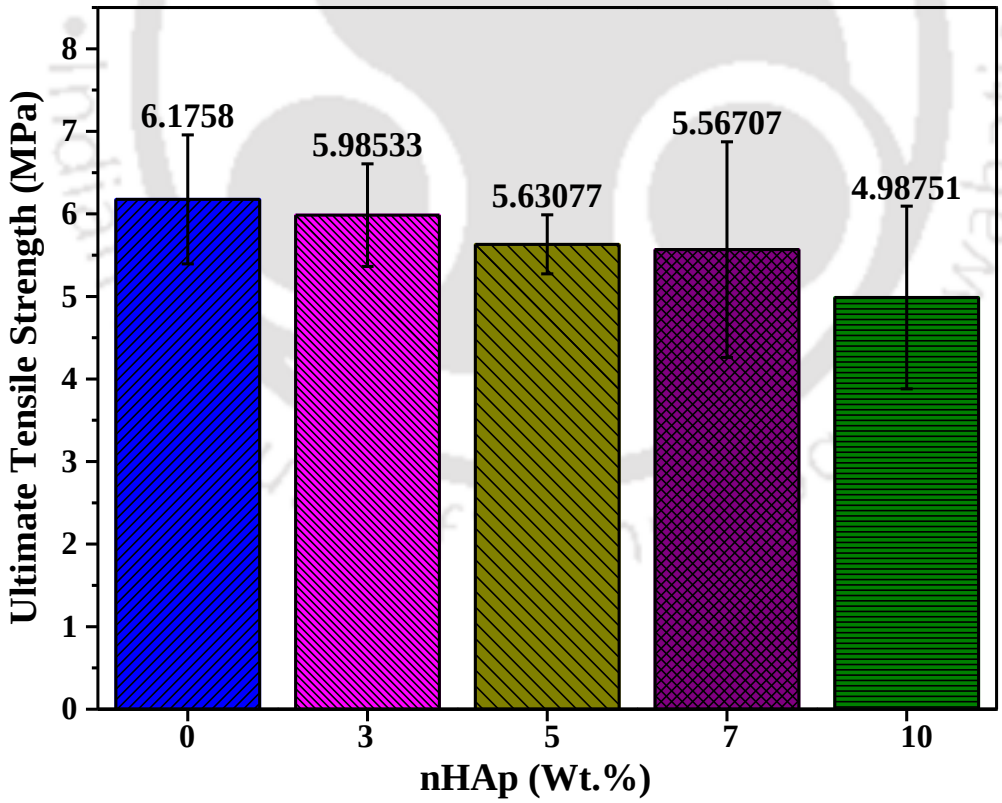

Figure 6.16: Ultimate Tensile Strength value of PLA/nHAp U-type staples concerning nHAp fillers.

The reduction of ultimate tensile strength varies between in the range of 3% to 20% corresponds to 3% nHAp to 10% nHAp. A similar reduction was also seen in the value of peak load as mentioned in Figure 6.17.

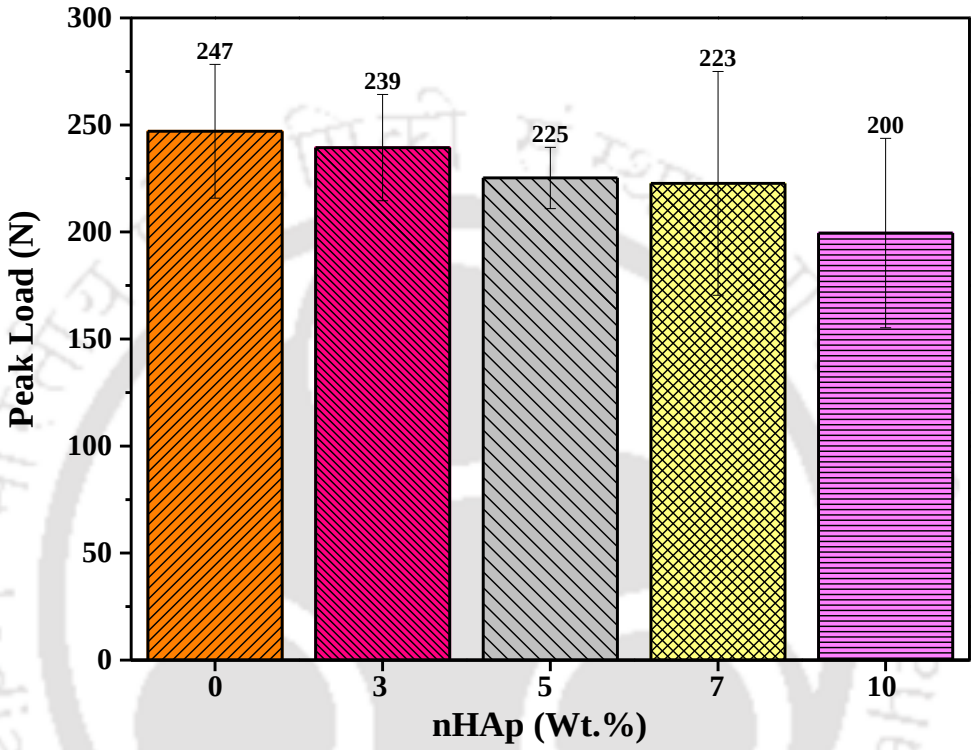

Figure 6.17: Peak load value of PLA/nHAp U-type staples concerning nHAp fillers.

Figure 6.18 and Figure 6.19 shows the value of ultimate tensile strength with corresponding peak value after *In vitro* hydrolytic degradation test of the U- type bone staples. It was observed that the rate of degradation of the neat PLA was faster compared to 3% nHAp. The reduction in tensile strength was observed 18% after 30 days and ~36 % reduction after 90 days in case of neat PLA. While in the case of 3% nHAp, ~21% reduction observed after 30 days and ~34%, after 90 days. The corresponding peak load after Invitro hydrolytic degradation was also observed similar trends.

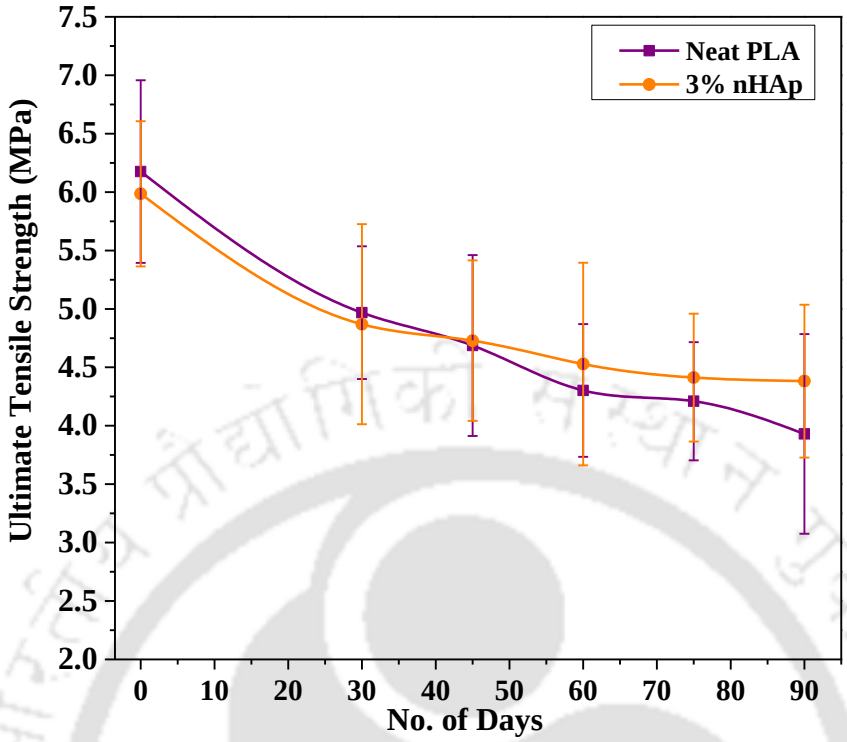

Figure 6.18: Ultimate tensile strength value of PLA/nHAp U-type staples concerning nHAp fillers.

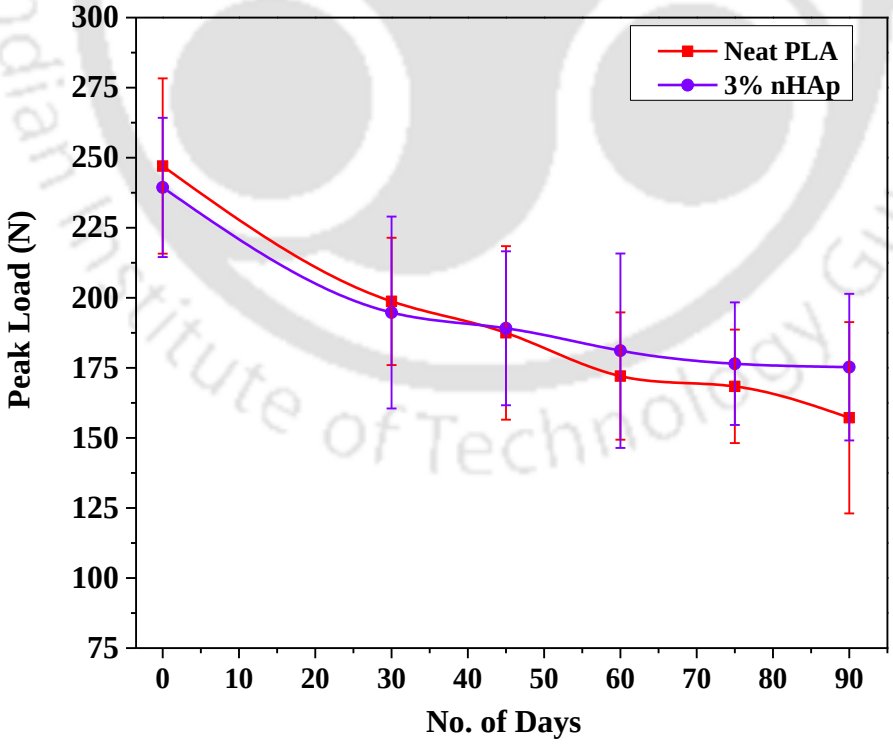

Figure 6.19: Peak load value of PLA/nHAp U-type staples concerning nHAp fillers.

6.6.2 Torsional test

The maximum torque, breaking angle were measured for the bone staples produced using fabricated torsion fixture. The measurement was done in torsion testing machine (make: Fuel instruments and equipment, India). The crosshead speed of the machine was one revolution per minute. The load cell capacity of the machine was 10kgf.m (9806.6599 mili Newton meter). The maximum torque was represented by the highest recorded value of the torque during the test, and the breaking angle was the rotation angle at the maximum torque. The measurement was carried out in triplicate.

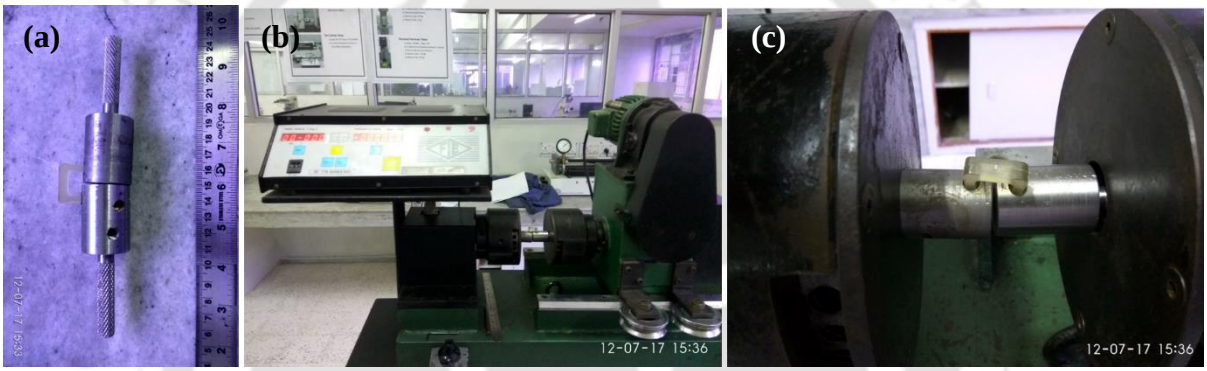

Figure 6.20: (a) Torsional test fixture for bone staples. (b) Torsion testing machine (c) Magnified photographic images of attached bone staples in the fabricated fixtures for torsion testing.

The fixture was made from mild steel metal. The room temperature was maintained at 24°C. Figure 6.21 shows the values of ultimate torque with varying filler concentration. The increment observed as 5% in the case of 3% nHAp concerning neat PLA. The breaking angle is also mentioned in Figure 6.22 corresponding to their ultimate torque value. The Figure 6.23 and Figure 6.24 shows the ultimate torque value and corresponding twisting value after hydrolytic degradation studies. It was observed that the torsional strength was reduced by ~19% after 30 days and ~37% reduction after 90 days in case of neat PLA. In the case of 3%

nHAp, ~21% reduction observed after 30 days and ~33%, after 90 days. The corresponding twisting angle also observed reducing.

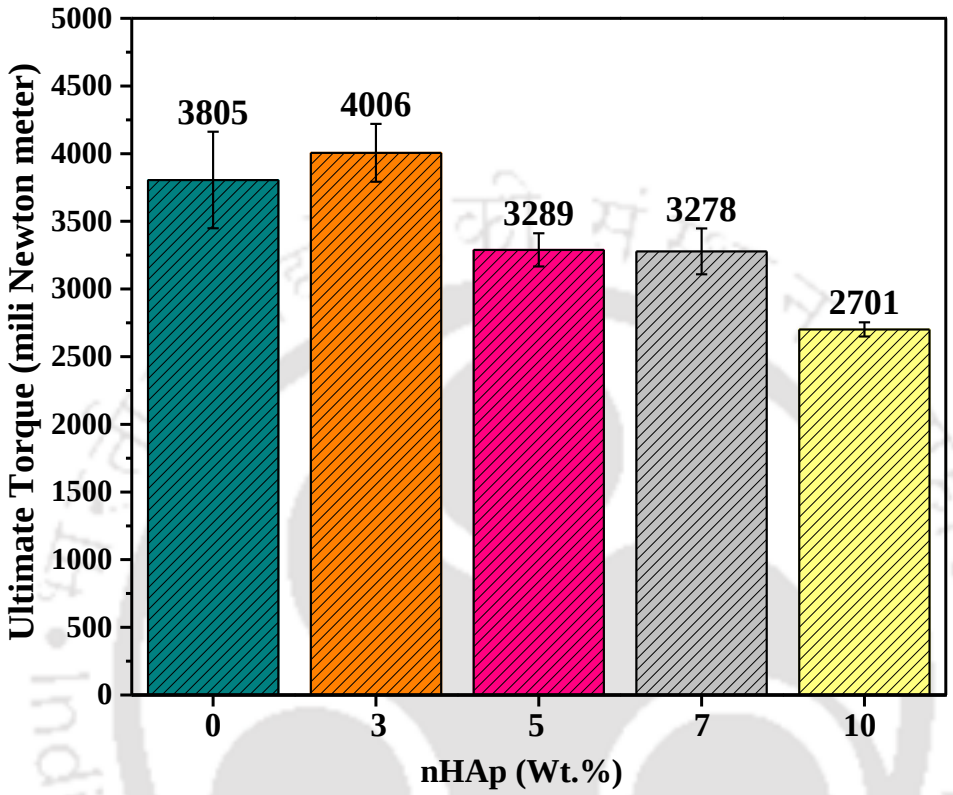

Figure 6.21: Value of ultimate torque concerning nHAp filler concentration.

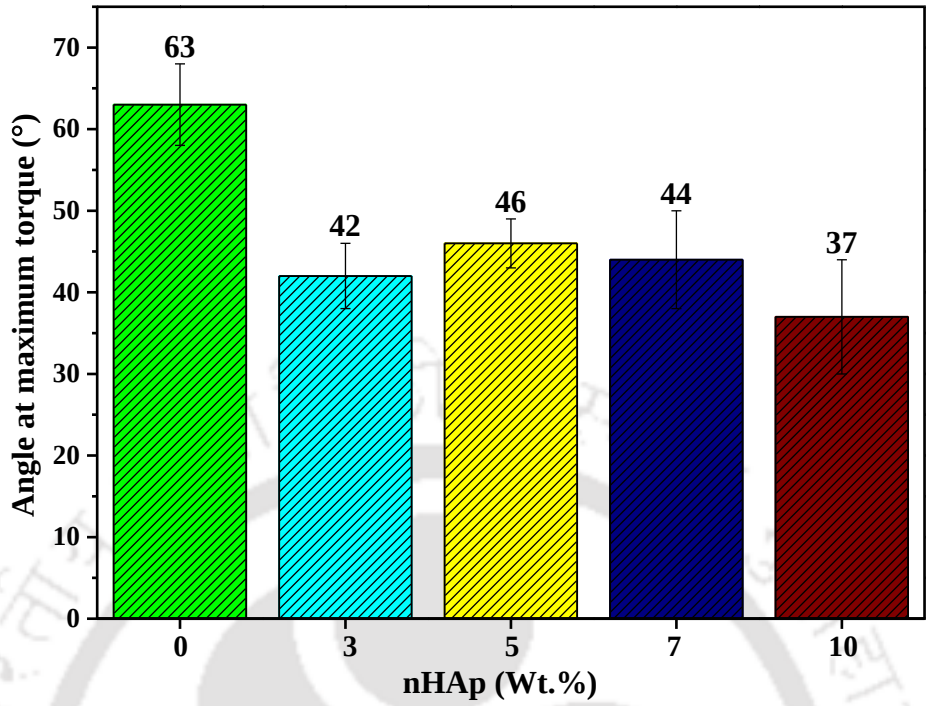

Figure 6.22: Value of breaking angle at which the maximum torque was observed concerning varying filler concentration.

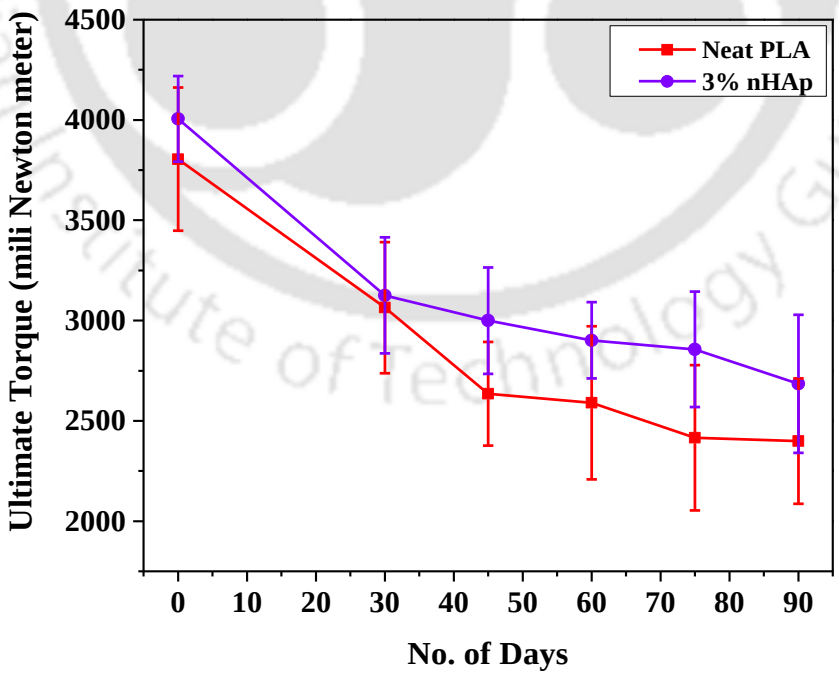

Figure 6.23: Torque value of neat PLA and 3 % nHAp after hydrolytic degradation studies.

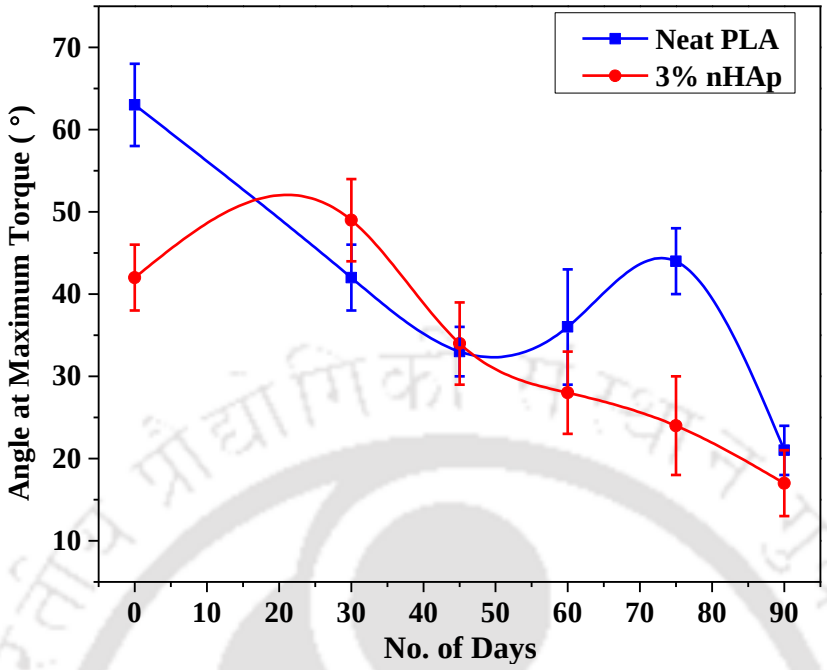

Figure 6.24: Angle at maximum torque of neat PLA and 3 % nHAp after degradation studies.

Figure 6.25: Photographic images of Fractured bone staples after torsion and ultimate tensile strength test.

Figure 6.25 shows the photographic images of a surface fracture of U-type bone staples conducted through torsion test and ultimate tensile strength.

6.7 Degradation studies

Figure *6.26* shows the mass loss profile of the steinmann pins (neat PLA) and optimized steinmann pins (7% nHAp) exposed in PBS solution for 90 days. It was observed that ~3%

reduction in mass loss after 30 days, ~11% reduction after 60 days and ~18% were a reduction in mass loss after 90 days in case of neat PLA. However, in the case of 7% nHAp, reduction of ~3% after 30days, ~7% after 60 days and ~12% after 90days mass loss observed. It was also observed that for the same duration of exposure towards PBS solution the rate of degradation of neat PLA was faster as compared with 7% nHAp. This studies also reveal that 100% degradation in a mass loss would be between 9 to 12 months and healing of fracture bone also takes 8-12 months. Hence for various age group peoples, steinmann pins can be tuned. Figure 6.27 shows the mass loss profile of the fabricated U-type bone staple (neat PLA) and optimized fabricated U-type bone staple (3% nHAp) exposed in PBS solution for 90 days.

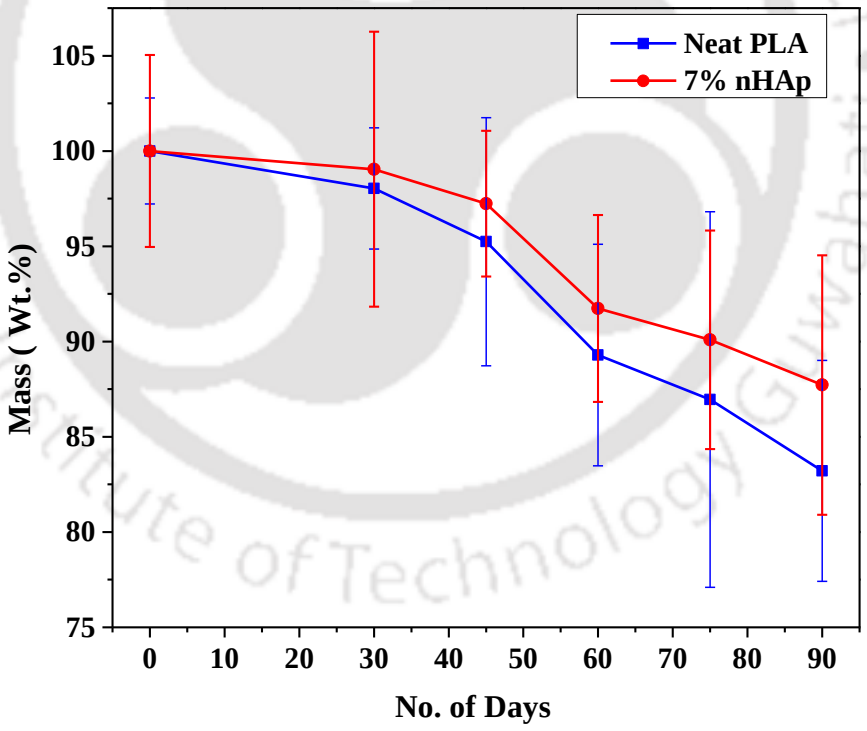

Figure 6.26: Loss of mass profile after In vitro hydrolytic degradation studies in case of neat PLA and 7 % nHAp in case of steinmann pins.

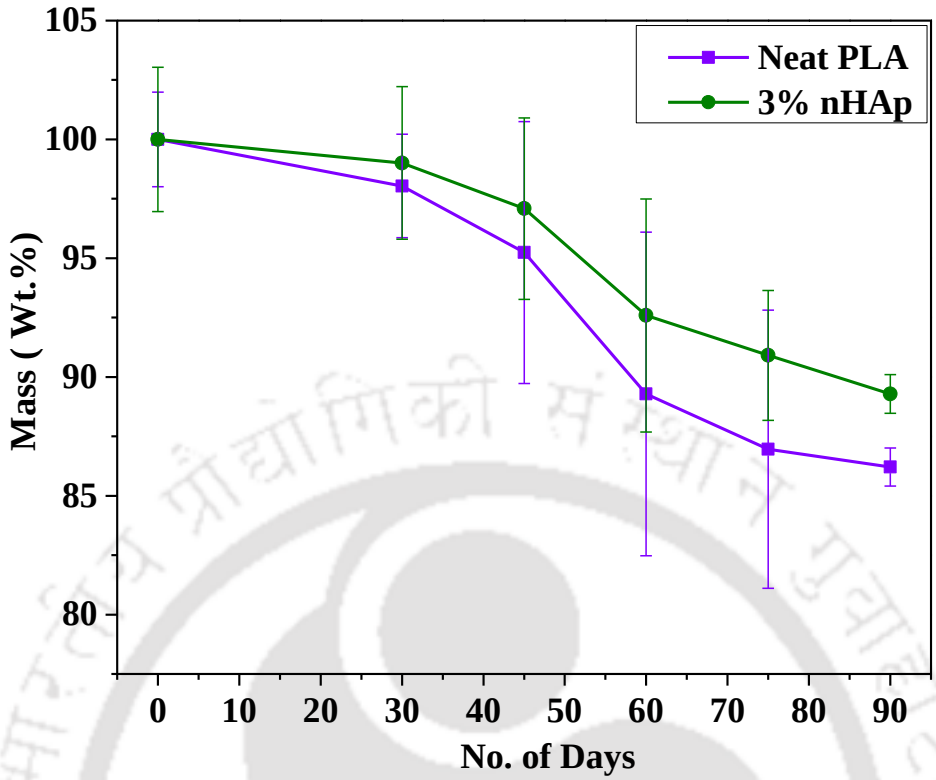

Figure 6.27: Loss of mass profile after In vitro hydrolytic degradation studies in case of neat PLA and 3% nHAp for U-type bone staples.

6.8 Dimensional deviation studies

In order to know the geometrical deviation from the standard geometry, fabricated steinmann pins and U-type bone staples were analyzed through optical surface profilometer (Optomech, vertical) at 10x (Figure 6.28 and Figure 6.29). It was observed that deviation of the fabricated steinmann pins and U-type bone staples was very less as compared with the standard dimension and later the deviated dimensions were neglected. Figure 6.30 shows the stereomicroscopic images of the surface of the U-type bone staple of neat PLA and PLA/nHAp composites. It was observed that the deviation in the teeth of the staples was in the range 1285µm-1361µm.

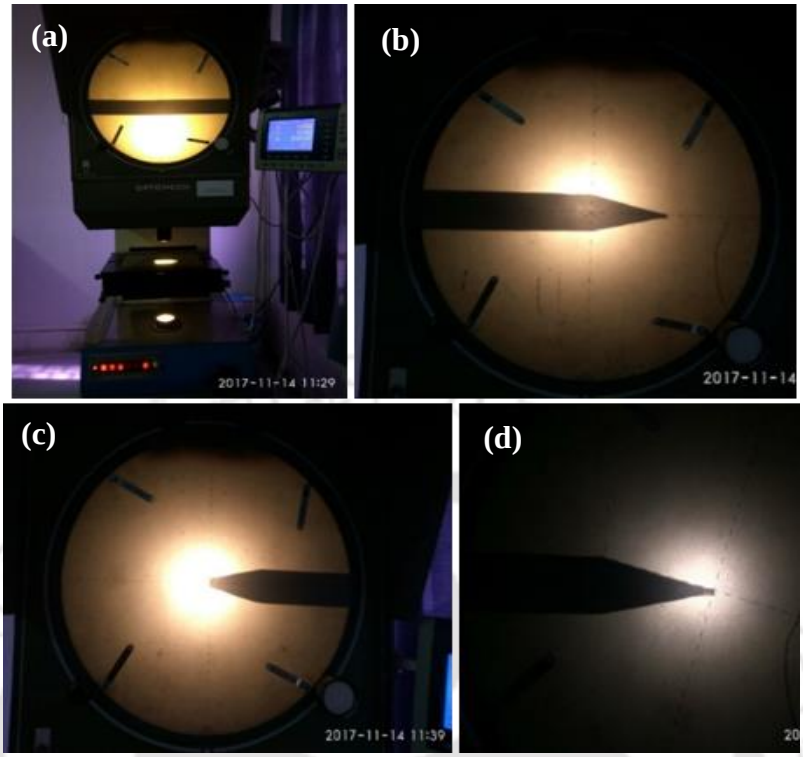

Figure 6.28: Optical profilometer of steinmann pins (a) steinmann pin on the bed (b) Magnified view of one of the ends (c) Enlarged view of one of the ends of steinmann pins (d) end view of the steinmann pins

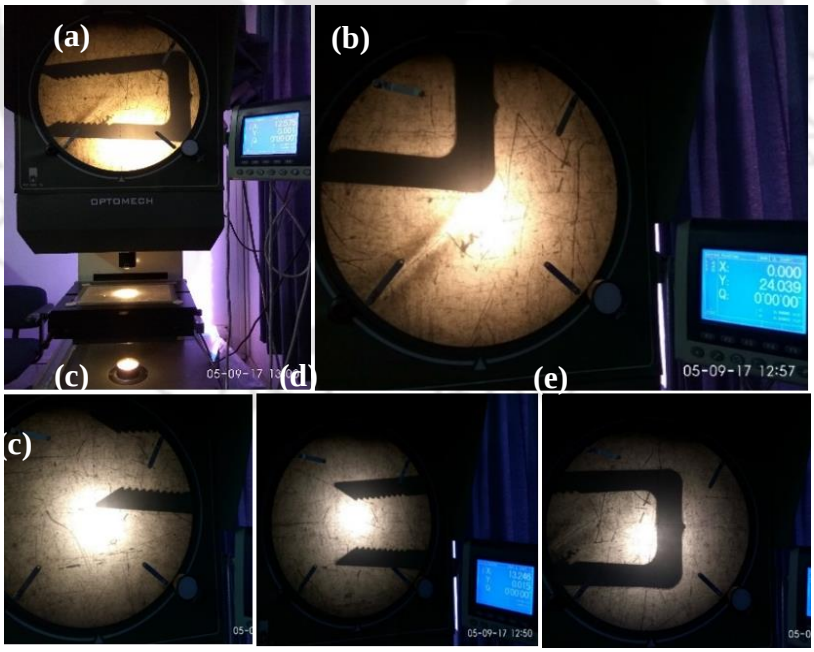

Figure 6.29: Optical surface profile of fabricated bone staples.(a) Staples kept on the profilometer base (b) Magnified view of the bridge length of the staples (c)leg of the staples (d) both leg of the staples(e) Bridge length of the staples.

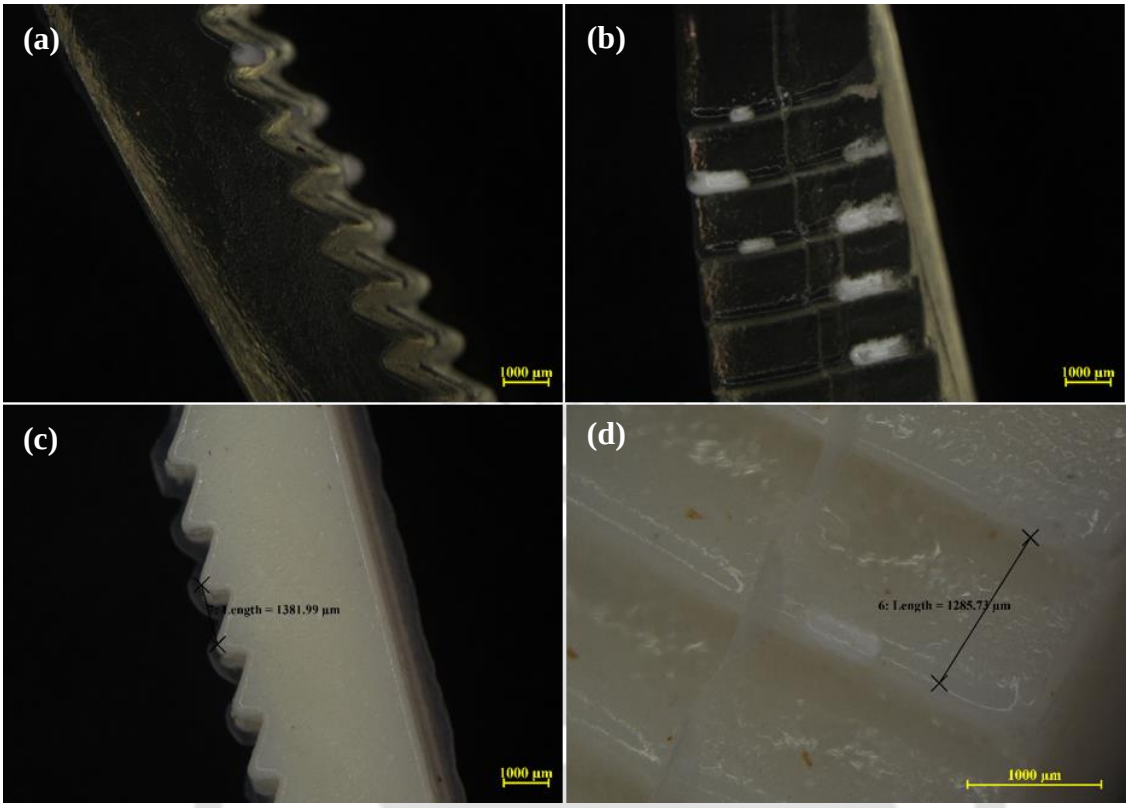

Figure 6.30: The stereomicroscopic images of U-type bone staples (a) neat PLA (b) Magnified view of neat PLA fabricated U-type bone staple (c) PLA/nHAp based U-type bone staples (d) Distance between two teeth of the fabricated U-type bone staple.

6.9 Summary

In this chapter, the following major points are summarized

1. The Steinmann pins and U-type bone staples based on purified PLA and PLA/nHAp has been successfully manufactured
2. The process parameters have been optimized in both product.
3. The development of the mold and related fixtures for performing mechanical testing of both steinmann pins and U-type bone staples has been discussed.
4. The mechanical test as per ASTM standards related to Steinmann pins and U-type bone staples has been performed.

5. The flexural strength of the Steinmann pins was also observed increment of 9% to 11% compared to neat PLA.
6. The double shear strength was also performed in the fabricated fixtures and as per ASTM standard. The maximum increase of 11% of 10 % nHAp was observed within the combinations.
7. The ultimate tensile strength of the bone staples was performed in a tension test as per ASTM standard. The reduction of 3% (3% nHAp) to 30 % (10% nHAp) was observed compared to neat PLA. Similar trends were also observed in peak load values also.
8. The torsional strength of 3% nHAp gives 5% increment concerning neat PLA.
9. The mechanical test was also conducted during the *In vitro* hydrolytic degradation test, and results were displayed.
10. The mass loss profiles show the reduction in mass as the time passes away in both the implants.

Chapter 7

Conclusion and Future Scope

7.1. Conclusion

This chapter discusses the major interferences drawn from the doctoral work and outlook for future studies. The major conclusions drawn by overall observation and major findings of the research work are as follows:

- Synthesis of nHAp from the fish scale biowaste and efficient application as bioactive biomaterials
- Purification of PLA in order to use as the base material to fabricate majorly used internal fixation devices
- Optimization of twin screw extruder cum injection molding parameter for successful fabrication of PLA/nHAp bioabsorbable composites
- Comprehensive characterization of neat PLA and PLA/nHAp composite
- Development and manufacturing of cortical screw mold to make "ready to fit" cortical screws as per dimension with commercial available metallic cortical screws.
- Development and manufacturing of cancellous screw mold to make "ready to fit" screw as per dimension with a commercial available metallic cancellous screw.
- Development and manufacturing of four combination hole bone plate mold to make a standard bone plate in which existing or fabricated bioabsorbable cortical or cancellous screw gets easily fitted.
- Development and manufacturing of steinmann pin and U-type bone staples molds to make bioabsorbable steinmann pin and U-type bone staples for specific orthopedic fracture fixations

- Fabrication of various fixtures related to respective mechanical test as per ASTM standard for the internal fixation devices and effectively conduction of mechanical test accordingly.
- Mechanical test of the fabricated internal fixation devices (cortical screw, cancellous screw. Bone plate, steinmann pin and bone staples) as per available ASTM standard.
- *In vitro* hydrolytic degradation, studies have been performed as per standard protocols.
- Mechanical studies of all the fabricated internal fixation devices during in vitro hydrolytic degradation studies were also conducted in order to tune with the varying concentration of the filler materials to target the product for the various age group of peoples.
- *In vitro* bioactivity studies in simulated body fluid and cytotoxicity studies of the same (cell viability, proliferation and differentiation) on the fabricated PLA/nHAp composite and internal fixation devices
- Identification of the optimum concentration of the nHAp filler for specific types of fabricated internal fixation devices. The dimensional deviation in their geometries and failure profile through photographic images has been discussed.
- Each internal fixation devices (cortical screws, cancellous screws, bone plate, steinmann pins and bone staples) has been summarized in their corresponding chapters for the optimum value of their properties in regards with their combinations.

7.2. Implication of the findings

This section discusses upon the key outcomes of the PhD research work

- Utilization of bioactive inorganic filler in forms of nano size hydroxyapatite powder fabricated through heat treatment of fish scales processed through mechanical ball milling process provides a cost effective production.
- Cost effective fabrication of majorly used bioabsorbable IFDs (cortical screws, cancellous screws, bone plates, U type staples and steinmann pins) for orthopedic fracture fixations so that needy person get it used economically.
- In India, all bioabsorbable orthopedic fracture fixations are imported from other country and very expensive, thus this research open the door to further investigate and establish the production of bioabsorbable internal fixation devices in India.
- Patients need not to visit the orthopedic doctor to surgery again for removal of IFDs as it is bioabsorbable.
- By tuning the concentration of nHAp in to PLA matrix, we can design the specific IFDs for various age group peoples, since the bone healing capacity differs upon various age group persons.

7.3. Future Scope

The following studies can be carried out to further explore this area of research:

- ❖ Detailed study of *In vitro* bioactivity studies of the fabricated internal fixation devices can be performed.
- ❖ In vivo studies of the developed internal fixation devices and their behavioral changes during real exposure toward living beings.
- ❖ The inclusion of computational validation along with experimental methods of fabrication.
- ❖ Development of other bioabsorbable internal fixation devices for craniofacial and maxillofacial surgeries applications.
- ❖ The inclusion of functional nanofillers with the existing matrix and reinforcement in order to fabricate functional internal fixation devices.

References

1. Orthopedic Devices Market-Global Industry Analysis, Size, Share, Growth, Trends and Forecast, Transparency market research, 2013-19.
2. White paper 2016, Indian Orthopedic Device Market a $2.4 Bn Opportunity by Sathguru management consultant report.
3. Medtech Report India: A hand book of Swiss start-ups published by Swissnex India, May, 2016.
4. Medical device manufacturing facility, government of Gujarat in the 8th Global Summit, 10-13, Jan 2017.
5. Report on "The fast progressing medical product market in India-Market overview and category insights", Redseer consulting, Delhi, 2015.
6. SKP report on the medical device industry in India: Therapeutic Areas, New Delhi, 2016.
7. Sathguru report on "Indian Orthopedic Device Market and forecast", October, 2016.
8. http://www.transparencymarketresearch.com/trauma-fixation-devices-market.html.,Date of access:27/06/2017.
9. India Medical Devices Report, Q1 2016, BMI Research
10. Indian Society of Hip and Knee Surgeons Joint Registry: A Preliminary Report, September, 2013.
11. Subbiah, T., Bhat, G. S., Tock, R. W., Parameswaran, S., and Ramkumar, S. S. (2005). Electrospinning of nanofibers. Journal of applied polymer science, 96(2), 557-569.
12. Strycker, M. L. (1995). Biodegradable internal fixation. The Journal of foot and ankle surgery, 34(1), 82-88.
13. Gut, G., and Śladowski, D. (2007). Mechanical properties of bone fixation devices prepared from a human allogenic bone. In Transplantation proceedings. 39 (9),2920-2922.

14. Felfel, R. M., Ahmed, I., Parsons, A. J., and Rudd, C. D. (2013). Bioresorbable screws reinforced with phosphate glass fibre: manufacturing and mechanical property characterisation. Journal of the mechanical behavior of biomedical materials, 17, 76-88.
15. Ricci, W. M., Tornetta III, P., Petteys, T., Gerlach, D., Cartner, J., Walker, Z., and Russell, T. A. (2010). A comparison of screw insertion torque and pullout strength. Journal of orthopaedic trauma, 24(6), 374-378.
16. Ratner, B. D., Hoffman, A. S., Schoen, F. J., and Lemons, J. E. (2004). Biomaterials science: an introduction to materials in medicine. Elsevier.
17. Pietrzak, W. S., Caminear, D. S., and Perns, S. V. (2002). Mechanical characteristics of an absorbable copolymer internal fixation pin. The Journal of foot and ankle surgery, 41(6), 379-388.
18. https://disposableinstrument.com/medical-components/fixation-pins-steinman-pins-k-wires/ (Date of website visit: 21/03/2019)
19. Knutsen, A. R., Sangiorgio, S. N., Liu, C., Zhou, S., Warganich, T., Fleming, J. and Ebramzadeh, E. (2016). Distal fibula fracture fixation: Biomechanical evaluation of three different fixation implants. Foot and Ankle Surgery, 22(4), 278-285.
20. Thomas F Smith,DPM, www.podiatryinstitute.com/pdfs/Update_2010/2010_41.pdf (Date of website visit: 21/03/2019)
21. Onche, I.I., Osagie, O.E., and Inuhu, S. (2011) Removal of orthopaedic implants: indications, outcome and economic implications. J. West African Coll. Surg., 1 (1), 101–112.
22. Son, S. H., Kang, Y. N., and Ryu, M. R. (2012). The effect of metallic implants on radiation therapy in spinal tumor patients with metallic spinal implants. Medical Dosimetry, 37(1), 98-107.
23. Yetkin, H., Senköylü, A., Cila, E., et al. (2000) Biodegradable Implants in Orthopaedics and Traumatology. Turk J Med Sci, 30 (1), 5.
24. Kim, S. S., Ahn, K. M., Park, M. S., Lee, J. H., Choi, C. Y., and Kim, B. S. (2007). A poly (lactide-co-glycolide)/hydroxyapatite composite scaffold with enhanced osteoconductivity. Journal of Biomedical Materials Research Part A: An Official Journal of The Society for Biomaterials, The Japanese Society for Biomaterials, and

The Australian Society for Biomaterials and the Korean Society for Biomaterials, 80(1), 206-215.

25. Spitalny, A. D. (2006). Bioabsorbable implants. Clinics in podiatric medicine and surgery, 23(4), 673-694.
26. Kontakis, G. M., Pagkalos, J. E., Tosounidis, T. I., Melissas, J., and Katonis, P. (2007). Bioabsorbable materials in orthopaedics. Acta orthopaedica belgica, 73(2), 159-169.
27. Klee, D., and Höcker, H. (2000). Polymers for biomedical applications: improvement of the interface compatibility. In Biomedical Applications Polymer Blends (pp. 1-57). Springer, Berlin, Heidelberg.
28. Choy, M. T., Tang, C. Y., Chen, L., Wong, C. T., and Tsui, C. P. (2014). In vitro and in vivo performance of bioactive Ti6Al4V/TiC/HA implants fabricated by a rapid microwave sintering technique. Materials Science and Engineering: C, 42, 746-756.
29. Ambrose, C. G., and Clanton, T. O. (2004). Bioabsorbable implants: review of clinical experience in orthopedic surgery. Annals of biomedical engineering, 32(1), 171-177.
30. Tielinen, L. (2002) Bioabsorbable Polymer and Bone Growth Factor Composites. Chondral Osseous Tissue Eng., 7, 2–12.
31. Gross, K. a., Komarovska, L., and Viksna, a. (2013).Efficient zinc incorporation in hydroxyapatite through crystallization of an amorphous phase could extend the properties of zinc apatites. J. Aust. Ceram. Soc., 49 (2), 129–135.
32. Unnithan, A. R., Arathyram, R. S., and Kim, C. S. (2015). Scaffolds with Antibacterial Properties. In Nanotechnology Applications for Tissue Engineering (pp. 103-123). William Andrew Publishing.
33. Pietrzak, W. S. (2000). Principles of development and use of absorbable internal fixation. Tissue engineering, 6(4), 425-433.
34. Rezwan, K., Chen, Q. Z., Blaker, J. J., and Boccaccini, A. R. (2006). Biodegradable and bioactive porous polymer/inorganic composite scaffolds for bone tissue engineering. Biomaterials, 27(18), 3413-3431.

35. Durucan, C., and Brown, P. W. (2001). Biodegradable hydroxyapatite–polymer composites. Advanced Engineering Materials, 3(4), 227-231.
36. Daniels, A. U., Chang, M. K., Andriano, K. P., and Heller, J. (1990). Mechanical properties of biodegradable polymers and composites proposed for internal fixation of bone. Journal of applied biomaterials, 1(1), 57-78.
37. Wendel, M., Sommarin, Y., and Heinegård, D. (1998). Bone matrix proteins: isolation and characterization of a novel cell-binding keratan sulfate proteoglycan (osteoadherin) from bovine bone. The Journal of cell biology, 141(3), 839-47.
38. Sheikh, Z., Najeeb, S., Khurshid, Z., Verma, V., Rashid, H., and Glogauer, M. (2015). Biodegradable materials for bone repair and tissue engineering applications. Materials, 8(9), 5744-5794.
39. Santos, D. V., Casadei, A. P. M., Pereira, R. V., Aragones, A., Salmoria, G. V., and Fredel, M. F. (2012). Development of polymer/nanoceramic composite material with potential application in biomedical engineering. In Materials Science Forum, 727, 1142–1146.
40. Shepherd, J. H., Shepherd, D. V., and Best, S. M. (2012). Substituted hydroxyapatites for bone repair. Journal of Materials Science: Materials in Medicine, 23(10), 2335-2347.
41. Describe the differences between primary and secondary bone healing. OrthopaedicsOne Clerkship. In: OrthopaedicsOne - The Orthopaedic Knowledge Network. Created Oct 30, 2011 05:49. Last modified Nov 28, 2011 11:04 ver.241. Retrieved 2019-03-22, from https://www.orthopaedicsone.com/x/bAJCB.
42. Perren, S.M. (2002) Evolution of the internal fixation of long bone fractures: The scientific basis of biological internal fixation: choosing a new balance between stability and biology. J. Bone Jt. Surg., 84 (8), 1093–1110.
43. Henderson, H. B., Ramaswamy, V., Wilson-Heid, A. E., Kesler, M. S., Allen, J. B., and Manuel, M. V. (2018). Mechanical and degradation property improvement in a biocompatible Mg-Ca-Sr alloy by thermomechanical processing. Journal of the mechanical behavior of biomedical materials, 80, 285-292.
44. Grandfield, K., Palmquist, A., Gonçalves, S., Taylor, A., Taylor, M., Emanuelsson, L., and Engqvist, H. (2011). Free form fabricated features on CoCr implants with

and without hydroxyapatite coating in vivo: a comparative study of bone contact and bone growth induction. Journal of Materials Science: Materials in Medicine, 22(4), 899-906.

45. Ratner, B. D., Hoffman, A. S., Schoen, F. J., and Lemons, J. E. (2006). Biomaterials science: an introduction to materials in medicine. MRS Bull, 31, 59.
46. Saini, M., Singh, Y., Arora, P., Arora, V., and Jain, K. (2015). Implant biomaterials: A comprehensive review. World journal of clinical cases, 3(1), 52-7.
47. Sykaras, N., Iacopino, A. M., Marker, V. A., Triplett, R. G., and Woody, R. D. (2000). Implant materials, designs, and surface topographies: their effect on osseointegration. A literature review. International Journal of Oral and Maxillofacial Implants, 15(5).
48. Törmälä, P., Pohjonen, T., and Rokkanen, P. (1998). Bioabsorbable polymers: materials technology and surgical applications. Proceedings of the Institution of Mechanical Engineers, Part H: Journal of Engineering in Medicine, 212(2), 101-111.
49. Gullberg, B., Johnell, O., and Kanis, J. A. (1997). World-wide projections for hip fracture. Osteoporosis international, 7(5), 407-413.
50. https://www.bones.nih.gov/health-info/bone/osteoporosis/overview___(Date of website visit: 21/03/2019)
51. Salgado, A. J., Coutinho, O. P., and Reis, R. L. (2004). Bone tissue engineering: state of the art and future trends. Macromolecular bioscience, 4(8), 743-765.
52. Morshed, S. (2014). Current options for determining fracture union. Advances in medicine, 2014.
53. https://boneandspine.com/bone-fracture-healing-occur/ (Date of website visit: 21/03/2019)
54. Salgado, A. J., Coutinho, O. P., and Reis, R. L. (2004). Bone tissue engineering: state of the art and future trends. Macromolecular bioscience, 4(8), 743-765.
55. Mondal, S., Mahata, S., Kundu, S., and Mondal, B. (2010). Processing of natural resourced hydroxyapatite ceramics from fish scale. Advances in Applied Ceramics, 109(4), 234-239.
56. Mondal, S., Mondal, B., Dey, A., and Mukhopadhyay, S. S. (2012). Studies on processing and characterization of hydroxyapatite biomaterials from different bio

wastes. Journal of Minerals and Materials Characterization and Engineering, 11(01), 55.

57. Prasad, A., Devendar, B., Sankar, M. R., and Robi, P. S. (2015). Micro-Scratch Based Tribological Characterization of Hydroxyapatite (HAp) Fabricated through Fish Scales. Materials Today: Proceedings, 2(4-5), 1216-1224.
58. Veljović, D., Jančić-Hajneman, R., Balać, I., Jokić, B., Putić, S., Petrović, R., and Janaćković, D. (2011). The effect of the shape and size of the pores on the mechanical properties of porous HAP-based bioceramics. Ceramics International, 37(2), 471-479.
59. Langer, R., Vacanti, J. P. (2003). Tissue Engineerng Science, 260, 920-926.
60. Suzuki, S., and Ikada, Y. (2012). Bioabsorbable Polymers. In Biomaterials for Surgical Operation (pp. 19-38). Humana Press.
61. Hutmacher, D. W., Schantz, T., Zein, I., Ng, K. W., Teoh, S. H., and Tan, K. C. (2001). Mechanical properties and cell cultural response of polycaprolactone scaffolds designed and fabricated via fused deposition modeling. Journal of Biomedical Materials Research: An Official Journal of The Society for Biomaterials, The Japanese Society for Biomaterials, and The Australian Society for Biomaterials and the Korean Society for Biomaterials, 55(2), 203-216.
62. Bhasney, S.M., Patwa, R., Kumar, A., and Katiyar, V. (2017) Plasticizing effect of coconut oil on morphological, mechanical, thermal, rheological, barrier, and optical properties of poly(lactic acid): A promising candidate for food packaging. Journal of Applied Polymer Science, 134(41), 1–12.
63. Reed, A. M., and Gilding, D. K. (1981). Biodegradable polymers for use in surgery—poly (glycolic)/poly (Iactic acid) homo and copolymers: 2. In vitro degradation. Polymer, 22(4), 494-498.
64. Dhillon, M. S., and Lokesh, A. V. (2006). Bioabsorbable implants in orthopaedics. Indian Journal of Orthopaedics, 40(4), 205.
65. Henkel, J., Woodruff, M. A., Epari, D. R., Steck, R., Glatt, V., Dickinson, I. C.,and Hutmacher, D. W. (2013). Bone regeneration based on tissue engineering conceptions—a 21st century perspective. Bone research, 1, 216.

66. Russias, J., Saiz, E., Nalla, R. K., Gryn, K., Ritchie, R. O., and Tomsia, A. P. (2006). Fabrication and mechanical properties of PLA/HA composites: a study of in vitro degradation. Materials Science and Engineering: C, 26(8), 1289-1295.
67. Kim, T. G., Shin, H., and Lim, D. W. (2012). Biomimetic scaffolds for tissue engineering. Advanced Functional Materials, 22(12), 2446-2468.
68. Daniels, A. U., Chang, M. K., Andriano, K. P., and Heller, J. (1990). Mechanical properties of biodegradable polymers and composites proposed for internal fixation of bone. Journal of applied biomaterials, 1(1), 57-78.
69. Durucan, C., and Brown, P. W. (2001). Biodegradable hydroxyapatite–polymer composites. Advanced Engineering Materials, 3(4), 227-231.
70. Rezwan, K., Chen, Q. Z., Blaker, J. J., and Boccaccini, A. R. (2006). Biodegradable and bioactive porous polymer/inorganic composite scaffolds for bone tissue engineering. Biomaterials, 27(18), 3413-3431.
71. Tripathi, N., and Katiyar, V. (2016) PLA/functionalized-gum arabic based bionanocomposite films for high gas barrier applications. Journal of Applied Polymer Science, 133(21), 1–8.
72. Saini, P., Arora, M., and Kumar, M. R. (2016). Poly (lactic acid) blends in biomedical applications. Advanced Drug Delivery Reviews, 107, 47-59.
73. Pietrzak, W. S. (2000). Principles of development and use of absorbable internal fixation. Tissue engineering, 6(4), 425-433.
74. Moser, R. C., McManus, A. J., Riley, S. L., and Thomas, K. A. (2005). Strength retention of 70: 30 poly (L-lactide-co-D, L-lactide) following real-time aging. Journal of Biomedical Materials Research Part B: Applied Biomaterials: An Official Journal of The Society for Biomaterials, The Japanese Society for Biomaterials, and The Australian Society for Biomaterials and the Korean Society for Biomaterials, 75(1), 56-63.
75. Wen, C. E., Mabuchi, M., Yamada, Y., Shimojima, K., Chino, Y., and Asahina, T. (2001). Processing of biocompatible porous Ti and Mg. Scripta Materialia, 45(10), 1147-1153.
76. Huang, G., Du, Z., Yuan, Z., Gu, L., Cai, Q., and Yang, X. (2018). Poly (L-lactide) nanocomposites containing poly (D-lactide) grafted nanohydroxyapatite with

improved interfacial adhesion via stereocomplexation. Journal of the mechanical behavior of biomedical materials, 78, 10-19.

77. Macha, I. J., Ben-Nissan, B., Santos, J., Cazalbou, S., Stamboulis, A., Grossin, D., and Giordano, G. (2017). Biocompatibility of a new biodegradable polymer-hydroxyapatite composite for biomedical applications. Journal of Drug Delivery Science and Technology, 38, 72–77.
78. Prati, J. L., Kim, D. H., and Matthewson, M. J. (2017). Application of static fatigue testing to the behavior of absorbable sutures. Journal of the Mechanical Behavior of Biomedical Materials, 74, 232–235.
79. Ozan, S., Lin, J., Li, Y., and Wen, C. (2017). New Ti-Ta-Zr-Nb alloys with ultrahigh strength for potential orthopedic implant applications. Journal of the mechanical behavior of biomedical materials, 75, 119-127.
80. Jaiswal, S., Kumar, R. M., Gupta, P., Kumaraswamy, M., Roy, P., and Lahiri, D. (2018). Mechanical, corrosion and biocompatibility behaviour of Mg-3Zn-HA biodegradable composites for orthopaedic fixture accessories. Journal of the mechanical behavior of biomedical materials, 78, 442-454.
81. Chen, Y., Frith, J. E., Dehghan-Manshadi, A., Attar, H., Kent, D., Soro, N. D. M.,and Dargusch, M. S. (2017). Mechanical properties and biocompatibility of porous titanium scaffolds for bone tissue engineering. Journal of the mechanical behavior of biomedical materials, 75, 169-174.
82. Kulkova, J., Moritz, N., Huhtinen, H., Mattila, R., Donati, I., Marsich, E.,and Vallittu, P. K. (2017). Hydroxyapatite and bioactive glass surfaces for fiber reinforced composite implants via surface ablation by Excimer laser. Journal of the mechanical behavior of biomedical materials, 75, 89-96.
83. Islam, M. T., Felfel, R. M., Abou Neel, E. A., Grant, D. M., Ahmed, I., and Hossain, K. M. Z. (2017). Bioactive calcium phosphate–based glasses and ceramics and their biomedical applications: A review. Journal of Tissue Engineering, 8, 1-16.
84. Tajbakhsh, S., and Hajiali, F. (2017). A comprehensive study on the fabrication and properties of biocomposites of poly(lactic acid)/ceramics for bone tissue engineering. Materials Science and Engineering C, 70, 897–912.

85. Lebre, F., Sridharan, R., Sawkins, M. J., Kelly, D. J., O'Brien, F. J., and Lavelle, E. C. (2017). The shape and size of hydroxyapatite particles dictate inflammatory responses following implantation. Scientific Reports, 7(1), 1–13.
86. Zhang, J., Liu, W., Gauthier, O., Sourice, S., Pilet, P., Rethore, G., and Weiss, P. (2016). A simple and effective approach to prepare injectable macroporous calcium phosphate cement for bone repair: Syringe-foaming using a viscous hydrophilic polymeric solution. Acta biomaterialia, 31, 326-338.
87. Bartolomé, J. F., Moya, J. S., Couceiro, R., Gutiérrez-González, C. F., Guitián, F., and Martinez-Insua, A. (2016). In vitro and in vivo evaluation of a new zirconia/niobium biocermet for hard tissue replacement. Biomaterials, 76, 313-320.
88. Inzana, J. A., Schwarz, E. M., Kates, S. L., and Awad, H. A. (2016). Biomaterials approaches to treating implant-associated osteomyelitis. Biomaterials, 81, 58-71.
89. Yang, H., Xia, K., Wang, T., Niu, J., Song, Y., Xiong, Z., and Lu, W. (2016). Growth, in vitro biodegradation and cytocompatibility properties of nano-hydroxyapatite coatings on biodegradable magnesium alloys. Journal of Alloys and Compounds, 672, 366-373.
90. De Medeiros, R. C., Sigua, E. A., Navarro, P., Olate, S., and Barbosa, J. R. A. (2016). In vitro mechanical analysis of different techniques of internal fixation of combined mandibular angle and body fractures. Journal of Oral and Maxillofacial Surgery, 74(4), 778-785.
91. Bellini, D., Cencetti, C., Sacchetta, A. C., Battista, A. M., Martinelli, A., Mazzucco, L., and Matricardi, P. (2016). PLA-grafting of collagen chains leading to a biomaterial with mechanical performances useful in tendon regeneration. Journal of the mechanical behavior of biomedical materials, 64, 151-160.
92. Kaavessina, M., Chafidz, A., Ali, I., and Al-Zahrani, S. M. (2015). Characterization of poly (lactic acid)/hydroxyapatite prepared by a solvent-blending technique: Viscoelasticity and in vitro hydrolytic degradation. Journal of Elastomers and Plastics, 47(8), 753-768.
93. Takayama, T., Daigaku, Y., Ito, H., and Takamori, H. (2014). Mechanical properties of bio-absorbable PLA/PGA fiber-reinforced composites. Journal of Mechanical Science and Technology, 28(10), 4151-4154.

94. Hassan, M. I., Sun, T., and Sultana, N. (2014). Fabrication of nanohydroxyapatite/poly (caprolactone) composite microfibers using electrospinning technique for tissue engineering applications. Journal of Nanomaterials, 2014, 65.
95. Arifin, A., Sulong, A. B., Muhamad, N., Syarif, J., and Ramli, M. I. (2014). Material processing of hydroxyapatite and titanium alloy (HA/Ti) composite as implant materials using powder metallurgy: a review. Materials and Design, 55, 165-175.
96. Wu, G. F., Liu, J., Ma, Y. W., Jiao, J. J., and Xiao, X. F. (2013). Fabrication and Characterization of Hydroxyapatite/Poly (L-Lactic Acid-Polycaprolactone Nanofibrous Composite Scaffolds. In Advanced Materials Research (Vol. 791, pp. 137-140). Trans Tech Publications.
97. Perrone, G. S., Leisk, G. G., Lo, T. J., Moreau, J. E., Haas, D. S., Papenburg, B. J. and Lin, S. J. (2014). The use of silk-based devices for fracture fixation. Nature communications, 5, 3385.
98. Wang, P., Zhao, L., Liu, J., Weir, M. D., Zhou, X., and Xu, H. H. (2014). Bone tissue engineering via nanostructured calcium phosphate biomaterials and stem cells. Bone research, 2, 1-13.
99. Abdal-hay, A., Barakat, N. A., and Lim, J. K. (2013). Hydroxyapatite-doped poly (lactic acid) porous film coating for enhanced bioactivity and corrosion behavior of AZ31 Mg alloy for orthopedic applications. Ceramics International, 39(1), 183-195.
100. Huang, J., Xiong, J., Liu, J., Zhu, W., and Wang, D. (2013). Investigation of the in vitro degradation of a novel polylactide/nanohydroxyapatite composite for artificial bone. Journal of Nanomaterials, 2013, 3.
101. Felfel, R. M., Ahmed, I., Parsons, A. J., and Rudd, C. D. (2013). Bioresorbable composite screws manufactured via forging process: pull-out, shear, flexural and degradation characteristics. Journal of the mechanical behavior of biomedical materials, 18, 108-122.
102. Felfel, R. M., Ahmed, I., Parsons, A. J., Walker, G. S., and Rudd, C. D. (2011). In vitro degradation, flexural, compressive and shear properties of fully bioresorbable composite rods. Journal of the mechanical behavior of biomedical materials, 4(7), 1462-1472.

103. Roeder, R. K., Converse, G. L., Kane, R. J., and Yue, W. (2008). Hydroxyapatite-reinforced polymer biocomposites for synthetic bone substitutes. Jom, 60(3), 38-45.
104. Russias, J., Saiz, E., Nalla, R. K., Gryn, K., Ritchie, R. O., and Tomsia, A. P. (2006). Fabrication and mechanical properties of PLA/HA composites: a study of in vitro degradation. Materials Science and Engineering: C, 26(8), 1289-1295.
105. Chaya, A., Yoshizawa, S., Verdelis, K., Myers, N., Costello, B. J., Chou, D. T., and Sfeir, C. (2015). In vivo study of magnesium plate and screw degradation and bone fracture healing. Acta biomaterialia, 18, 262-269.
106. Böstman, O., and Pihlajamäki, H. (2000). Clinical biocompatibility of biodegradable orthopaedic implants for internal fixation: a review. Biomaterials, 21(24), 2615-2621.
107. Bergsma, J. E., De Bruijn, W. C., Rozema, F. R., Bos, R. R. M., and Boering, G. (1995). Late degradation tissue response to poly (L-lactide) bone plates and screws. Biomaterials, 16(1), 25-31.
108. Fan, Y., Xiu, K., Duan, H., and Zhang, M. (2008). Biomechanical and histological evaluation of the application of biodegradable poly-L-lactic cushion to the plate internal fixation for bone fracture healing. Clinical Biomechanics, 23, S7-S16.
109. Zheng, N., Price, C. T., Indelicato, P. A., and Gao, B. (2008). Tibial fixation of bone-patellar tendon-bone grafts in anterior cruciate ligament reconstruction: a cadaveric study of bovine bone screw and biodegradable interference screw. The American journal of sports medicine, 36(12), 2322-2327.
110. Sukegawa, S., Kanno, T., Kawai, H., Shibata, A., Takahashi, Y., Nagatsuka, H., and Furuki, Y. (2015). Long-term bioresorption of bone fixation devices made from composites of unsintered hydroxyapatite particles and poly-L-lactide. Journal of Hard Tissue Biology, 24(2), 219-224.
111. Wang, Y., Tie, D., Guan, R., Wang, N., Shang, Y., Cui, T., and Li, J. (2018). Microstructures, mechanical properties, and degradation behaviors of heat-treated Mg-Sr alloys as potential biodegradable implant materials. Journal of the mechanical behavior of biomedical materials, 77, 47-57.

112. Chaya, A., Yoshizawa, S., Verdelis, K., Myers, N., Costello, B. J., Chou, D. T., and Sfeir, C. (2015). In vivo study of magnesium plate and screw degradation and bone fracture healing. Acta biomaterialia, 18, 262-269.

113. Grandfield, K., Palmquist, A., Gonçalves, S., Taylor, A., Taylor, M., Emanuelsson, L., and Engqvist, H. (2011). Free form fabricated features on CoCr implants with and without hydroxyapatite coating in vivo: a comparative study of bone contact and bone growth induction. Journal of Materials Science: Materials in Medicine, 22(4), 899-906.

114. Zhang, Q., Lv, S., Lu, J., Jiang, S., and Lin, L. (2015). Characterization of polycaprolactone/collagen fibrous scaffolds by electrospinning and their bioactivity. International journal of biological macromolecules, 76, 94-101.

115. Bos, R. R. M., Rozema, F. B., Boering, G., Nijenhius, A. J., Pennings, A. J., Verwey, A. B., ... and Jansen, H. W. B. (1991). Degradation of and tissue reaction to biodegradable poly (L-lactide) for use as internal fixation of fractures: a study in rats. Biomaterials, 12(1), 32-36.

116. Dhar, P., Tarafder, D., Kumar, A., and Katiyar, V. (2016). Thermally recyclable polylactic acid/cellulose nanocrystal films through reactive extrusion process. Polymer, 87, 268-282.

117. Pal, A. K., and Katiyar, V. (2017). Thermal degradation behaviour of nanoamphiphilic chitosan dispersed poly (lactic acid) bionanocomposite films. International journal of biological macromolecules, 95, 1267-1279.

118. Pal, A. K., and Katiyar, V. (2016). Nanoamphiphilic chitosan dispersed poly (lactic acid) bionanocomposite films with improved thermal, mechanical, and gas barrier properties. Biomacromolecules, 17(8), 2603-2618.

119. Dhar, P., Tarafder, D., Kumar, A., and Katiyar, V. (2015). Effect of cellulose nanocrystal polymorphs on mechanical, barrier and thermal properties of poly (lactic acid) based bionanocomposites. RSC Advances, 5(74), 60426-60440.

120. Tesfaye, M., Patwa, R., Kommadath, R., Kotecha, P., and Katiyar, V. (2016). Silk nanocrystals stabilized melt extruded poly (lactic acid) nanocomposite films: Effect of recycling on thermal degradation kinetics and optimization studies. Thermochimica Acta, 643, 41-52.

121. Gross, K. a., Komarovska, L., and Viksna, a. (2013). Efficient zinc incorporation in hydroxyapatite through crystallization of an amorphous phase could extend the properties of zinc apatites. J. Aust. Ceram. Soc., 49 (2), 129–135.
122. Arora, A., Sharma, P., and Katti, D. S. (2015). Pullulan-based composite scaffolds for bone tissue engineering: improved osteoconductivity by pore wall mineralization. Carbohydrate polymers, 123, 180-189.
123. Gupta, A., Prasad, A., Mulchandani, N., Shah, M., Ravi Sankar, M., Kumar, S., and Katiyar, V. (2017). Multifunctional nanohydroxyapatite-promoted toughened high-molecular-weight stereocomplex poly (lactic acid)-based bionanocomposite for both 3D-printed orthopedic implants and high-temperature engineering applications. ACS omega, 2(7), 4039-4052.
124. Armentano, I., Dottori, M., Fortunati, E., Mattioli, S., and Kenny, J. M. (2010). Biodegradable polymer matrix nanocomposites for tissue engineering: a review. Polymer degradation and stability, 95(11), 2126-2146.
125. Valapa, R. B., Pugazhenthi, G., and Katiyar, V. (2015). Fabrication and characterization of sucrose palmitate reinforced poly (lactic acid) bionanocomposite films. Journal of Applied Polymer Science, 132(3),1-10.
126. Gupta, A., Pal, A. K., Woo, E. M., and Katiyar, V. (2018). Effects of Amphiphilic Chitosan on Stereocomplexation and Properties of Poly (lactic acid) Nano-biocomposite. Scientific reports, 8(1), 4351.
127. Dhar, P., Bhasney, S. M., Kumar, A., and Katiyar, V. (2016). Acid functionalized cellulose nanocrystals and its effect on mechanical, thermal, crystallization and surfaces properties of poly (lactic acid) bionanocomposites films: A comprehensive study. Polymer, 101, 75-92.
128. Gupta, A., Prasad, A., Mulchandani, N., Shah, M., Ravi Sankar, M., Kumar, S., and Katiyar, V. (2017). Multifunctional nanohydroxyapatite-promoted toughened high-molecular-weight stereocomplex poly (lactic acid)-based bionanocomposite for both 3D-printed orthopedic implants and high-temperature engineering applications. ACS omega, 2(7), 4039-4052.

129. Dhar, P., Tarafder, D., Kumar, A., and Katiyar, V. (2015). Effect of cellulose nanocrystal polymorphs on mechanical, barrier and thermal properties of poly (lactic acid) based bionanocomposites. RSC Advances, 5(74), 60426-60440.

130. Pal, A. K., Bhattacharjee, S. K., Gaur, S. S., Pal, A., and Katiyar, V. (2018). Chemomechanical, morphological, and rheological studies of chitosan-graft-lactic acid oligomer reinforced poly (lactic acid) bionanocomposite films. Journal of Applied Polymer Science, 135(3), 45546.

131. Kokubo, T., Kushitani, H., Sakka, S., Kitsugi, T., and Yamamuro, T. (1990). Solutions able to reproduce in vivo surface-structure changes in bioactive glass-ceramic A-W3. Journal of biomedical materials research, 24(6), 721-734.

132. Kang, Y. Q., Yin, G. F., Wang, K. F., Luo, L., Liao, L., and Yao, Y. D. (2007). A study of bone-like apatite formation on β-TCP/PLLA scaffold in static and dynamic Simulated Body Fluid. In Key Engineering Materials (Vol. 330, pp. 483-486). Trans Tech Publications.

133. Gu, Y. W., Khor, K. A., and Cheang, P. (2003). In vitro studies of plasma-sprayed hydroxyapatite/Ti-6Al-4V composite coatings in simulated body fluid (SBF). Biomaterials, 24(9), 1603-1611.

134. Chavan, P. N., Bahir, M. M., Mene, R. U., Mahabole, M. P., and Khairnar, R. S. (2010). Study of nanobiomaterial hydroxyapatite in simulated body fluid: Formation and growth of apatite. Materials Science and Engineering: B, 168(1-3), 224-230.

135. Li, M. X., Kim, S. H., Choi, S. W., Goda, K., and Lee, W. I. (2016). Effect of reinforcing particles on hydrolytic degradation behavior of poly (lactic acid) composites. Composites Part B: Engineering, 96, 248-254.

136. Amirouche, F., Solitro, G. F., and Magnan, B. P. (2016). Stability and Spine Pedicle Screws Fixation Strength-A Comparative Study of Bone Density and Insertion Angle. Spine deformity, 4(4), 261-267.

137. Joukainen, A., Partio, E. K., Waris, P., Joukainen, J., Kröger, H., Törmälä, P., and Rokkanen, P. (2007). Bioabsorbable screw fixation for the treatment of ankle fractures. Journal of orthopaedic science, 12(1), 28-34.

138. Sides, S. D., Fetter, N. L., Glisson, R., and Nunley, J. A. (2006). Bending stiffness and pull-out strength of tapered, variable pitch screws, and 6.5-mm cancellous screws in acute Jones fractures. Foot and ankle international, 27(10), 821-825.

139. Spitalny, A. D. (2006). Bioabsorbable implants. Clinics in podiatric medicine and surgery, 23(4), 673-694.

140. Perrone, G. S., Leisk, G. G., Lo, T. J., Moreau, J. E., Haas, D. S., Papenburg, B. J. and Lin, S. J. (2014). The use of silk-based devices for fracture fixation. Nature communications, 5, 3385.

141. Hughes, A. N., and Jordan, B. A. (1972). The mechanical properties of surgical bone screws and some aspects of insertion practice. Injury, 4(1), 25-38.

142. Mageed, M., Steinberg, T., Drumm, N., Stubbs, N., Wegert, J., and Koene, M. (2018). Internal fixation of proximal fractures of the 2nd and 4th metacarpal and metatarsal bones using bioabsorbable screws. Australian veterinary journal, 96(3), 76-81.

143. Kim, B. J., Piao, Y., Wufuer, M., Son, W. C., and Choi, T. H. (2018). Biocompatibility and efficiency of biodegradable magnesium-based plates and screws in the facial fracture model of beagles. Journal of Oral and Maxillofacial Surgery, 76(5), 1055-e1.

144. Yu, K., Dai, Y., Luo, Z., Long, H., Zeng, M., Li, Z., and Zhu, Y. (2018). In vitro and in vivo evaluation of novel biodegradable Mg-Ag-Y alloys for use as resorbable bone fixation implant. Journal of Biomedical Materials Research Part A, 106(7), 2059-2069.

145. Lai, D. M., Shih, Y. T., Chen, Y. H., Chien, A., and Wang, J. L. (2018). Effect of pedicle screw diameter on screw fixation efficacy in human osteoporotic thoracic vertebrae. Journal of Biomechanics, 70, 196-203.

146. Schumacher, T. C., Tushtev, K., Wagner, U., Becker, C., große Holthaus, M., Hein, S. B., and Rezwan, K. (2017). A novel, hydroxyapatite-based screw-like device for anterior cruciate ligament (ACL) reconstructions. The Knee, 24(5), 933-939.

147. Varghese, V., Kumar, G. S., and Krishnan, V. (2017). Effect of various factors on pull out strength of pedicle screw in normal and osteoporotic cancellous bone models. Medical engineering and physics, 40, 28-38.

148. Charles, Y. P., Pelletier, H., Hydier, P., Schuller, S., Garnon, J., Sauleau, E. A., and Clavert, P. (2015). Pullout characteristics of percutaneous pedicle screws with different cement augmentation methods in elderly spines: an in vitro biomechanical study. Orthopaedics and Traumatology: Surgery and Research, 101(3), 369-374.

149. Downey, M. W., Kosmopoulos, V., and Carpenter, B. B. (2015). Fully threaded versus partially threaded screws: determining shear in cancellous bone fixation. The Journal of Foot and Ankle Surgery, 54(6), 1021-1024.

150. Perrone, G. S., Leisk, G. G., Lo, T. J., Moreau, J. E., Haas, D. S., Papenburg, B. J., and Lin, S. J. (2014). The use of silk-based devices for fracture fixation. Nature communications, 5, 3385.

151. Ferretti, C. (2008). A prospective trial of poly-L-lactic/polyglycolic acid co-polymer plates and screws for internal fixation of mandibular fractures. International journal of oral and maxillofacial surgery, 37(3), 242-248.

152. Costi, J. J., Kelly, A. J., Hearn, T. C., and Martin, D. K. (2001). Comparison of torsional strengths of bioabsorbable screws for anterior cruciate ligament reconstruction. The American journal of sports medicine, 29(5), 575-580.

153. Chapman, J. R., Harrington, R. M., Lee, K. M., Anderson, P. A., Tencer, A. F., and Kowalski, D. (1996). Factors affecting the pullout strength of cancellous bone screws. Journal of biomechanical engineering, 118(3), 391-398.

154. Ching, Y. C., Rosiyah, Y. Y., and Li, G. (2013). Preparation and characterization of nanoparticle reinforced polyactides composite. In Journal of nano research (Vol. 23, pp. 7-15). Trans Tech Publications.

155. Fan, H., Gu, Y., Wang, S., Li, M., and Zhang, Z. (2018). Characterization and analysis of torsion property of carbon fiber bundle combined with epoxy resin. Polymer Composites, 39(S4), E2529-E2539.

156. Pal, A. K., and Katiyar, V. (2016). Nanoamphiphilic chitosan dispersed poly (lactic acid) bionanocomposite films with improved thermal, mechanical, and gas barrier properties. Biomacromolecules, 17(8), 2603-2618.

157. Gupta, A., Prasad, A., Mulchandani, N., Shah, M., Ravi Sankar, M., Kumar, S., and Katiyar, V. (2017). Multifunctional nanohydroxyapatite-promoted toughened high-molecular-weight stereocomplex poly (lactic acid)-based bionanocomposite for both

3D-printed orthopedic implants and high-temperature engineering applications. ACS omega, 2(7), 4039-4052.

158. babu Valapa, R., Pugazhenthi, G., and Katiyar, V. (2016). Hydrolytic degradation behaviour of sucrose palmitate reinforced poly (lactic acid) nanocomposites. International journal of biological macromolecules, 89, 70-80.
159. Dhar, P., Tarafder, D., Kumar, A., and Katiyar, V. (2015). Effect of cellulose nanocrystal polymorphs on mechanical, barrier and thermal properties of poly (lactic acid) based bionanocomposites. RSC Advances, 5(74), 60426-60440.
160. Felfel, R. M., Ahmed, I., Parsons, A. J., and Rudd, C. D. (2013). Bioresorbable composite screws manufactured via forging process: pull-out, shear, flexural and degradation characteristics. Journal of the mechanical behavior of biomedical materials, 18, 108-122.
161. Hernigou, P., and Pariat, J. (2017). History of internal fixation with plates (part 2): new developments after World War II; compressing plates and locked plates. International orthopaedics, 41(7), 1489-1500.
162. Downey, M. W., Kosmopoulos, V., and Carpenter, B. B. (2015). Fully threaded versus partially threaded screws: determining shear in cancellous bone fixation. The Journal of Foot and Ankle Surgery, 54(6), 1021-1024.
163. Johnson, L. L., and Eda vanDyk, G. (1996). Metal and biodegradable interference screws: comparison of failure strength. Arthroscopy: The Journal of Arthroscopic and Related Surgery, 12(4), 452-456.
164. Ricci, W. M., Tornetta III, P., Petteys, T., Gerlach, D., Cartner, J., Walker, Z., and Russell, T. A. (2010). A comparison of screw insertion torque and pullout strength. Journal of orthopaedic trauma, 24(6), 374-378.
165. http://orthopaedicprinciples.com/2013/06/bone-screws-in-orthopaedic-surgery/(Date of website visit: 21/03/2019)
166. Amirouche, F., Solitro, G. F., and Magnan, B. P. (2016). Stability and Spine Pedicle Screws Fixation Strength—A Comparative Study of Bone Density and Insertion Angle. Spine deformity, 4(4), 261-267.

167. Knutsen, A. R., Sangiorgio, S. N., Liu, C., Zhou, S., Warganich, T., Fleming, J., and Ebramzadeh, E. (2016). Distal fibula fracture fixation: Biomechanical evaluation of three different fixation implants. Foot and Ankle Surgery, 22(4), 278-285.

168. Kim, J. K., Yoon, J. O., and Baek, H. (2018). Corticocancellous bone graft vs cancellous bone graft for the management of unstable scaphoid nonunion. Orthopaedics and Traumatology: Surgery and Research, 104(1), 115-120.

169. Kulper, S. A., Sze, K. Y., Fang, C. X., Ren, X., Guo, M., Schneider, K., ... and Ngan, A. (2018). A novel fracture mechanics model explaining the axial penetration of bone-like porous, compressible solids by various orthopaedic implant tips. Journal of the mechanical behavior of biomedical materials, 80, 128-136.

170. Li, Z., Shizhao, S., Chen, M., Fahlman, B. D., Liu, D., and Bi, H. (2017). In vitro and in vivo corrosion, mechanical properties and biocompatibility evaluation of MgF2-coated Mg-Zn-Zr alloy as cancellous screws. Materials Science and Engineering: C, 75, 1268-1280.

171. Roesler, C. R. M., Salmoria, G. V., Moré, A. D. O., Vassoler, J. M., and Fancello, E. A. (2014). Torsion test method for mechanical characterization of PLDLA 70/30 ACL interference screws. Polymer Testing, 34, 34-41.

172. Baums, M. H., Zelle, B. A., Schultz, W., Ernstberger, T., and Klinger, H. M. (2006). Intraarticular migration of a broken biodegradable interference screw after anterior cruciate ligament reconstruction. Knee Surgery, Sports Traumatology, Arthroscopy, 14(9), 865-868.

173. Heimbach, B., Grassie, K., Shaw, M. T., Olson, J. R., and Wei, M. (2017). Effect of hydroxyapatite concentration on high-modulus composite for biodegradable bone-fixation devices. Journal of Biomedical Materials Research Part B: Applied Biomaterials, 105(7), 1963-1971.

174. Sahoo, N.G., Pan, Y.Z., Li, L., and He, C. Bin (2013). Nanocomposites for bone tissue regeneration. Nanomedicine, 8 (4), 639–653.

175. Niinomi, M., Liu, Y., Nakai, M., Liu, H., and Li, H. (2016). Biomedical titanium alloys with Young's moduli close to that of cortical bone. Regenerative biomaterials, 3(3), 173-185.

176. Nasution, A.K., Ulum, M.F., Abdul Kadir, M.R., and Hermawan, H. (2017). Mechanical and corrosion properties of partially degradable bone screws made of pure iron and stainless steel 316L by friction welding. Sci. China Mater., 61, 1–14.
177. Zhu, C., Ahmed, I., Parsons, A., Wang, Y., Tan, C., Liu, J., and Liu, X. (2018). Novel bioresorbable phosphate glass fiber textile composites for medical applications. Polymer Composites, 39, E140-E151.
178. Moser, J. E., Kunkel, K. A., and Gerard, P. D. (2017). Pullout strength of 2.0 mm cancellous and cortical screws in synthetic bone. Veterinary surgery, 46(8), 1110-1115.
179. Downey, M. W., Kosmopoulos, V., and Carpenter, B. B. (2015). Fully threaded versus partially threaded screws: determining shear in cancellous bone fixation. The Journal of Foot and Ankle Surgery, 54(6), 1021-1024.
180. Varghese, V., Kumar, G. S., and Krishnan, V. (2017). Effect of various factors on pull out strength of pedicle screw in normal and osteoporotic cancellous bone models. Medical engineering and physics, 40, 28-38.
181. Chapman, J. R., Harrington, R. M., Lee, K. M., Anderson, P. A., Tencer, A. F., and Kowalski, D. (1996). Factors affecting the pullout strength of cancellous bone screws. Journal of biomechanical engineering, 118(3), 391-398.
182. Sides, S. D., Fetter, N. L., Glisson, R., and Nunley, J. A. (2006). Bending stiffness and pull-out strength of tapered, variable pitch screws, and 6.5-mm cancellous screws in acute Jones fractures. Foot and ankle international, 27(10), 821-825.
183. Shi, C., Pu, X., Zheng, G., Feng, X., Yang, X., Zhang, B., and Xia, H. (2016). An antibacterial and absorbable silk-based fixation material with impressive mechanical properties and biocompatibility. Scientific reports, 6, 37418.
184. Liu, Y., Shao, J., Sun, J., Bian, X., Feng, L., Xiang, S., and Chen, X. (2014). Improved mechanical and thermal properties of PLLA by solvent blending with PDLA-b-PEG-b-PDLA. Polymer degradation and stability, 101, 10-17.
185. Ballo, A., Lassila, L. V., Narhi, T., and Vallittu, P. K. (2008). In vitro mechanical testing of glass fiber-reinforced composite used as dental implants. J Contemp Dent Pract, 9(2), 41-48.

186. Pal, A. K., and Katiyar, V. (2016). Nanoamphiphilic chitosan dispersed poly (lactic acid) bionanocomposite films with improved thermal, mechanical, and gas barrier properties. Biomacromolecules, 17(8), 2603-2618.

187. Tripathi, N., and Katiyar, V. (2016). PLA/functionalized-gum arabic based bionanocomposite films for high gas barrier applications. Journal of Applied Polymer Science, 133(21), 1-8.

188. Valapa, R. B., Pugazhenthi, G., and Katiyar, V. (2015). Fabrication and characterization of sucrose palmitate reinforced poly (lactic acid) bionanocomposite films. Journal of Applied Polymer Science, 132(3).

189. Dhar, P., Gaur, S. S., Kumar, A., and Katiyar, V. (2018). Cellulose Nanocrystal Templated Graphene Nanoscrolls for High Performance Supercapacitors and Hydrogen Storage: An Experimental and Molecular Simulation Study. Scientific reports, 8(1), 3886.

190. Engineer, C., Parikh, J., and Raval, A. (2011). Review on Hydrolytic Degradation Behavior of Biodegradable Polymers from Controlled Drug Delivery System. Trends in Biomaterials and Artificial Organs, 25(2), 79-85.

191. Wang, Y. P., Xiao, Y. J., Duan, J., Yang, J. H., Wang, Y., and Zhang, C. L. (2016). Accelerated hydrolytic degradation of poly (lactic acid) achieved by adding poly (butylene succinate). Polymer Bulletin, 73(4), 1067-1083.

192. Anderson, J.M., and Shive, M.S. (2012) Biodegradation and biocompatibility of PLA and PLGA microspheres . Adv. Drug Deliv. Rev., 64, 72–82.

193. Chaya, A., Yoshizawa, S., Verdelis, K., Myers, N., Costello, B. J., Chou, D. T., and Sfeir, C. (2015). In vivo study of magnesium plate and screw degradation and bone fracture healing. Acta biomaterialia, 18, 262-269.

194. Ferretti, C. (2008). A prospective trial of poly-L-lactic/polyglycolic acid co-polymer plates and screws for internal fixation of mandibular fractures. International journal of oral and maxillofacial surgery, 37(3), 242-248.

195. Ahmad, M., Nanda, R., Bajwa, A. S., Candal-Couto, J., Green, S., and Hui, A. C. (2007). Biomechanical testing of the locking compression plate: when does the distance between bone and implant significantly reduce construct stability. Injury, 38(3), 358-364.

196. Dewo, P., Van Der Houwen, E. B., Sharma, P. K., Magetsari, R., Bor, T. C., Vargas-Llona, L. D., ... and Verkerke, G. J. (2012). Mechanical properties of Indonesian-made narrow dynamic compression plate. Journal of the mechanical behavior of biomedical materials, 13, 93-101.

197. Amirouche, F., Solitro, G. F., and Magnan, B. P. (2016). Stability and Spine Pedicle Screws Fixation Strength-A Comparative Study of Bone Density and Insertion Angle. Spine deformity, 4(4), 261-267.

198. Kulper, S. A., Sze, K. Y., Fang, C. X., Ren, X., Guo, M., Schneider, K., ... and Ngan, A. (2018). A novel fracture mechanics model explaining the axial penetration of bone-like porous, compressible solids by various orthopaedic implant tips. Journal of the mechanical behavior of biomedical materials, 80, 128-136.

199. Middleton, J. C., and Tipton, A. J. (2000). Synthetic biodegradable polymers as orthopedic devices. Biomaterials, 21 (23), 2335–2346.

200. Nasiri, F., Ajeli, S., Semnani, D., Jahanshahi, M., and Emadi, R. (2018). Design, fabrication and structural optimization of tubular carbon/Kevlar®/PMMA/graphene nanoplate composite for bone fixation prosthesis. Biomedical Materials, 13(4), 045010.

201. Frigg, R. (2003). Development of the locking compression plate. Injury, 34, B6-10.

202. Frigg, R., Frenk, A., and Wagner, M. (2007). Biomechanics of plate osteosynthesis. Techniques in orthopaedics, 22(4), 203-208.

203. Mehboob, H., and Chang, S. H. (2015). Optimal design of a functionally graded biodegradable composite bone plate by using the Taguchi method and finite element analysis. Composite Structures, 119, 166-173.

204. Mehboob, H., and Chang, S. H. (2014b). Evaluation of healing performance of biodegradable composite bone plates for a simulated fractured tibia model by finite element analysis. Composite Structures, 111, 193-204.

205. Mehboob, H., and Chang, S. H. (2014a). Application of composites to orthopedic prostheses for effective bone healing: A review. Composite Structures, 118, 328-341.

206. Kohal, R. J., Bächle, M., Att, W., Chaar, S., Altmann, B., Renz, A., and Butz, F. (2013). Osteoblast and bone tissue response to surface modified zirconia and titanium implant materials. Dental Materials, 29(7), 763-776.

207. Allgöwer, M., Matter, P., Perren, S. M., and Rüedi, T. (2012). The dynamic compression plate DCP. Springer Science and Business Media.

208. Huang, Z. M., and Fujihara, K. (2005). Stiffness and strength design of composite bone plates. Composites science and technology, 65(1), 73-85.

209. Ferretti, C. (2008). A prospective trial of poly-L-lactic/polyglycolic acid co-polymer plates and screws for internal fixation of mandibular fractures. International journal of oral and maxillofacial surgery, 37(3), 242-248.

210. Kim, S. H., Chang, S. H., and Son, D. S. (2011). Finite element analysis of the effect of bending stiffness and contact condition of composite bone plates with simple rectangular cross-section on the bio-mechanical behaviour of fractured long bones. Composites Part B: Engineering, 42(6), 1731-1738.

211. Montufar, E. B., Casas-Luna, M., Horynová, M., Tkachenko, S., Fohlerová, Z., Diaz-de-la-Torre, S.,and Kaiser, J. (2018). High strength, biodegradable and cytocompatible alpha tricalcium phosphate-iron composites for temporal reduction of bone fractures. Acta biomaterialia, 70, 293-303.

212. Samiezadeh, S., Avval, P. T., Fawaz, Z., and Bougherara, H. (2015). On optimization of a composite bone plate using the selective stress shielding approach. Journal of the mechanical behavior of biomedical materials, 42, 138-153.

213. Dewo, P., van der Houwen, E. B., Marius, R., Magetsari, R., and Verkerke, G. J. (2015). Redesign of Indonesian-made osteosynthesis plates to enhance their mechanical behavior. Journal of the mechanical behavior of biomedical materials, 42, 274-281.

214. Dewo, P., Van Der Houwen, E. B., Sharma, P. K., Magetsari, R., Bor, T. C., Vargas-Llona, L. D., ... and Verkerke, G. J. (2012). Mechanical properties of Indonesian-made narrow dynamic compression plate. Journal of the mechanical behavior of biomedical materials, 13, 93-101.

215. Chakladar, N. D., Harper, L. T., and Parsons, A. J. (2016). Optimisation of composite bone plates for ulnar transverse fractures. Journal of the mechanical behavior of biomedical materials, 57, 334-346.

216. Sukegawa, S., Kanno, T., Kawai, H., Shibata, A., Takahashi, Y., Nagatsuka, H., and Furuki, Y. (2015). Long-term bioresorption of bone fixation devices made from composites of unsintered hydroxyapatite particles and poly-L-lactide. Journal of Hard Tissue Biology, 24(2), 219-224.

217. Uhthoff, H. K., Poitras, P., and Backman, D. S. (2006). Internal plate fixation of fractures: short history and recent developments. Journal of orthopaedic science, 11(2), 118-126.

218. Roeder, R. K., Converse, G. L., Kane, R. J., and Yue, W. (2008). Hydroxyapatite-reinforced polymer biocomposites for synthetic bone substitutes. Jom, 60(3), 38-45.

219. Nourisa, J., and Rouhi, G. (2016). Biomechanical evaluation of intramedullary nail and bone plate for the fixation of distal metaphyseal fractures. Journal of the mechanical behavior of biomedical materials, 56, 34-44.

220. Kharazi, A. Z., Fathi, M. H., and Bahmany, F. (2010). Design of a textile composite bone plate using 3D-finite element method. Materials and Design, 31(3), 1468-1474.

221. Gaball, C., Lovald, S., Baack, B., and Olson, G. (2011). Minimally invasive bioabsorbable bone plates for rigid internal fixation of mandible fractures. Archives of facial plastic surgery, 13(1), 31-35.

222. Hur, W., Park, M., Lee, J. Y., Kim, M. H., Lee, S. H., Park, C. G., and Lee, S. J. (2016). Bioabsorbable bone plates enabled with local, sustained delivery of alendronate for bone regeneration. Journal of controlled release, 222, 97-106.

223. Ahmad, M., Nanda, R., Bajwa, A. S., Candal-Couto, J., Green, S., and Hui, A. C. (2007). Biomechanical testing of the locking compression plate: when does the distance between bone and implant significantly reduce construct stability. Injury, 38(3), 358-364.

224. Grizzi, I., Garreau, H., Li, S., and Vert, M. (1995). Hydrolytic degradation of devices based on poly (DL-lactic acid) size-dependence. Biomaterials, 16(4), 305-311.

225. Proikakis, C. S., Mamouzelos, N. J., Tarantili, P. A., and Andreopoulos, A. G. (2006). Swelling and hydrolytic degradation of poly (D, L-lactic acid) in aqueous solutions. Polymer Degradation and Stability, 91(3), 614-619.

226. Mageed, M., Steinberg, T., Drumm, N., Stubbs, N., Wegert, J., and Koene, M. (2018). Internal fixation of proximal fractures of the 2nd and 4th metacarpal and metatarsal bones using bioabsorbable screws. Australian veterinary journal, 96(3), 76-81.

227. Antoci, V., Ono, C. M., Antoci Jr, V., and Raney, E. M. (2008). Pin-tract infection during limb lengthening using external fixation. Am J Orthop (Belle Mead NJ), 37(9), E150-E1544.

228. Kofman, K. E., Buckley, T., and McGrouther, D. A. (2012). Complications of transcutaneous metal devices. European journal of plastic surgery, 35(9), 673-682.

229. Hsu, L. P., Schwartz, E. G., Kalainov, D. M., Chen, F., and Makowiec, R. L. (2011). Complications of K-wire fixation in procedures involving the hand and wrist. The Journal of hand surgery, 36(4), 610-616.

230. Gut, G., and Śladowski, D. (2007, November). Mechanical properties of bone fixation devices prepared from a human allogenic bone. In Transplantation proceedings (Vol. 39, No. 9, pp. 2920-2922).

231. Hirvensalo, E., Böstman, O., and Rokkanen, P. (1990). Absorbable polyglycolide pins in fixation of displaced fractures of the radial head. Archives of orthopaedic and trauma surgery, 109(5), 258-261.

232. Jensen, C. H., and Jensen, C. M. (1996). Biodegradable pins versus Kirschner wires in hand surgery. Journal of Hand Surgery, 21(4), 507-510.

233. Weimann, A., Zantop, T., Rümmler, M., Hassenpflug, J., and Petersen, W. (2003). Primary stability of bone-patellar tendon-bone graft fixation with biodegradable pins. Arthroscopy: The Journal of Arthroscopic and Related Surgery, 19(10), 1097-1102.

234. Pietrzak, W. S., Lessek, T. P., and Perns, S. V. (2006). A bioabsorbable fixation implant for use in proximal interphalangeal joint (hammer toe) arthrodesis: biomechanical testing in a synthetic bone substrate. The Journal of foot and ankle surgery, 45(5), 288-294.

235. Antoci, V., Ono, C. M., Antoci Jr, V., and Raney, E. M. (2008). Pin-tract infection during limb lengthening using external fixation. Am J Orthop (Belle Mead NJ), 37(9), E150-E1544.

236. Bellisari, G.E., Kaeding, C.C., and Litsky, A.S. (2010). Mechanical evaluation of cross pins used for femoral fixation of hamstring grafts in ACL reconstructions. Orthopedics, **33** (10), 722.

237. Kembhavi, R.S., Menon, J., and Patro, D.K. (2015). Outcome of fractures fixed with biodegradable pins – a case series. International journal of medical and applied science,4 (1),50-58.

238. Singh, R., Tripathy, S. K., Naik, M. A., Sujir, P., and Rao, S. K. (2017). ACL reconstruction using femoral Rigid-fix and tibial Bio-intrafix devices. Journal of clinical orthopaedics and trauma, 8(3), 254-258.

239. Lekston, Z., Stróż, D., and Jędrusik-Pawłowska, M. (2012). Preparation and characterization of nitinol bone staples for cranio-maxillofacial surgery. Journal of materials engineering and performance, 21(12), 2650-2656.

240. Russell, S. M. (2009). Design considerations for nitinol bone staples. Journal of materials engineering and performance, 18(5-6), 831-835.

241. Koukoubis, T. D., Glisson, R. R., Feagin Jr, J. A., Seaber, A. V., Schenkman, D., Korompilias, A. V., and Stahl, D. L. (1997). Meniscal fixation with an absorbable staple: An experimental study in dogs. Knee Surgery, Sports Traumatology, Arthroscopy, 5(1), 22-30.

242. Rethnam, U., Kuiper, J., and Makwana, N. (2009). Mechanical characteristics of three staples commonly used in foot surgery. Journal of foot and ankle research, 2(1), 5.

243. www.podiatryinstitute.com/pdfs/Update_2010/2010_41.pdf (Date of website visit: 21/03/2019)

244. Parvaiz, M., and Mahanwar, P. (2010) Morphological, Mechanical, Thermal, Electrical and Rheological Properties of Polycarbonate Composites Reinforced with Surfaces Modified Mica. J. Miner., 9 (11), 985–996.

245. Wu, G.F., Liu, J., Ma, Y.W., et al. (2013) Fabrication and Characterization of Hydroxyapatite/Poly (L-Lactic Acid-Polycaprolactone Nanofibrous Composite Scaffolds. Adv. Mater. Res., 791–793, 137–140.

Research Outcomes

Patents

1. Vimal Katiyar, Ravi M. Sankar and Arbind Prasad, Resorbable Polymer Composite Bone Plate, Indian Patent Application No: 201831011253.
2. Vimal Katiyar, Ravi M. Sankar and Arbind Prasad, Resorbable Cortical Screw, Indian Patent Application No: 201831011251.
3. Vimal Katiyar, Ravi M. Sankar and Arbind Prasad, Siddharth Bhasney, Process for the preparation of polymer composite based Cancellous Screws and Pins, Indian Patent Application No: 201831011252.
4. Vimal Katiyar, Ravi M. Sankar, Arbind Prasad,"Process for preparation of Resorbable Polymeric Composite U type Bone Staple, Indian Patent Application No: 201831011250.

Book Chapter

1. Neha Mulchandani, Arbind Prasad and Vimal Katiyar, "Resorbable Polymers in bone repair and regeneration", Materials for Biomedical Engineering: Absorbable Polymers, (ISBN: 9780128184158), Elsevier, 18th June, 2019.

Journals

1. Arvind Gupta, Arbind Prasad, Neha Mulchandani, Manisha Shah, Mamilla Ravi Sankar, Sachin Kumar, Vimal Katiyar, Multifunctional Nano-Hydroxyapatite promoted Toughened High Molecular Weight Stereo-complex Poly(lactic acid) based Bionanocomposite for both 3D Printed Orthopedic Implants and High-Temperature Engineering Applications, ACS Omega 2017, 2, 4039−4052, DOI: 10.1021/acsomega.7b00915.

2. Arbind Prasad, Siddharth Mohan Bhasney, M. Ravi Sankar, Vimal Katiyar, "Fish Scale Derived Hydroxyapatite reinforced Poly (Lactic acid) Polymeric Bio-films: Possibilities for Sealing/locking the Internal Fixation Devices", Materials Today: Proceedings, Volume 4, Issue 2, Part A, 2017, Pages 1340-1349, ISSN 2214-7853, https://doi.org/10.1016/j.matpr.2017.01.155.
3. Arbind Prasad, M. Ravi Sankar, Vimal Katiyar, "State of Art on Solvent Casting Particulate Leaching Method for Orthopedic Scaffolds Fabrication", Materials Today: Proceedings, Volume 4, Issue 2, Part A, 2017, Pages 898-907, ISSN 2214-7853, https://doi.org/10.1016/j.matpr.2017.01.101.
4. Arbind Prasad, Siddharth Bhasney, Vimal Katiyar, M. Ravi Sankar, "Biowastes Processed Hydroxyapatite filled Poly (Lactic acid) Bio-Composite for Open Reduction Internal Fixation of Small Bones". Materials Today: Proceedings, (2017), 4 (9), 10153–10157. http://doi.org/10.1016/j.matpr.2017.06.339.
5. Arbind Prasad, B. Devendar, M. Ravi Sankar, P.S. Robi,"Micro-Scratch Based Tribological Characterization of Hydroxyapatite (HAp) Fabricated through Fish Scales", Materials Today: Proceedings (2015), 2(4-5), 1216–1224. http://doi.org/10.1016/j.matpr.2015.07.034.

Conferences

1. Y. Chittara, A. Yadav, M. Ravi Sankar, Arbind Prasad, B. N Mondal, N Mondal, U. Batra, " Effect of Calcination Temperature on Quality of Hydroxyapatite that Fabricated from fish scales Biowastes", 23rd Processing and Fabrication of Advanced Materials(PFAM-XXIII), 5-7 December, 2014, IIT Roorkee (India), Pages 65-77.
2. Arbind Prasad, Dheeraj Gupta, M. Ravi Sankar, A. Narayana Reddy," Experimental Investigations of Ni/La_2O_3 Composite Micro-Cladding on AISI 1040 Steel through Microwave Irradiation ", 5th International and 26th All India Manufacturing Technology, Design and Research conference(AIMTDR-2014),12-14 December 2014, IIT Guwahati (India), Pages (55)1-6.
3. Arbind Prasad, M. Ravi Sankar, Vimal Katiyar " Fabrication and Invitro studies of Biodegradable strands shaped polymeric pin for fixation of Proximal Interphalangeal

Joints", Advances in Sustainable polymers (ASP,2016) organized by Kyoto Institute of Technology ,Japan and Indian Institute of Technology Guwahati on 4-6 August,2016 in Japan.

4. Arbind Prasad, Melakuu Tesfaye, M. Ravi Sankar, Vimal Katiyar "Rheological and Thermal Studies of Poly Lactic acid/Hydroxyapatite Composites ", International conference on Polymer science and Technology and advances in polymer science and new generation technologies Spsi-acs jubilee symposium, (MACRO 2017), January 9-11, 2017 at VSSC, Thiruvananthapuram, Kerala, India
5. Arbind Prasad, Aditya Sinha, M. Ravi Sankar, Vimal Katiyar " Effect of Hydroxyapatite Loading on Polylactic acid/Hydroxyapatite Composites on its Mechanical, Thermal and Degradation Properties", International conference on Polymer science and Technology and advances in polymer science and new generation technologies Spsi-acs jubilee symposium, (MACRO 2017), January 9-11, 2017 at VSSC, Thiruvananthapuram, Kerala, India.
6. Arbind Prasad, M. Ravi Sankar, A. N. Reddy "Quality of Hydroxyapatite from Fish Scales Bio-waste Calcinated at Various Temperatures" Research Conclave organized by PhD Council of Student's Academic Board (SAB), Indian Institute of Technology Guwahati on 23-26 March, 2015.
7. Arbind Prasad, M. Ravi Sankar, Vimal Katiyar, "Studies on Fabrication and characterization of Poly (Lactic acid)/ Hydroxyapatite Bio-composite for Orthopedic Fixation Applications" Indian Chemical Engineering Congress and 68th Annual Session of Indian Institute of Chemical engineers (CHEMCON 2015) organized by Guwahati Regional Centre and Indian Institute of Chemical Engineers at IIT Guwahati on 27-30 December 2015.
8. Arbind Prasad, M. Ravi Sankar, Vimal Katiyar, "Nano Hydroxyapatite fabrication through fish scales bio wastes" Materials Research Society of India Symposium on Advance Materials for Sustainable Applications & 27th Annual General meeting of MRSI jointly organized by CSIR-NEIST Jorhat, IIT Guwahati and Tezpur University at CSIR-North East Institute of Science and Technology, Jorhat on 18-20 February 2016.

9. Arbind Prasad, M. Ravi Sankar, Vimal Katiyar, " Bio-waste processed composites for orthopedic fixation applications" Research Conclave organized by PhD Council of Student's Academic Board (SAB), Indian Institute of Technology Guwahati on 23-26 March, 2015.
10. Arbind Prasad, M. Ravi Sankar, Vimal Katiyar, "Fabrication and Invitro studies of Biodegradable strands shaped polymeric pin for fixation of Proximal Interphalangeal Joints" Advances in Sustainable polymers (ASP,2016) organized by Kyoto Institute of Technology ,Japan and Indian Institute of Technology Guwahati on 4-6 August, 2016 in Japan.
11. Arbind Prasad, M. Ravi Sankar, Vimal Katiyar, "Fabrication and characterization of Poly (lactic acid)/Hydroxyapatite biofilms for bone graft harvest site fixations " 252nd ACS National Meeting in Philadelphia (Paper Id:2516802), PA,USA, August 21-25, 2016.
12. Arvind Gupta, Arbind Prasad, M. Ravi Sankar, Vimal Katiyar, Fabrication and Characterization of the Stereo-complex Poly-(lactic acid) and Hydroxyapatite Biocomposite, AIChE Annual Meeting in San Francisco, CA (2016).
13. Arbind Prasad, M. Ravi Sankar, Vimal Katiyar, " Fabrication and Invitro studies of Biodegradable strands shaped polymeric pin for fixation of Proximal Interphalangeal Joints "Advances in Sustainable polymers (ASP 16) organized by Kyoto Institute of Technology ,Japan and Indian Institute of Technology Guwahati on 4-6 August, 2016 in Japan.
14. Arbind Prasad, M. Ravi Sankar, Vimal Katiyar, "Poly Lactic acid/ nano Hydroxyapatite based resorbable composites: Device to fix Podiatry fixations" Fourth International Symposium on Advances in Sustainable Polymers (ASP 17), January 8-11, 2018
15. Arbind Prasad, M. Ravi Sankar, Vimal Katiyar, "Value added Bioactive Biomaterials from Biowaste: The North East Perspective", Indo-Japan Bilateral Symposium on Future Perspective of Bio-resource Utilization in North-East India (IJBS 17), February 1-4, 2018.

Awards

1. Cleared stage 1 and stage 2 online quiz conducted by Science Direct (Elsevier Publication)
2. Won best Paper Presentation Awards (worth 600 Euros) from Springer publications in Advances in sustainable polymers conferences, ASP 17, 2018.
3. Won best Poster award and cash award in Research Conclave organized by PhD Council of Student's Academic Board (SAB), Indian Institute of Technology Guwahati on 14-17 March, 2019.
4. Won best poster award in 4th international conference "Technological advancement in Polymers" at IIT Kanpur
5. Won best poster cum SRIC IIT Kharagpur award (Sponsored Research Industrial Consultancy, IIT Kharagpur) in 4th international conference on "Nanotechnology for Better Living" on theme: Technological Advancement of Polymer Composites jointly organized by IIT Kanpur, NIT Srinagar, CSJM University and HBTU Kanpur on 6-7 April, 2019.

Invited talks

- Arbind Prasad, M. Ravi Sankar, Vimal Katiyar " Nano Bioactive Ceramics based Bioresorbable Composite for Bone Fracture Fixations" KIT-IITG Joint Symposium, organized by Kyoto Institute of Technology, Japan and Indian Institute of Technology Guwahati on January 8-11, 2018.

Publications under preparation

1. Fabrication and characterization of cortical screws for bone fracture fixations (to be communicated)
2. Fabrication and characterization of cancellous screw for bone fracture fixations (to be communicated)
3. Fabrication and characterization of bioabsorbable bone plates for open reduction of orthopedics fixations (to be communicated)
4. Fabrication and characterization of steinmann pins and staples for fixations of interphalangeal joints (to be communicated)